

copyright of this thesis rests with its author.

This copy of the thesis has been supplied on condition that anyone who consults it is understood to recognise that its copyright rests with its author and that no quotation from the thesis and no information derived from it may be published without the author's prior written consent.

307

D47328/83

YAZDANI PEDRAMI M

307

472

PHYSICO-CHEMICAL STUDIES ON RANDOM AND BLOCK  
COPOLYMERS BASED ON DERIVATIVES  
OF ITACONIC ACID

A thesis submitted to the University of Stirling  
for the degree of  
Doctor of Philosophy

Mehrdad, Yazdani Pedram

Department of Chemistry

June 1982

7/83

## PREFACE

This thesis is submitted for the degree of Doctor of Philosophy at the University of Stirling, having been submitted for no other degree. It is a record of research undertaken in the Department of Chemistry. This work is wholly original except where due reference is made.

### ACKNOWLEDGEMENTS

I wish to thank my supervisor, Professor J.M.G. Cowie, for his frequent advice, encouragement and support throughout this work. I also wish to thank Dr. I. J. McEwen for his practical assistance and many discussions which have helped me to further my knowledge and understanding of the thermal and mechanical properties of polymers.

My thanks also go to the members of the Chemistry Department for their assistance during my period of studies at Stirling, particularly to Mrs. J. Weber for typing the manuscript and to Mr. R. Ferguson for developing the computer programs used during this work.

Finally, I wish to express my sincere gratitude to my family and to my parents for their support without which I could not have undertaken this study.

## ABSTRACT

The thermal and mechanical properties of homopolymers, random copolymers, mixed ester polymers, block copolymers and ionomers, all based on itaconic acid have been studied.

The heat capacity behaviour of random copolymers and mixed ester polymers has been measured and compared with their mechanical spectra. A major relaxation process in the glassy state of some of the polymers has been detected and identified with the independent relaxation of long n-alkyl side chains. A theoretical model has been developed which describes the relaxation and accounts for the heat capacity behaviour in these systems.

Thermoplastic block copolymers have been synthesized using dimethylitaconate as the glassy component and butadiene as the rubbery component. The mechanical and thermal properties of the block copolymers have been established and useful materials can be obtained from this system.

Finally, a series of ionomers from mono-n-pentyl itaconate and di-n-pentyl itaconate was synthesized and the effect of variation of the ion content on the mechanical behaviour was investigated.

## CONTENTS

	<u>Page</u>
1. <u>CHAPTER ONE</u>	
<u>INTRODUCTION</u>	1
1.1 Itaconic acid and its esters	2
1.2 Polymerization of itaconic acid esters	3
1.3 Mechanical properties and the glass transition of amorphous polymers	5
1.4 The heat capacity and glass transition of amorphous polymers	8
1.5 Copolymers	10
1.6 Properties of copolymers	12
1.7 Ionomers	13
1.8 Scope of present work	14
2. <u>CHAPTER TWO</u>	
<u>EXPERIMENTAL AND INSTRUMENTATION</u>	15
2.1 Preparation and characterization of monomers and other reagents	17
2.2 Polymerizations and copolymerizations	22
2.3 Polymer characterization	34
3. <u>CHAPTER THREE</u>	
<u>COPOLYMERS FROM DIESTERS OF ITACONIC ACID</u>	58
3.1 Copolymer compositions, reactivity ratios and molecular weights	60
3.2 TBA measurements	73
3.3 DSC measurements	92
3.4 $\Delta C_p$ behaviour in the systems studied	115
3.5 Theoretical interpretation of $T_g^L$ in the homopolymers	129
3.6 Analysis of the variation of $T_g^U$ with copolymer composition	147

	<u>Page</u>
4. <u>CHAPTER FOUR</u>	
<u>MIXED ESTER POLYMERS FROM ITACONIC ACID</u>	165
4.1 Mixed esters	167
4.2 TBA measurements	172
4.3 DSC measurements	181
4.4 Conclusions	181
5. <u>CHAPTER FIVE</u>	
<u>BLOCK COPOLYMERS</u>	190
5.1 Sequential initiators	191
5.2 Block copolymers of butadiene and dimethyl itaconate	201
5.3 Thermal and mechanical properties of copolymers from polybutadienes, hydrogenated polybutadiene and dimethyl itaconate	229
5.4 Block copolymers of isoprene and dimethyl itaconate	256
6. <u>CHAPTER SIX</u>	
<u>IONOMERS</u>	262
6.1 Copolymer characterization	263
6.2 TBA measurements	273
REFERENCES	285
APPENDICES	

CHAPTER ONE

CHAPTER ONE

INTRODUCTION

The first part of the book is devoted to a general survey of the subject matter. It is intended to give the reader a broad view of the field and to point out the main lines of development.

The second part of the book is devoted to a detailed study of the various aspects of the subject. It is intended to give the reader a more complete knowledge of the subject and to show the progress of research in the field.

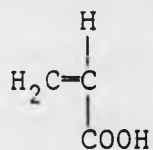
The third part of the book is devoted to a study of the various applications of the subject. It is intended to show the reader how the principles of the subject can be applied to practical problems.

The fourth part of the book is devoted to a study of the various methods of research in the field. It is intended to show the reader the various techniques that are used in the study of the subject and to give the reader a more complete knowledge of the subject.

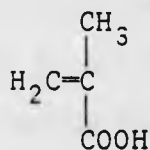


### 1.1 ITACONIC ACID AND ITS ESTERS

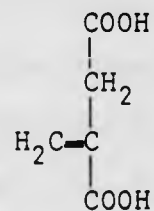
Itaconic acid (2-methylene butane-1,4-dioic acid) is a dicarboxylic acid with an external methylene group and may be regarded as a structural variant of acrylic and methacrylic acids.



acrylic acid



methacrylic acid



itaconic acid

Itaconic acid was originally isolated by Baup<sup>(1)</sup>, in 1836, from the pyrolysis products of citric acid and it was characterized by solubility and melting point. The name "itaconic acid" was given a few years later but it was not until the 1880's that further investigations were undertaken, both on itaconic acid itself and on a number of its esters<sup>(2)</sup>.

In 1931, Kinoshita<sup>(3)</sup> reported for the first time the preparation of itaconic acid by a fermentation process. He isolated from dried and salted plums, a fungus (Aspergillus itaonicus) which was found to be capable of fermenting sugars to itaconic acid in yields of up to 24%. The preparation of itaconic acid by this process never attained a commercial scale due to the high cost involved, resulting in limited applied research being undertaken. A large scale fermentation process for the production of itaconic acid using Aspergillus terreus, with molasses as the source of carbohydrate, has been developed during the last decade by Pfizer Chemicals in the U.K. and has

considerably reduced the price of this useful and versatile acid.

Esterification of itaconic acid was first reported by Swarts<sup>(4)</sup> in 1873. Resin formation by itaconic acid esters was observed early in this century causing substantial interest and efforts in this field. Various patents<sup>(5)</sup> relating to esters based on itaconic acid have been issued since that time. These describe their use in such applications as oil additives, plasticizers, coatings and synthetic fibres.

## 1.2 POLYMERIZATION OF ITACONIC ACID ESTERS

The first detailed study of the homopolymerization of dimethyl-, diethyl- and di-n-butyl itaconates was published by Marvel and Shepherd<sup>(6)</sup> in 1958. Nagai and his co-workers<sup>(7)</sup> carried out a dilatometric study of the kinetics of the bulk polymerization of dimethyl-, diethyl-, di-n-propyl, di-n-butyl- and di-n-octyl itaconates at 323K using  $\alpha, \alpha'$ -Azobis iso-butyronitrile (AIBN) as initiator, in 1960. They suggested the following rate equation,

$$R_p = k[M][I]^{\frac{1}{2}} \quad (1)$$

where  $R_p$  is the rate of polymerization,  $k$  the apparent rate constant,  $[M]$  and  $[I]$  the concentrations of monomer and initiator respectively.

A review on the polymerization of itaconic acid and its esters was published by Tate<sup>(8,9)</sup> in 1967. He also found that under controlled conditions, it is possible to obtain good yields of mono alkyl esters of itaconic acid which could then be polymerized to poly(mono alkyl itaconates)<sup>(10)</sup>. He

suggested that polymers of dialkyl itaconates are similar in hardness to the corresponding polymers of alkyl methacrylates and quoted the softening point of poly(dimethyl itaconate) to be about 385K.

Velickovic and his co-workers<sup>(11-15)</sup>, have published a series of papers on the hydrodynamic properties of itaconic acid based polymers. They measured the refractive index increment of a comprehensive series of di-n-alkyl itaconate polymers and copolymers and have established the Kuhn-Mark Houwink-Sakurada (KMHS) relations and unperturbed dimensions for these systems. The same workers have also polymerized dicyclohexyl itaconate, using AIBN as initiator, and have established the solubility parameters and the KMHS relationship for the product. The hydrodynamic properties of random copolymers of mono-n-butylitaconate and di-n-butylitaconate have also been studied<sup>(16,17)</sup>.

The most extensive study of the physical properties of polymers based on esters of itaconic acid has been carried out by Cowie and his co-workers<sup>(18-25)</sup> whose main interests have been in determining structure-property relationships. Di-n-alkyl itaconates with side chain lengths of up to 20 carbons have been prepared and the effect of chain length on the glass transition ( $T_g$ ) has been determined. When the side chain contains from 7-11 carbons the polymers exhibit evidence of a double glass transition, and for side chains of 12 or more carbon atoms crystallinity is observed in these otherwise amorphous polymers. An analogous series of di-cycloalkyl itaconate polymers has been used to elucidate the nature of molecular motions in the glassy state<sup>(26)</sup>.

Ion containing polymers (Ionomers) have been prepared from poly(monoesters) and from copolymers of mono and diesters. The morphology, mechanical and thermal properties of these systems have been determined<sup>(19)</sup>. Further studies exploiting the potential for modification of the difunctional nature of monomers from itaconic acid are being actively pursued.

### 1.3 MECHANICAL PROPERTIES AND THE GLASS TRANSITION OF AMORPHOUS POLYMERS

The mechanical properties of elastic solids can be described in classical terms by Hook's law and the corresponding description for liquids is embodied in Newton's law. In many cases, polymeric materials exhibit the characteristic of both solids and liquids, and they are said to be in a viscoelastic state<sup>(27)</sup>.

The physical nature of an amorphous polymer is related to the extent of molecular motion in the sample. In the glassy state, cooperative motion along the chain is frozen and the material has most of the characteristics of an elastic solid. When thermal energy is supplied so that cooperative movement of the polymer chains is generated by rotation about the single bonds connecting the atoms of the chain, a transition from the glass to the rubber-like state begins to take place. At this temperature, called the glass transition temperature ( $T_g$ ), dramatic changes in the physical properties, such as hardness and elasticity, are observed. As the temperature is further raised an increasing number of polymer chains begin to move with greater freedom. Finally, when molecular motion has increased to a sufficient level, viscous flow of the polymer will occur.

From the experimental point of view  $T_g$  may be detected by monitoring any one of a number of properties which can be measured as a function of temperature. These include specific heat, specific volume, dielectric and mechanical behaviour<sup>(28,29)</sup>.

The molecular basis for the glass transition is widely accepted as the onset of long range cooperative motion of the polymer backbone (micro-Brownian motion)<sup>(30)</sup> which is frozen in below  $T_g$ . Although, for any particular polymer,  $T_g$  is normally quoted as a single temperature, the changes measured at  $T_g$  occur over a temperature range of perhaps 20K. The point of maximum change in properties is traditionally designated  $T_g$ . This may be illustrated with reference to figure 1 where the mechanical modulus is plotted against temperature.

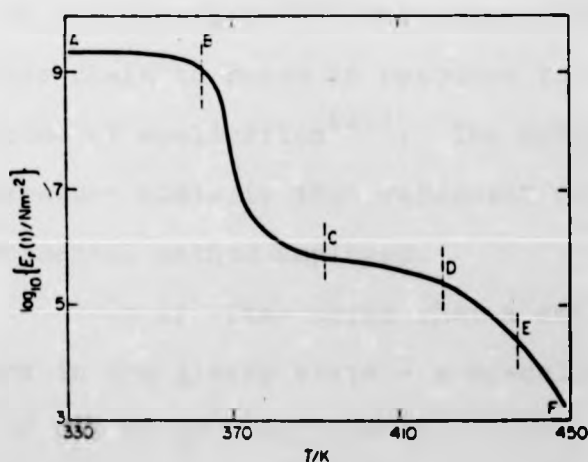


Figure 1: Schematic diagram of log (mechanical modulus) versus temperature.

- A-B Glassy state
- B-C Transition region ( $T_g$ )
- C-D Leathery region
- D-E Rubbery state
- E-F Flow region

Around  $T_g$  the modulus drops from its glassy state value ( $\sim 10^9 \text{ Nm}^{-2}$ ) by several orders of magnitude but does not immediately drop to a value characteristic of a viscous liquid. If the molecular weight is above some critical value chain entanglements will give rise to a "rubbery plateau" region, the extent of which is dependent on molecular weight. Other factors which will affect the extent of the rubbery region are the presence of chemical cross links ("permanent entanglement") and/or crystallinity<sup>(31)</sup>.

The mechanical modulus of a polymer may be measured by a number of low frequency or quasi-static mechanical tests such as stress relaxation, creep under load, and stress-strain behaviour where the rate of testing is relatively low (much less than 1 Hz). Techniques such as the torsional pendulum and dynamic mechanical analysis essentially apply an oscillating stress to the sample at higher frequencies from  $\sim 1$  Hz to  $\sim 100$  Hz. The viscoelastic nature of polymers, is readily measured by any one of these methods<sup>(28)</sup> and arises from the ability of the polymer chain to relax in response to an applied stress during its time of application<sup>(27)</sup>. The actual position of  $T_g$  on the temperature scale is thus dependent on the frequency of the experimental method employed.

It is often noted that a small change in modulus occurs in the glassy state - a so-called sub-glass transition - and is due to limited molecular motions within the glass<sup>(30)</sup>. Sub-glass transition has been ascribed to local segmental motion of the chain and motions within or of a side chain unit. The origins of sub-glass transitions have been extensively discussed by both Heijboer<sup>(32)</sup> and Cowie<sup>(33)</sup>.

Since the glass transition reflects the amount of energy necessary to overcome rotational barriers in the polymer chain backbone, it is therefore a function of chemical structure. For example, poly(dimethyl siloxane) has a  $T_g = 150\text{K}$  as a result of the relatively flexible o-Si-o linkages, whereas the  $T_g$  of poly(p-phenylene oxide) is 350K due to the inclusion of the particularly rigid p-phenylene ring in the polymer chain backbone. In addition to the effect of the flexibility of the backbone, there is a steric effect in polymers with the repeat unit type  $\langle \text{CH}_2\text{-CHX} \rangle$  due to pendant group X. Bulky groups hinder rotation about the backbone and cause a rise in  $T_g$ . This effect is well illustrated by considering the series polyethylene, polypropylene, polystyrene, whose respective values of  $T_g$  are 195K, 253K and 373K.

Cross-linking is another important factor in determining  $T_g$  since this obviously restricts chain mobility. Cross-linking may result from covalent bonding or ionic interactions between polymer chains. The inclusion of crystalline regions or other aggregated structures in an amorphous polymer may also limit chain mobility at the glass transition.

#### 1.4 THE HEAT CAPACITY AND GLASS TRANSITION OF AMORPHOUS POLYMERS

The heat capacity ( $C_p$ ) is the amount of heat which must be added to a system to raise its temperature under conditions of constant pressure and is formally defined as

$$C_p = \left( \frac{\delta H}{\delta T} \right)_p \quad (2)$$

where H is the enthalpy. The heat capacity at constant volume is analogously defined by

$$C_V = \left( \frac{\delta U}{\delta T} \right)_V \quad (3)$$

where  $U$  is the internal energy of the system.  $C_V$  is much more difficult to measure than  $C_P$ , and if required is usually obtained via the relation,

$$C_P = C_V + \alpha^2 T V_m / \kappa_T \quad (4)$$

$\kappa_T$  is the isothermal compressibility,  $\alpha$  the coefficient of expansion and  $V_m$  the molar volume.

Heat capacities are normally well understood<sup>(34)</sup> and in the solid state arise mainly from vibrational contributions (which are effectively the only motions permitted at low temperatures). They may be calculated with a high degree of accuracy for simple structures where the geometry and bond force constants are known.

Calculation of  $C_P$  for polymers, however, is a much more difficult task. Firstly the chemical structure is usually complex, variations in chain length and chain atom arrangement alter the skeletal vibrations and thus change the low temperature heat capacity. An approximation of the vibrations in linear macromolecules is possible by separation of the normal modes into group vibrations and skeletal vibrations<sup>(35)</sup>. Contributions from the former can be calculated from summing the Einstein terms for the isolated chain units, and the remaining skeletal vibrations can be looked on as vibrations of structureless "beads" each with the mass of a chain unit. Only the polymer melt is in true thermodynamic equilibrium whereas a polymer glass is in a supercooled state and its heat capacity, especially in the  $T_g$  region, is critically dependent on thermal



history. A comprehensive review by Wunderlich and Bauer<sup>(34)</sup> describes how carbon backboned polymers may be treated as a chain of structureless "beads" for the purpose of estimating  $C_p$  and a more recent contribution by DiMarzio and Dowell<sup>(36)</sup> allows prediction of the discontinuity in  $C_p$  at  $T_g$  to be estimated from a knowledge of the chemical structure. In this thesis we are mainly concerned with changes in  $C_p$  ( $\Delta C_p$ ) occurring at the glass transition, the magnitude of  $\Delta C_p$  being a measure of the extent of the extra molecular motion occurring at  $T_g$ .

As noted above, when a glassy polymer is heated through  $T_g$  there is an abrupt increase in  $C_p$  as molecular vibrations are supplemented by the conformational changes occurring in the liquid or rubbery state which is achieved above  $T_g$ . This statement should be qualified, however, since it is now widely accepted that limited molecular motions, other than vibrational, can occur in the glassy state<sup>(32,33)</sup>. The contribution of such motions to the glassy state heat capacity can be calculated<sup>(34)</sup> and has recently been experimentally determined for poly(dicyclooctylitaconate)<sup>(37)</sup>. This thesis will present further evidence of detectable heat capacity contributions in the glassy state arising from specific molecular motions.

### 1.5 COPOLYMERS

Since it is often found that homopolymers have widely differing properties which, in combination, would be desirable for a particular application, it might be thought that physical mixtures of various types would be one way of achieving this end.

Unfortunately this is not so, mainly due to the inherent incompatibility of many polymer pairs, and the alternative approach of copolymerization is more likely to be used.

Several important types of copolymer exist.

(I) Random copolymers, these are formed when irregular propagation occurs and the units A and B enter the chain in a random fashion.



The physical properties of random copolymers are often very close to the average of the two corresponding homopolymers.

(II) Alternating copolymers, here equimolar amounts of A and B enter the chain in a regular alternating fashion,

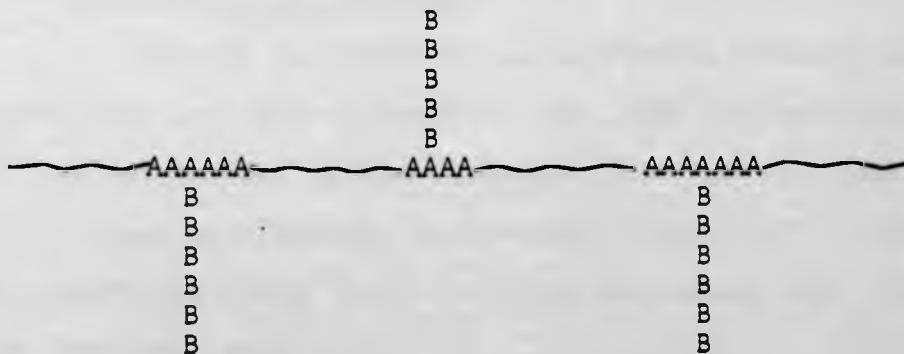


(III) Block copolymers, here long sequences of one monomer unit form a block which is then joined to a sequence of the other monomer,



i.e. an {A}{B} linear block copolymer. Other types of block copolymers exist such as {A}{B}{A} or [{A}{B}]<sub>n</sub>.

(IV) Graft copolymers, are block copolymers in which one monomer forms the backbone and another the side chain,



Types (I) and (II) are most frequently synthesized using free radical initiation, the latter under special conditions, while type (III) is most often synthesized using "living" polymerization techniques<sup>(38)</sup>. Here the propagating species is ionic in nature and remains active even after complete consumption of monomer, a second monomer can then be added to provide the second block.

In principle, a "living" free radical chain end could also be used to construct block copolymers and numerous methods of achieving this have been reported in the literature. However, due to the extreme reactivity of radicals these are experimentally inconvenient, especially for commercial exploitation<sup>(39-41)</sup>. An alternative is to provide a chain end which is stable but can be reactivated under chosen conditions in the presence of the second monomer<sup>(42)</sup>. Details of this method will be discussed later.

Type (IV) copolymers are normally synthesized by providing reactive sites on a preformed backbone which can then be attacked by the second monomer. High energy radiation is usually the preferred technique.

#### 1.6 PROPERTIES OF COPOLYMERS

Random and alternating copolymers normally provide mechanical and other properties which are averaged between those of the two respective homopolymers. This is most ideally reached in the case of alternating copolymers since they can be considered as homopolymers in which the repeat unit consists of the comonomer pair.

Block and Graft copolymers consist of two (or more) types of chain segments which are normally dissimilar in chemical nature. Contacts between segments of different types are enthalpically unfavourable, thus the solid state morphology of block and graft copolymers is dictated by the tendency towards phase separation of the two components. There is a restriction to the extent to which the phases can separate from the inter block chemical linkages so that the mechanical properties of the system are superior to those of a corresponding phase separated blend.

Because of the greater degree of control over the synthesis of block copolymers they have distinct advantages in comparison with graft copolymers and it is possible to achieve material with predictable mechanical, thermal and other properties. The most common type of block copolymer usually consists of "hard" {A} and "rubbery" {B} segments in the sequences {A}{B}{A} or [ $\{A\}\{B\}$ ]<sub>n</sub>. These are phase separated and display multiple thermal transitions, such as melting or glass transitions, characteristic of the respective components. Between the two transitions such materials behave as an elastomer and may be processed above the upper transition as a thermoplastic. The chemistry and properties of block copolymers has been extensively reviewed<sup>(38)</sup>.

### 1.7 IONOMERS

Ionomers are thermoplastic ionic polymers having hydrocarbon backbones with small amounts of pendant carboxylic acid or other ionizable groups which are neutralized either

partially or completely with metal cations. Introduction of the metal in the polymer chain increases the association forces between the carboxyl groups and acts as a so-called ionic cross-link. The presence of these ionic cross-links restricts molecular mobility in the polymer chain thus having a profound effect on the mechanical and thermal properties of the system. The most extensive studies on ionomers have been carried out on polyethylene based ionomers<sup>(43)</sup>, but ionomers based on other systems have also been reported<sup>(19,44)</sup>. Studies of the morphology of ionomers suggest that the ions aggregate into clusters embedded in a hydrocarbon matrix. The precise size and shape of these ionic clusters is still a matter of controversy<sup>(45-47)</sup>.

#### 1.8 SCOPE OF PRESENT WORK

This thesis covers a number of aspects. In Chapter 3 the heat capacities of selected copolymer systems are presented and analysed to provide unequivocal evidence of the presence of two glass transitions in polyitaconates with long ester side chains. Chapter 4 describes how the dual functionality of itaconic acid may be used to obtain mixed esters and investigates some of the properties of the derived poly (mixed esters).

Block copolymer synthesis involving PDMI as the "hard" segment, and studies of the thermomechanical properties of the resulting materials are presented in Chapter 5. Finally, a further series of ionomers based on itaconic acid esters are investigated in Chapter 6.

CHAPTER TWO

EXPERIMENTAL AND INSTRUMENTATION

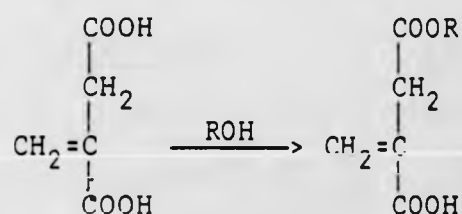
Abbreviated names of itaconic acid based diesters, mono-esters and mixed esters used in this thesis.

Dimethyl itaconate	DMI
Di-n-propyl itaconate	DPrI
Di-n-butyl itaconate	DBI
Di-n-pentyl itaconate	DPI
Di-n-heptyl itaconate	DHpI
Di-n-octyl itaconate	DOI
Di-n-nonyl itaconate	DNI
Monomethyl itaconate	MMI
Mono-n-pentyl itaconate	MPI
Methyl ethyl itaconate	MeEI
Methyl-n-propyl itaconate	MePrI
Methyl-n-butyl itaconate	MeBI
Methyl-n-pentyl itaconate	MePI
Methyl-n-hexyl itaconate	MeHxI
Methyl-n-heptyl itaconate	MeHpI
Methyl-n-octyl itaconate	MeOI
Methyl-n-nonyl itaconate	MeNI
Methyl-n-decyl itaconate	MeDI

## 2.1 PREPARATION AND CHARACTERIZATION OF MONOMERS AND OTHER REAGENTS

(i) Di-n-alkyl itaconates, were prepared by esterification of itaconic acid (Aldrich Chemicals) in benzene using sulphuric acid as catalyst and the appropriate alcohol (BDH, A.R. or Aldrich reagent grades, fractionally distilled before use). A 3-4 mole excess of alcohol was used and refluxing of the mixture was continued for 6-9 hours. After neutralization with a dilute solution of sodium bicarbonate and washing with water, the benzene layer was removed, dried over magnesium sulphate and fractionally vacuum distilled to yield the pure diester. The products were characterized by ir, nmr and refractive index (Table 2.1).

(ii) Mono-n-alkyl itaconates. Monomethyl and mono-n-pentyl itaconate were prepared according to the method of Baker et al.<sup>(10)</sup> by refluxing a mixture of itaconic acid and a 3-4 mole excess of the required alcohol for 20-30 minutes with acetyl chloride as catalyst.



The excess unreacted alcohol was removed rapidly under reduced pressure and the crude monoester was isolated by vacuum distillation or crystallization. The products were characterized by melting point, potentiometric titration of free carboxyl groups (see section 2.3.3), nmr and ir analysis (Table 2.2).



TABLE 2.1

Details of reaction products from preparation of diesters of itaconic acid.

<u>MONOMER</u>	<u>BOILING RANGE</u>		<u>YIELD</u> (mole %)	<u>REFRACTIVE INDEX</u> ( $n_D^{293K}$ )
	temp./ (K)	pressure/(torr)		
DMI	328-330	0.05-0.04	72	1.4418
DPrI	357-361	0.5 -0.4	68	-
DBI	395-401	0.4 -0.1	66	1.4426
DPI	392-398	0.05-0.04	55	1.4435
DHpI	427-429	0.45-0.4	60	1.4477
DOI	449-452	0.1 -0.15	68	1.4493
DNI	481-485	0.7 -0.6	37	1.4511

TABLE 2.2

Details of reaction products from preparation of monoesters of itaconic acid.

<u>MONOMER</u>	<u>BOILING RANGE</u>		<u>YIELD</u> (mole %)	<u>MELTING POINT</u> (K)
	temp./ (K)	pressure/(torr)		
MMI	379-385	0.05-0.04	60	340-343
MPI*	-	-	56	311-313

\* purified by recrystallization

(iii) Methyl-n-alkyl itaconates (mixed esters), were prepared by reaction of monomethyl itaconate with a 2-3 mole excess of the appropriate alcohol using p-toluene sulphonic acid as catalyst. After the required reaction time (Table 2.3) the excess unreacted alcohol was rapidly removed under reduced pressure and the crude product was further purified by up to 3 fractional vacuum distillations at the pressure and temperature ranges shown in Table 2.3. For mixed esters containing a heptyl or higher group, unreacted monomethyl itaconate was found to co-distil with the required product. This was removed by dissolving the monomethyl itaconate contaminated ester in benzene, washing with water until the washings were neutral, drying and finally removing the benzene under vacuum.

Characterization of the mixed esters was carried out by nmr, ir and refractive index measurement (Table 2.3). The structure of the mixed esters prepared are discussed in section 4.1.

(iv) 4,4'-Azobis(4-cyanopentanoyl dichloride), was prepared according to the procedure described by Smith<sup>(48)</sup>. 4,4'-Azobis(4-cyanopentanoic acid) (Aldrich Chemicals, 65% in water) was dried at 298K under vacuum until constant weight. A slurry of 0.1 mole of acid in 300 cm<sup>3</sup> of distilled, sodium dried, benzene was cooled to 273K with constant stirring under a nitrogen blanket and 0.2 mole phosphorus pentachloride (Aldrich Chemicals) was then added slowly over a period of 20-30 minutes. The reaction mixture was allowed to warm up to room temperature until a small amount of insoluble residue was left. After filtration, the solvent was removed under reduced

TABLE 2.3

Details of reaction products from preparation of mixed esters of itaconic acid.

<u>MONOMER</u>	<u>BOILING RANGE</u>		<u>REACTION TIME</u>	<u>YIELD</u>	<u>REFRACTIVE INDEX</u>
	temp./(K)	pressure/(torr)	(h)	(mole %)	( $n_D^{293K}$ )
MeEI	355-356	0.06-0.1	1.5	19	-
MePrI	333-337	0.1 -0.4	2.0	25	1.4395
MeBI	347-351	0.05-0.045	1.5	14	1.4413
MePI	377-395.	0.45-0.5	2.5	12	1.4437
MeHxI	376-384	0.8 -1.1	2.5	19	1.4442
MeHpI	379-393	0.15-0.2	3.0	14	1.4484
MeOI	391-413	0.5 -0.6	4.0	16	-
MeNI	395-415	0.25-0.3	4.0	18	1.4538
MeDI	403-431	0.4 -0.5	4.5	17	1.4451

pressure. The yellow pasty solid remaining was leached with  $3 \times 100 \text{ cm}^3$  portions of a 1:3 mixture of diethyl ether/hexane, (both distilled and sodium dried) to remove phosphorus oxychloride. This crude product was then dissolved in the minimum amount of dried chloroform and reprecipitated in hexane to yield a white solid with melting point of 349-354K. This was further purified by recrystallization from a 1:1 mixture of dried chloroform/diethyl ether<sup>(49)</sup> to give a pure product with melting point 364-367K which was characterized by ir and nmr spectroscopy.

(v) Di-t-butyl-4,4'-Azobis(4-cyanoperoxy-pentanoate).

This sequential initiator was prepared by treating 4,4'-Azobis(4-cyanopentanoyl dichloride) with t-butylhydroperoxide (Fluka, 80% in di-t-butylperoxide) as follows. A mixture of 0.06 mole of pyridine (distilled and dried over molecular sieves) and 0.17 mole of t-butylhydroperoxide in  $150 \text{ cm}^3$  sodium-dried and distilled benzene, cooled to ice temperature under dry nitrogen, and a solution of 0.03 mole diacid chloride in  $100 \text{ cm}^3$  benzene was added dropwise with constant stirring over ca. 30 minutes. The reaction mixture was then allowed to warm up to room temperature while stirring continued. After the required reaction time (12 hours) precipitated pyridinium hydrochloride was separated by filtration and the solvent was removed under reduced pressure at 293K to yield a yellow pasty solid. This was dissolved in a small amount of either chloroform or dichloromethane and reprecipitated in hexane to yield a white solid. After at least three reprecipitations the product was further purified by recrystallization from a 1:1 mixture of chloroform/diethyl ether. A product with a melting point of 374-377K was obtained

after recrystallization and was characterized by ir, nmr and elemental analysis.

## 2.2 POLYMERIZATIONS AND COPOLYMERIZATIONS

(i) Di-n-alkyl itaconates. The homo- and copolymerization of diesters and the homopolymerization of the mixed esters of itaconic acid were carried out in bulk under nitrogen using recrystallized  $\alpha\alpha'$  azobisisobutyronitrile-AIBN (BDH) as initiator (0.5 mole %) at 333K. Polymers were isolated by precipitation from their chloroform solutions using methanol as non-solvent until the ir spectra showed them to be free of C=C absorptions from contaminating monomer. Polymer number average molecular weights ( $\bar{M}_n$ ) were measured in either xylene, toluene or chlorobenzene, at 319K by membrane osmometry (see section 2.3.3). Copolymer compositions were estimated by nmr analysis. All polymers were vacuum dried before use.

(ii) Copolymers of mono- and di-n-pentyl itaconate. Mono-n-pentyl itaconate was homopolymerized and copolymerized with di-n-pentyl itaconate in bulk under nitrogen at 321K using AIBN as initiator. Polymers were isolated by precipitation from their ethanol or chloroform solutions using an appropriate precipitant (see Table 2.4) and  $\bar{M}_n$  values were obtained by membrane osmometry in ethanol at 310K. The copolymer compositions were determined by potentiometric titration (see section 2.3.3). Polymers were vacuum dried at room temperature.

(iii) Polybutadiene macroinitiator. Low molecular weight hydroxyl-terminated polybutadiene (Polysciences) was condensed with 4,4'-Azobis(4-cyanopentanoyl dichloride) as

TABLE 2.4

Details of polymerization conditions for homo- and copolymers of mono- and di-n-pentyl itaconate

<u>SAMPLE No:</u>	<u>Mol.% MPI IN FEED</u>	<u>AIBN (mol %)</u>	<u>REACTION TIME (h)</u>	<u>SOLVENT</u> EtOH+CHCl <sub>3</sub>	<u>PRECIPITANT</u>
1	24	0.30	9.5	EtOH+CHCl <sub>3</sub>	
2	25	0.33	2.6	"	
3	25	0.10	8.5	"	
4	25	0.30	4.5	"	CH <sub>3</sub> OH + H <sub>2</sub> O
5	39	0.29	8.25	"	
6	45	0.28	5.0	"	
7	47	0.28	2.5	EtOH	
8	52	0.27	5.0	"	
9	59	0.26	4.5	"	
10	67	0.08	7.5	"	
11	67	0.27	2.0	"	PET. ETHER
12	71	0.30	8.5	"	
13	84	0.08	2.0	"	
14	84	0.25	-	"	

follows. A 2-3 wt. % benzene solution of 4,4'-Azobis(4-cyanopentanoyl dichloride) was added, with stirring, over a period of 20-30 minutes to a 15-20 wt. % solution of polybutadiene in the presence of triethylamine (TEA) as hydrochloric acid scavenger, at 298K. The reaction mixture was left stirring for a period of at least 20 hours. The polybutadiene macro-initiator - a macroazonitrile PBD(MAZN) - was isolated by precipitation of the filtered reaction mixture into methanol. At least three further reprecipitations from chloroform solutions of the PBD(MAZN) using methanol were carried out to purify the product. Four PBD(MAZN) preparations (see Table 2.5) were carried out after a number of test experiments to find the optimum conditions for the condensation. The products were characterized by vapour pressure osmometry (VPO, see section 2.3.3) and ir spectroscopy.

(iv) Poly(butadiene-b-dimethyl itaconate) samples were prepared by thermal decomposition of the azo linkage of PBD(MAZN)'s in the presence of dimethyl itaconate alone or dimethyl itaconate in benzene solution. A septum sealed flask was charged with the required quantities of PBD(MAZN), dimethyl itaconate and benzene (when used) and flushed with nitrogen for 10-15 minutes. The flask was then placed in a thermostatted bath at 333K or 338K and gently shaken for the required reaction time. Chloroform was then added and the products were isolated by precipitation with methanol. A further three precipitations from chloroform solutions with methanol were carried out before the products were finally dried under vacuum, in the dark, at room temperature. Copolymer compositions were determined by

TABLE 2.5

Details of the preparation of polybutadiene macroinitiators  
(PBD(MAZN)'s)

<u>SAMPLE CODE:</u>	<u>POLYBUTA- DIENE</u>	$\bar{M}_n^*$	<u>ACID CHLORIDE</u>	<u>T.E.A</u>	<u>BENZENE</u>	<u>REACTION TIME</u>
	(mole $\times 10^2$ )	(g mole $^{-1}$ )	(mole $\times 10^2$ )	(cm $^3$ )	(cm $^3$ )	(h)
PBD(MAZN-IV)	1.47	1220	1.05	25	170	23
PBD(MAZN-B)	0.66	3270	0.65	20	300	20
PBD(MAZN-V)	5.34	1220	3.40	65	700	24
PBD(MAZN-VI)	3.44	1220	3.27	30	500	22

\* Number average molecular weights of the polybutadienes  
were determined by VPO as described in section 2.3.3.



nmr analysis and  $\bar{M}_n$  values were measured by membrane osmometry in chlorobenzene solutions at 319K. Details of the polymerization conditions are listed in Tables 2.6-2.9.

(v) Hydrogenated hydroxyl-terminated polybutadiene.

Quantitative hydrogenation of low molecular weight hydroxyl-terminated polybutadiene (polysciences) was carried out by heterogenous catalytic reaction with hydrogen. A 2 wt. % solution of polybutadiene  $\bar{M}_n = 3270 \text{ g mol}^{-1}$  in toluene was mixed with 0.6 g of 10% Pd on charcoal in a high pressure hydrogenator under 60 atmospheres  $\text{H}_2$  at room temperature. After 24 hours the reaction mixture was filtered and the polymer isolated by pouring the reaction mixture into methanol. Complete hydrogenation was verified by ir and nmr spectroscopy.

(vi) Hydrogenated polybutadiene macroinitiator

(HPBD(MAZN)) was prepared from hydrogenated hydroxyl-terminated polybutadiene in the same manner as the unhydrogenated polybutadiene macroinitiator (PBD(MAZN)). The product was characterized by VPO and ir spectroscopy. Details of the preparation of HPBD(MAZN) is shown in Table 2.10.

TABLE 2.10

Details of the preparation of hydrogenated polybutadiene macroinitiator.

<u>SAMPLE CODE:</u>	<u>HYDROGENATED POLYBUTADIENE</u>	<u>ACID CHLORIDE</u>	<u>TEA</u>	<u>BENZENE</u>	<u>REACTION TIME</u>
	(mole x $10^3$ )	(mole x $10^3$ )	( $\text{cm}^3$ )	( $\text{cm}^3$ )	(h)
HPBD(MAZN-C)	3.05	2.92	15	250	25

TABLE 2.6

Polymerization conditions for poly(butadiene-b-dimethyl itaconate) using PBD(MAZN-IV).

<u>SAMPLE CODE</u>	<u>PBD(MAZN-IV)</u> (mole x 10 <sup>4</sup> )	<u>DMI</u> (mole x 10 <sup>2</sup> )	<u>TEMP.</u> (K)	<u>REACTION TIME</u> (h)
P(BD- <u>b</u> -DMI)-I(1)	0.45	6.33	338	19.0
P(BD- <u>b</u> -DMI)-I(2)	0.90	"	"	13.0
P(BD- <u>b</u> -DMI)-I(3)	1.80	"	"	9.5
P(BD- <u>b</u> -DMI)-I(4)	3.60	"	"	5.0
P(BD- <u>b</u> -DMI)-I(5)	9.00	"	"	4.5

TABLE 2.7

Polymerization conditions for poly(butadiene-b-dimethyl itaconate) using PBD(MAZN-B).

<u>SAMPLE CODE</u>	<u>PBD(MAZN-B)</u> (mole x 10 <sup>4</sup> )	<u>DMI</u> (mole x 10 <sup>2</sup> )	<u>BENZENE</u> (cm <sup>3</sup> )	<u>TEMP.</u> (K)	<u>REACTION TIME</u> (h)
P(BD- <u>b</u> -DMI)-II(1)	1.57	3.164	5	338	5.3
P(BD- <u>b</u> -DMI)-II(2)	2.01	"	"	"	4.5
P(BD- <u>b</u> -DMI)-II(3)	2.68	"	"	"	4.0
P(BD- <u>b</u> -DMI)-II(4)	3.92	"	"	"	4.0

TABLE 2.8

Polymerization conditions for poly(butadiene-b-dimethyl itaconate) using PBD(MAZN-V)

<u>SAMPLE CODE</u>	<u>PBD(MAZN-V)</u> (mole x 10 <sup>4</sup> )	<u>DMI</u> (mole x 10 <sup>2</sup> )	<u>TEMP.</u> (K)	<u>REACTION TIME</u> (h)
P(BD- <u>b</u> -DMI)-III(1)	5.58	6.33	333	5.0
P(BD- <u>b</u> -DMI)-III(2)	8.72	"	"	5.5
P(BD- <u>b</u> -DMI)-III(3)	12.10	"	"	6.0
P(BD- <u>b</u> -DMI)-III(4)	10.85	"	338*	16.5

\* 5 cm<sup>3</sup> benzene was used.

TABLE 2.9

Polymerization conditions for poly(butadiene-b-dimethyl itaconate) using PBD(MAZN-VI)

<u>SAMPLE CODE</u>	<u>PBD(MAZN-VI)</u> (mole x 10 <sup>4</sup> )	<u>DMI</u> (mole x 10 <sup>2</sup> )	<u>TEMP.</u> (K)	<u>REACTION TIME</u> (h)
P(BD- <u>b</u> -DMI)-IV(1)	1.77	6.33	338	6.5
P(BD- <u>b</u> -DMI)-IV(2)	3.54	"	"	6.3
P(BD- <u>b</u> -DMI)-IV(3)	5.31	"	"	5.5
P(BD- <u>b</u> -DMI)-IV(4)	8.85	"	"	4.3
P(BD- <u>b</u> -DMI)-IV(5)	10.62	"	"	4.0

(vii) Poly(hydrogenated butadiene-*b*-dimethyl itaconate). These samples were prepared by the same method used for the poly(butadiene-*b*-dimethyl itaconate) samples. Copolymer composition was estimated by nmr analysis and  $\bar{M}_n$  values determined by membrane osmometry in chlorobenzene at 319K. Details of the polymerization conditions are shown in Table 2.11.

(viii) Polyisoprene macroinitiator (PI(M)) samples were prepared by standard emulsion techniques using di-*t*-butyl-4,4'-Azobis(4-cyanoperoxypentanoate) sequential initiator and sodium lauryl sulphate as emulsifier. Isoprene (Aldrich Chemicals, gold lable) was distilled prior to polymerization. Polyisoprene macroinitiators were prepared at 328 and/or 333K using the azo linkages as the initiating site, or at 307K where decomposition of the perester bonds can be activated using tetraethylenepentamine (TEPA) as reducing agent. Specially designed 100-150 cm<sup>3</sup> "quickfit" flasks were charged with required quantities of monomer, initiator and a 5% wt/vol aqueous solution of sodium lauryl sulphate and sealed under vacuum after 3 freeze-thaw cycles. The flasks were then placed in a thermostat bath at the desired temperature and shaken at a rate which ensured that a stable emulsion was formed. After the required reaction time the polymer was isolated by pouring the reaction mixture into methanol. Further precipitations were carried out by dissolving the product in chloroform and precipitating with methanol before the polymer was finally dried under vacuum in the dark at 293K.

Polyisoprene macroinitiators were characterized by ir and nmr spectroscopy and  $\bar{M}_n$  values were determined by

TABLE 2.11

Polymerization conditions for poly(hydrogenated butadiene-b-dimethyl itaconate) using HPBD(MAZN-C)

<u>SAMPLE CODE:</u>	<u>HPBD(MAZN-C)</u> (mole x 10 <sup>4</sup> )	<u>DMI</u> (mole x 10 <sup>2</sup> )	<u>BENZENE</u> (cm <sup>3</sup> )	<u>TEMP.</u> (K)	<u>REACTION TIME</u> (h)
P(HBD- <u>b</u> -DMI)-V(1)	1.042	2.40	3	343	24
P(HBD- <u>b</u> -DMI)-V(2)	1.127	1.00	"	"	"
P(HBD- <u>b</u> -DMI)-V(3)	1.127	0.82	"	"	21
P(HBD- <u>b</u> -DMI)-V(4)	1.144	0.41	2	"	"
P(HBD- <u>b</u> -DMI)-V(5)	0.720	0.64	"	328	23

membrane osmometry in either toluene or chlorobenzene solutions at 319K. The polymerization conditions are shown in Table 2.12.

(x) Poly(dimethyl itaconate) macroinitiators (PDMI(M)), were prepared either in bulk, solution or by the emulsion technique employed for polyisoprene macroinitiator, using di-*t*-butyl-4,4'-Azobis(4-cyanoperoxy-pentanoate) as sequential initiator. After the required reaction time, polymers were isolated by precipitation with methanol and further precipitations of their chloroform solution with methanol were carried out to purify them. The polymers were vacuum dried prior to further use. Characterization of poly(dimethyl itaconate) macroinitiators was carried out by ir and nmr spectroscopy and  $\bar{M}_n$  values were determined either by membrane osmometry in chlorobenzene solutions at 319K or by viscometry (see section 2.3.3) in benzene at 298K. Details of the polymerization conditions for poly(dimethyl itaconate) macroinitiators are listed in Table 2.13.

(xi) Poly(isoprene-*b*-dimethyl itaconate), samples were prepared in several ways.

(a) Polyisoprene macroinitiator (PI(M)) with perester end groups was decomposed in benzene solution under nitrogen atmosphere in the presence of dimethyl itaconate (DMI) at 307K. Tetraethylenepentamine (TEPA) was used as reducing agent to activate the perester linkages in the macroinitiator.

(b) Poly(dimethyl itaconate) macroinitiator (PDMI(M)) dissolved in benzene, was decomposed in the presence of isoprene

TABLE 2.12

Polymerization conditions for polyisoprene macroinitiators  
(PI(M)'s)

<u>SAMPLE CODE:</u>	<u>ISOPRENE</u> (mole x 10 <sup>2</sup> )	<u>INITIATOR</u> (mole %)	<u>EMULSIFIER*</u> (cm <sup>3</sup> )	<u>TEMP.</u> (K)	<u>REACTION TIME</u> (h)
PI(M-I)	3.81	1.0	8.0	328	24
PI(M-II)	9.0	0.7	24	333	48
PI(M-III)	9.3	0.65	24	"	60
PI(M-IV)	9.0	1.0	20	308 <sup>**</sup>	185

\* Emulsifier solution volume

\*\* Initiator activated by addition of  $1.8 \times 10^{-3}$  mol TEPA.

TABLE 2.13

Polymerization conditions for poly(dimethyl itaconate)  
macroinitiators (PDMI(M)'s)

<u>SAMPLE CODE:</u>	<u>DMI</u> (mole x 10 <sup>2</sup> )	<u>INITIATOR</u> (mole %)	<u>TEPA</u> (mole x 10 <sup>3</sup> )	<u>METHOD</u>	<u>TEMP.</u> (K)	<u>REACTION TIME</u> (h)
PDMI(M-I)	1.6	1.0	-	BULK	333	16
PDMI(M-II)	3.8	3.0	-	"	"	20
PDMI(M-III)	2.5	4.0	-	"	"	4.5
PDMI(M-IV)	3.1	1.0	0.32	SOLUTION*	301	168
PDMI(M-V)	3.8	2.0	0.76	BULK	310	120
PDMI(M-VI)	14	2.0	5.7	EMULSION	"	26

\* 3 cm<sup>3</sup> benzene used.



monomer at 307K, using TEPA as activator,

and (c) at 333K using an emulsion system sealed under vacuum.

The products were isolated by precipitation in methanol and were purified by further reprecipitation from their chloroform solutions with methanol. Characterization of the products was carried out by nmr and ir spectroscopy and  $\bar{M}_n$  values were determined by membrane osmometry at 319K in chlorobenzene. Polymerization conditions are shown in Tables 2.14-2.22.

## 2.3 POLYMER CHARACTERIZATION

### 2.3.1 THERMAL METHODS

(i) Heat capacities (Cp) were measured as a function of temperature for all homo- and copolymers of itaconic acid based esters and for the block copolymers prepared in this study by the differential scanning calorimetry (DSC) technique, using a Perkin-Elmer model DSC-2 equipped with a low temperature mode accessory and capable of measurements in the temperature range 100-1000K<sup>(50)</sup>. Basically the instrument records the differential power required to maintain a zero temperature difference between the sample and an inert reference as the temperature of both is changed at a linear programmed rate. A schematic diagram of the DSC system is shown in Figure 2.1.

A signal, proportional to the difference between the heat input to the sample and that to the reference,  $dH/dt$ , is fed into a recorder. In practice, this recorder is also used to register the average temperature of the sample and reference.

monomer at 307K, using TEPA as activator,

and (c) at 333K using an emulsion system sealed under vacuum.

The products were isolated by precipitation in methanol and were purified by further reprecipitation from their chloroform solutions with methanol. Characterization of the products was carried out by nmr and ir spectroscopy and  $\bar{M}_n$  values were determined by membrane osmometry at 319K in chlorobenzene. Polymerization conditions are shown in Tables 2.14-2.22.

## 2.3 POLYMER CHARACTERIZATION

### 2.3.1 THERMAL METHODS

(i) Heat capacities (Cp) were measured as a function of temperature for all homo- and copolymers of itaconic acid based esters and for the block copolymers prepared in this study by the differential scanning calorimetry (DSC) technique, using a Perkin-Elmer model DSC-2 equipped with a low temperature mode accessory and capable of measurements in the temperature range 100-1000K<sup>(50)</sup>. Basically the instrument records the differential power required to maintain a zero temperature difference between the sample and an inert reference as the temperature of both is changed at a linear programmed rate. A schematic diagram of the DSC system is shown in Figure 2.1.

A signal, proportional to the difference between the heat input to the sample and that to the reference,  $dH/dt$ , is fed into a recorder. In practice, this recorder is also used to register the average temperature of the sample and reference.

TABLE 2.14

Polymerization conditions for poly(isoprene-b-dimethyl itaconate) using (PI(M-I)).

<u>SAMPLE CODE:</u>	<u>PI(M-I)</u> (mole x 10 <sup>5</sup> )	<u>DMI</u> (mole x 10 <sup>3</sup> )	<u>TEPA</u> (mole x 10 <sup>5</sup> )	<u>BENZENE</u> (cm <sup>3</sup> )	<u>REACTION TIME</u> (h)
P(I- <u>b</u> -DMI)-I	1.78	3.54	3.57	4	95

TABLE 2.15

Polymerization conditions for poly(isoprene-b-dimethyl itaconate) using (PI(M-II)).

<u>SAMPLE CODE:</u>	<u>PI(M-II)</u> (mole x 10 <sup>5</sup> )	<u>DMI</u> (mole x 10 <sup>3</sup> )	<u>TEPA</u> (mole x 10 <sup>5</sup> )	<u>BENZENE</u> (cm <sup>3</sup> )	<u>REACTION TIME</u> (h)
P(I- <u>b</u> -DMI)-II(1)	1.92	9.5	3.84	8.0	144
P(I- <u>b</u> -DMI)-II(2)	"	9.5	"	14	100
P(I- <u>b</u> -DMI)-II(3)	"	12.65	"	10	144
P(I- <u>b</u> -DMI)-II(4)	"	19.0	"	16	144
P(I- <u>b</u> -DMI)-II(5)	"	12.65	"	3.0	17
P(I- <u>b</u> -DMI)-II(6)	1.06	15.82	12.2	4.5	144

TABLE 2.16

Polymerization conditions for poly(isoprene-b-dimethyl itaconate) using (PI(M-III)).

<u>SAMPLE CODE:</u>	<u>PI(M-III)</u> (mole x 10 <sup>5</sup> )	<u>DMI</u> (mole x 10 <sup>2</sup> )	<u>TEPA</u> (mole x 10 <sup>5</sup> )	<u>BENZENE</u> (cm <sup>3</sup> )	<u>REACTION TIME</u> (h)
P(I- <u>b</u> -DMI)-III(1)	1.4	3.80	2.8	7.0	159
P(I- <u>b</u> -DMI)-III(2)	"	6.33	"	15	"
P(I- <u>b</u> -DMI)-III(3)	"	"	"	18	"
P(I- <u>b</u> -DMI)-III(4)	"	"	1.4	17	"
P(I- <u>b</u> -DMI)-III(5)	"	3.16	2.0	15	"
P(I- <u>b</u> -DMI)-III(6)	"	"	11.2	15	"

TABLE 2.17

Polymerization conditions for poly(dimethyl itaconate-b-isoprene) using (PDMI(M-I)).

<u>SAMPLE CODE:</u>	<u>PDMI(M-I)</u> (mole x 10 <sup>6</sup> )	<u>ISOPRENE</u> (mole x 10 <sup>2</sup> )	<u>TEPA</u> (mole x 10 <sup>5</sup> )	<u>BENZENE</u> (cm <sup>3</sup> )	<u>TEMP.</u> (K)	<u>REACTION TIME</u> (h)
P(DMI- <u>b</u> -I)-I	2.93	9.0	1.00	10	307	282

TABLE 2.18

Polymerization conditions for poly(dimethyl itaconate-b-isoprene) using (PDMI(M-II)).

<u>SAMPLE CODE:</u>	<u>PDMI(M-II)</u> (mole x 10 <sup>6</sup> )	<u>ISOPRENE</u> (mole x 10 <sup>2</sup> )	<u>TEPA</u> (mole x 10 <sup>5</sup> )	<u>BENZENE</u> (cm <sup>3</sup> )	<u>TEMP.</u> (K)	<u>REACTION TIME</u> (h)
P(DMI- <u>b</u> -I)-II(1)	10.64	10.0	2.13	10	307	165
P(DMI- <u>b</u> -I)-II(2)	5.32	6.35	1.06	"	"	100

TABLE 2.19

Polymerization conditions for poly(dimethyl itaconate-b-isoprene) using (PDMI(M-III)).

<u>SAMPLE CODE:</u>	<u>PDMI(M-III)</u> (mole x 10 <sup>6</sup> )	<u>ISOPRENE</u> (mole x 10 <sup>2</sup> )	<u>TEPA</u> (mole x 10 <sup>5</sup> )	<u>BENZENE</u> (cm <sup>3</sup> )	<u>TEMP.</u> (K)	<u>REACTION TIME</u> (h)
P(DMI- <u>b</u> -I)-III	8.26	5.0	1.65	7	307	168

TABLE 2.20

Polymerization conditions for poly(dimethyl itaconate-b-isoprene) using (PDMI(M-IV)).

<u>SAMPLE CODE:</u>	<u>PDMI(M-IV)</u> (mole x 10 <sup>6</sup> )	<u>ISOPRENE</u> (mole x 10 <sup>2</sup> )	<u>EMULSIFIER</u> (cm <sup>3</sup> )	<u>BENZENE</u> (cm <sup>3</sup> )	<u>TEMP.</u> (K)	<u>REACTION TIME</u> (h)
P(DMI- <u>b</u> -I)-IV	1.41	0.74	5.5	4	333	66

TABLE 2.21

Polymerization conditions for poly(dimethyl itaconate-b-isoprene) using (PDMI(M-V)).

<u>SAMPLE CODE:</u>	<u>PDMI(M-V)</u> (mole x 10 <sup>6</sup> )	<u>ISOPRENE</u> (mole x 10 <sup>2</sup> )	<u>EMULSIFIER</u> (cm <sup>3</sup> )	<u>BENZENE</u> (cm <sup>3</sup> )	<u>TEMP.</u> (K)	<u>REACTION TIME</u> (h)
P(DMI- <u>b</u> -I)-V	6.0	10.5	25	6	333	24

TABLE 2.22

Polymerization conditions for poly(dimethyl itaconate-b-isoprene) using (PDMI(M-VI)).

<u>SAMPLE CODE:</u>	<u>PDMI(M-VI)</u> (mole x 10 <sup>6</sup> )	<u>ISOPRENE</u> (mole x 10 <sup>2</sup> )	<u>EMULSIFIER</u> (cm <sup>3</sup> )	<u>BENZENE</u> (cm <sup>3</sup> )	<u>TEMP.</u> (K)	<u>REACTION TIME</u> (h)
P(DMI- <u>b</u> -I)-VI	29.17	17.6	35	25	333	26

Details of the theory and design of differential scanning calorimeters have been described by Watson et al.<sup>(51)</sup> and by O'Neill<sup>(52)</sup>. Some of the more important points are the following.

When a sample material is subjected to a linear temperature increase, the rate of heat flow into the sample is proportional to its instantaneous specific heat. By measuring this rate of heat flow as a function of temperature and comparing it with that for a standard material under the same conditions, one can obtain the specific heat,  $C_p$ , as a function of temperature. The procedure has been described in detail by O'Neill<sup>(53)</sup> and other workers<sup>(54,55)</sup>. O'Neill claims a precision of 0.3% or better in specific heat determinations. Wunderlich<sup>(35)</sup> quotes an accuracy of  $\pm 0.5\%$  for the scanning technique in comparison with conventional adiabatic calorimetry, however at subambient temperatures the error limits are larger (3% at 100K).

The procedure for measurement of the heat capacity by DSC is described as follows. Empty aluminium pans are placed in the sample and reference holders. An isothermal base line is recorded at the lowest temperature chosen and the temperature is then programmed to increase over the required range, at an appropriate rate. An isothermal base line is then recorded at the higher temperature as indicated in Figure 2.2. The two isothermal base lines are used to interpolate a base line over the scanning section as shown in the same figure. The above procedure is repeated with a known mass of sample in the sample pan and a trace of  $dH/dt$  against time is recorded. There is a recorder deflection due to the absorption of heat by the sample

and thus

$$dH/dt = mC_p \cdot dT_p/dt \quad (2.1)$$

where  $m$  is the mass of the sample and  $dT_p/dt$  is the programmed rate of temperature increase.

This equation could be used to obtain values of  $C_p$  directly, but any errors in recorder read out of  $dH/dt$ , and in the programming rate  $dT_p/dt$  would reduce the accuracy. To minimize these errors the procedure is repeated with a known mass of sapphire in the sample pan, the specific heat of which is well established<sup>(56)</sup>, and a new trace is recorded. Thus two ordinate deflections  $D_{\text{sample}}$  and  $D_{\text{sapphire}}$  at any chosen temperature are obtained as shown in Figure 2.2 and yield the ratio of the  $C_p$  values of sample and sapphire. The value of  $C_p$  for the sample can then be evaluated from the following equation.

$$C_{p \text{ sample}} = \frac{m_{\text{sapphire}}}{m_{\text{sample}}} \times \frac{D_{\text{sample}}}{D_{\text{sapphire}}} \times C_{p \text{ sapphire}} \quad (2.2)$$

Evaluation of  $C_{p \text{ sample}}$  at convenient temperature intervals in the chosen scan range yields the  $C_p$  versus temperature ( $T$ ) behaviour for the sample under study.

In this work polymer samples in the range of 15-25 mg were used at a scan rate of  $20 \text{ K min}^{-1}$ . The temperature readout of the instrument was calibrated with pure metal standards (Hg, Ga, In and Pb) to  $\pm 0.2\text{K}$ . In experiments involving sub-ambient scans dry helium was used as purge gas, above ambient measurements were performed in an atmosphere of dry nitrogen. In all cases samples were first heated to the upper limit of the scan and held there for ca. 5 minutes before quenching at  $320 \text{ K min}^{-1}$  to the lower starting limit.

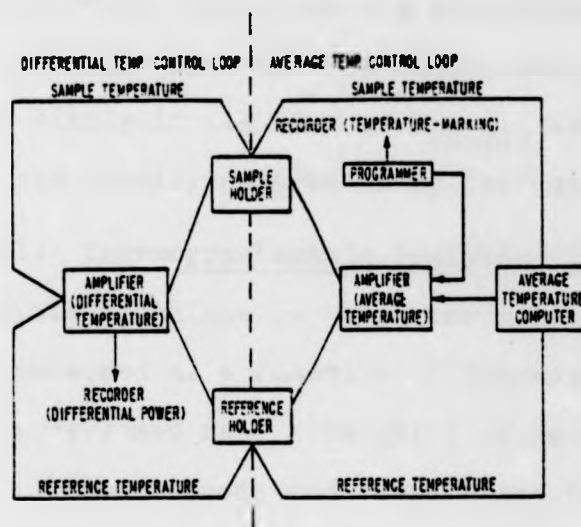


Figure 2.1: Schematic diagram of DSC-2 differential scanning calorimeter.

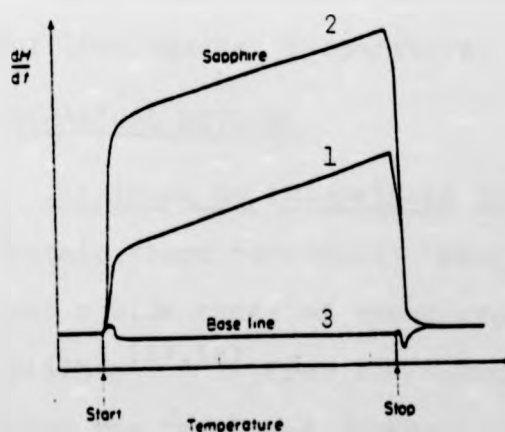


Figure 2.2: Schematic diagram of DSC traces for sample (1), standard (2-sapphire) and empty pans (3-baseline).



In certain cases, where a knowledge of the absolute value of  $C_p$  as a function of temperature was not required, data is displayed simply in the form of  $D_{\text{sample}}$  versus  $T$ . Features, such as  $T_g$ , are readily determined by this method.

(ii) Thermogravimetric analysis (TGA) is a dynamic thermal analysis technique in which the weight loss of a material is measured as a function of increasing temperature at a linear programmed rate. Weight loss can also be measured as function of time at constant temperature if required. The technique was applied to all polymer samples synthesized in this work in order to evaluate their thermal stability and degradation temperatures.

A Perkin-Elmer Thermogravimetric System model TGS-2 connected to a Perkin-Elmer DSC-2 temperature programmer was used in this study. Thermal degradation of all polymer samples was carried out under a nitrogen atmosphere at heating rates of 20 or/and  $40 \text{ K min}^{-1}$ . The results are displayed as a graph of % sample weight loss against temperature.

### 2.3.2 MECHANICAL METHODS

(i) Torsional braid analysis (TBA) is a technique whereby the dynamic thermomechanical behaviour of polymers can be measured over a wide range of temperature. TBA was originally developed by Gillham<sup>(57,58)</sup> from the conventional torsional pendulum. Unlike the torsional pendulum, TBA measurements can be made on relatively small (ca. 100 mg) amounts of material which is impregnated into a multifilament glass-braid acting as a support for mechanically weak materials. This permits the study of thermoplastic materials to be carried out above their

melting or softening points. Perhaps the major disadvantage of the TBA technique is that it cannot provide absolute measurements (for example, a polymer's mechanical modulus) since the specimen under test is a composite and not a pure polymer of known dimensions. Another restriction in the torsional braid method is due to the fact that the frequency varies with changes in temperature, owing to the changing of the composite's stiffness. This, however, applies to most conventional torsion pendulums.

A torsional braid analyser model 100-B1, manufactured by Chemical Instruments Corporation of New York was used in this work (see Figure 2.3). This instrument is based on Gillham's original apparatus with some minor modification being carried out in this laboratory. The nominal frequency of this instrument is approximately 1 Hz, and it may be operated over the temperature range 83K-773K.

Samples were prepared for measurement by impregnating a glass-fibre braid with polymer. This was achieved by soaking the braid in a polymer solution (10-15% wt./vol.) for about 1 hour. The excess solvent was evaporated from the sample firstly by suspending the braids in the open laboratory for about 2 hours under slight tension ( $\sim 35$  g) and then were either drying under vacuum or heating to a temperature above their  $T_g$  inside the TBA apparatus under a nitrogen purge. The glass braids used in this work were either supplied by the manufacturer or they were fabricated in the laboratory from material supplied by James Stroud Insulation, Preston, England. This latter material is a woven glass-fibre which has an unwanted surface coating which can interfere with the measurement. Cleaning of

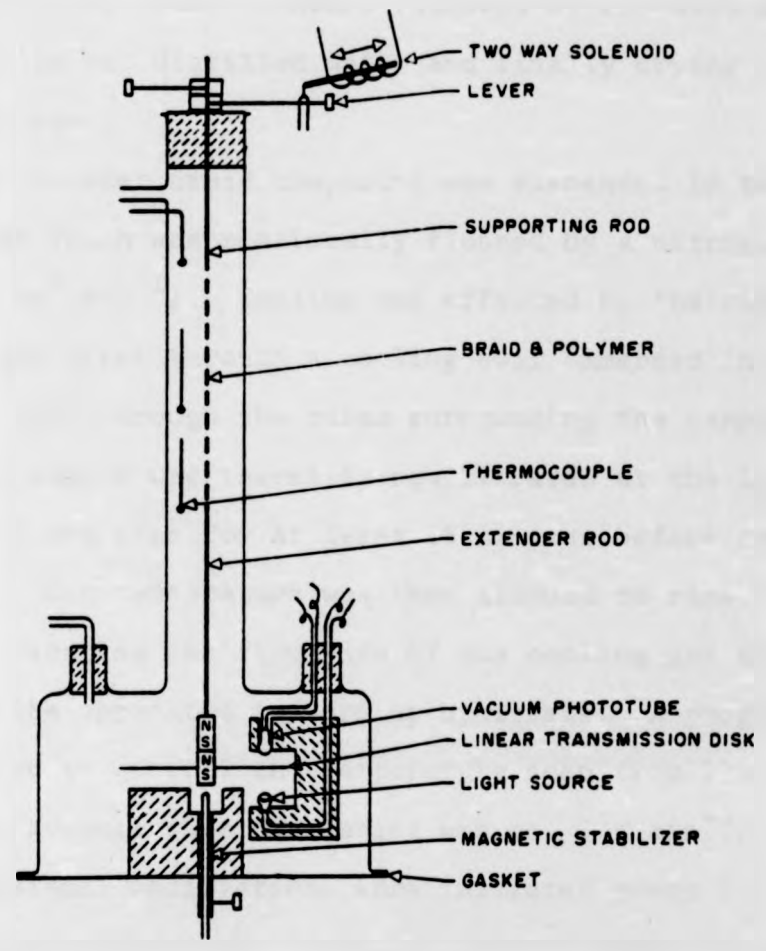


Figure 2.3:

Schematic diagram of torsional braid analyser (TBA).

Temperature of the braid/polymer composite was measured at the centre thermocouple position.

this coating material was easily achieved by immersion in chromic acid for at least 48 hours followed by repeated washing of the braids in hot distilled water and finally drying at  $\sim 373\text{K}$  before use.

The polymer braid composite was suspended in the sample chamber which was continually flushed by a nitrogen stream ( $\sim 20 \text{ cm}^3 \text{ min}^{-1}$ ). Cooling was effected by the circulation of nitrogen gas first through a cooling coil immersed in liquid nitrogen and then through the tubes surrounding the sample chamber. The sample was thermally equilibrated at the lowest temperature of the scan for at least 15 minutes before commencing measurements. The temperature was then allowed to rise slowly by gradually reducing the flow rate of the cooling gas to zero and allowing the apparatus to warm up by itself. A programmed heater was used to control the temperature scan from  $273\text{K}$  upwards. The average rate of heating was ca.  $2 \text{ K min}^{-1}$ .

Torsional oscillations were initiated every 2.5 minutes throughout the scan. A typical set of damped sinusoidal oscillations is shown in Figure 2.4. From these the relative damping index ( $-\log(1/n)$ ) was obtained, where  $n$  is the number of oscillation between two arbitrary fixed amplitudes. This is directly proportional to the logarithmic decrement<sup>(28)</sup> and describes the damping characteristics of the sample. Approximately 100-150 data points were collected to construct each thermogram. These are plotted as  $-\log(1/n)$  against temperature for all the samples studied to give a TBA thermogram.

The relative rigidity ( $1/p^2$ ) where  $p$  is the period of the sinusoidal oscillation was also evaluated as a function of temperature in some cases. ( $1/p^2$ ) is proportional to the

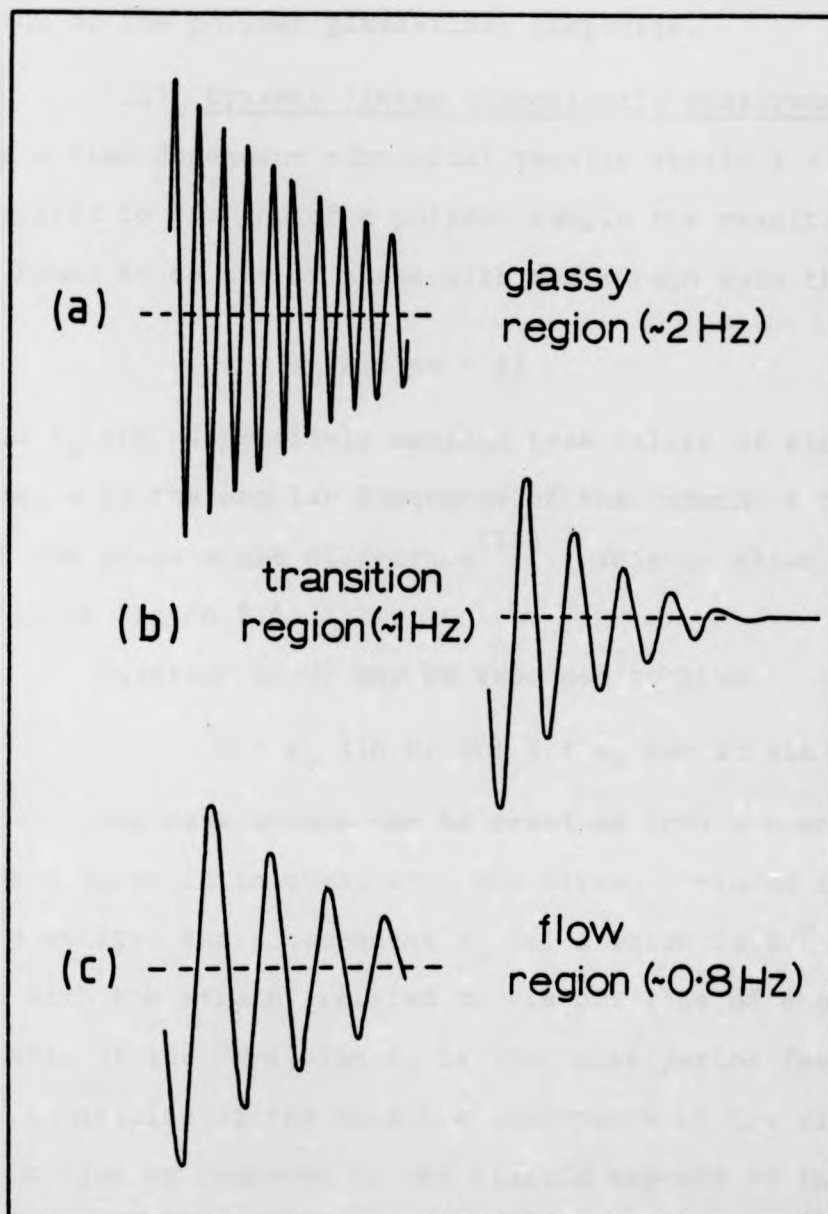


Figure 2.4: Characteristic output of the TBA instrument:

- (a) glassy state,  
(b) transition region,  
and (c) flow region.

modulus of the polymer/glass-fibre composite.

(ii) Dynamic linear viscoelastic measurements,

where a time dependent sinusoidal tensile strain  $\epsilon = \epsilon_0 \sin \omega t$  is applied to one end of a polymer sample the resulting stress  $\sigma$  is found to be out of phase with the strain such that

$$\sigma = \sigma_0 \sin(\omega t + \delta) \quad (2.3)$$

$\epsilon_0$  and  $\sigma_0$  are respectively maximum peak values of strain and stress,  $\omega$  is the angular frequency of the strain,  $t$  the time and  $\delta$  the phase angle difference<sup>(59)</sup>. This is shown diagrammatically in Figure 2.5.

Equation (2.3) may be expanded to give

$$\sigma = \sigma_0 \sin \omega t \cos \delta + \sigma_0 \cos \omega t \sin \delta \quad (2.4)$$

The peak stress can be resolved into a component  $\sigma_0 \cos \delta$  which is in phase with the strain (related to the stored energy) and a component  $\sigma_0 \sin \delta$  which is  $90^\circ$  out of phase with the strain (related to viscous loss of energy). The ratio of the two,  $\tan \delta$ , is the "dissipation factor" which is an indication of the relative importance of the viscous contribution as compared to the elastic aspects of the material's behaviour.

Two elastic moduli can be defined<sup>(59)</sup>

$$E' = (\sigma_0/\gamma_0) \cos \delta \quad (2.5)$$

and

$$E'' = (\sigma_0/\gamma_0) \sin \delta \quad (2.6)$$

whose ratio is also the dissipation factor. The complex elastic

modulus can then be expressed by

$$E^* = E' + iE'' \quad (2.7)$$

the absolute value of which is

$$E^* = (E'^2 + E''^2)^{\frac{1}{2}} \quad (2.8)$$

The complex elastic modulus is a function which completely describes the dynamic mechanical behaviour of the material for small tensile strains.

A Rheovibron model DDV IIC direct reading dynamic viscoelastometer (see Figure 2.6) manufactured by Toyo Baldwin Co. Ltd., Japan, was used in this work.

Polymer samples, in the form of thin strips, either melt pressed or cast from a solvent, were mounted in the instrument which was then brought to the starting temperature of the measurement. After heating had been initiated, readings of the dynamic force and  $\tan \delta$  were taken at approximately 2 minute intervals. The dynamic force (D) is an instrumental parameter which is related to the modulus of the test sample by the equation

$$E^* = (2l/F \times D \times A) \times 10^8 \quad (2.9)$$

where  $l$  is the length of the sample in cm.,  $A$  is the sample cross section area in  $\text{cm}^2$  (measured by micrometer) and  $F$  is the amplitude factor which can be calculated from the instrumental settings. Equation (2.9) gives the values of  $E^*$  in  $\text{Nm}^{-2}$ .

The values of  $\tan \delta$  and/or  $E^*$  were plotted as a function of temperature using log-linear graph paper.

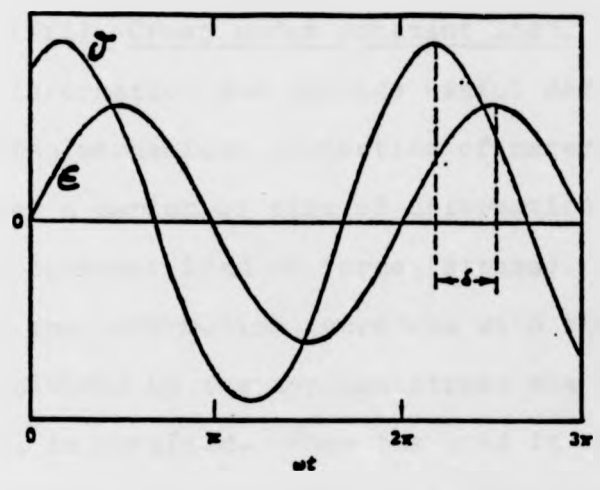


Figure 2.5: Stress and strain as a function of time in the application of a sinusoidal strain to a viscoelastic sample.

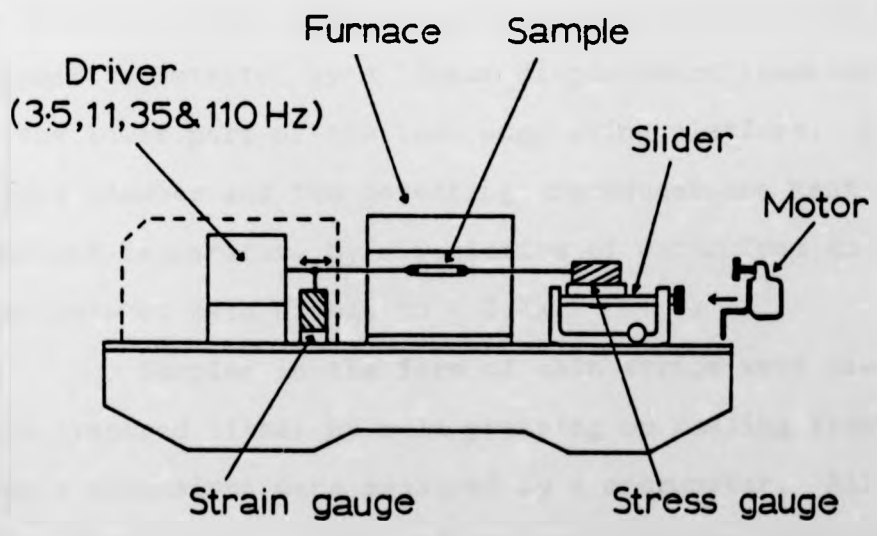


Figure 2.6: Schematic diagram of Rheovibron DDV-IIC



(iii) Creep under constant load. Creep tests give practical information and provide useful data pertinent to the theory of the mechanical properties of materials. Measurement is made over a period of time of deformation (strain) brought about by a constant load or force (stress). In a creep experiment the deformation increases with time and when the strain is divided by the applied stress the quantity  $J$ , the compliance, is obtained. When the load is removed from a creep specimen after some time there is a tendency for the specimen to return to its original length and a recovery curve may then be obtained if the deformation is plotted as a function of time after the removal of the load.

The creep apparatus which was used in this work was designed and built in the laboratory (see Figure 2.7). The instrument can be used to test relatively tough thermoplastics as well as rubbers. The increase in the length of the sample polymer is detected by a linear displacement transducer located in the lower part of the load supporting platform. Both the sample chamber and the detecting transducer are kept at a constant temperature by circulation of water from an external thermostated bath stable to  $\pm 0.1\text{K}$ .

Samples in the form of thin strips were used. These were prepared either by melt pressing or casting from a solution. Sample dimensions were measured by a micrometer. All experiments were carried out at 298K and ambient relative humidity. The output of the transducer is proportional to sample elongation  $(l-l_0/l_0)$  and is displayed on a chart recorder as a function of time.

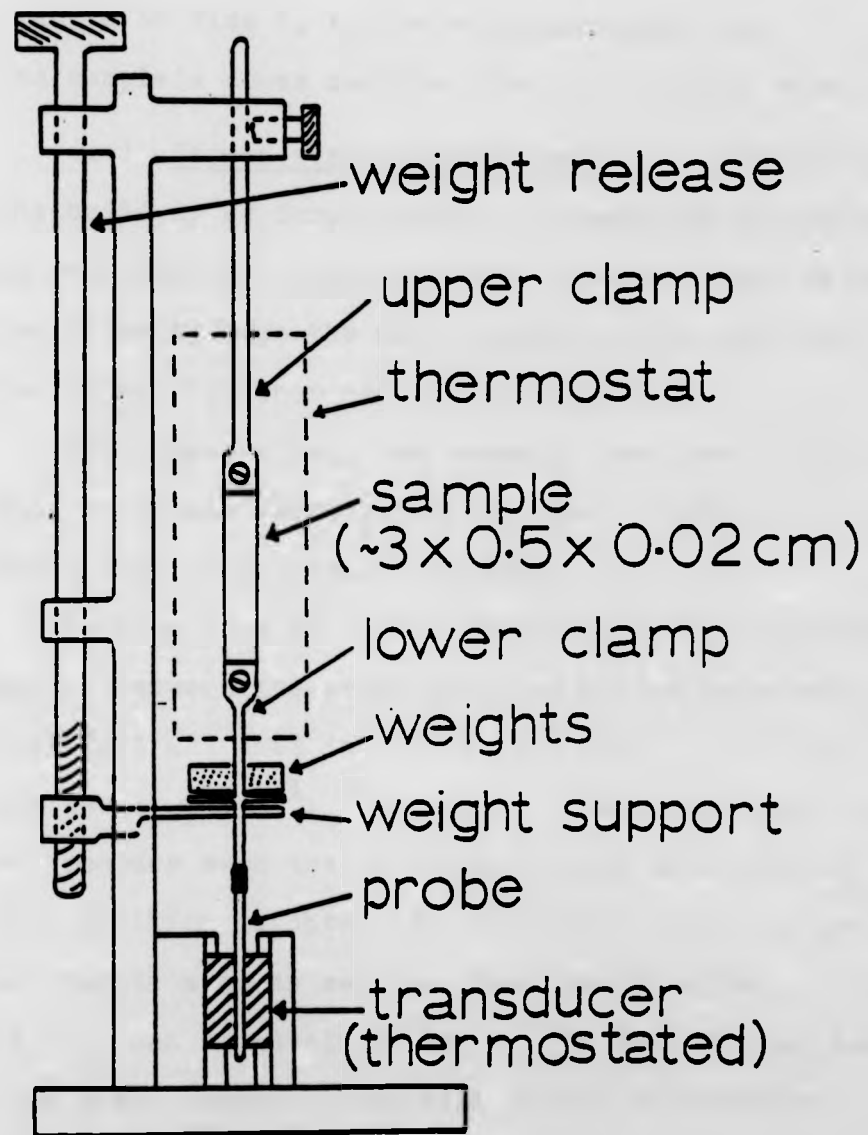


Figure 2.7: Schematic diagram of Creep apparatus.

The quantity  $J(t) = \frac{l(t) - l_0}{l_0} / \sigma$  as a function of  $\log(t)$  was plotted on a log-linear graph paper.  $l(t)$  is sample length at time  $t$ ,  $l_0$  the original length and  $\sigma = (\text{load/sample's cross section area})$  the applied stress.

(iv) Stress-strain measurements. In stress-strain tests the build-up of force (stress) is measured as the sample is being deformed at a constant rate. Stress-strain measurements have traditionally been the most popular and widely used technique among all other mechanical tests.

The stress-strain measurements were carried out at 293K using a tensile testing machine (Model T5003, J. J. Lloyd Instruments Ltd., Southampton, England).

Polymer samples in the form of solvent cast strips were mounted between the stationary and moving cross head grips. A 50N load cell was used in the tension mode and the rate of extension was  $1 \text{ cm min}^{-1}$ . The output of the instrument was fed to a X-Y recorder such that a trace of load cell reading versus cross head position is obtained. From this a plot of stress ( $\sigma = \text{load/sample's cross section area}$ ) versus strain ( $\epsilon = l - l_0 / l_0$ ) can be obtained where  $l_0$  is the original sample length and  $l$  the length at any time during deformation.

### 2.3.3 SOLUTION METHODS

(i) Membrane osmometry. Measurements of the osmotic pressure ( $\pi$ ) of a polymer solution enables the number average molecular weight ( $\bar{M}_n$ ) to be determined from the relation<sup>(60)</sup>

$$(\pi/c)_{c \rightarrow 0} = RT/\bar{M}_n \quad (2.10)$$

where  $(\pi/c)_{c \rightarrow 0}$  is the limiting value at zero concentration ( $c$ )

of the osmotic pressure divided by the concentration. The gas constant is  $R$  and  $T$  is the temperature in Kelvins. Only under special conditions, when the polymer is dissolved in a pseudo-ideal solvent, e.g. a  $\theta$  solvent, is  $(\pi/c)$  independent of concentration. Experimentally, a series of concentrations is studied and the results treated according to a virial expansion, the most familiar of which is,

$$(\pi/c) = RT(\bar{M}_n^{-1} + A_2c + A_3c^2 + \dots) \quad (2.11)$$

where  $A_2$ ,  $A_3$  are the second and third virial coefficients respectively. When solutions are sufficiently dilute a plot of  $(\pi/c)$  against  $(c)$  is linear ( $A_3 = 0$ ). The intercept of such a graph at zero concentration gives  $(\pi/c)_{c \rightarrow 0}$ .

In this work a Knauer membrane osmometer and detecting bridge (K.G. Dr.-Ing. H. Knauer & Co. GmbH, 1 Berlin 37 (West), Holstweg 18) were used. The basic features of this instrument are shown in Figure 2.8. Calibration is by the application of a known external pressure to the inlet tube. On addition of polymer solution to the upper chamber the pressure change in the lower chamber is detected by the diaphragm and a signal proportional to the pressure change is registered on a recorder.

Membranes (Sartorius, regenerated cellulose (11539#50)) were conditioned to toluene, xylene and/or chlorobenzene and proved satisfactory for  $\bar{M}_n$  measurements down to ca.  $12 \times 10^3 \text{ g mol}^{-1}$ , where permeation of solute molecules through the membrane was the limiting factor. Concentrations in the range  $0-20 \text{ g dm}^{-3}$  were employed. In any concentration series the solution with the lowest concentration was measured first followed by others in order of increasing concentration.

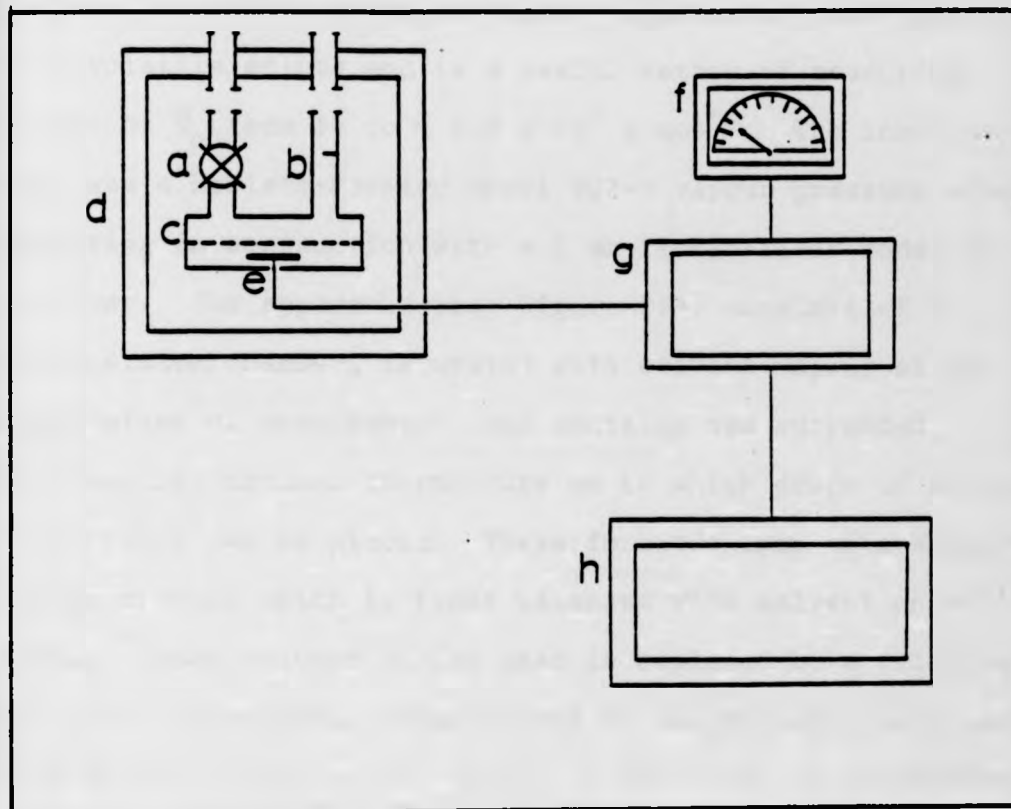


Figure 2.8: Schematic diagram of membrane osmometer:

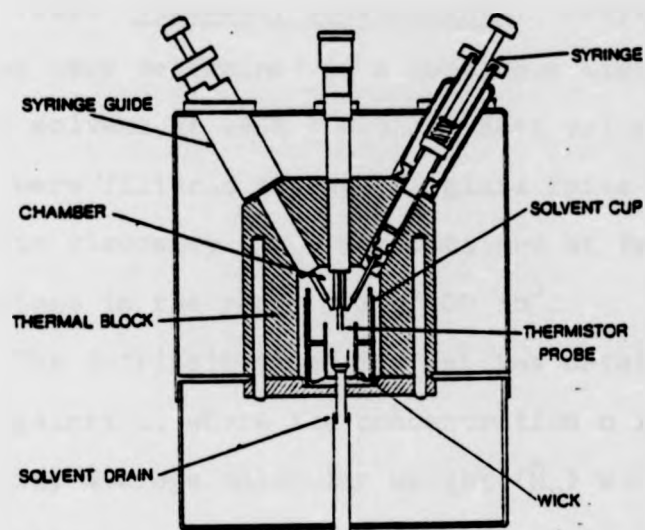
- (a) outlet valve
- (b) inlet tube
- (c) membrane
- (d) thermostatted chamber
- (e) pressure detecting membrane
- (f) osmotic pressure dial
- (g) Wheatstone's bridge circuit
- (h) recorder (Heathkit, model no. IR-18M)

(ii) Vapour pressure osmometry. This technique is based on the lowering of vapour pressure of a solvent by an involatile solute and is a useful method of measuring values of  $\bar{M}_n$  from 50 to  $\sim 2.0 \times 10^4$  g mol<sup>-1</sup>. The instrument used was a Hewlett-Packard Model 302-B vapour pressure osmometer operating in conjunction with a 1 mv Perkin-Elmer Model 56 recorder. The apparatus (see Figure 2.9) consists of a thermostatted chamber, saturated with solvent vapour at the temperature of measurement, and contains two suspended differential matched thermistors on to which drops of solution and solvent can be placed. These form two arms of a Wheatstone bridge circuit which is first balanced with solvent on both beads. When solvent on one bead is replaced by a solution an out of balance signal proportional to concentration and inversely proportional to molecular weight is obtained. A calibration constant  $K$  is first determined by calibrating the instrument with a standard substance of high purity and known molecular weight. Benzil (BDH, MW = 210.23 g mol<sup>-1</sup>) was used as a calibrant in this work. The  $\bar{M}_n$  values of an unknown compound can then be calculated from the relation,

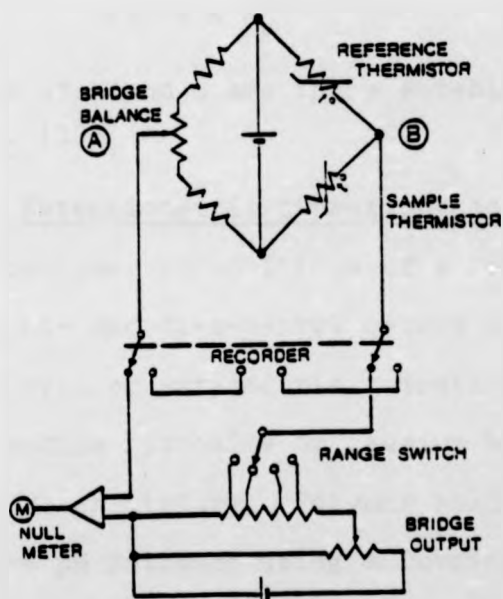
$$\bar{M}_n = K / \left( \frac{v}{c} \right)_{c=0} \quad (2.12)$$

where  $v$  is a measure of the bridge imbalance with solution of concentration  $c$ , and  $K$ , the empirical calibration factor, is regarded as a kind of cell constant and is determined for each thermistor pair/solvent/temperature combination.

The  $\bar{M}_n$  values were obtained by plotting  $(v/c)^{1/2}$  against  $c$  for a series of concentrations in the range 0-50 g dm<sup>-3</sup> and determining  $\left( \frac{v}{c} \right)_{c=0}$  from the intercept.



(a)



(b)

Figure 2.9: Schematic diagram of vapour pressure osmometer (VPO):

(a) thermal chamber showing probe and syringes

(b) simplified circuit diagram

(iii) Viscosity measurements. Polymer solution viscosities were determined in a Ubbelohde viscometer using benzene as solvent at  $298\text{K} \pm 0.01\text{K}$ . Both solvent and polymer solutions were filtered through  $G_3$  glass frits before use. The specific viscosity ( $\eta_{sp}$ ) was obtained at four different concentrations in the range  $0-1 \text{ g}/100 \text{ cm}^3$ .

The intrinsic viscosity  $[\eta]$  was obtained from plot of  $\eta_{sp}/c$  against  $c$ , where the concentration  $c$  is in  $\text{g}/100 \text{ cm}^3$ . The viscosity average molecular weight ( $\bar{M}_v$ ) was calculated from the relation

$$[\eta] = K \cdot \bar{M}_v^\alpha \quad (2.13)$$

where the values of  $K$  and  $\alpha$  are those established by Velickovic et al.<sup>(13)</sup>.

(iv) Potentiometric titration and ionomer preparation. Copolymer compositions of a series of random copolymers of mono- and di-*n*-pentyl esters of itaconic acid were determined by a potentiometric titration of their ethanol solutions with sodium hydroxide or caesium hydroxide in a (90:10) ethanol/water mixture. Polymer solution of  $1 - 1.5 \text{ g dm}^{-3}$  were used and the pH followed using a Corning-EEL, Model 7 pH meter connected to a chart recorder.

The amount of free acid groups in any copolymer sample, and hence the number of moles of the monoester incorporated in the copolymer was calculated from the end point of the titration curve. The ionomers, produced by neutralisation of the free acid groups, normally precipitated from solution close to the end point and were isolated by evaporation of the solvent. They were finally dried under vacuum at room temperature.



#### 2.3.4 MISCELLANEOUS TECHNIQUES

(i) Infrared spectroscopy. Infrared analysis (ir) was carried out using a Perkin-Elmer 577 Grating Infrared Spectrometer. Monomer and polymer samples were studied by casting films on NaCl plates or as KBr discs.

(ii) Nuclear magnetic resonance (nmr) spectra of monomer and polymer samples were recorded on a Hitachi Perkin-Elmer R24 (60 MHz) NMR spectrometer in its standard mode. Samples were studied as 10-15% wt./vol. solution in  $\text{CDCl}_3$  with TMS as internal reference.

(iii) Small angle X-ray scattering (SAXS) studies of some ionomer samples were kindly carried out by Dr. D.L.Handlin at the University of Massachusetts. X-ray scattering at small angles reveals features with a Bragg spacing of the order of tens of Ångstrom units as opposed to conventional X-ray scattering which resolves dimensions of the order of 0.1 Ångstrom unit. It is therefore a useful technique for investigating the morphology of polymers on a macroscale.

(iv) Elemental analysis was carried out on a Model 1106 Carlo-Erba Elemental Analyzer (Milan, Italy) under standard conditions. C, H and N are determined directly, and O by difference.

CHAPTER THREE

COPOLYMERS FROM DIESTERS OF ITACONIC ACID

RESULTS AND DISCUSSION

Abbreviated names of the homopolymers from diesters of itaconic acid used in this thesis.

Poly(dimethyl itaconate)	PDMI
Poly(di-n-propyl itaconate)	PDPPrI
Poly(di-n-butyl itaconate)	PDBI
Poly(di-n-hexyl itaconate)	PDHxI
Poly(di-n-heptyl itaconate)	PDHpI
Poly(di-n-octyl itaconate)	PDOI
Poly(di-n-nonyl itaconate)	PDNI
Poly(di-n-decyl itaconate)	PDDI

### 3.1 COPOLYMER COMPOSITIONS, REACTIVITY RATIOS AND MOLECULAR WEIGHTS

Three series of copolymers were prepared, with DMI as the shorter side chain comonomer and DHpI, DOI and DNI as the longer side chain comonomers. Additionally, a series of copolymers from DPrI and DOI were synthesized to compare the effects of lengthening the shorter chain component. A series of copolymers from DMI and DBI were prepared for comparison with the corresponding mixed ester polymer described in Chapter 4.

#### 3.1.1 COPOLYMER MOLECULAR WEIGHTS

Copolymer molecular weights were measured in xylene by membrane osmometry. During the measurements no permeation effects were observed. Permeation is known to occur at  $\bar{M}_n \approx 17000$   $\text{g mol}^{-1}$  with the membranes used, so no significant low molecular weight "tails" were present in the distributions. All samples had  $\bar{M}_n$  values in the region of  $10^5$   $\text{g mol}^{-1}$ , thus the effect of low molecular weight on the thermal and mechanical properties will be negligible.<sup>(61)</sup> The  $\bar{M}_n$  values obtained are listed in Tables 3.1-3.5.

#### 3.1.2 COPOLYMER COMPOSITION

Copolymer compositions were estimated by nmr spectroscopy using the total integrals between 4.5 and 3.1 ppm ( $I_A$ ) and between 3.1 and 0.5 ppm ( $I_B$ ). The former integral arises from  $-\text{OCH}_3$  groups (from DMI units) and  $-\text{OCH}_2$  groups (from any longer chain ester). The latter integral arises from the  $-\text{CH}_2-$  units in the main chain,  $-\text{CH}_2-$  units of the n-alkyl side chains, terminal  $-\text{CH}_3$  units and the  $-\text{CH}_2$  units attached directly to the main chain.

TABLE 3.1

Copolymer compositions and  $\bar{M}_n$  values for poly(dimethyl itaconate -co-di-n-butyl itaconate) series

SAMPLE	MOL.% DBI		CONVERSION (wt. %)	$\bar{M}_n \times 10^{-5}$ (g mol <sup>-1</sup> )	SAMPLE CODE
	Feed	Copolymer			
PDBI	-	-	53	1.45	-
1	92.55	88	11	0.96	P(DMI+DBI) 12/88
2	85.50	80	13	1.67	P(DMI+DBI) 20/80
3	78.72	73	7.0	1.63	P(DMI+DBI) 27/73
4	66.20	62	5.0	1.52	P(DMI+DBI) 38/62
5	44.40	39	16	1.23	P(DMI+DBI) 61/39
6	26.00	22	17	0.95	P(DMI+DBI) 78/22
PDMI	-	-	17	0.71	-

TABLE 3.2

Copolymer compositions and  $\bar{M}_n$  values for poly(dimethyl itaconate -co-di-n-heptyl itaconate) series

SAMPLE	MOL.% DHpI		CONVERSION (wt. %)	$\bar{M}_n \times 10^{-4}$ (g mol <sup>-1</sup> )	SAMPLE CODE
	Feed	Copolymer			
PDHpI	-	-	60	9.68	-
1	90.20	90	28	9.71	P(DMI+DHpI) 10/90
2	85.45	77	25	10.3	P(DMI+DHpI) 23/77
3	78.70	67	26	9.86	P(DMI+DHpI) 33/67
4	66.20	56	27	7.72	P(DMI+DHpI) 44/56
5	44.40	35	22	13.1	P(DMI+DHpI) 65/35
6	26.00	14	23	10.6	P(DMI+DHpI) 86/14
PDMI	-	-	17	7.10	-

TABLE 3.3

Copolymer compositions and  $\bar{M}_n$  values for poly(dimethyl itaconate -co-di-n-octyl itaconate) series

SAMPLE	MOL.% DOI		CONVERSION (wt. %)	$\bar{M}_n \times 10^{-5}$ (g mol <sup>-1</sup> )	SAMPLE CODE
	Feed	Copolymer			
PDMI	-	-	17	0.71	-
1	10.04	8.0	16	1.20	P(DMI+DOI) 92/8
2	26.73	22	22	1.54	P(DMI+DOI) 78/22
3	40.18	36	18	1.47	P(DMI+DOI) 64/36
4	57.27	56	31	1.48	P(DMI+DOI) 44/56
5	80.06	78	30	1.22	P(DMI+DOI) 22/78
6	93.52	93	21	1.25	P(DMI+DOI) 7/93
PDOI	-	-	12	1.17	-

TABLE 3.4

Copolymer compositions and  $\bar{M}_n$  values for poly(dimethyl itaconate -co-di-n-nonyl itaconate) series

SAMPLE	MOL.% DNI		CONVERSION (wt. %)	$\bar{M}_n \times 10^{-5}$ (g mol <sup>-1</sup> )	SAMPLE CODE
	Feed	Copolymer			
PDMI	-	-	17	0.71	-
1	9.40	7.0	19	1.22	P(DMI+DNI) 93/7
2	25.3	20	17	1.25	P(DMI+DNI) 80/20
3	38.3	30	15	1.35	P(DMI+DNI) 70/30
4	55.3	46	19	1.48	P(DMI+DNI) 54/46
5	78.8	66	20	1.45	P(DMI+DNI) 34/66
6	94.1	77	23	1.35	P(DMI+DNI) 23/77
PDNI	-	-	24	1.22	-

TABLE 3.5

Copolymer compositions and  $\bar{M}_n$  values for poly(di-n-propyl itaconate-co-di-n-octyl itaconate) series

SAMPLE	MOL.% DOI		CONVERSION (wt. %)	$\bar{M}_n \times 10^{-5}$ (g mol <sup>-1</sup> )	SAMPLE CODE
	Feed	Copolymer			
PDPPrI	-	-	48	0.83	-
1	12.12	8.0	15	1.35	P(DPrI+DOI) 92/8
2	31.15	21	22	1.69	P(DPrI+DOI) 79/21
3	45.30	40	26	0.80	P(DPrI+DOI) 60/40
4	62.36	58	18	0.78	P(DPrI+DOI) 42/58
5	83.50	72	17	0.93	P(DPrI+DOI) 28/72
6	91.30	82	31	1.26	P(DPrI+DOI) 18/82
PDOI	-	-	12	1.17	-

Two simultaneous equations can be set up for any copolymer system containing DMI in the form

$$6x + 4y = I_A \quad (3.1)$$

$$4x + ny = I_B \quad (3.2)$$

where  $x$  = mol fraction of DMI in the copolymer and  $y$  = mol fraction of the second comonomer. The value of  $n$  depends on the length of the ester side chains of the second comonomer as shown in Table 3.6.

TABLE 3.6

Values of  $n$  for copolymer systems with DMI as first comonomer.

<u>SECOND COMONOMER</u>	<u><math>n</math></u>
DBI	18
DHpI	30
DOI	34
DNI	38

In the case of P(DPrI + DOI) copolymers the relevant equations are

$$4x + 4y = I_A \quad (3.3)$$

$$14x + 34y = I_B \quad (3.4)$$

where  $x$  = mol fraction of DPrI and  $y$  = mol fraction of the DOI in the copolymer.

A representative nmr spectrum from the P(DMI + DBI) series and one from the P(DMI + DOI) series are shown in figures 3.1 and 3.2 respectively. As can be seen the signals are viscosity broadened and the integration steps are difficult to define. The accuracy of the analysis is consequently not high and the error is estimated to be ca.  $\pm 5\%$ .



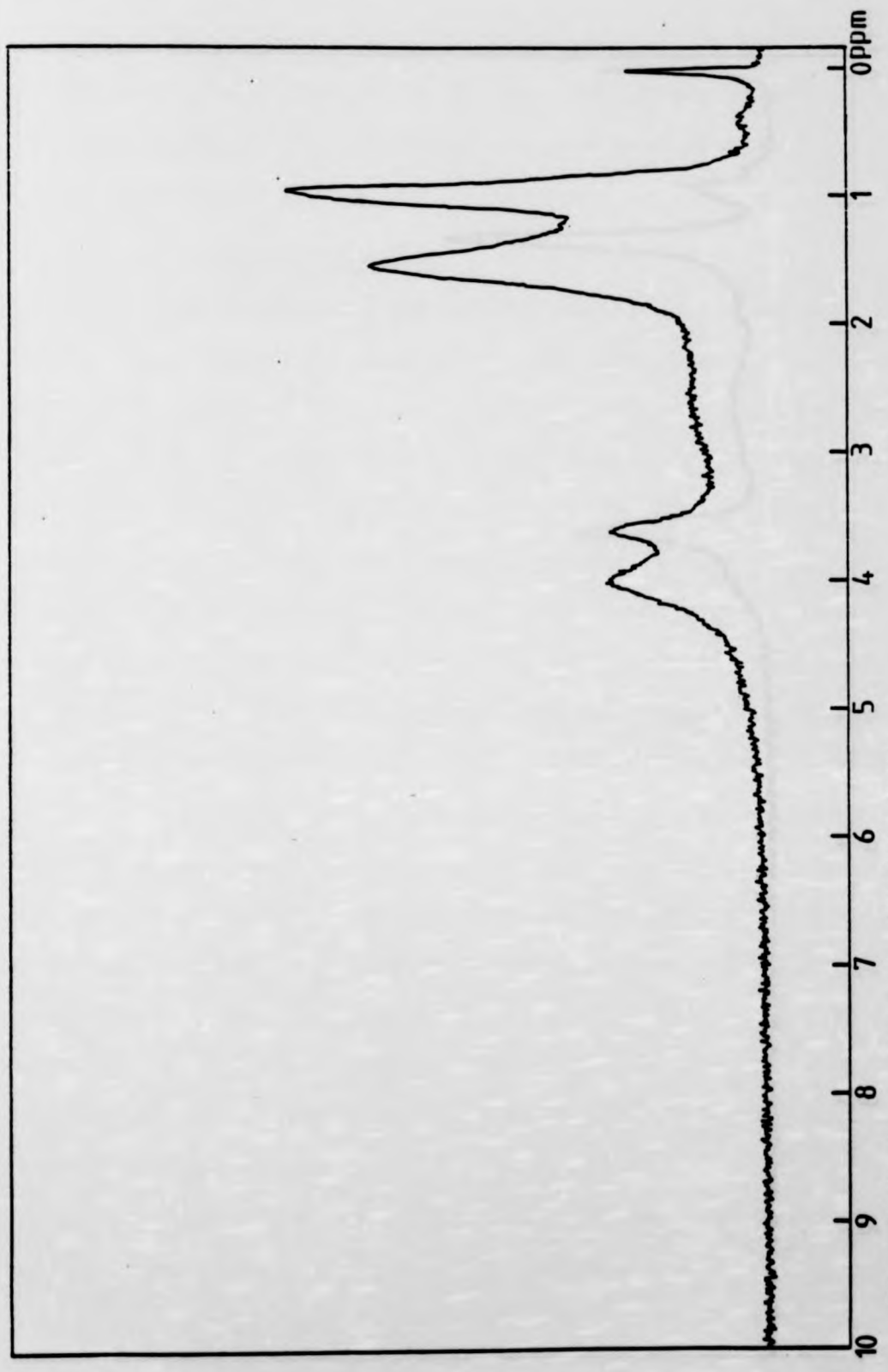


Figure 3.1: Nmr spectrum of P(DMI+DBI) 27/73.

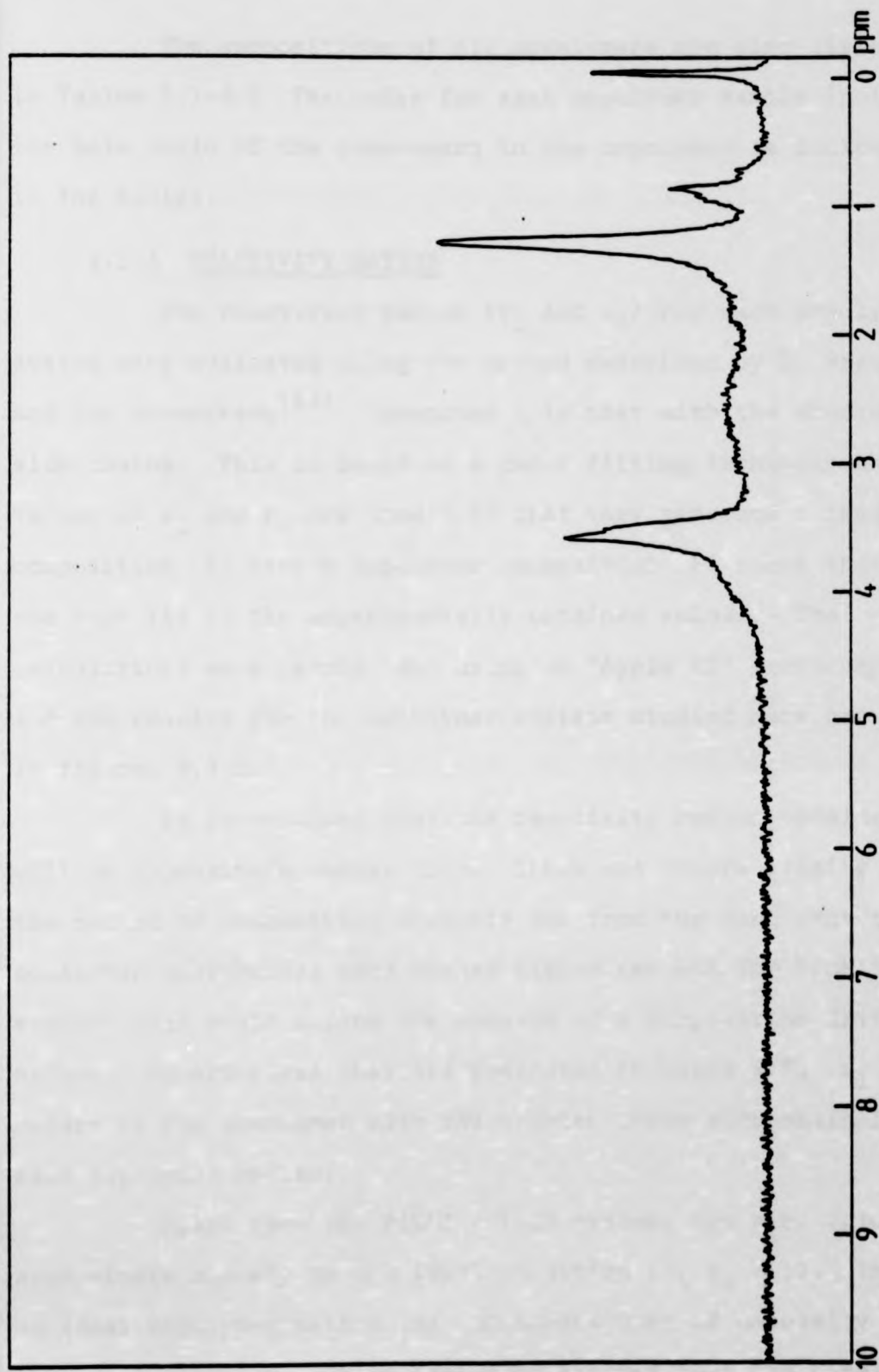


Figure 3.2: Nmr spectrum of P(DMI+DOI) 78/22.

The compositions of all copolymers are also listed in Tables 3.1-3.5. The codes for each copolymer sample include the mole ratio of the comonomers in the copolymer as indicated in the tables.

### 3.1.3 REACTIVITY RATIOS

The reactivity ratios ( $r_1$  and  $r_2$ ) for each copolymer system were evaluated using the method described by D. Braun and his co-workers.<sup>(62)</sup> Comonomer 1 is that with the shorter side chains. This is based on a curve fitting technique whereby values of  $r_1$  and  $r_2$  are chosen so that they generate a feed composition (f) versus copolymer composition (F) curve that is the best fit to the experimentally obtained values. The calculations were carried out using an "Apple II" microcomputer and the results for the copolymer systems studied here are shown in figures 3.3-3.7.

It is realised that the reactivity ratios obtained will be approximate values only. There are errors arising from the method of composition analysis and from the fact that the copolymer conversions were rather higher (except for P(DMI + DBI) series) than would ensure the absence of a composition drift effect. Nevertheless they are presented in Table 3.7;  $r_1$  refers to the comonomer with the shorter ester side chain in each copolymer system.

Apart from the P(DMI + DMI) system, the  $r_1 r_2$  values approximate closely to the ideal condition ( $r_1 \cdot r_2 = 1$ ). In an ideal copolymerization the comonomers must of necessity enter the chain randomly. It is therefore assumed that the copolymer systems studied in this work are essentially random copolymers.

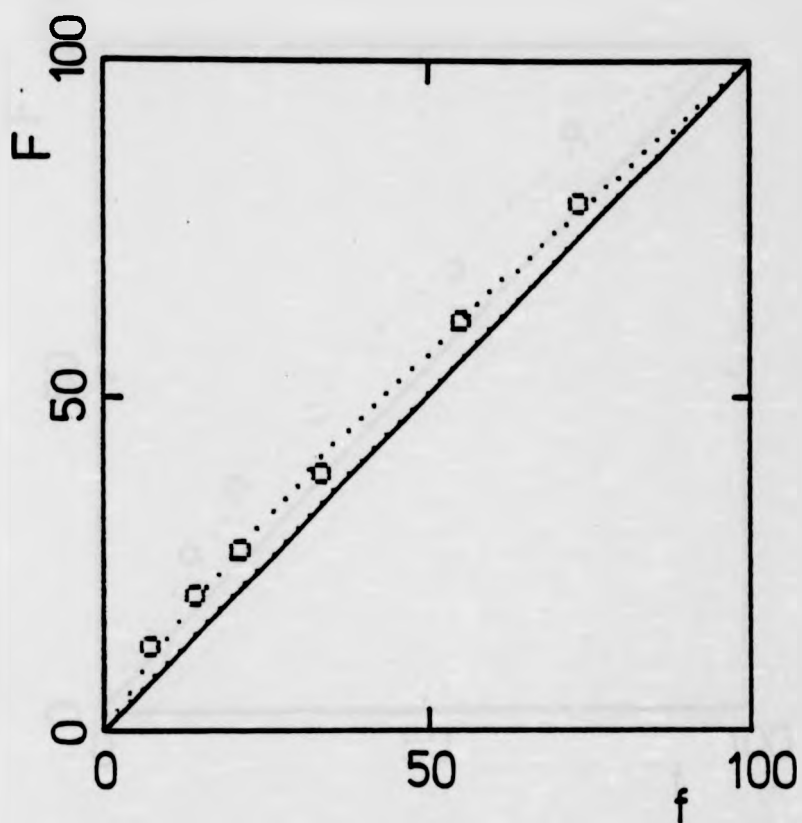


Figure 3.3: Plot of mol fraction DMI in feed ( $f$ ) versus mol fraction DMI in copolymer ( $F$ ) for P(DMI+DBI) copolymer series.

□, Experimental points;  
(.....) calculated curve with  $r_1 = 1.16$   
and  $r_2 = 0.69$ .

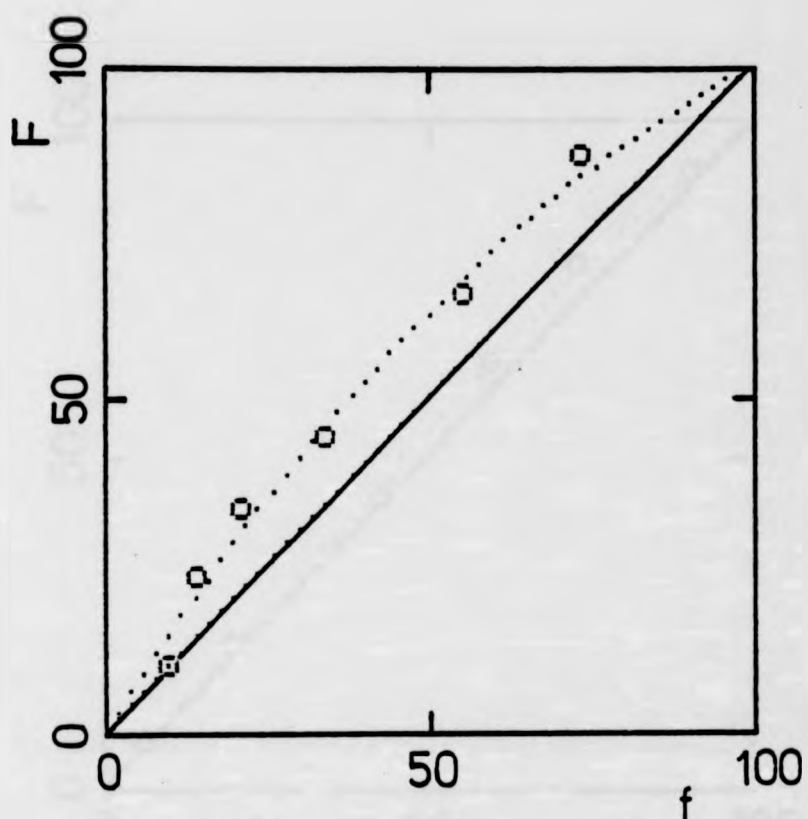


Figure 3.4: Plot of mol fraction DMI in feed ( $f$ ) versus mol fraction DMI in copolymer ( $F$ ) for P(DMI+DHpI) copolymer series.

□, Experimental points;  
(.....) calculated curve with  
 $r_1 = 1.81$  and  $r_2 = 0.68$ .

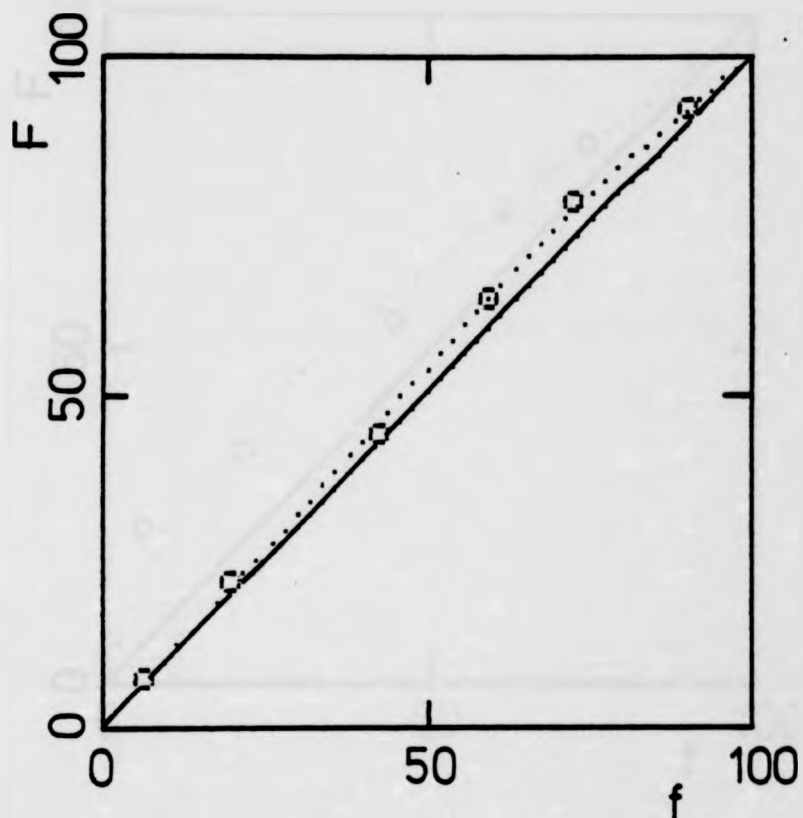


Figure 3.5: Plot of mol fraction DMI in feed ( $f$ ) versus mol fraction DMI in copolymer for P(DMI+DOI) copolymer series.

□, Experimental points;

(.....) calculated curve with

$r_1 = 1.36$  and  $r_2 = 1.03$ .

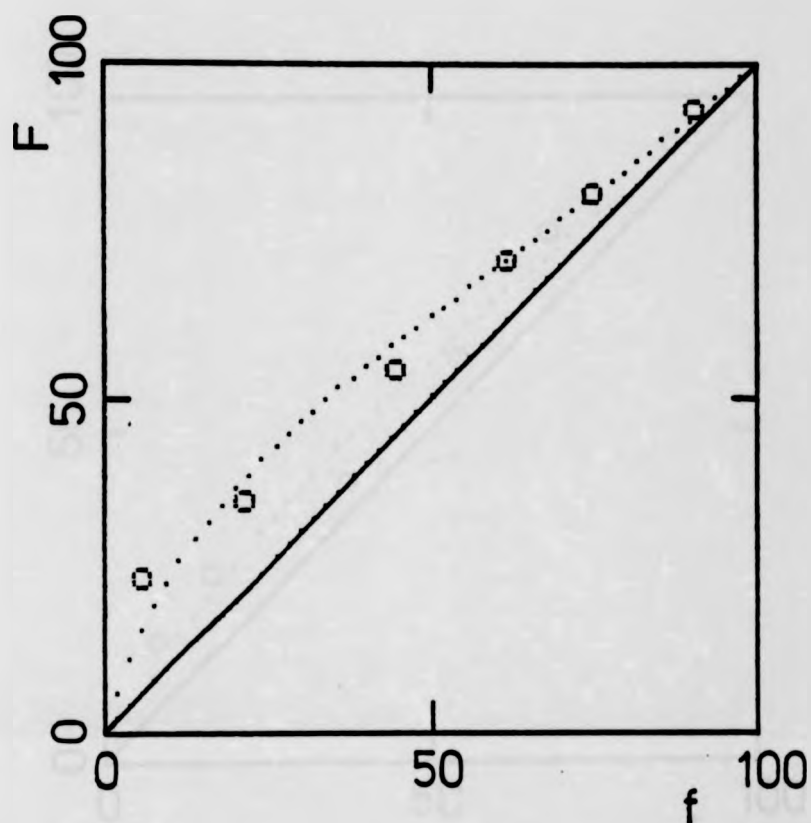


Figure 3.6: Plot of mol fraction DMI in feed ( $f$ ) versus mol fraction DMI in copolymer ( $F$ ) for P(DMI+DNI) copolymer series.

□ , Experimental points;  
(.....) calculated curve with  
 $r_1 = 1.17$  and  $r_2 = 0.32$ .

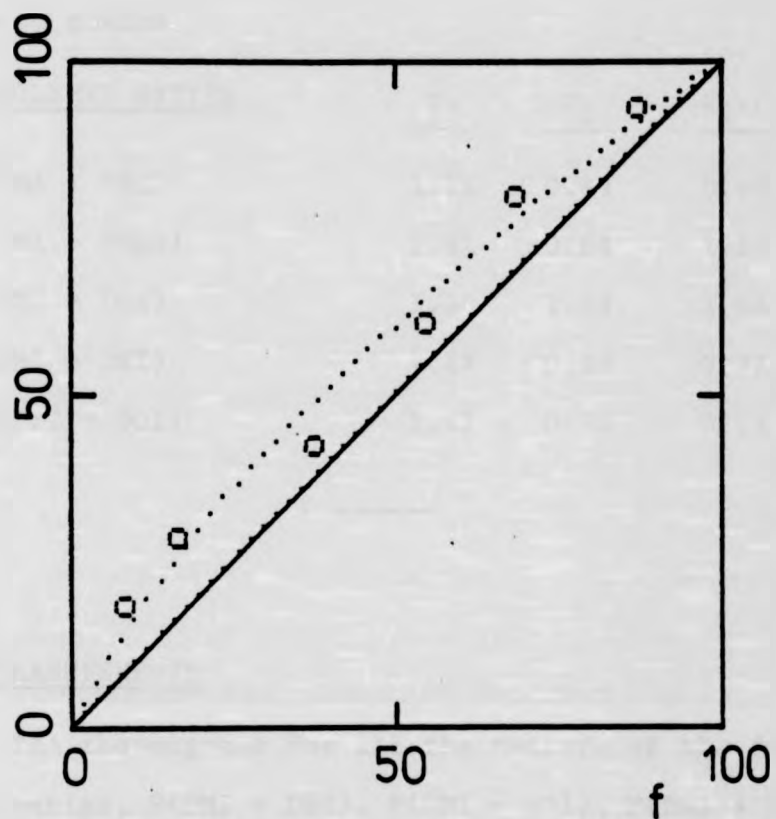


Figure 3.7: Plot of mol fraction DPrI in feed ( $f$ ) versus mol fraction DPrI in copolymer ( $F$ ) for P(DPrI+DOI) copolymer series.

□, Experimental points;  
(.....) calculated curve with  
 $r_1 = 1.33$  and  $r_2 = 0.55$ .



TABLE 3.7

Values of the reactivity ratios  $r_1$  and  $r_2$  for indicated copolymer systems. Comonomer 1 is that with the shorter n-alkyl side chains.

<u>COPOLYMER SYSTEM</u>	<u><math>r_1</math></u>	<u><math>r_2</math></u>	<u><math>r_1 \cdot r_2</math></u>
P(DMI + DBI)	1.16	0.69	0.80
P(DMI + DHpI)	1.81	0.68	1.23
P(DMI + DOI)	1.36	1.03	1.40
P(DMI + DNI)	1.17	0.32	0.37
P(DPrI + DOI)	1.33	0.55	0.73

### 3.2 TBA MEASUREMENTS

TBA thermograms for all the members of the four copolymer series, P(DMI + DBI), P(DMI + DOI), P(DMI + DNI) and P(DPrI + DOI) were obtained as plots of the damping index ( $-\log 1/n$ ) (which is a relative quantity) against temperature, and are displaced vertically on an arbitrary scale for clarity. In general the copolymers of each series show one major damping maximum and one or more secondary features. It is convenient to discuss the results for each series of copolymers in turn.

#### 3.2.1 P(DMI + DBI) SERIES

This series was studied to provide a comparison for the mixed ester polymer from methyl n-butyl itaconate which can be regarded as a 50/50 "copolymer" with methyl and n-butyl moieties on the same repeat unit.

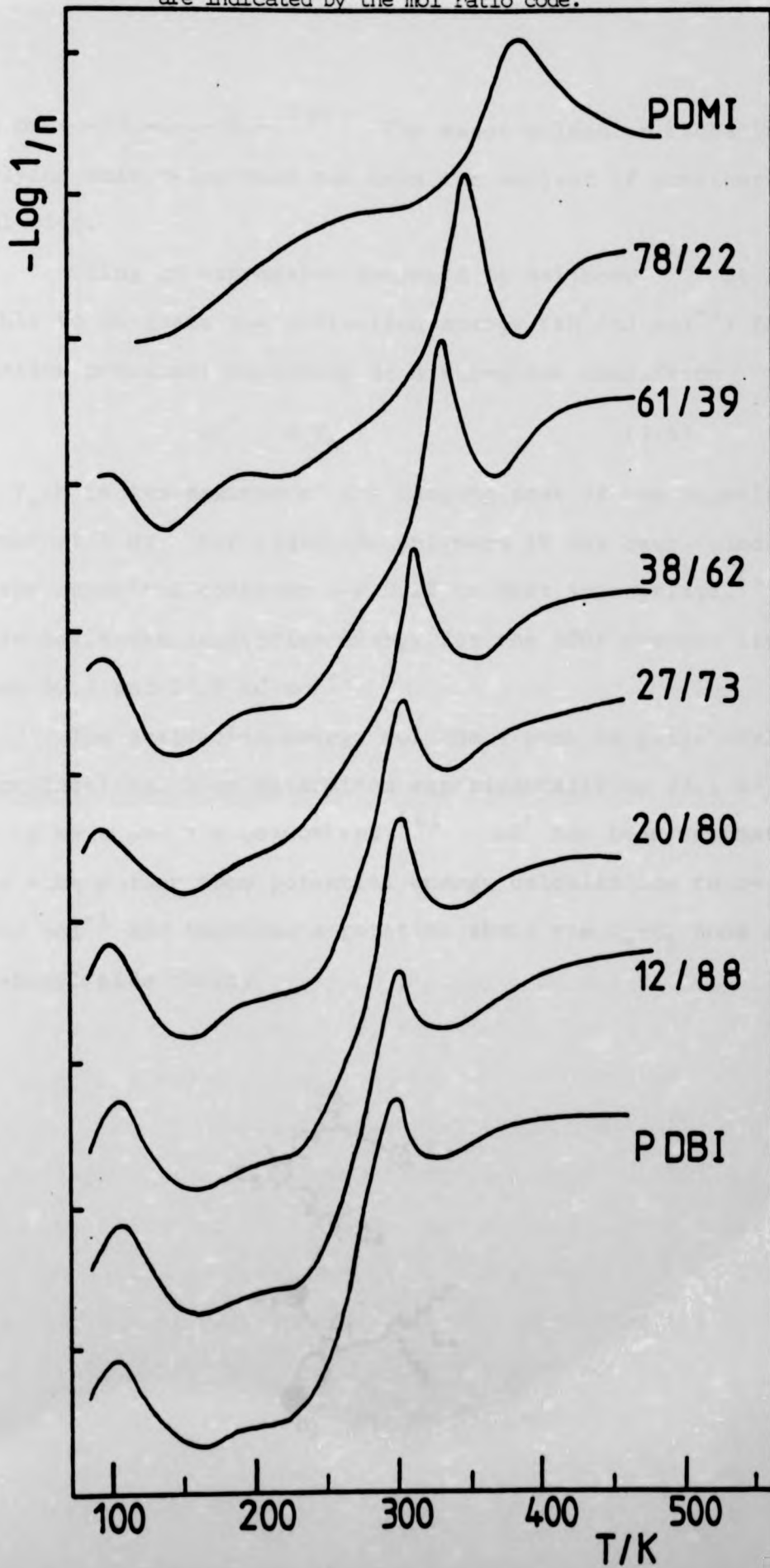
The TBA thermograms for the series are shown in figure 3.8. The two homopolymers and the copolymers all show one prominent damping maximum which is identified as the glass transition ( $T_g$ ) and which changes smoothly from 296K in PDBI to 373K in PDMI (see figure 3.8). The  $T_g$  values for the series are listed in Table 3.8 along with the corresponding DSC determined  $T_g$  values, which agree closely. The DSC glass transition temperatures were taken as the point of intersection of the base line and the tangent through the steepest point of the inflection on the heat capacity ( $C_p$ ) versus temperature curves for the series which are shown in figure 3.17 and will be discussed later.

The relaxation processes which give rise to the damping maxima at  $T_g$  are agreed to involve long-range co-operative motion of the polymer backbone which is frozen in below  $T_g$ . However, small scale relaxation processes can occur in the glass involving only a small number of units. (33)

It has become common (63) to label peaks in the mechanical spectra of amorphous polymers using  $\alpha$ ,  $\beta$ ,  $\gamma$ , etc., where  $T_\alpha = T_g$ , the highest temperature peak, with  $T_\beta$ ,  $T_\gamma$ , etc. referring to sub-glass transition peaks at increasingly lower temperatures.

The  $\gamma$  process. A relaxation is present at  $\sim 100$ K in most members of the series and becomes less prominent as the DBI content decreases, being completely absent in PDMI. This peak is labelled  $T_\gamma$  and the values are listed in Table 3.8. A transition with a maximum in this temperature region is always found in polymers which contain sequences of at least four  $-\text{CH}_2-$

Figure 3.8: Plots of the mechanical damping index ( $-\log 1/n$ ) versus temperature for P(DMI+DBI) copolymer series. Samples are indicated by the mol ratio code.



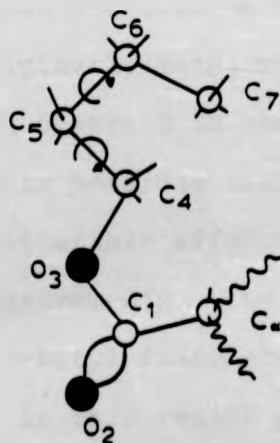
units or  $-O-CH_2-CH_2-CH_2-$ .<sup>(33)</sup> The exact molecular mechanism underlying this relaxation has been the subject of considerable speculation.

Using an expression proposed by Heijboer<sup>(32)</sup> it is possible to estimate the activation energy ( $\Delta H^\ddagger/kJ\ mol^{-1}$ ) for relaxation processes occurring at a sub-glass transition

$$\Delta H^\ddagger = A T_m \quad (3.5)$$

where  $T_m/K$  is the maximum of the damping peak of the transition measured at 1 Hz. For itaconate polymers it has been found that the numerical constant  $A = 0.29$  is most appropriate.<sup>(64)</sup> On this basis the activation energy for the 100K process lies between 30.5 and 27.5  $kJ\ mol^{-1}$ .

The activation energy for the  $\gamma$  peak in poly(butyl methacrylate) has been determined experimentally as 23.1  $kJ\ mol^{-1}$  by Wada and his co-workers.<sup>(65)</sup>  $\Delta H^\ddagger$  has been estimated by the same author from potential energy calculations to be 20.2  $kJ\ mol^{-1}$  and involves a rotation about the  $C_4-C_5$  bond of the n-butyl side chain.



Alternatively, rotation about the  $C_5-C_6$  would be expected to have the same activation energy as the rotation about the middle bond of n-butane\* itself ( $\sim 29 \text{ kJ mol}^{-1}$ ).<sup>(66)</sup> Either of these two motions would seem to explain adequately the damping process at  $\sim 100\text{K}$  in this copolymer series, although both motions cannot be occurring synchronically or the activation energy for the  $\gamma$  peak would be approximately  $29 + 23 = 52 \text{ kJ mol}^{-1}$ .

Implicit in the above argument is the assumption that any relaxation process (rotation, wagging, etc.) has an activation energy which is dependent only on the intramolecular potentials and that the surrounding matrix has no effect. This assumption has been verified by Heijboer<sup>(32)</sup> in his extensive studies of poly(cyclohexylmethacrylate). Limited motions in the rigid glassy state are therefore pictured as occurring in "holes" of adequate size such that the matrix does not impede the rearrangement in question.

The  $\beta$  process. A third peak is observed in the spectra of the series (see figure 3.8) in the region of  $180-200\text{K}$  and is of rather low intensity. This peak is not present in PDMI itself which has a long low-temperature shoulder from  $\sim 200\text{K}$  to  $T_g$  and which has been ascribed to motion of the ester linkage,<sup>(28)</sup> similar to that in poly(methylmethacrylate) (PMMA).<sup>(32)</sup> A peak at  $\sim 180\text{K}$  has been observed in the spectrum of PMMA due to absorbed water and it is possible that a similar origin pertains here, even though considerable efforts were made to keep the samples dry during measurements. The corresponding mixed ester polymer (poly(methyl n-butyl itaconate)) does not have an observable relaxation in this region although poly(methyl n-propyl

\* See illustration on p.82.

itaconate, poly(methyl n-pentyl itaconate) and poly(methyl n-hexyl itaconate) do show similar features (see section 4.2). The origin of this peak is not clear at this time.

If the values of  $T_g$  and  $T_\gamma$  for the series are plotted against copolymer composition (see figure 3.9), it can be seen that the values of  $T_g$  increase as the DBI content decreases. In this case DBI acts as an internal plasticizer and thus lowers the  $T_g$ .  $T_\gamma$  values vary only very slightly and go through a shallow maximum and then minimum with increasing DMI content of the copolymer.

### 3.2.2 P(DMI + DOI) SERIES

This series of copolymers and the P(DMI + DNI) series were synthesized to investigate more fully the behaviour of previously studied poly(di-n-alkyl itaconates) with side groups containing 7-10 carbon atoms. <sup>(24)</sup> These have been proposed as possessing two glass transitions, " $T_g^L$ " and " $T_g^U$ " (L = lower, U = upper) where the lower temperature process involves the side chain and the upper the main chain. In particular heat capacity measurements were sought and these are discussed in the following section (3.3).

The  $\gamma$  process. The TBA thermograms for P(DMI + DOI) series are shown in figure 3.10 and display a number of features. A prominent  $T_\gamma$  peak at  $\sim 100K$  (see Table 3.9) is present as would be expected for polymers with long  $-CH_2-$  sequences in the side chain. The peak diminishes as the concentration of DOI units decreases. This could be due to a similar relaxation mechanism as described for the  $\gamma$  process in the P(DMI + DBI)

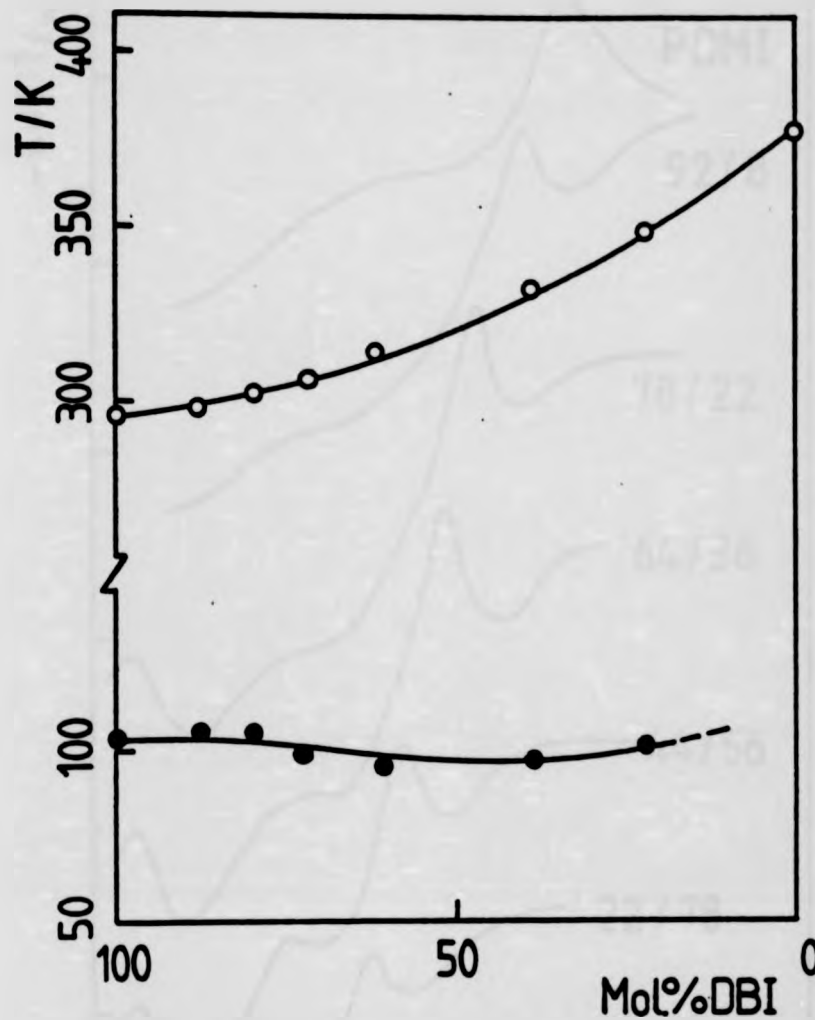
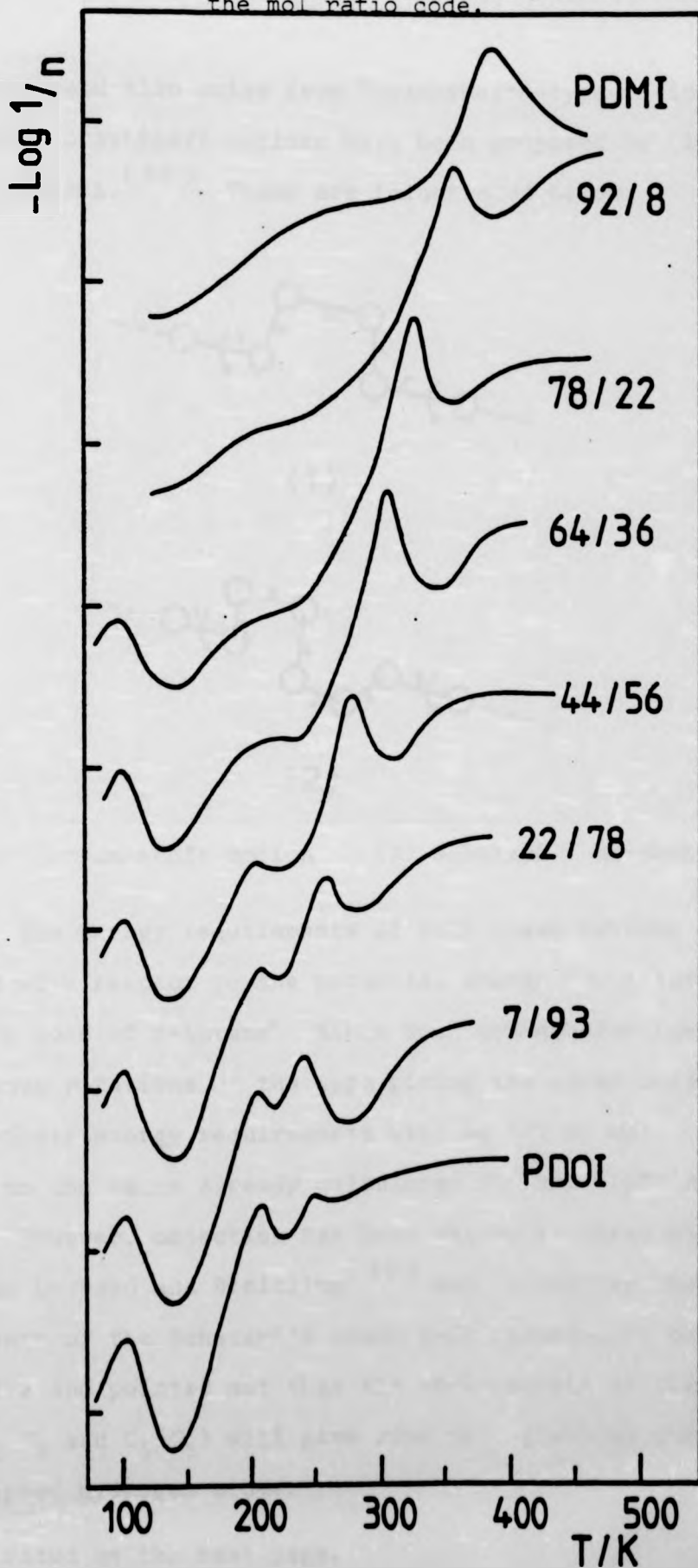


Figure 3.9: Plots of  $T_g$  ( $\circ$ ) and  $T_y$  ( $\bullet$ ) values versus copolymer composition for P(DMI+DBI) copolymer series.

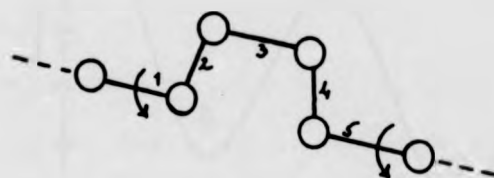
Figure 3.10: Plots of the mechanical damping index ( $-\log 1/n$ ) versus temperature for P(DMI+DOI) copolymer series. Samples are indicated by the mol ratio code.



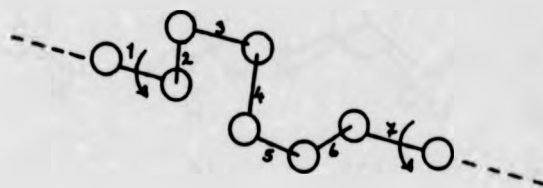


system but could also arise from "crankshaft"-type motions.

Two types of crankshaft motions have been proposed by (1) Boyer<sup>(67)</sup> and (2) Schatzki.<sup>(68)</sup> These are illustrated below.



(1)

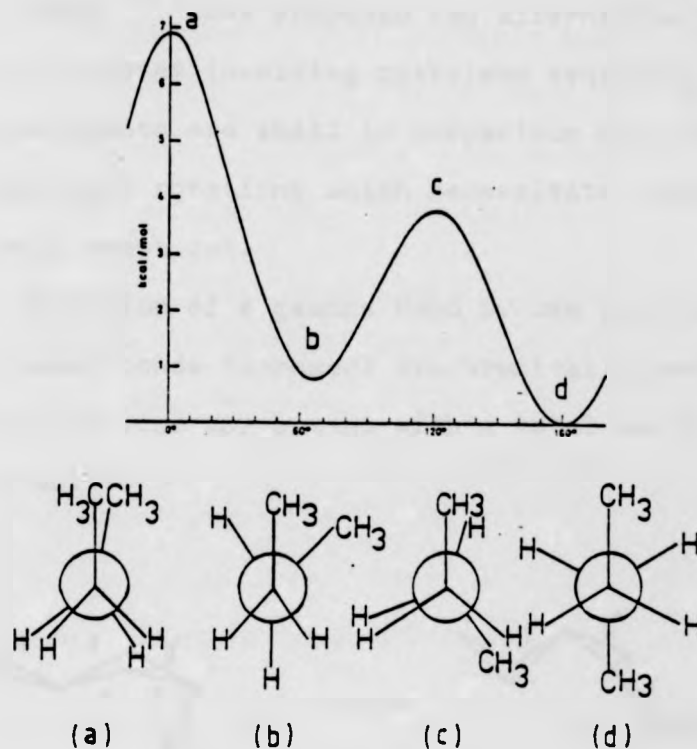


(2)

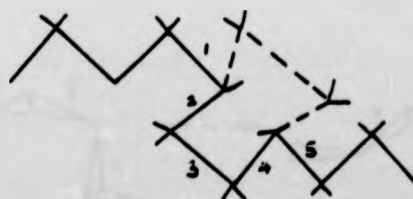
(1) Boyer crankshaft motion      (2) Schatzki crankshaft motion

The energy requirements of both these motions can be estimated with respect to the potential energy for rotation about the centre bond of n-butane\*. Since both crankshafts involve two simultaneous rotations of the type giving the lower butane barrier, their energy requirements will be  $\approx 32 \text{ kJ mol}^{-1}$ , which is close to the value already calculated for the  $\approx 100\text{K}$  damping process. However, objection has been raised to these simple mechanisms by Boyd and Breitling<sup>(69)</sup> who calculated the steric requirements of the Schatzki's crankshaft rotation to be prohibitive and pointed out that the co-linearity of the stem bonds ( $\text{C}_1\text{-C}_2$  and  $\text{C}_5\text{-C}_6$ ) will give rise to a strained structure with eclipsed hydrogen atoms.

\* Illustrated on the next page.



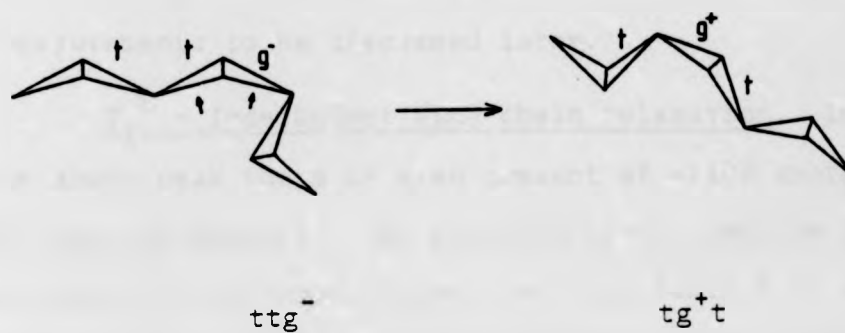
The same authors have modified the Boyer crankshaft rotation by allowing the stem bonds to be non-colinear and have carried out strain energy calculations which reveal a "flip-flop" type of motion (shown below) with an approximate  $42 \text{ kJ mol}^{-1}$  barrier which was unaffected by the matrix.



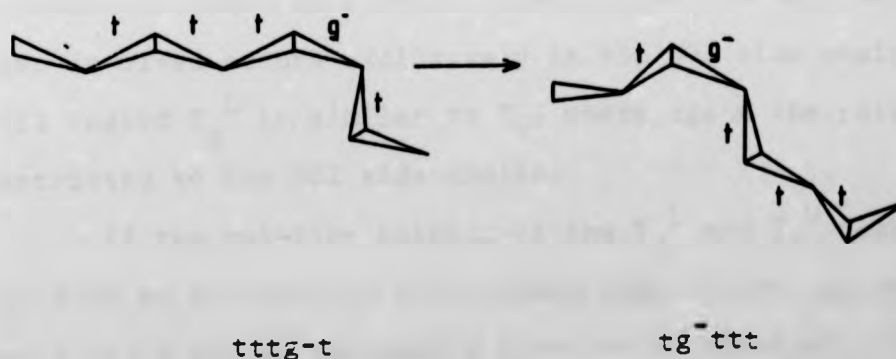
Boyd-Breitling flip-flop motion

Cowie<sup>(33)</sup> has proposed two alternative possible relaxation processes involving methylene sequences whose volume requirements are small in comparison with that required by the crankshaft rotations which necessitate relatively large volumes being swept out.

(i) Migration of a gauche bond by one position will result if two adjacent bonds (arrowed) synchronically passing over the lower energy barrier for butane with a total energy requirement of  $\leq 32 \text{ kJ mol}^{-1}$ .



(ii) Migration of a gauche bond by two positions will be possible if two non-adjacent bonds pass over the lower energy barrier for butane.



This latter rearrangement is particularly appealing as an explanation for relaxations in longer alkyl side chains since the volume required is relatively small and there is very little geometric change outside the three-bond unit.

$T_g^U$  - The main chain relaxation process. In any series of copolymers the glass transition temperature is a smooth function of the copolymer composition. <sup>(70)</sup> Using this criterion it is possible to identify the main chain relaxation as the highest temperature peak in each thermogram, moving from 248K in PDOI to 373K in PDMI (see Table 3.9). This is confirmed by DSC measurements to be discussed later.

$T_g^L$  - Independent side chain relaxation. In addition to the above peak there is also present at  $\sim 210$ K another significant damping process. The position of the peak is almost independent of copolymer composition (see Table 3.9) and its intensity diminishes as the concentration of DOI side chain reduces. This behaviour is analogous to that reported for the P(DMI + DHpI) system <sup>(23)</sup> and the peak is identified similarly as the  $T_g^L$  for this copolymer series. The fact that the position of this peak is essentially independent of the copolymer composition and that its intensity diminishes with decreasing DOI content is taken as strong evidence that the relaxation process involved occurs exclusively in the DOI side chain regions. In this regard  $T_g^L$  is similar to  $T_g^Y$ , where again the relaxation is restricted to the DOI side chains.

If the relative heights of the  $T_g^L$  and  $T_g^U$  peaks are plotted as a function of copolymer composition, as shown in figure 3.11, a smooth decreasing function is obtained. It is

TABLE 3.8

Glass transition temperatures and  $T_g$  values for P(DMI+DBI) series determined by TBA and DSC

<u>SAMPLE</u>	<u>MOL.% DBI</u>	$T_g$ /K (TBA)	$T_g$ /K (DSC)	$T_g$ /K (TBA)
PDBI	100	296	282	103
1	88	298	286	105
2	80	302	292	105
3	73	306	296	99
4	62	314	308	95
5	39	332	321	97
6	22	349	334	101
PDMI	0	373	377	-

TABLE 3.9

TBA determined glass transition temperatures ( $T_g^U$ ), ( $T_g^L$ ) and  $T_g$  values for P(DMI+DOI) series

<u>SAMPLE</u>	<u>MOL.% DOI</u>	$T_g^U$ /K	$T_g^L$ /K	$T_g$ /K
PDOI	0	373	-	-
1	8.0	359	-	-
2	22	325	~213	98
3	36	305	~218	102
4	56	278	~215	103
5	78	257	209	104
6	92	243	207	104
PDOI	100	248	209	106

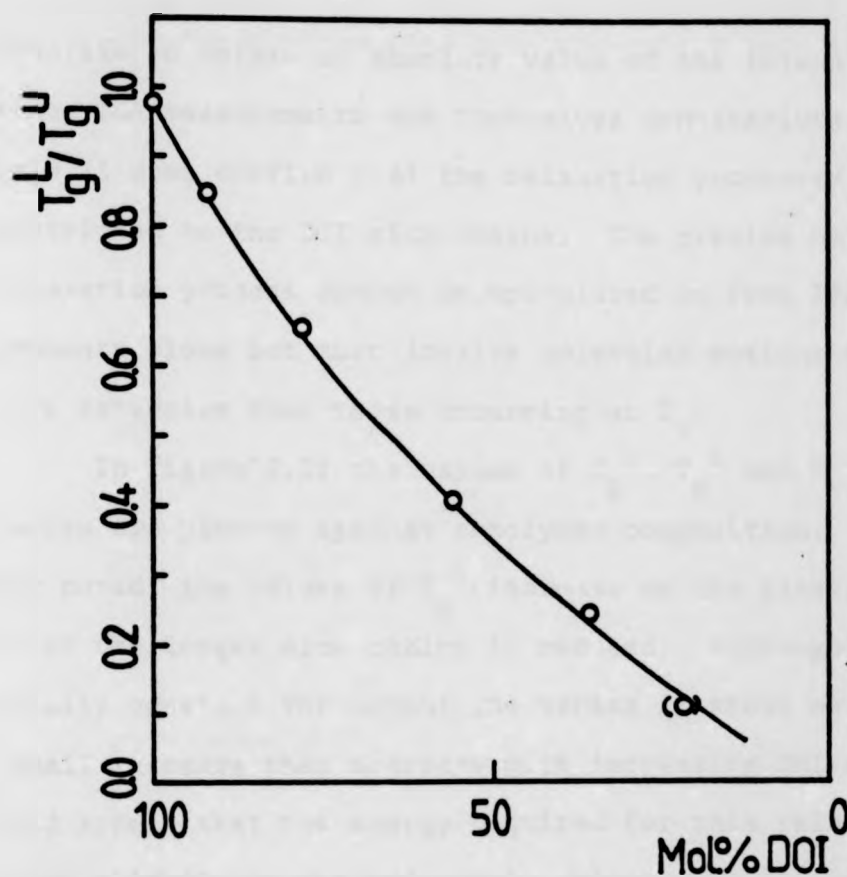


Figure 3.11 Plots of the relative heights of  $T_g^L$  and  $T_g^U$  peaks in the TBA spectra of P(DMI+DOI) copolymer series as a function of copolymer composition. Relative intensity of a peak is arbitrarily measured as

$$\frac{-\log 1/n \text{ at } T_g^L}{-\log 1/n \text{ at } T_g^U}$$

not possible to obtain an absolute value of the intensity of  $T_g^L$  since TBA measurements are themselves non-absolute, but figure 3.11 does confirm that the relaxation processes involved are restricted to the DOI side chains. The precise nature of the relaxation process cannot be speculated on from TBA measurements alone but must involve molecular motions which are more extensive than those occurring at  $T_\gamma$ .

In figure 3.12 the values of  $T_g^U$ ,  $T_g^L$  and  $T_\gamma$  for the series are plotted against copolymer composition. As already noted, the values of  $T_g^U$  increase as the plasticizing effect of the longer side chains is reduced. Although  $T_g^L$  is essentially constant throughout the series it shows evidence of a small increase then decrease with increasing DMI content. It would appear that the energy required for this relaxation is increased slightly as the main chain units start to come closer together, but that eventually this effect disappears.  $T_\gamma$ , if anything, falls slightly as the DMI content increases. The behaviour of  $T_g^L$  and  $T_\gamma$  in this manner may be taken as evidence for a small effect of a changing matrix on the molecular motion involved.

### 3.2.3 P(DMI + DNI) SERIES

This copolymer system should show similar features to the P(DMI + DOI) series. The TBA thermograms for the series are shown in figure 3.13.

The  $\gamma$  process. Again a low temperature relaxation at  $\sim 100K$  is present which diminishes in intensity with decreasing DNI side chain content. The mechanisms already discussed also apply to  $T_\gamma$  of this series. The  $T_\gamma$  values obtained are listed in Table 3.10.

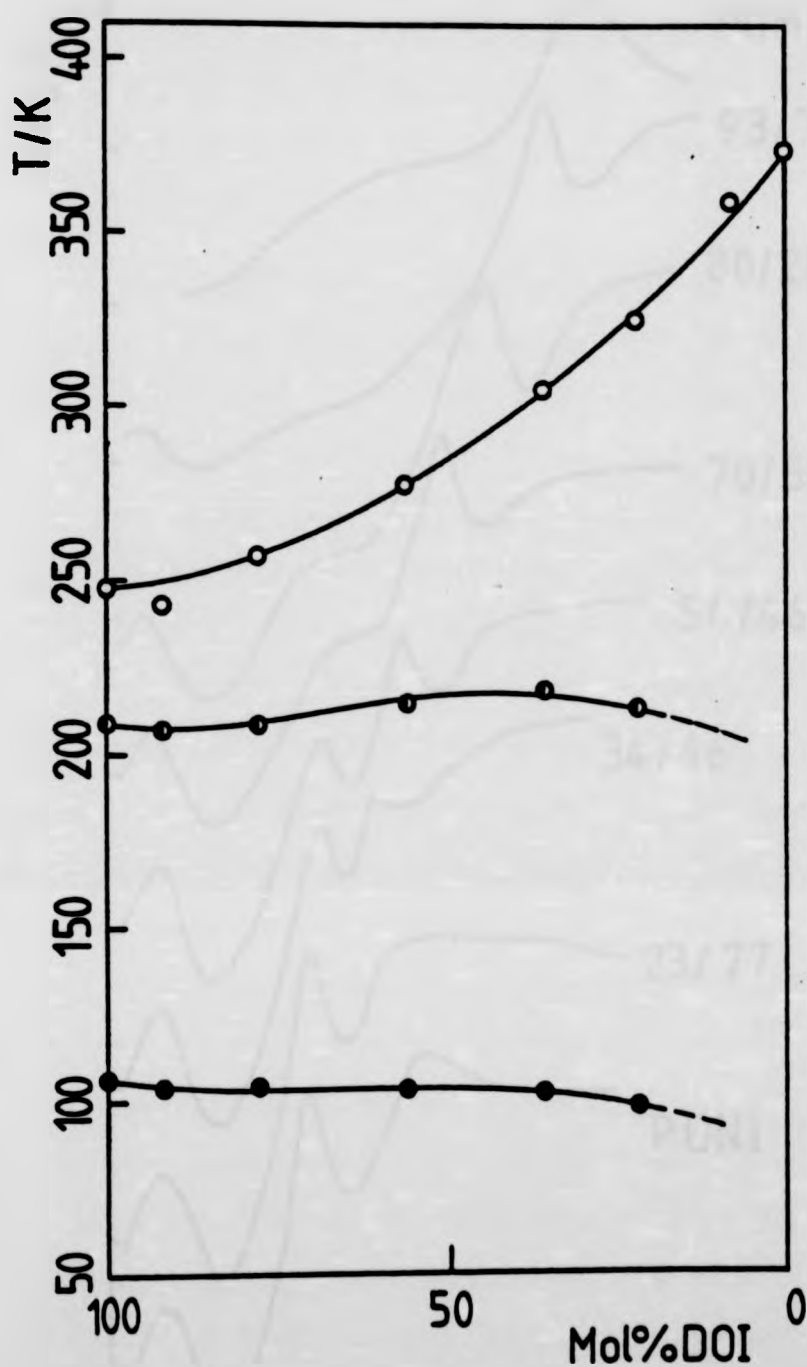


Figure 3.12: Plots of  $T_g^U$  (—○—),  $T_g^L$  (—○—) and  $T_g$  (—●—) values versus copolymer composition for P(DMI+DOI) copolymer series.



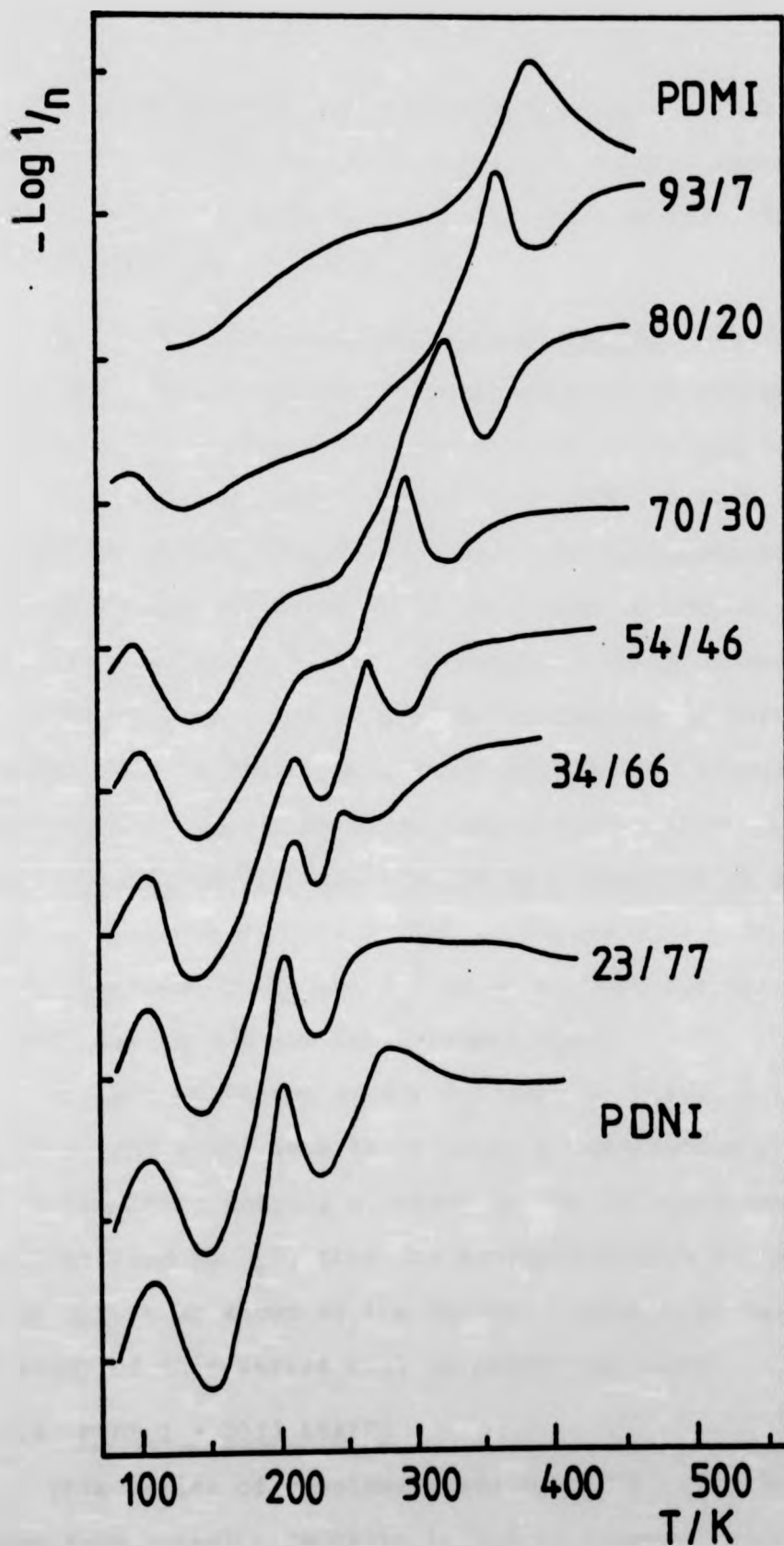


Figure 3.13: Plots of the mechanical damping index ( $-\log 1/\eta$ ) versus temperature for P(DMI+DNI) copolymer series. Samples are indicated by the mol ratio code.

$T_g^L$ -independent side chain relaxation. A peak which diminishes in intensity with decreasing DMI content again appears at  $\sim 210\text{K}$  and this is assigned to  $T_g^L$  for this series. The values of  $T_g^L$  are also listed in Table 3.10.

$T_g^U$  - The main chain relaxation process. The main chain relaxation which changes with composition is obvious for those members of the series with DMI content of 44 mol % or greater. This peak decreases from 373K in PDMI to 267K at sample 4 of the series (see Table 3.10). It is impossible to estimate accurately the position of this peak in sample 5 but the approximate value is  $\sim 243\text{K}$ . In sample 6 the peak seems to have been absorbed into the general broad damping at high temperatures, but in PDNI itself there appears to be increasing resolution in the high temperature region with a broad peak ( $T_g^U$ ) at  $\sim 280\text{K}$ .  $T_g^U$ ,  $T_g^L$  and  $T_\gamma$  are plotted as a function of the copolymer composition for the series in figure 3.14. The same trends are observed for  $T_\gamma$  and  $T_g^L$  as were found for the P(DMI + DOI) series and the same remarks apply.

The extrapolation of the  $T_g^U$  data in figure 3.14 to give  $T_g^U$  for PDNI would seem to indicate a temperature of  $\sim 230\text{K}$ . However if the broad damping at  $\sim 280\text{K}$  in the TBA spectrum of PDNI is identified as  $T_g^U$ , then the extrapolation will have to undergo an upturn as shown in the figure. Additional data from the DSC study of this series will be presented later.

#### 3.2.4 P(DPrI + DOI) SERIES

This series of copolymers was synthesized to see if the change from methyl side chain ( $-\text{CH}_3$ ) to n-propyl side chain ( $-\text{CH}_2-\text{CH}_2-\text{CH}_3$ ) affected the relaxation behaviour of the longer

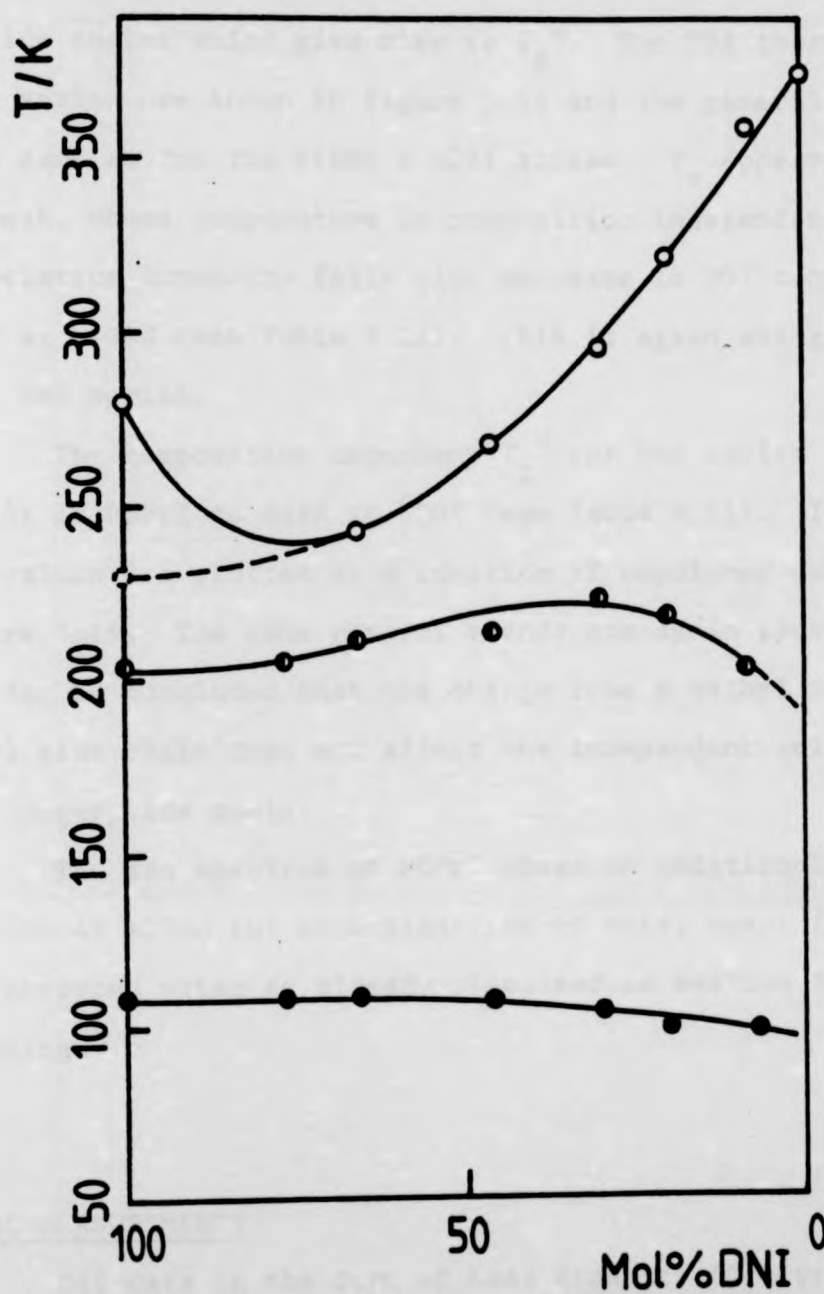


Figure 3.14: Plots of  $T_g^U$  ( $\circ$ ),  $T_g^L$  ( $\circ$ ), and  $T_g$  ( $\bullet$ ) values versus copolymer composition for P(DMI+DNI) copolymer series.

(DOI) side chains which give rise to  $T_g^L$ . The TBA thermograms for the series are shown in figure 3.15 and the general features are the same as for the P(DMI + DOI) series.  $T_\gamma$  appears at  $\sim 100K$  and a peak, whose temperature is composition independent but whose relative intensity falls with decrease in DOI content, is present at  $\sim 205K$  (see Table 3.11). This is again assigned as  $T_g^L$  for the series.

The composition dependent  $T_g^U$  for the series changes from 315K in PDPrI to 248K in PDOI (see Table 3.11).  $T_g^U$ ,  $T_g^L$  and  $T_\gamma$  values are plotted as a function of copolymer composition in figure 3.16. The same general trends are again present here and it can be concluded that the change from a methyl to an n-propyl side chain does not affect the independent relaxation of the longer side chain.

The TBA spectrum of PDPrI shows an additional minor relaxation at  $\sim 170K$  but no explanation of this, apart from being due to absorbed water as already discussed in section 3.2.1, is forthcoming.

### 3.3 DSC MEASUREMENTS

DSC data in the form of heat capacity ( $C_p$ ) versus temperature plots were obtained for all the copolymer series. Of particular interest was the behaviour of  $C_p$  in the region of  $T_g^L$ , already defined from the TBA studies of the copolymers with DOI and DNI as the longer side chain comonomer. In addition, the  $C_p$  behaviour of a series of copolymers from DMI and DHpI was measured. The TBA data for this copolymer system has already been published. (23)

Figure 3.15: Plots of the mechanical damping index ( $-\log 1/n$ ) versus temperature for P(DPrI+DOI) copolymer series. Samples are indicated by the mol ratio code.

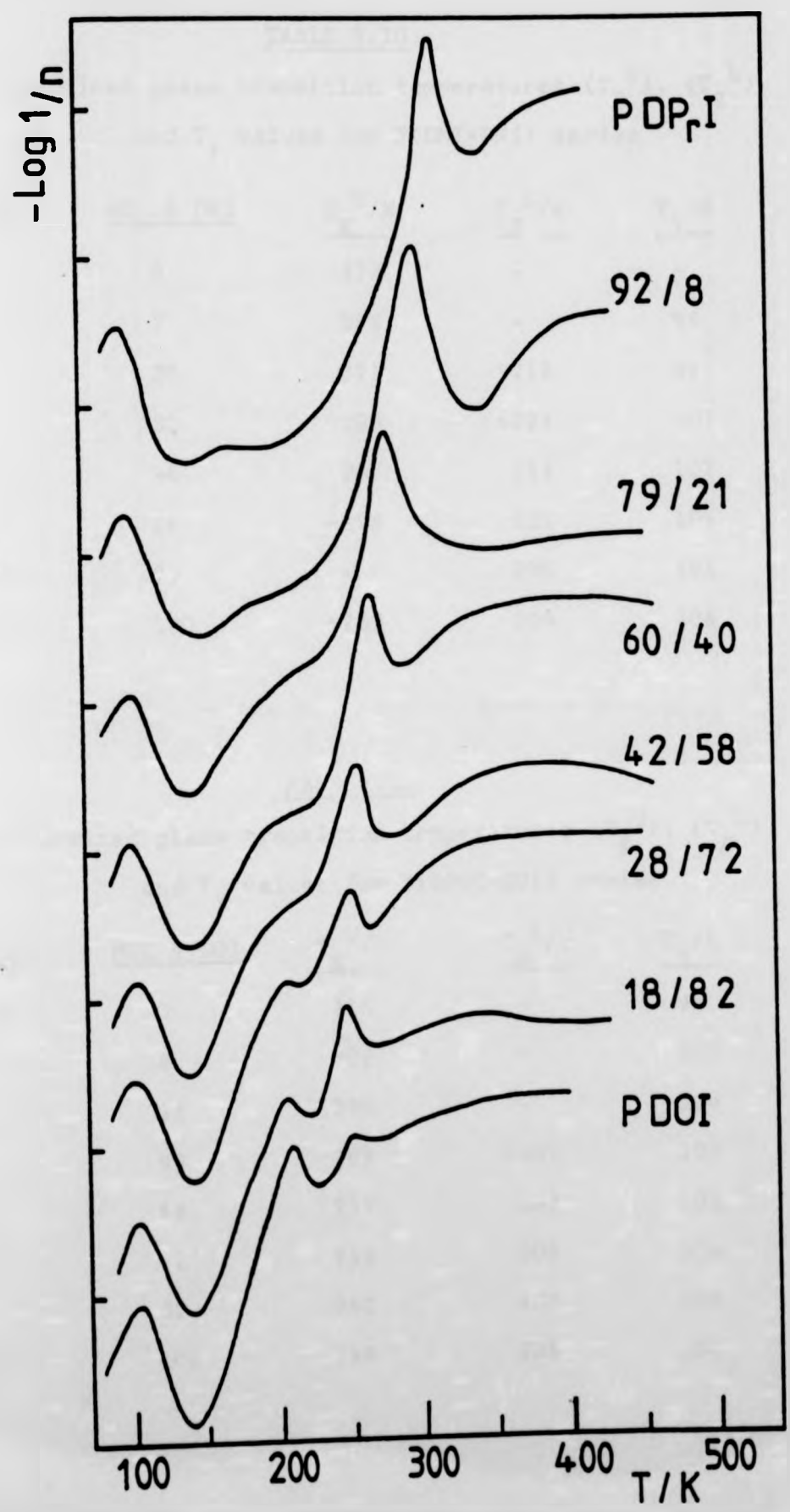


TABLE 3.10

TBA determined glass transition temperatures ( $T_g^U$ ), ( $T_g^L$ )  
and  $T_Y$  values for P(DMI+DNI) series

<u>SAMPLE</u>	<u>MOL.% DNI</u>	<u><math>T_g^U</math>/K</u>	<u><math>T_g^L</math>/K</u>	<u><math>T_Y</math>/K</u>
PDMI	0	373	-	-
1	7	358	-	98
2	20	321	~218	99
3	30	295	~223	103
4	46	267	213	107
5	66	~243	211	108
6	77	-	205	108
PDNI	100	~280	204	108

TABLE 3.11

TBA determined glass transition temperatures ( $T_g^U$ ), ( $T_g^L$ )  
and  $T_Y$  values for P(DPrI+DOI) series

<u>SAMPLE</u>	<u>MOL.% DOI</u>	<u><math>T_g^U</math>/K</u>	<u><math>T_g^L</math>/K</u>	<u><math>T_Y</math>/K</u>
PDPrI	0	315	-	98
1	8	302	-	102
2	21	280	-	104
3	40	269	~201	103
4	58	259	~203	105
5	72	253	205	104
6	82	250	207	105
PDOI	100	248	209	106

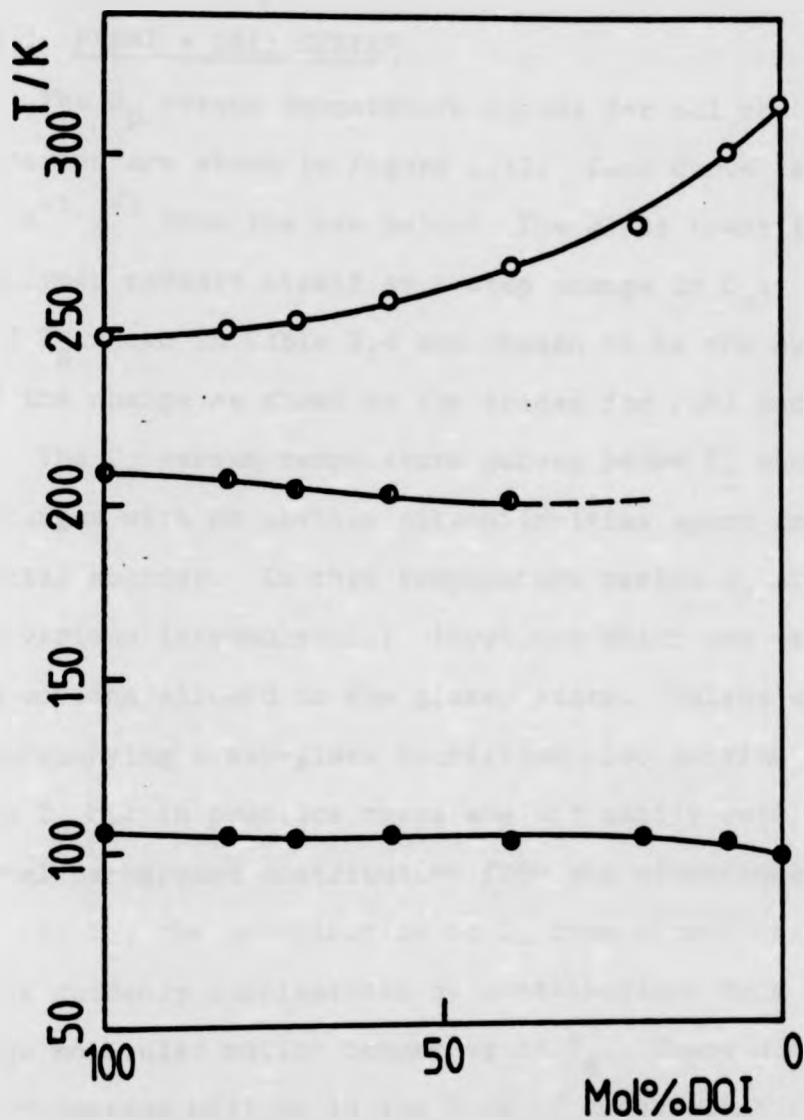


Figure 3.16: Plots of  $T_g^U$  ( $\circ$ ),  $T_g^L$  ( $\bullet$ ), and  $T_g$  ( $\bullet$ ) values versus copolymer composition for P(DPrI+DOI) copolymer series.

### 3.3.1 P(DMI + DBI) SERIES

The  $C_p$  versus temperature curves for all the members of this series are shown in figure 3.17. Each curve is displaced by  $0.5 \text{ J K}^{-1} \text{ g}^{-1}$  from the one below. The glass transition of each copolymer reveals itself as a step change in  $C_p$ . The values of  $T_g$  shown in Table 3.8 are chosen to be the extrapolated onset of the change as shown on the traces for PDBI and PDMI.

The  $C_p$  versus temperature curves below  $T_g$  show only smooth changes with no obvious discontinuities apart from experimental scatter. In this temperature region  $C_p$  arises from the various intramolecular vibrations which are essentially the only motions allowed in the glassy state. Molecular relaxations accompanying a sub-glass transition also provide a contribution to  $C_p$  but in practice these are not easily resolved from the general background contribution from the vibrational modes.<sup>(34)</sup>

At  $T_g$ , the contribution to  $C_p$  from vibrational sources is suddenly supplemented by contributions from the long-range molecular motion occurring at  $T_g$ . These additional degrees of freedom will be in the form of cooperative rotations about the bonds of the polymer backbone and side chains and from translations of long sequences of the polymer as the fluid state is approached. It has also been suggested that some change in the vibrational contribution also occurs at  $T_g$ .<sup>(71)</sup>

The change in heat capacity at  $T_g$  ( $\Delta C_p$ ) is a parameter which is a measure of the degrees of freedom that become frozen in the glass. Wunderlich<sup>(34)</sup> has shown that  $\Delta C_p = 11.5 \text{ J K}^{-1}$  per mole of "beads" where a bead is defined as the smallest section of the solid that can move as a unit in internal rotation.



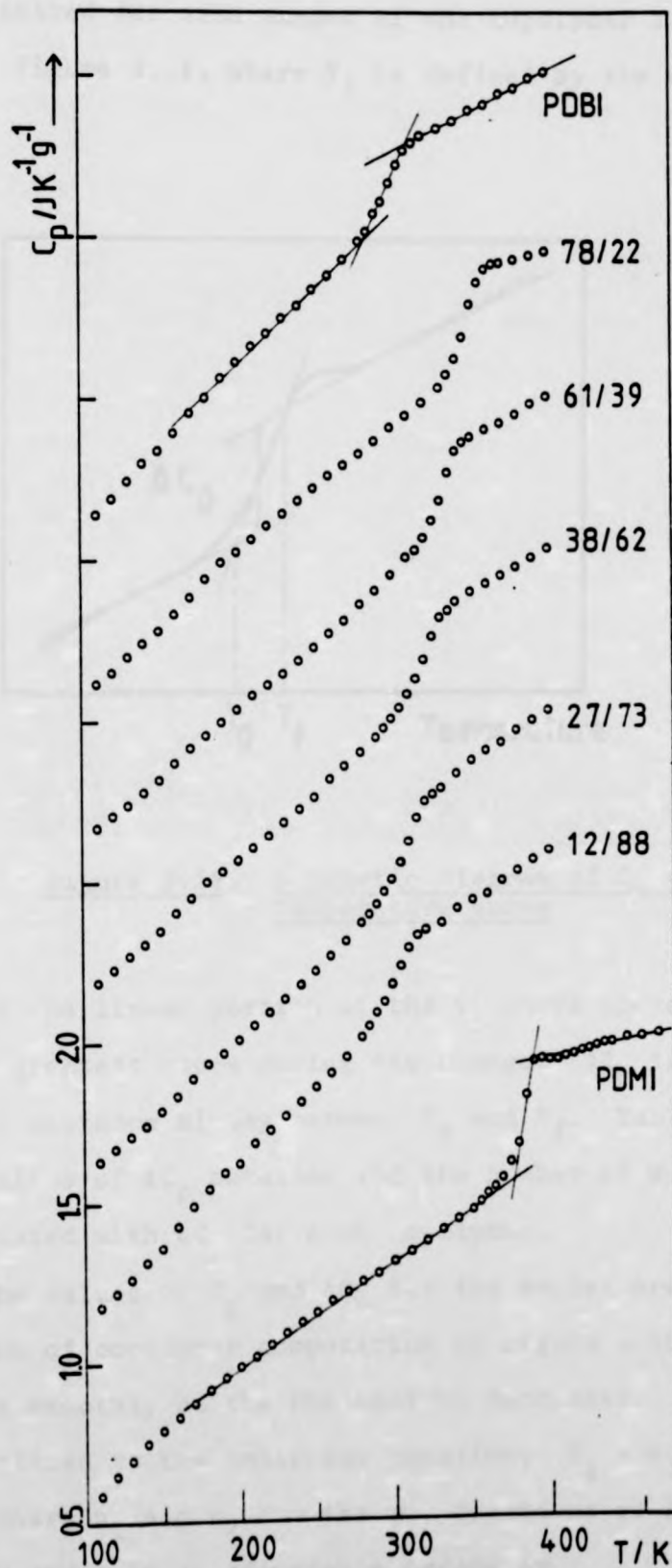


Figure 3.17: Plots of  $C_p/\text{JK}^{-1}\text{g}^{-1}$  versus temperature for P(DMI+DBI) copolymer series.

$\Delta C_p$  was estimated for each member of the copolymer series as shown in figure 3.18, where  $T_f$  is defined by the extrapolated

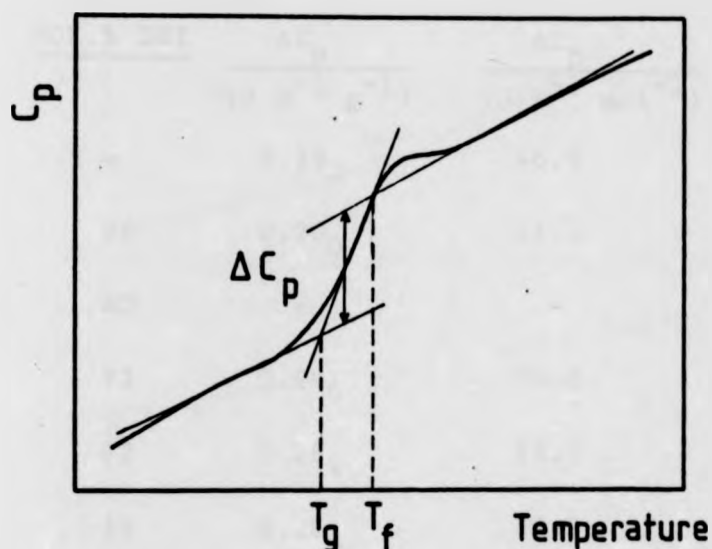


Figure 3.18. Schematic diagram of  $C_p$  versus temperature curve

intersect of the linear portion of the  $C_p$  curve above  $T_g$  with the line of greatest slope during the change.  $\Delta C_p$  is taken as the vertical distance midway between  $T_g$  and  $T_f$ . Table 3.12 shows the values of  $\Delta C_p$  obtained and the number of Wunderlich beads associated with  $\Delta C_p$  for each copolymer.

The values of  $T_g$  and  $\Delta C_p$  for the series are plotted as a function of copolymer composition in figure 3.19.  $T_g$  and  $\Delta C_p$  increase smoothly as the DBI content decreases. The  $T_g$  values are fitted to the empirical equation;  $T_g = n_1 T_{g1} + n_2 T_{g2} + n_1 n_2 K^{(72)}$  where  $n_1$  and  $n_2$  are the mol fractions of DMI and DBI respectively and  $K$  is an adjustable parameter.

TABLE 3.12

$\Delta C_p$  values and the number of Wunderlich beads for P(DMI + DBI) series

<u>SAMPLE</u>	<u>MOL. % DBI</u>	$\Delta C_p$ (J K <sup>-1</sup> g <sup>-1</sup> )	$\Delta C_p$ (J K <sup>-1</sup> mol <sup>-1</sup> )	<u>NUMBER OF BEADS</u>
PDBI	-	0.19 <sub>2</sub>	46.5	4.0
1	88	0.20 <sub>0</sub>	46.4	4.0
2	80	-	-	-
3	73	0.24 <sub>0</sub>	52.6	4.6
4	62	0.25 <sub>4</sub>	53.3	4.6
5	39	0.26 <sub>3</sub>	50.2	4.4
6	22	0.31 <sub>1</sub>	54.7	4.8
PDMI	-	0.35 <sub>2</sub>	55.6	4.8

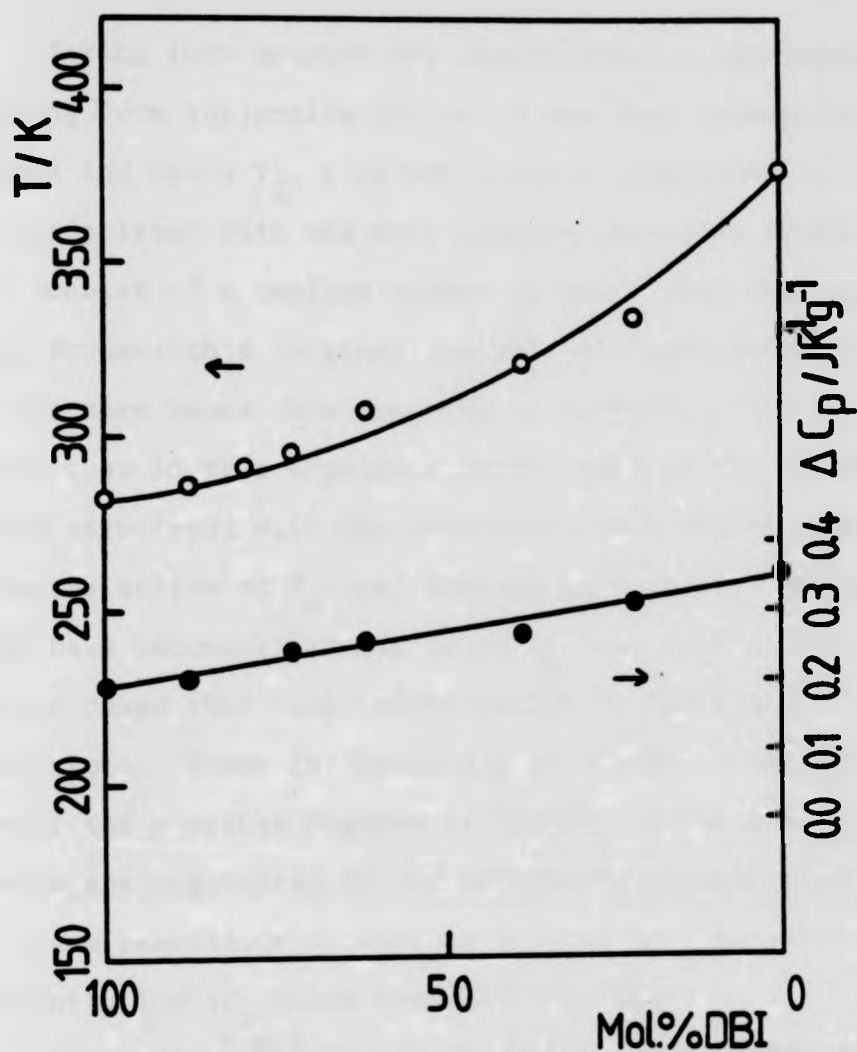


Figure 3.19: Plots of  $T_g$  (—○—), and  $\Delta C_p$  (—●—) values against copolymer composition for P(DMI+DBI) copolymer series.

$T_g$  versus composition curve is fitted to  $T_g = n_1 T_{g1} + n_2 T_{g2} + n_1 n_2 K$  with  $K = -75$ ,  $n_1 = \text{mol fraction of DMI}$  and  $n_2 = \text{mol fraction of DBI}$ .

Taking into account the uncertainty in determining  $\Delta C_p$ , arising from subjective choice of the best extrapolation lines above and below  $T_g$ , a rather unusual conclusion is found. Namely, the polymer with the more complex structure (PDBI) seems to consist of a smaller number of beads than the simpler PDMI. In Wunderlich's original analysis the more complex the polymer the more beads were proposed to contribute to  $\Delta C_p$ . It appears that in this copolymer series some of the degrees of freedom associated with the di-n-butyl side chains that should become active at  $T_g$  (and thereby enhance  $\Delta C_p$ ) are either absent or have become activated below  $T_g$  over such a wide temperature range that their contribution to the glassy state  $C_p$  is unnoticed. There is absolutely no reason to suppose that any of the possible degrees of freedom of the n-butyl side chains are suppressed in the structures studied here so it would seem reasonable to explore a possible explanation of the apparently low  $\Delta C_p$  value obtained for PDBI.

Wunderlich<sup>(34)</sup> has shown that it is possible to estimate the heat capacity of poly(1-butane) from that of polypropylene by adding the heat capacity contribution from a  $\text{CH}_2$  unit and has used a similar additive procedure to deduce  $C_p$  contributions in the polyacrylates. The heat capacity of a  $\text{CH}_2$  unit is taken as that of amorphous polyethylene (per  $\text{CH}_2$  unit) between 50 and 200K. Above 200K, amorphous polyethylene undergoes its glass transition. It is then possible to estimate the heat capacity of PDBI from that of PDMI by adding six times the value of  $C_p$  per mole of  $\text{CH}_2$  units.

Figure 3.20 shows the experimental  $C_p$  versus temperature curve for PDMI and PDBI recalculated per mol of repeat unit. Also

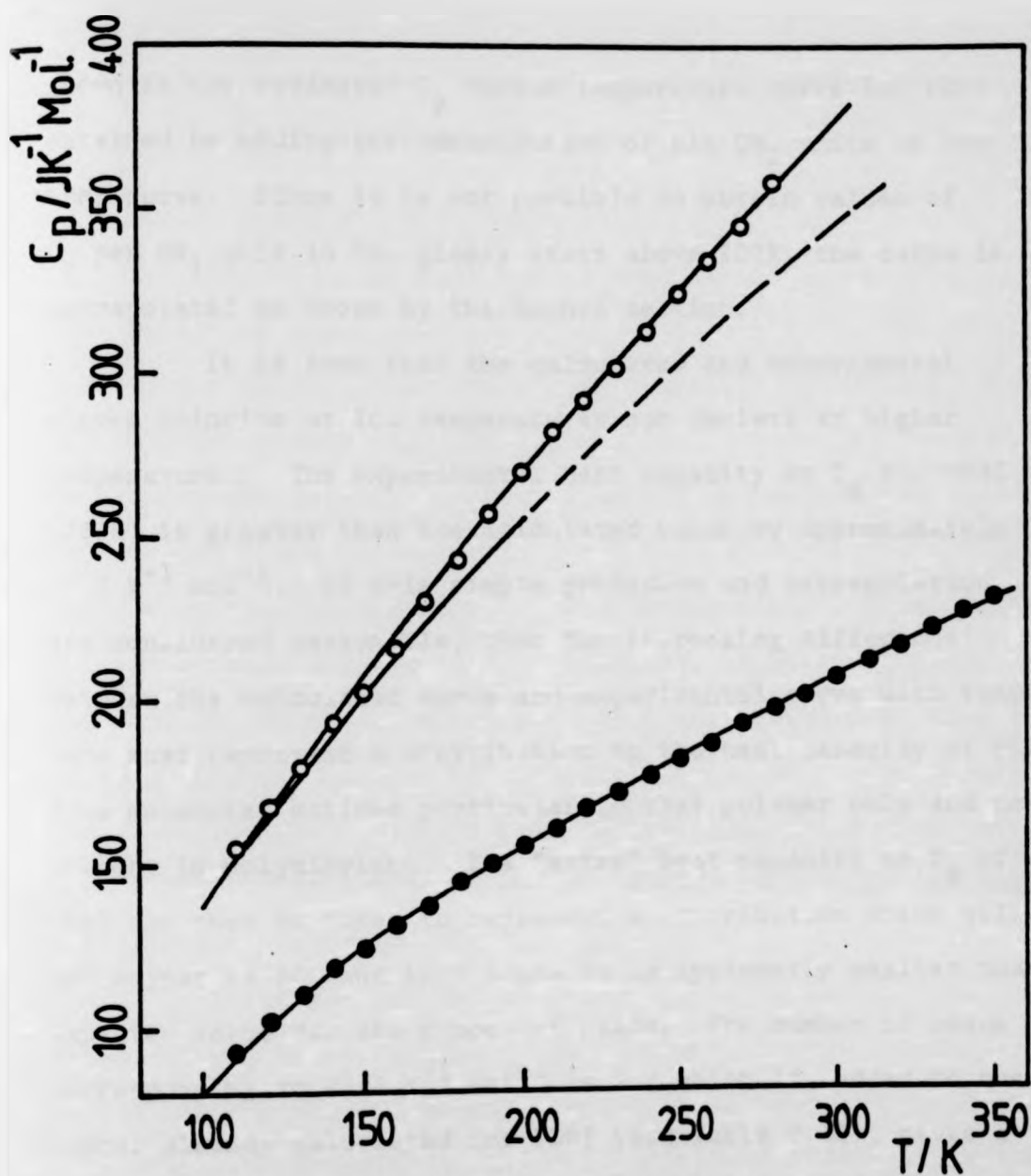


Figure 3.20: Plots of experimental  $C_p/\text{JK}^{-1}\text{mol}^{-1}$  versus temperature for PDMI ( $\bullet$ ) and PDBI ( $\circ$ ).  $C_p$  versus temperature curve for PDBI ( $\text{---}$ ) calculated from the heat capacity of PDMI +  $6 \times C_p$  (polyethylene) from 100 to 200K as described in the text, extrapolated section shown by ( $\text{-----}$ ).

shown is the estimated  $C_p$  versus temperature curve for PDBI obtained by adding the contribution of six  $\text{CH}_2$  units to the PDMI curve. Since it is not possible to obtain values of  $C_p$  per  $\text{CH}_2$  unit in the glassy state above 200K, the curve is extrapolated as shown by the dashed section.

It is seen that the calculated and experimental curves coincide at low temperatures but deviate at higher temperatures. The experimental heat capacity at  $T_g$  for PDBI (282K) is greater than the calculated value by approximately  $27 \text{ J K}^{-1} \text{ mol}^{-1}$ . If this simple procedure and extrapolation are considered reasonable, then the increasing difference between the calculated curve and experimental curve with temperature must represent a contribution to the heat capacity of PDBI from molecular motions particular to that polymer only and not present in polyethylene. The "extra" heat capacity at  $T_g$  of PDBI can then be taken to represent a contribution which will not appear in  $\Delta C_p$  and thus leads to an apparently smaller than expected value for the number of beads. The number of beads corresponding to  $27 \text{ J K}^{-1} \text{ mol}^{-1}$  is 2.3 which if, added to the number already calculated for PDBI (see Table 3.12), gives a total of 6.3 beads. Although a bead is not defined rigorously, a value of 6.3 is more acceptable for PDBI when compared with PDMI (4.8 beads) and PMMA (3-4 beads).<sup>(34)</sup>

What the molecular motions are that occur below  $T_g$  of PDBI are not known. The "extra" heat capacity below  $T_g$  does not agree with the calculated heat capacity from internal rotation of the side chain (see section 3.5.3 for details of this type of analysis). It could be due to limited motions made possible in the glassy state of PDBI (which must possess

greater free volume than PDMI) due to the plasticising effect of the n-butyl side chains.

### 3.3.2 P(DMI + DHpI) SERIES

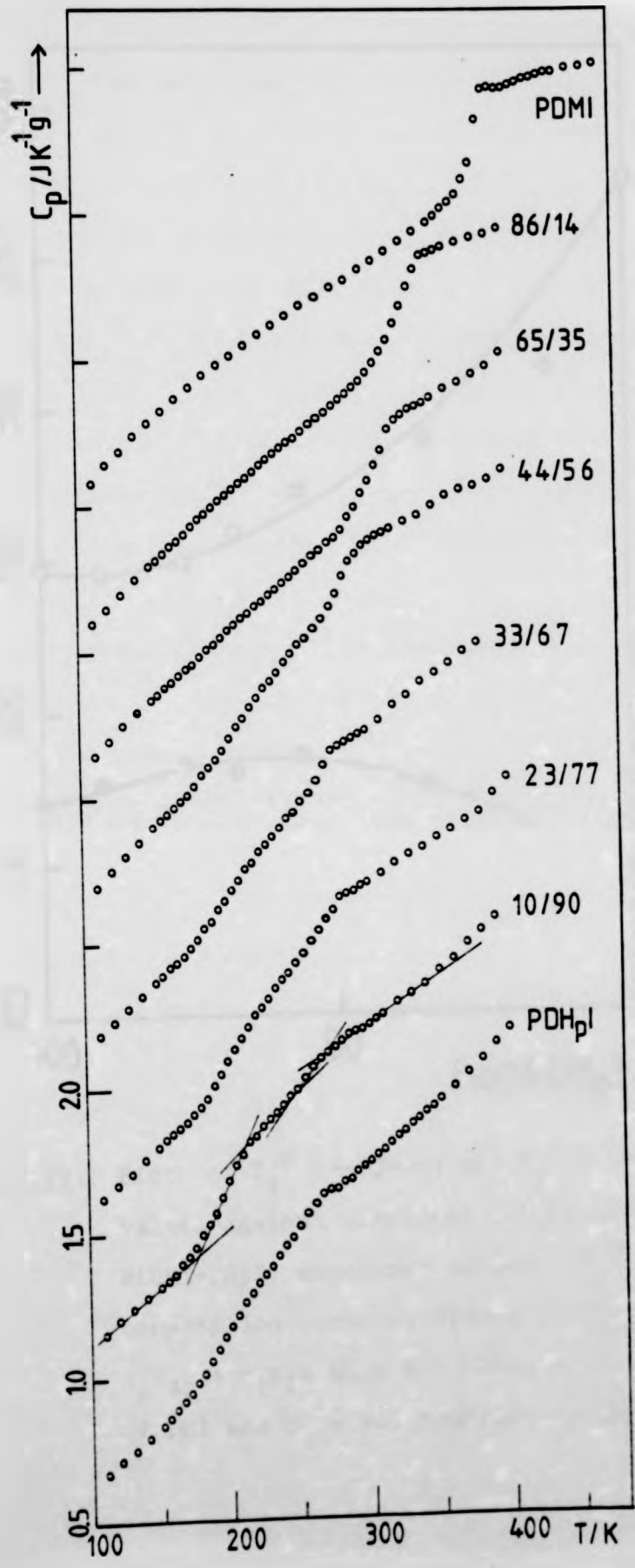
The heat capacity versus temperature curves for this series of copolymers are shown in figure 3.21. It is immediately obvious that the smooth change in  $C_p$  below  $T_g$  for the copolymers with high DMI content is not repeated for other members of the series. For PDHpI itself and copolymers with DMI content of up to 65% there are two discontinuities in the curve with the characteristics of  $T_g$  inflections. These inflections have been defined by the intersections of the linear portions of the curves above and below the transitions with the lines of greatest slope, as indicated on the trace for sample 1. The transition temperatures are then taken as the extrapolated onsets and  $\Delta C_p$  values obtained at the mean temperature of each transition as described earlier.

The higher of the two transitions is composition dependent and moves to higher temperatures, becoming more intense as the DMI content increases. The position of the lower transition is essentially independent of composition but reduces in intensity as the DHpI content decreases. These transitions are thus assigned as the  $T_g^L$  and  $T_g^U$  previously identified by TBA studies on this copolymer system. (23)

Table 3.13 lists the values of both  $T_g^L$  and  $T_g^U$  for each member of the series and these are plotted as functions of copolymer composition in figure 3.22.  $T_g^U$  is a smoothly increasing function of composition as would be expected for the relaxation temperature of the main chain.  $T_g^L$  shows similar



Figure 3.21: Plots of  $C_p / JK^{-1}g^{-1}$  versus temperature for P(DMI+DHpI) copolymer series.



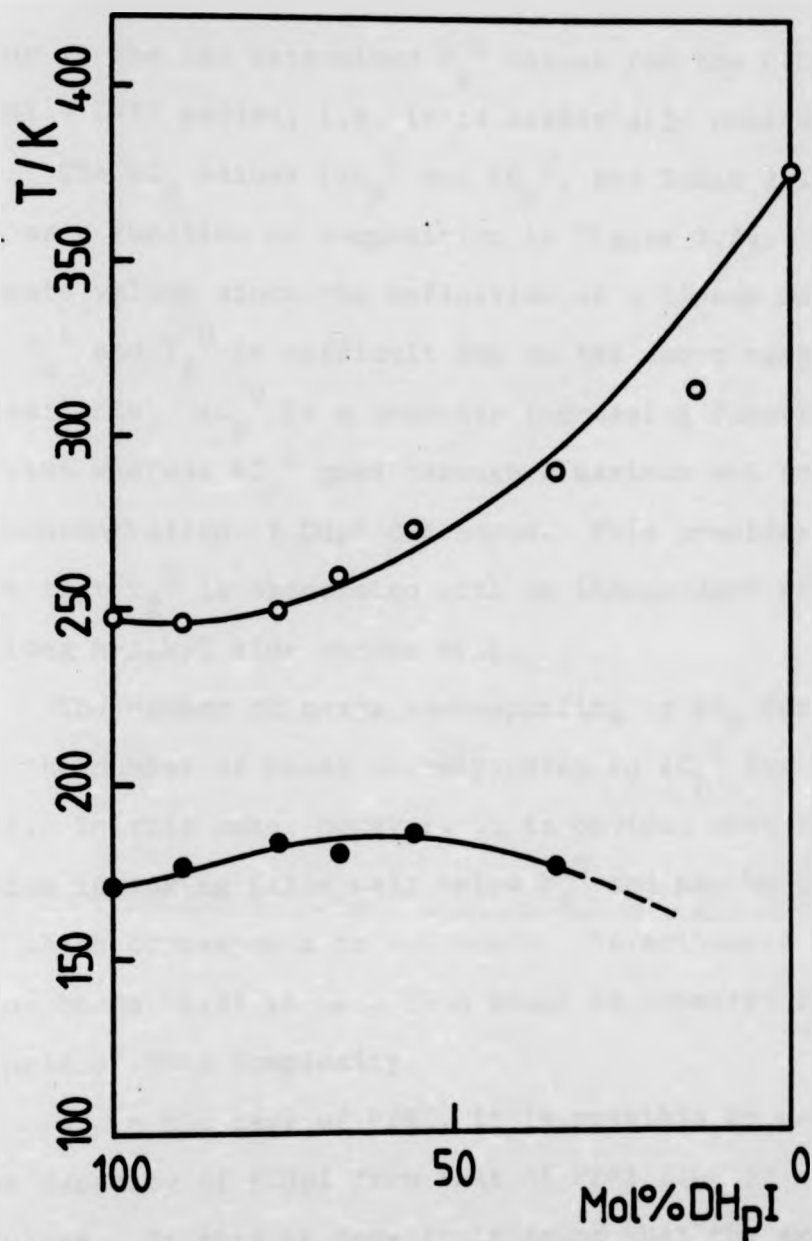


Figure 3.22: Plots of  $T_g^U$  (—○—) and  $T_g^L$  (—●—) values against copolymer composition for P(DMI+DHpI) copolymer series.  $T_g^U$  versus composition curve is fitted to  $T_g^U = n_1 T_{g1} + n_2 T_{g2} + n_1 n_2 K$  with  $K = -155$ ,  $n_1$  = mol fraction of DMI and  $n_2$  = mol fraction of DHpI.

behaviour to the TBA determined  $T_g^L$  values for the P(DMI + DOI) and P(DMI + DNI) series, i.e. it is essentially constant.

The  $\Delta C_p$  values ( $\Delta C_p^L$  and  $\Delta C_p^U$ , see Table 3.13) are plotted as a function of composition in figure 3.23. These are approximate values since the definition of a linear base line between  $T_g^L$  and  $T_g^U$  is difficult due to the short temperature range available.  $\Delta C_p^U$  is a smoothly increasing function of composition whereas  $\Delta C_p^L$  goes through a maximum and then decreases as the concentration of DHpI decreases. This provides further evidence that  $T_g^L$  is associated with an independent relaxation of the long n-alkyl side chains only.

The number of beads corresponding to  $\Delta C_p$  for PDMI is 4.8 and the number of beads corresponding to  $\Delta C_p^U$  for PDHpI is only 1.2. In this case, however, it is obvious that considerable relaxation is taking place well below  $T_g^U$  and may be quantified by  $\Delta C_p^L$  which corresponds to 4.1 beads. Nevertheless the total number of beads (5.3) is less than would be expected for a repeat unit of this complexity.

As in the case of PDBI, it is possible to calculate the heat capacity of PDHpI from that of PDMI plus  $12 \times C_p$  of polyethylene. If this is done it is found that the experimental and calculated  $C_p$  values in the glassy state of PDHpI (100K to ca. 170K) agree closely (within 2.5%). It would seem reasonable then that the total change in  $C_p$  between 170K (glass) and 260K (rubber) should be chosen to give a more realistic measure of the number of beads present. This can be evaluated at  $\sim 0.34 \text{ J K}^{-1} \text{ g}^{-1}$  corresponding to 9.6 beads, and is a much more acceptable value for the complex DHpI unit.

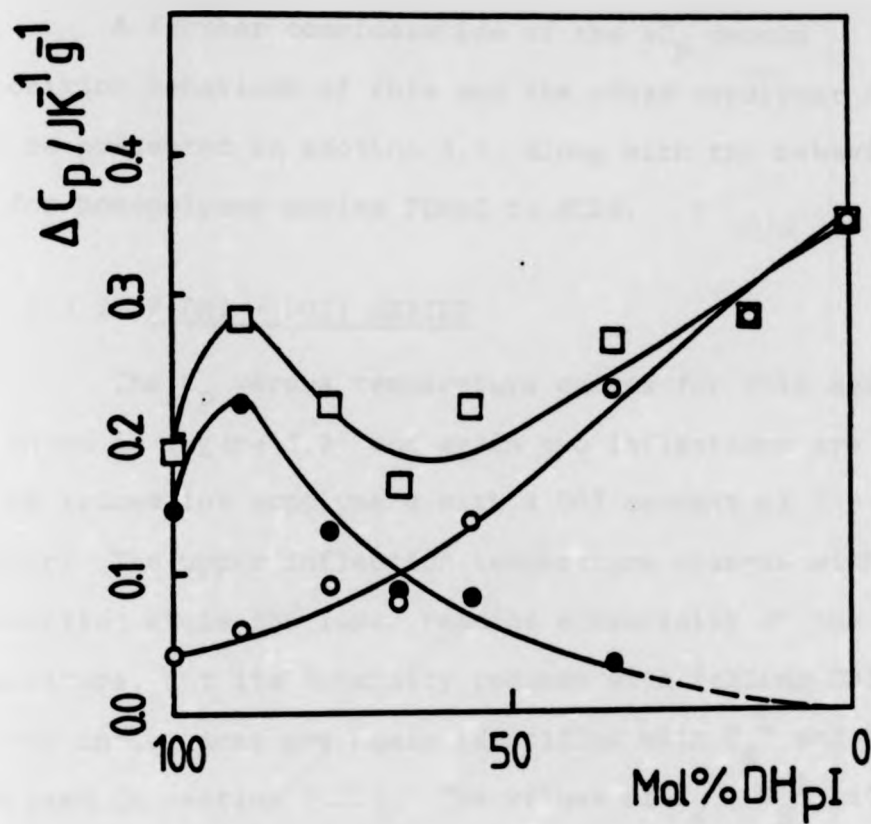


Figure 3.23: Plots of  $\Delta C_p^U$  ( $\circ$ ),  $\Delta C_p^L$  ( $\bullet$ ) and  $\Delta C_p^{tot.}$  ( $\square$ ) values against copolymer composition for P(DMI+DHpI) copolymer series.

A further consideration of the  $\Delta C_p$  versus composition behaviour of this and the other copolymer series will be presented in section 3.4, along with the behaviour of  $\Delta C_p$  for homopolymer series PDHpI to PDDI.

### 3.3.3 P(DMI + DOI) SERIES

The  $C_p$  versus temperature curves for this series are shown in figure 3.24 and again two inflections are found on the traces for copolymers with a DOI content of 36% or greater. The upper inflection temperature changes with composition while the lower remains essentially at the same temperature, but its intensity reduces with falling DOI content. The two inflections are again identified with  $T_g^L$  and  $T_g^U$  as discussed in section 3.2.2. The values of  $T_g^U$ ,  $T_g^L$ ,  $\Delta C_p^U$  and  $\Delta C_p^L$  for the series are listed in Table 3.14.

Figures 3.25 and 3.26 show the behaviour of  $T_g^L$  and  $T_g^U$  and of  $\Delta C_p^L$  and  $\Delta C_p^U$  respectively as a function of copolymer composition.

The number of Wunderlich beads corresponding to  $\Delta C_p^L$  is 8.8 and  $\Delta C_p^U$  is 1.5. Since  $T_g^L$  is associated with the ester side chain, the increase in the number of beads at  $T_g^L$  reflects the increased side chain length. A comparison of all  $\Delta C_p$  data will be given later.

### 3.3.4 P(DMI + DNI) SERIES

The  $C_p$  versus temperature data for this series are displayed in figure 3.27 and the extent to which  $T_g^L$  now dominates the heat capacity behaviour is obvious in the traces

Figure 3.24: Plots of  $C_p/JK^{-1}g^{-1}$  versus temperature for P(DMI+DOI) copolymer series.

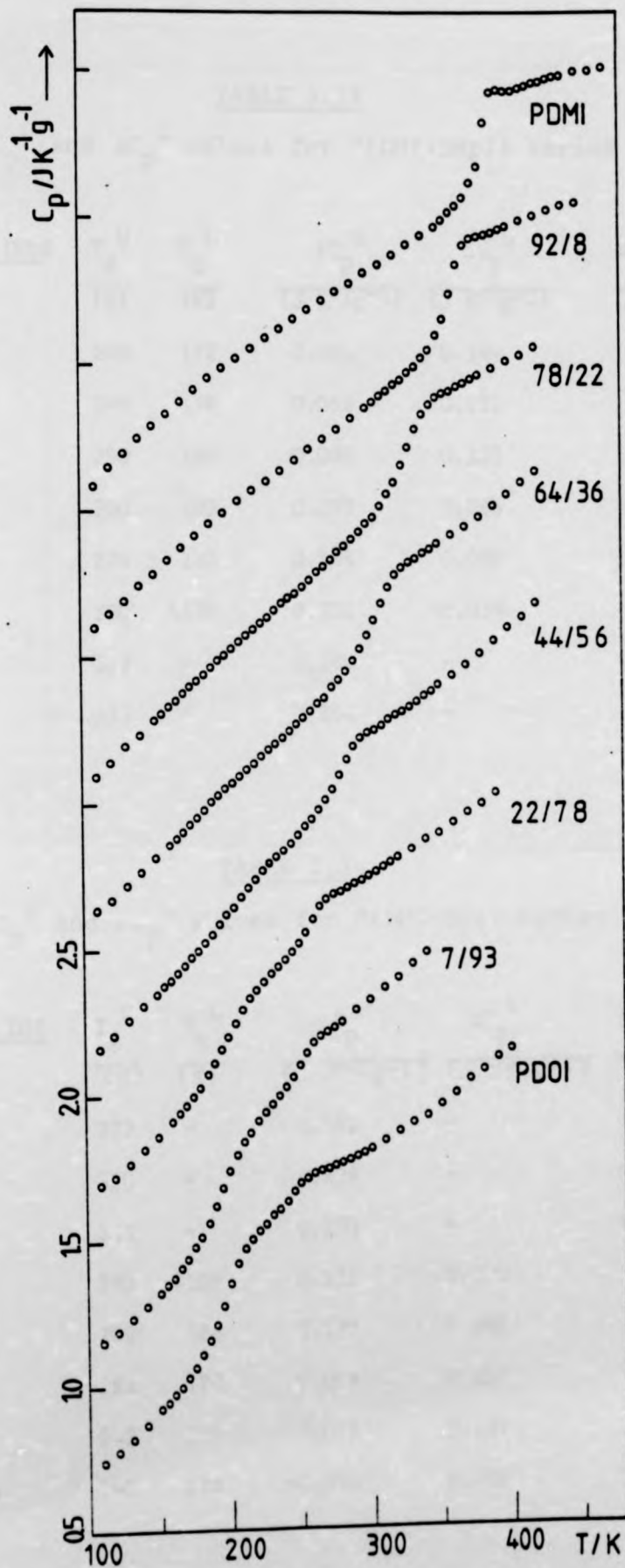


TABLE 3.13

 $T_g^U$ ,  $T_g^L$ ,  $\Delta C_p^U$  and  $\Delta C_p^L$  values for P(DMI+DHpI) series

SAMPLE	MOL.% DHpI	$T_g^U$ (K)	$T_g^L$ (K)	$\Delta C_p^U$ (J K <sup>-1</sup> g <sup>-1</sup> )	$\Delta C_p^L$ (J K <sup>-1</sup> g <sup>-1</sup> )	$\Delta C_p$ (TOTAL) (J K <sup>-1</sup> g <sup>-1</sup> )
PDHPI	100	248	172	0.043	0.144	0.187
1	90	246	176	0.059	0.221	0.280
2	77	250	183	0.089	0.130	0.219
3	67	260	180	0.077	0.085	0.162
4	56	274	185	0.136	0.082	0.218
5	35	290	~176	0.231	~0.034	0.265
6	14	312	-	0.284	-	~0.284
PDMI	0	377	-	0.352	-	0.352

TABLE 3.14

 $T_g^U$ ,  $T_g^L$ ,  $\Delta C_p^U$  and  $\Delta C_p^L$  values for P(DMI+DOI) series

SAMPLE	MOL.% DOI	$T_g^U$ (K)	$T_g^L$ (K)	$\Delta C_p^U$ (J K <sup>-1</sup> g <sup>-1</sup> )	$\Delta C_p^L$ (J K <sup>-1</sup> g <sup>-1</sup> )	$\Delta C_p$ (TOTAL) (J K <sup>-1</sup> g <sup>-1</sup> )
PDMI	0	377	-	0.352	-	0.352
1	8	350	-	0.338	-	~0.338
2	22	313	-	0.270	-	~0.270
3	36	290	~185	0.216	~0.020	0.236
4	56	269	188	0.130	0.046	0.176
5	78	252	178	0.068	0.152	0.220
6	93	242	175	0.055	0.237	0.292
PDOI	100	240	178	~0.049	0.285	0.334

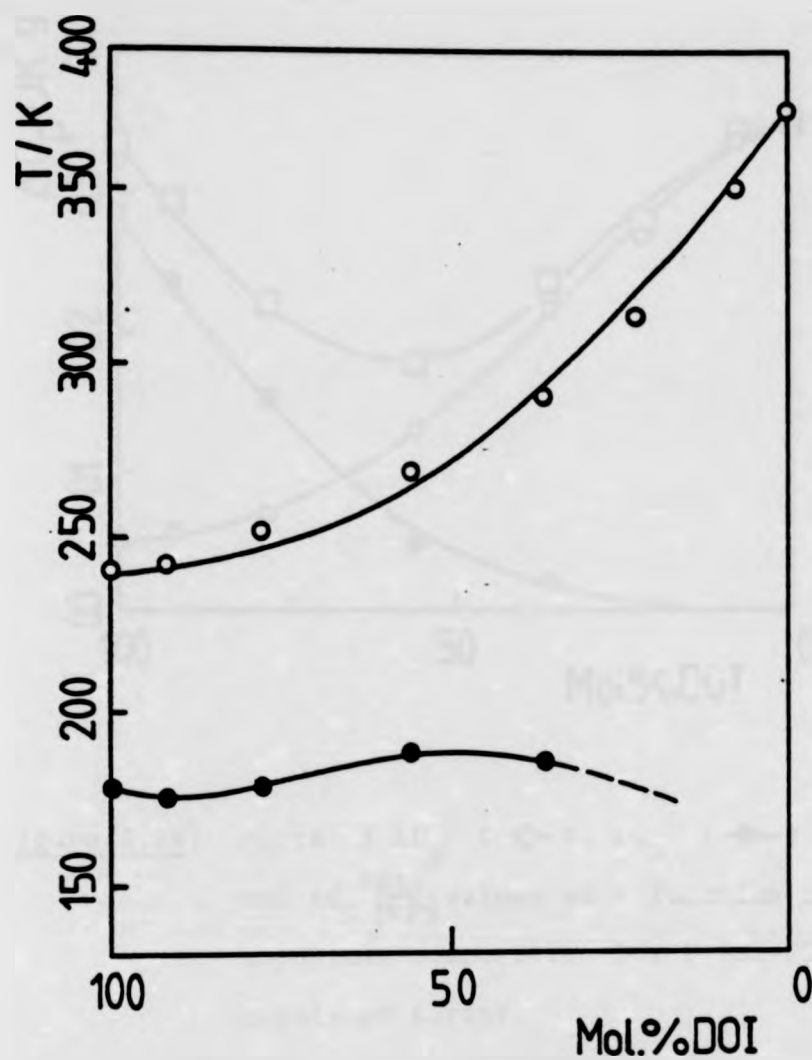


Figure 3.25: Plots of  $T_g^U$  (—○—) and  $T_g^L$  (—●—) values against copolymer composition for P(DMI+DOI) copolymer series.  $T_g^U$  versus composition curve is fitted to  $T_g = n_1 T_{g1} + n_2 T_{g2} + n_1 n_2 K$  with  $K = -140$ ,  $n_1 =$  mol fraction of DMI and  $n_2 =$  mol fraction of DOI.



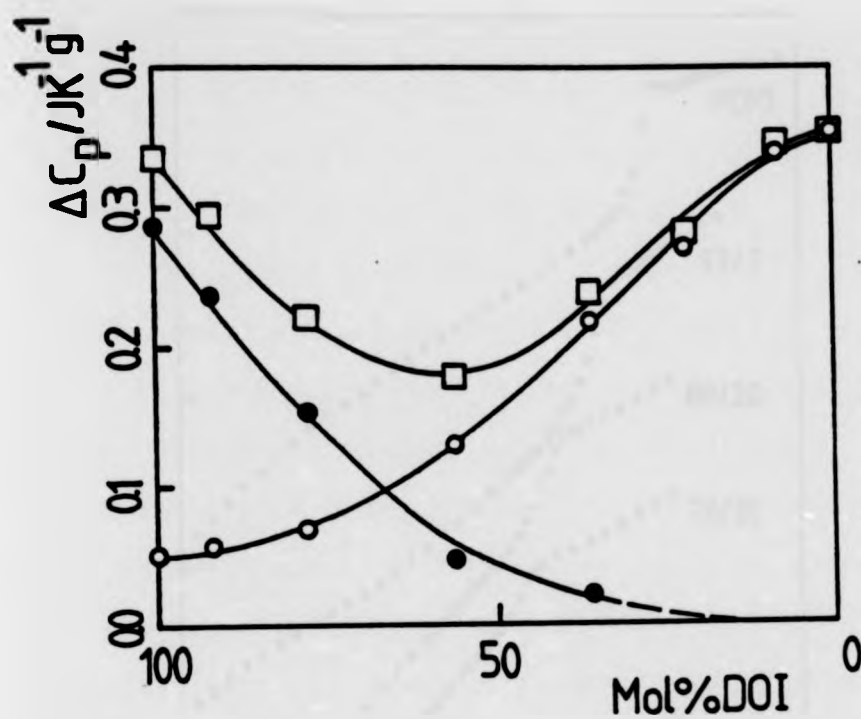
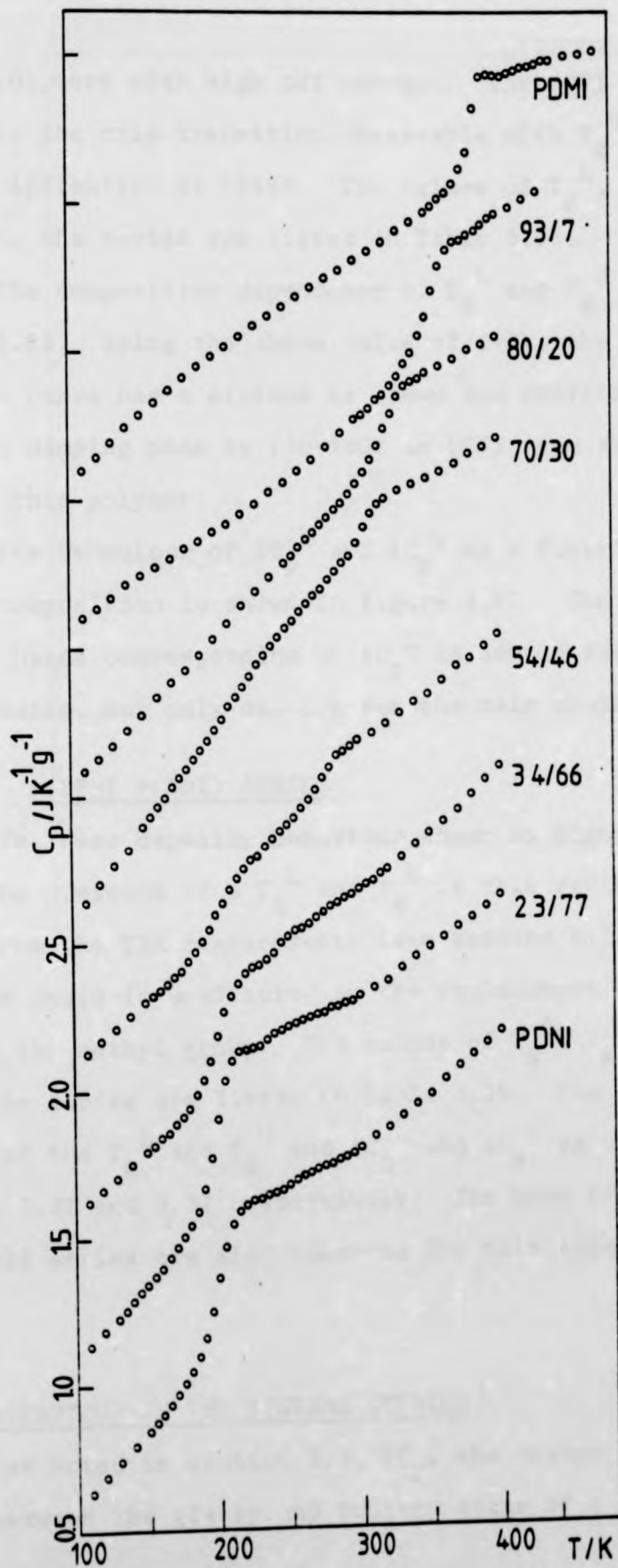


Figure 3.26: Plots of  $\Delta C_p^U$  (—○—),  $\Delta C_p^L$  (—●—) and  $\Delta C_p^{tot.}$  (—□—) values as a function of copolymer composition for P(DMI+DOI) copolymer series.

Figure 3.27: Plots of  $C_p / JK^{-1}g^{-1}$  versus temperature for P(DMI+DNI) copolymer series.



for the copolymers with high DNI content. For PDNI itself  $T_g^L$  is virtually the only transition observable with  $T_g^U$  appearing as a faint inflection at  $\sim 245K$ . The values of  $T_g^L$ ,  $T_g^U$ ,  $\Delta C_p^L$  and  $\Delta C_p^U$  for the series are listed in Table 3.15.

The composition dependence of  $T_g^L$  and  $T_g^U$  is shown in figure 3.28. Using the above value of  $245K$ , the  $T_g^U$  versus composition curve has a minimum as shown and confirms the assignment of the damping peak at  $270-280K$  in PDNI (see section 3.2.3) as  $T_g^U$  for this polymer.

The behaviour of  $\Delta C_p^L$  and  $\Delta C_p^U$  as a function of copolymer composition is shown in figure 3.29. The number of Wunderlich beads corresponding to  $\Delta C_p^L$  is now 15 for the long DNI side chains, but only ca. 1.1 for the main chain transition.

### 3.3.5 P(DPrI + DOI) SERIES

The heat capacity behaviour shown in figure 3.30 confirms the presence of a  $T_g^L$  and  $T_g^U$  in this series also. As expected from the TBA measurements (see section 3.2.4) the longer side chain is unaffected by the replacement of the n-propyl groups for the methyl group. The values of  $T_g^U$ ,  $T_g^L$ ,  $\Delta C_p^U$  and  $\Delta C_p^L$  for the series are listed in Table 3.16. The composition behaviour of the  $T_g^L$  and  $T_g^U$  and  $\Delta C_p^L$  and  $\Delta C_p^U$  values are shown in figures 3.31 and 3.32 respectively. The same trends as P(DMI + DOI) series are also observed for this copolymer system.

## 3.4 $\Delta C_p$ BEHAVIOUR IN THE SYSTEMS STUDIED

As noted in section 3.3,  $\Delta C_p$ , the change in heat capacity between the glassy and rubbery state of a polymer,

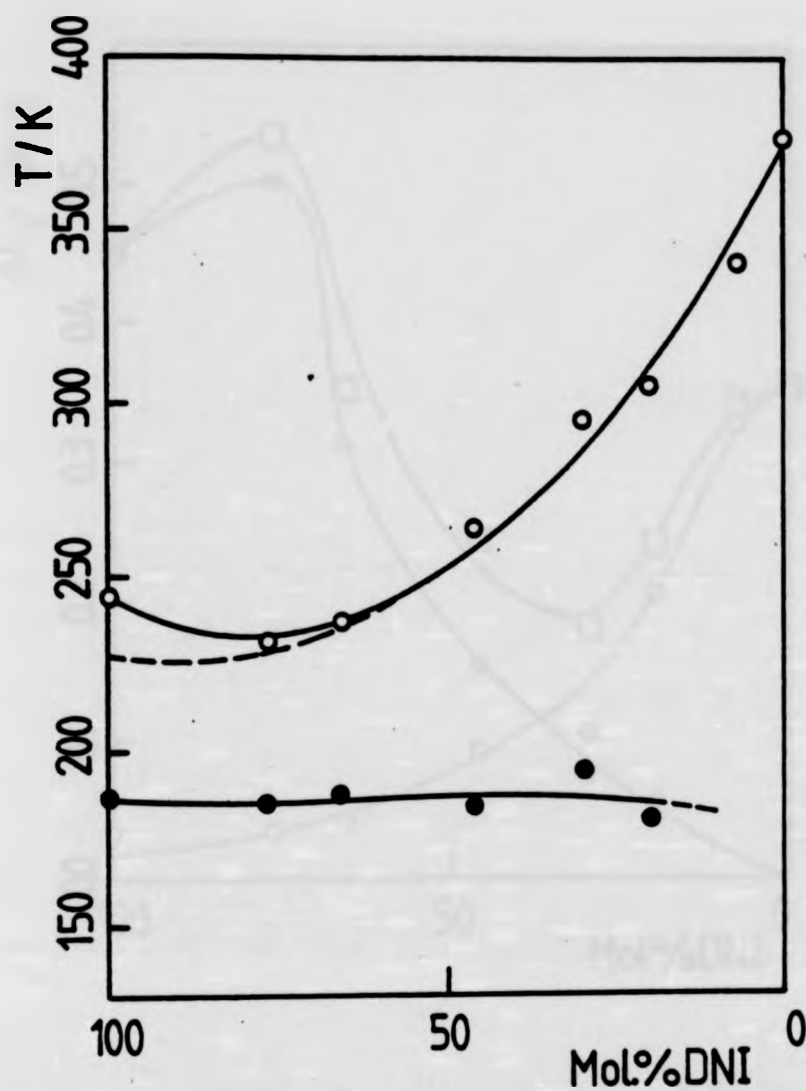


Figure 3.28: Plots of  $T_g^U$  (—○—) and  $T_g^L$  (—●—) values against copolymer composition for P(DMI+DNI) series.  $T_g^U$  versus composition curve is fitted to  $T_g = n_1 T_{g1} + n_2 T_{g2} + n_1 n_2 K$  with  $K = -230$ ,  $n_1$  = mol fraction of DMI and  $n_2$  = mol fraction of DNI.

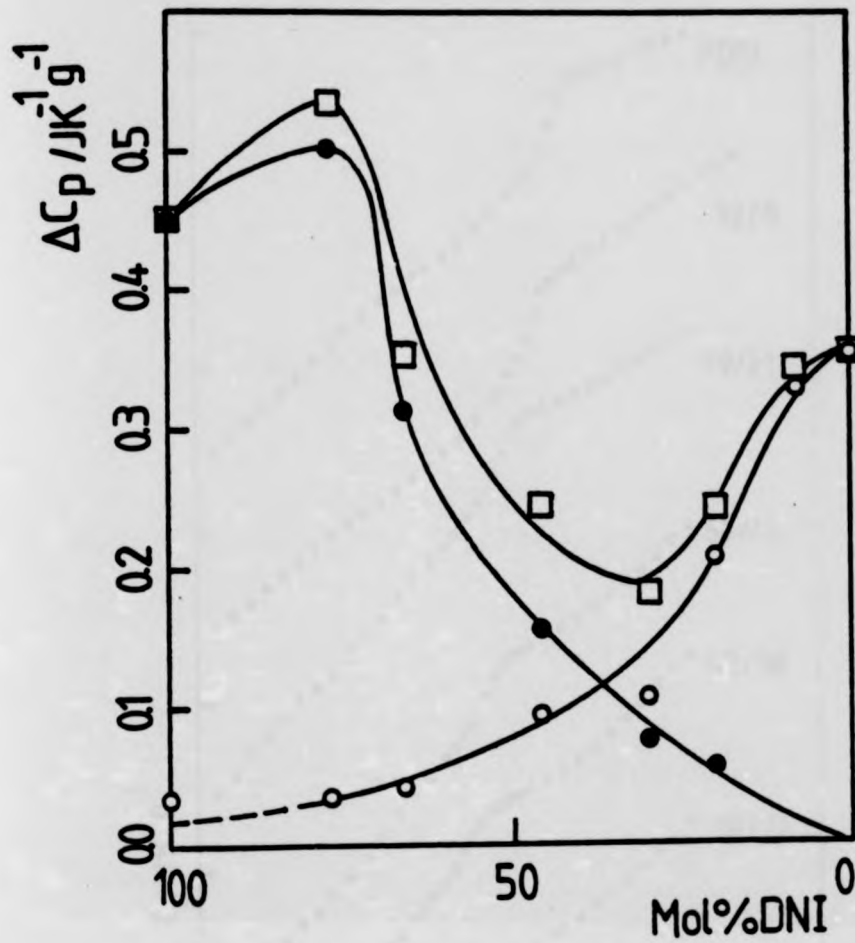


Figure 3.29: Plots of  $\Delta C_p^U$  (—○—),  $\Delta C_p^L$  (—●—) and  $\Delta C_p^{tot.}$  (—□—) values as a function of copolymer composition for P(DMI+DNI) copolymer series.

Figure 3.30: Plots of  $C_p/JK^{-1}g^{-1}$  versus temperature for P(DPrI+DOI) copolymer series.

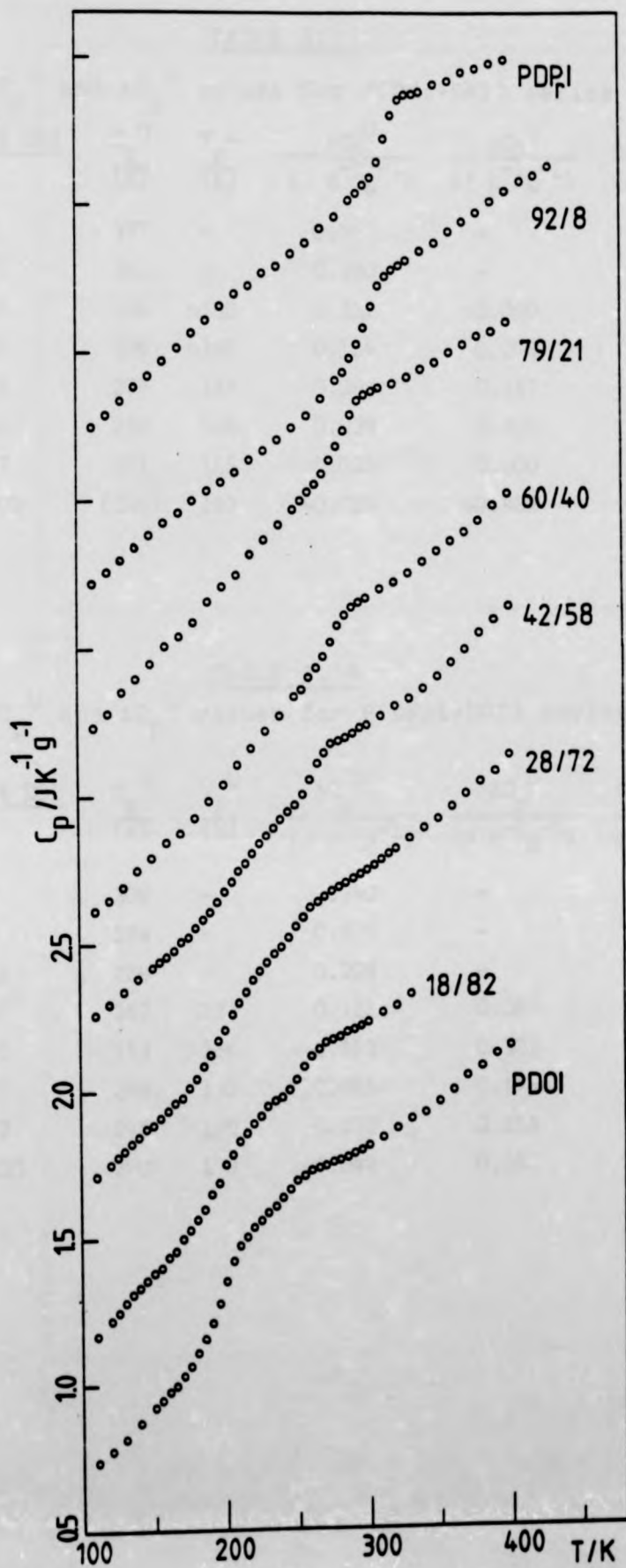


TABLE 3.15

 $T_g^U$ ,  $T_g^L$ ,  $\Delta C_p^U$  and  $\Delta C_p^L$  values for P(DMI+DNI) series

SAMPLE	MOL.% DNI	$T_g^U$ (K)	$T_g^L$ (K)	$\Delta C_p^U$ (J K <sup>-1</sup> g <sup>-1</sup> )	$\Delta C_p^L$ (J K <sup>-1</sup> g <sup>-1</sup> )	$\Delta C_p$ (TOTAL) (J K <sup>-1</sup> g <sup>-1</sup> )
PDMI	0	377	-	0.352	-	0.352
1	7	341	-	0.330	-	~0.330
2	20	306	~180	0.212	~0.030	~0.242
3	30	296	~195	0.104	0.076	0.180
4	46	264	184	0.093	0.157	0.244
5	66	238	188	0.038	0.314	0.352
6	77	231	185	0.035	0.500	0.535
PDNI	100	(245)	187	~0.034	~0.487	~0.521

TABLE 3.16

 $T_g^U$ ,  $T_g^L$ ,  $\Delta C_p^U$  and  $\Delta C_p^L$  values for P(DPrI+DOI) series

SAMPLE	MOL.% DOI	$T_g^U$ (K)	$T_g^L$ (K)	$\Delta C_p^U$ (J K <sup>-1</sup> g <sup>-1</sup> )	$\Delta C_p^L$ (J K <sup>-1</sup> g <sup>-1</sup> )	$\Delta C_p$ (TOTAL) (J K <sup>-1</sup> g <sup>-1</sup> )
PDPri	0	304	-	0.250	-	0.250
1	8	284	-	0.274	-	~0.274
2	21	264	-	0.209	-	~0.209
3	40	257	188	0.181	0.067	0.248
4	58	253	186	0.113	0.103	0.216
5	72	248	182	0.065	0.176	0.241
6	82	245	180	0.070	0.213	0.283
PDOI	100	240	178	~0.049	0.285	0.334

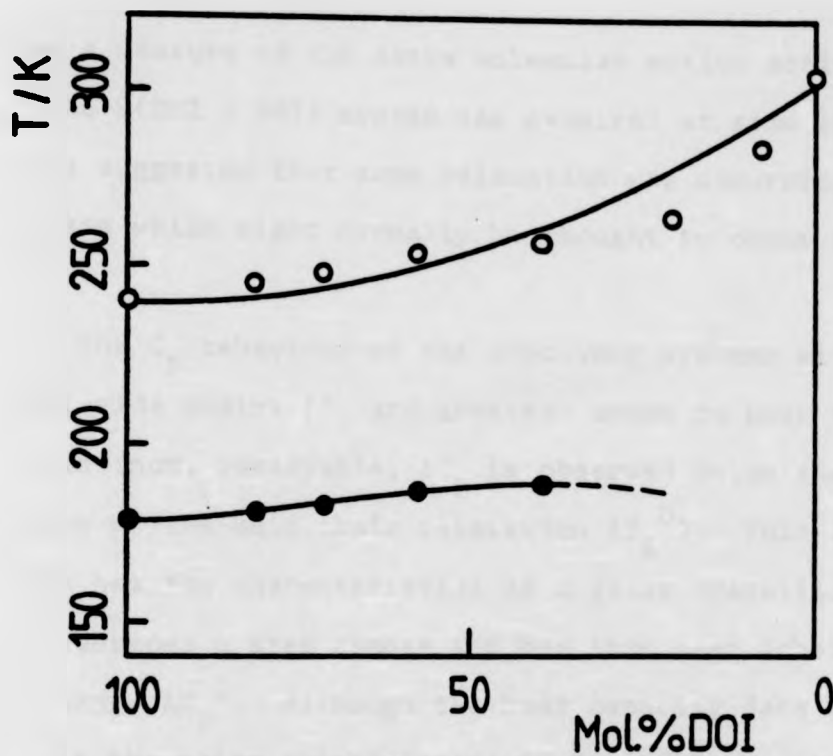


Figure 3.31: Plots of  $T_g^U$  (—○—) and  $T_g^L$  (—●—) values against copolymer composition for P(DPrI+DOI) copolymer series.  $T_g^U$  versus composition curve is fitted to  $T_g = n_1 T_{g1} + n_2 T_{g2} + n_1 n_2 K$  with  $K = -70$ ,  $n_1$  = mol fraction of DPrI and  $n_2$  = mol fraction of DOI.

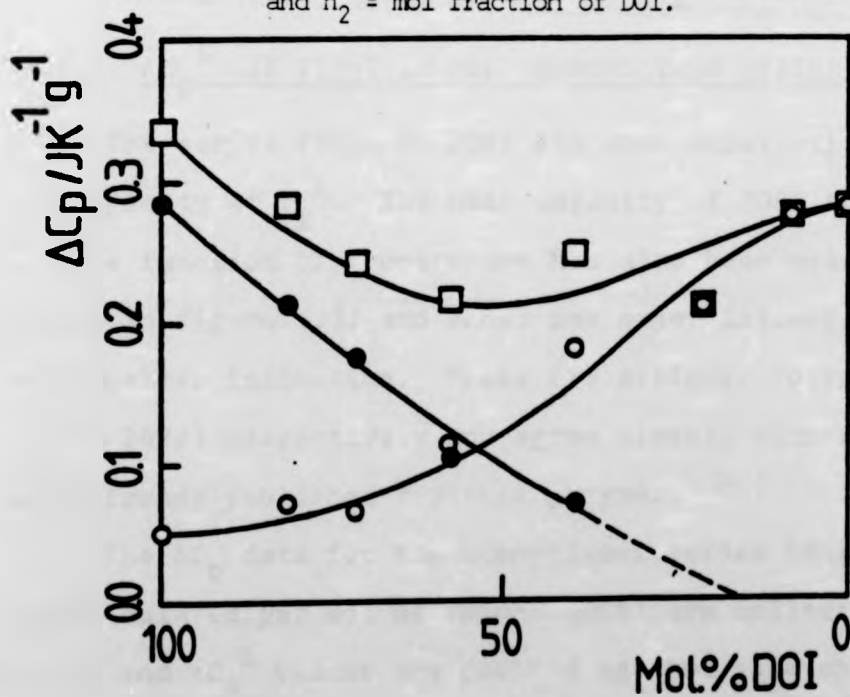


Figure 3.32: Plots of  $\Delta C_p^U$  (—○—),  $\Delta C_p^L$  (—●—) and  $\Delta C_p^{\text{tot.}}$  (—□—) values as a function of copolymer composition for P(DPrI+DOI) copolymer series.



should be a measure of the extra molecular motion activated at  $T_g$ . The P(DMI + DBI) system was examined at some length and it was suggested that some relaxation was occurring in the glassy state which might normally be thought to occur only at  $T_g$ .

The  $C_p$  behaviour of the copolymer systems with longer di-n-alkyl side chains ( $C_7$  and greater) seems to bear this out, since a distinct, observable,  $\Delta C_p$  is observed below the temperature of the main chain relaxation ( $T_g^U$ ). This lower transition has the characteristics of a glass transition in that  $C_p$  undergoes a step change and has thus been labelled  $T_g^L$  and the change  $\Delta C_p^L$ . Although the heat capacity data suggest that  $T_g^L$  is the major change (since  $\Delta C_p^L > \Delta C_p^U$  when the content of the longer side chain is high) it is not the temperature at which the polymer softens, this occurs at  $T_g^U$  (73)

#### 3.4.1 $\Delta C_p^L$ FOR PDHpI TO PDDI HOMOPOLYMER SERIES

The series PDHpI to PDNI all show substantial changes in heat capacity at  $T_g^L$ . The heat capacity of PDDI ( $C_{10}$  side chain) as a function of temperature has also been measured and is plotted in figure 3.33 and shows one major inflection plus one much smaller inflection. These are assigned to  $T_g^L$  (191K) and  $T_g^U$  ( $\sim 262K$ ) respectively and agree closely with DSC and TBA data already published for this polymer. (24)

The  $\Delta C_p$  data for the homopolymer series PDHpI to PDDI (recalculated per mol of repeat unit) are collected in Table 3.17 and  $\Delta C_p^L$  values are plotted against side chain length in figure 3.34.

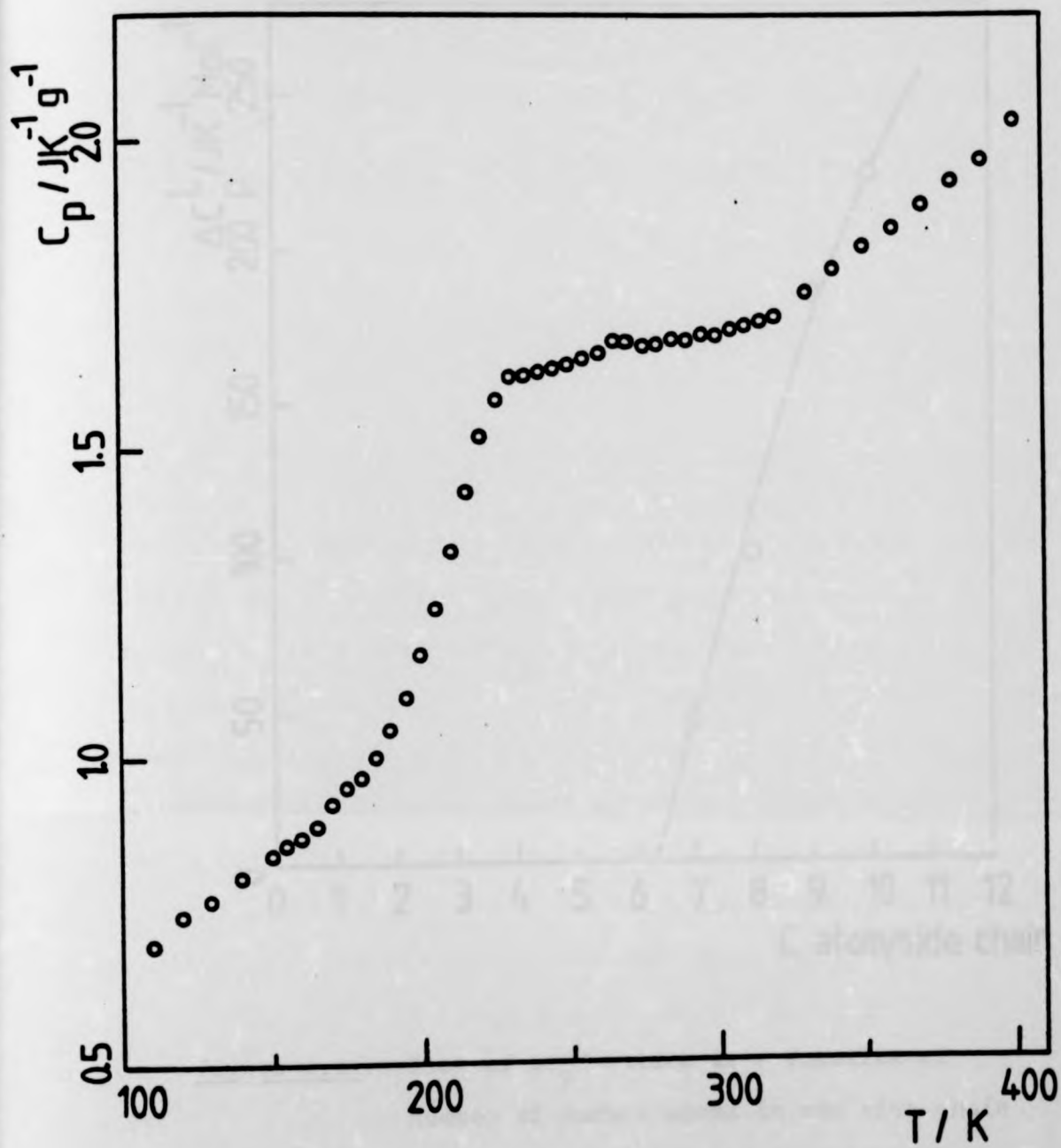


Figure 3.33: Plot of  $C_p / \text{JK}^{-1}\text{g}^{-1}$  versus temperature for PDDI.

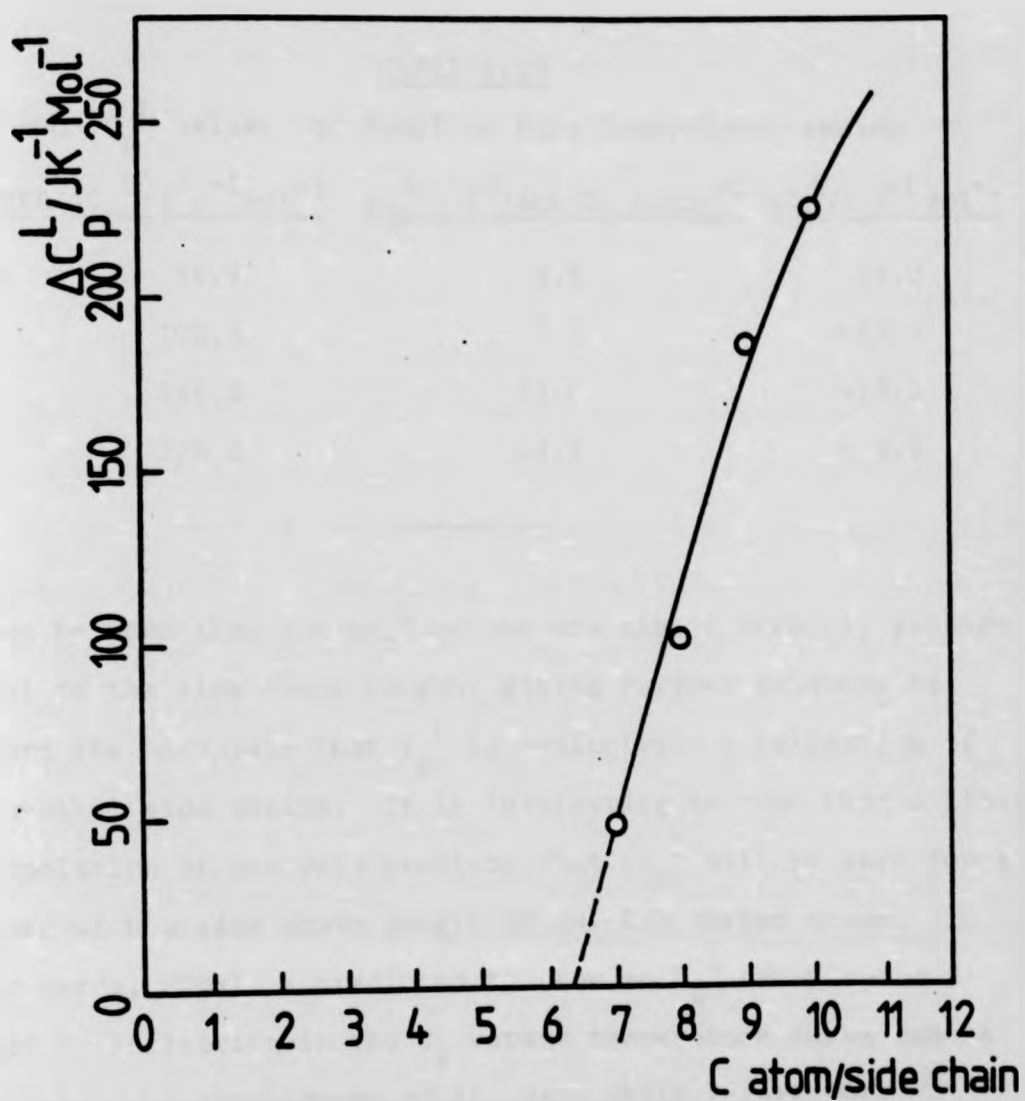


Figure 3.34: Plot of  $\Delta C_p^L$  values as a function of number of carbon atoms in one side chain for PDHpI to PDDI homopolymer series.

TABLE 3.17

$\Delta C_p^U$  and  $C_p^L$  values for PDHpI to PDDI homopolymer series

POLYMER	$\Delta C_p^L / J K^{-1} mol^{-1}$	$\Delta C_p^L / J K^{-1} (mol CH_2 \text{ units})^{-1}$	$\Delta C_p^U / J K^{-1} mol^{-1}$
PDHpI	46.9	3.9	14.0
PDOI	100.9	7.2	~17.3
PDNI	186.0	11.6	~13.0
PDDI	225.1	12.5	~ 8.2

It can be seen that the  $\Delta C_p^L$  values are almost directly proportional to the side chain length, giving further evidence to support the postulate that  $T_g^L$  is exclusively a relaxation of the n-alkyl side chains. It is interesting to note that a linear extrapolation of the data predicts that  $\Delta C_p^L$  will be zero for a polymer with a side chain length of ca. 6.3 carbon atoms. In other words, PDHxI is predicted to show no  $T_g^L$  behaviour and indeed no inflection in the  $C_p$  versus temperature curve can be seen below the temperature of the main chain relaxation. (21)

The values of  $\Delta C_p^L$  are not available for polymers with n-alkyl side chains containing more than ca. 11 carbon atoms (24) since side chain crystallisation occurs and the systems are no longer amorphous. An upper limit to  $\Delta C_p^L$  (in the absence of crystallisation) for an infinitely long n-alkyl side chain would be the value of  $\Delta C_p$  (per mol of  $CH_2$  units) at the glass transition of amorphous polyethylene. This can be estimated from published data (34) as ca.  $15.4 J K^{-1} mol^{-1}$  which is sensibly higher than the  $\Delta C_p^L$  values obtained here.

The values of  $\Delta C_p^U$  for the homopolymer series PDHpI to PDDI show no dramatic or identifiable changes with increasing side chain length as would be expected if  $T_g^U$  represents the onset of the main chain motion only.

The  $\Delta C_p$  behaviour as a function of side chain length thus furnishes further evidence for the assignment of  $T_g^L$  to side chain relaxation and  $T_g^U$  to main chain relaxation. The appearance of two such separate relaxations for the same polymer implies that there is little or no mixing on the molecular scale between the main and side chains. Molecular models of itaconate polymers confirm this. The main chain of a poly di-n-alkyl itaconate is almost completely shielded by the pendant ester linkages which provide a polar "barrier" to the approach of an n-alkyl side chain unit. Polymers with long n-alkyl side chains are thus visualised as "comb-type" copolymers where the side chains are densely packed in the regions of space round the polymer backbone but do not penetrate or entangle with the backbone itself.

#### 3.4.2 $\Delta C_p$ BEHAVIOUR IN THE COPOLYMER SYSTEMS

For four copolymer series, plots of  $\Delta C_p^U$  and  $\Delta C_p^L$  values as a function of copolymer composition are shown in figures 3.23, 3.26, 3.29 and 3.32. In every case  $\Delta C_p^U$  values increase smoothly as the mol % of the shorter side chain ester increases and  $\Delta C_p^L$  values decrease as the mole % of the longer side chain ester decreases. In two cases maxima in  $\Delta C_p^L$  are present before the decrease occurs (P(DMI + DHpI) and P(DMI + DNI)). The total  $\Delta C_p^{tot} = \Delta C_p^L + \Delta C_p^U$  values go through a minimum in every copolymer system.

$\Delta C_p^L$  values (recalculated per mol of repeat unit) are plotted for the four copolymer systems as a function of copolymer composition in figure 3.35. In every system  $\Delta C_p^L$  decreases as the mole fraction of the longer side chain ester in the copolymer decreases, indicating once again that  $T_g^L$  results from molecular motions exclusive to these side chains. The maximum in the  $\Delta C_p^L$  versus composition curve for P(DMI + DHpI) is not readily explained, a tendency to go through a maximum can also be seen in  $\Delta C_p^L$  versus composition curve for the P(DMI + DNI) system. There may be some particular packing behaviour, which restricts molecular motion of the side chains to some extent in the odd numbered side chain homopolymers, and which is released by the incorporation of a few DMI units. On the other hand it should be remembered that the actual value of  $\Delta C_p^L$  is very sensitive to the extrapolation lines chosen below and above  $T_g^L$ .

$\Delta C_p^U$  values are plotted as a function of copolymer composition in figure 3.36. A definite trend of increasing  $\Delta C_p^U$  with increasing content of the shorter ester side chain is seen, although there is considerable scatter in the points, especially those for the P(DMI + DNI) system. Such a trend, from low  $\Delta C_p^U$  values when the long ester side chain content is high, to high  $\Delta C_p^U$  values when it is low, is rationalised by postulating that  $\Delta C_p^U$  originates from main chain relaxations. The relative number of relaxing main chain units or segments is small in copolymers with a high concentration of long ester side chains but increases as the copolymer becomes richer in DMI or DPrI units.

$\Delta C_p^{\text{tot.}} = \Delta C_p^L + \Delta C_p^U$  values are plotted as a function

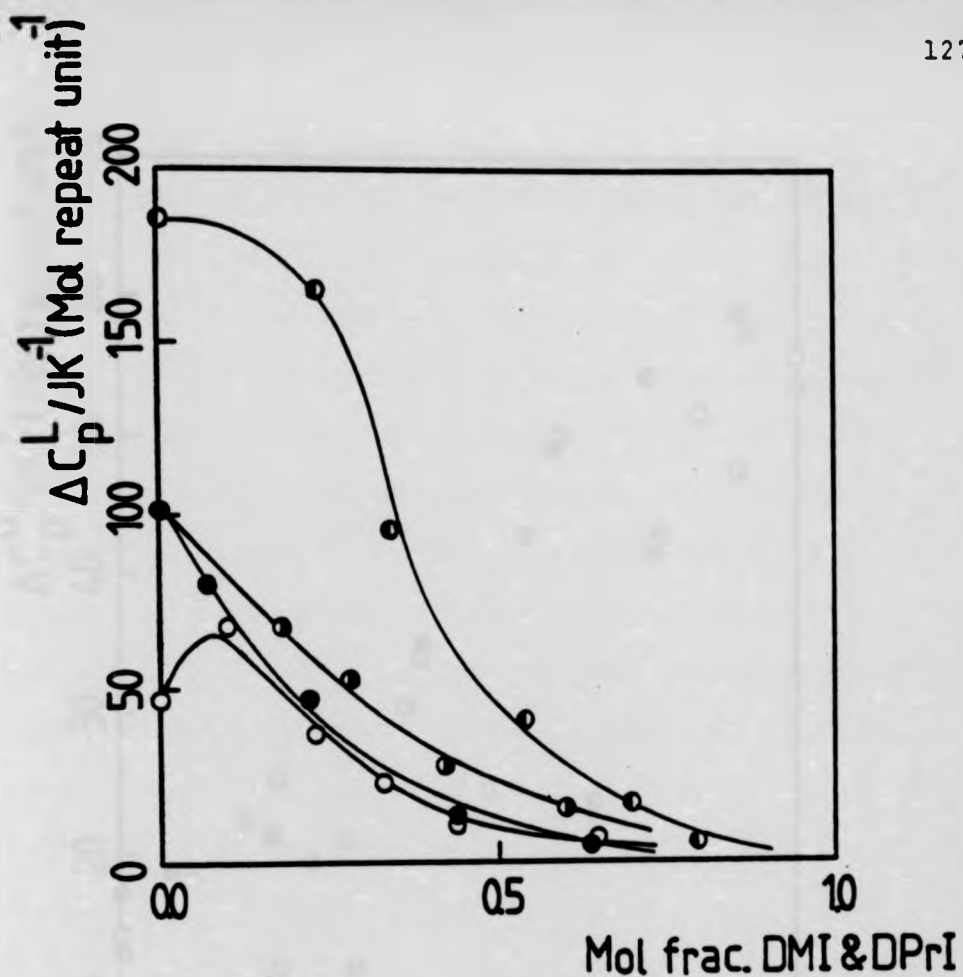


Figure 3.35: Plots of  $\Delta C_p^L / JK^{-1} \text{mol}^{-1}$  values versus mol fraction of DMI in the copolymer for P(DMI+DHpI) series, (  $\circ$  ); P(DMI+DOI) series, (  $\bullet$  ); P(DMI+DNI) series, (  $\odot$  ) and versus mol fraction of DPrI in the copolymer for P(DPrI+DOI) series, (  $\bullet$  ).

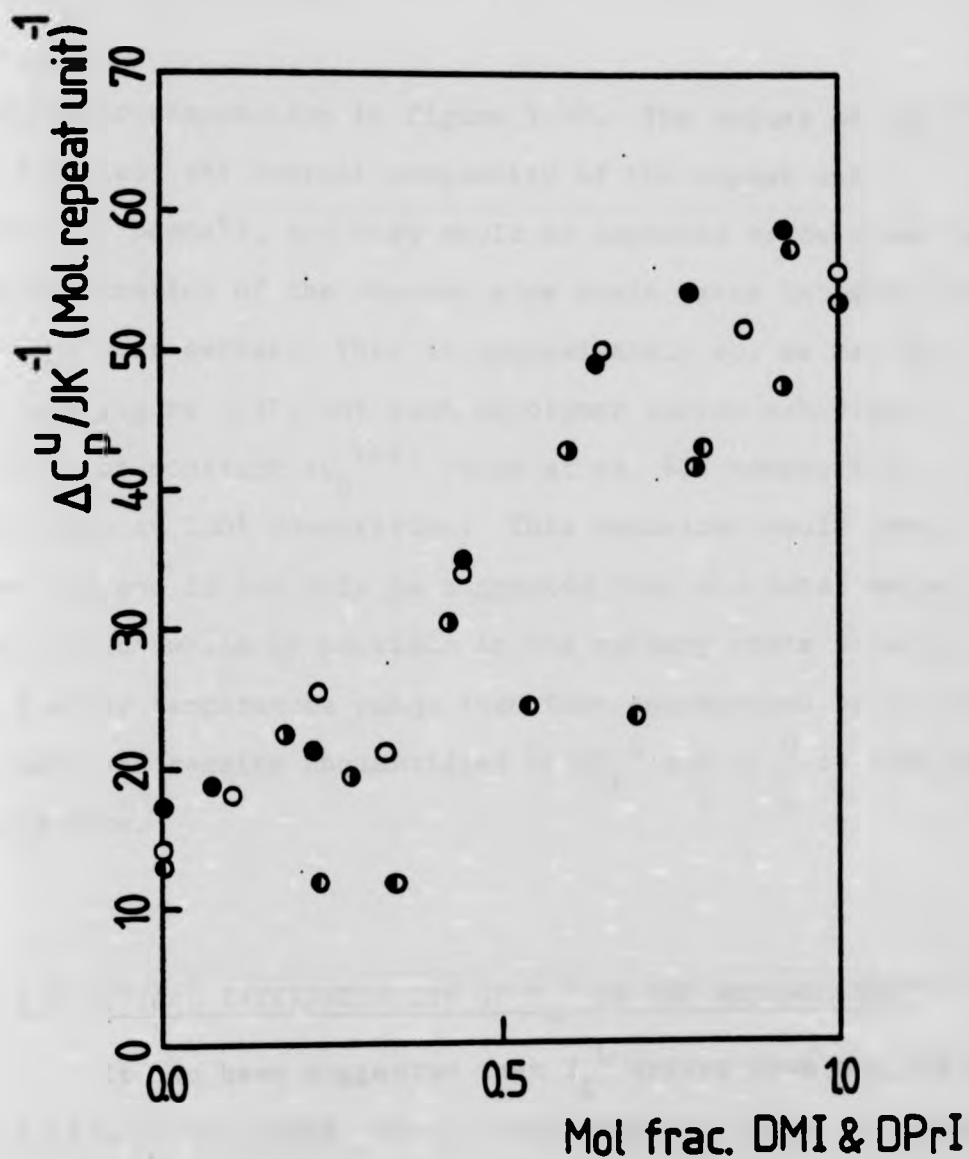


Figure 3.36: Plots of  $\Delta C_p^U / JK^{-1} \text{mol}^{-1}$  values versus mol fraction of DMI in the copolymer for P(DMI+DHpI) series, (  $\circ$  ); P(DMI+DOI) series, (  $\bullet$  ); P(DMI+DNI) series, (  $\bullet$  ) and versus mol fraction of DPrI in the copolymer for P(DPrI+DOI) series, (  $\bullet$  ).



of copolymer composition in figure 3.37. The values of  $\Delta C_p^{\text{tot.}}$  should reflect the overall complexity of the repeat unit (number of "beads"), and they would be expected to decrease as the concentration of the shorter side chain ester increases in each copolymer series. This is approximately so, as can be seen from figure 3.37, but each copolymer series achieves a more or less constant  $\Delta C_p^{\text{tot.}}$  value at ca. 50% composition rather than at 100% composition. This behaviour would seem rather odd and it can only be suggested that the total amount of relaxation which is possible in the rubbery state occurs over a wider temperature range than that encompassed by the two  $\Delta C_p$  jumps and remains unquantified by  $\Delta C_p^L$  and  $\Delta C_p^U$  as they are defined here.

### 3.5 THEORETICAL INTERPRETATION OF $T_g^L$ IN THE HOMOPOLYMERS

It has been suggested that  $T_g^L$  arises from motions of the side chains alone, and it would seem in order to attempt some theoretical predictions based on a reasonable molecular model. Firstly, however, we will consider an analysis of heat capacity based on the expression for the energy of a simple harmonic oscillator.

#### 3.5.1 POLYMERS AS A COLLECTION OF HARMONIC OSCILLATORS

The energy of a simple harmonic oscillator is given by

$$\epsilon = \frac{1}{2} h\nu_0 + kT \frac{\theta/T}{(e^{\theta/T} - 1)} \quad (3.6)$$

where  $h$  is Planck's constant,  $k$  is Boltzman constant,  $\theta = h\nu/k$

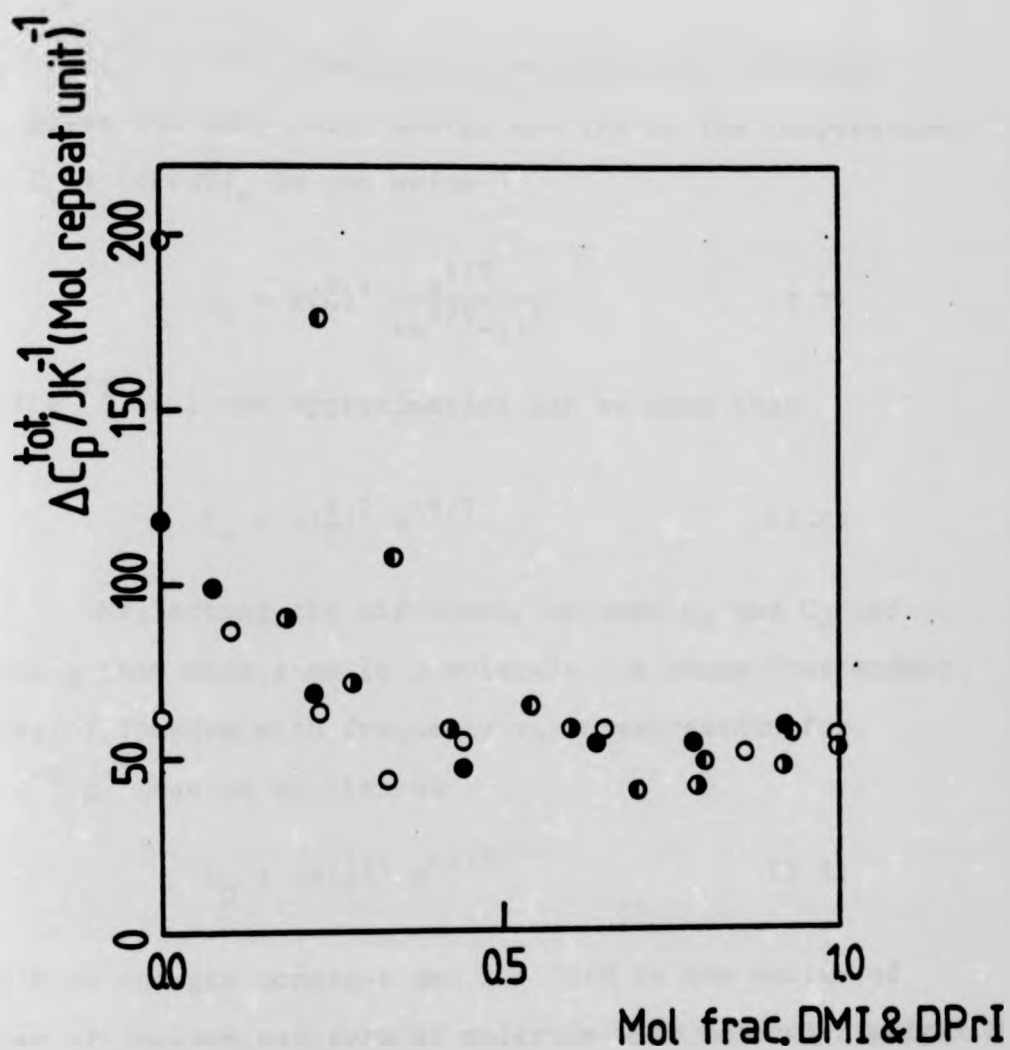


Figure 3.37: Plots of  $\Delta C_p^{\text{tot.}} / \text{JK}^{-1} \text{mol}^{-1}$  values versus mol fraction of DMI in the copolymer for P(DMI+DHpI) series, (  $\circ$  ); P(DMI+DOI) series, (  $\bullet$  ); P(DMI+DNI) series, (  $\bullet$  ) and versus mol fraction of DPrI in the copolymer for P(DPrI+DOI) series, (  $\bullet$  ).

where  $\nu/\text{sec}^{-1}$  is the frequency of oscillation. The term  $\frac{1}{2} h\nu_0$  gives the zero point energy and  $T/K$  is the temperature. Since  $C_v = (d\varepsilon/dT)_v$  we can write

$$C_v = k\left(\frac{\theta}{T}\right)^2 \frac{e^{\theta/T}}{(e^{\theta/T}-1)^2} \quad (3.7)$$

and if  $e^{\theta/T} \gg 1$  the approximation can be made that

$$C_v \approx k\left(\frac{\theta}{T}\right)^2 e^{-\theta/T} \quad (3.8)$$

Neglecting the difference between  $C_v$  and  $C_p$  and proposing that each atom in a molecule has three independent degrees of freedom with frequency  $\nu$ , an expression for  $C_p/J K^{-1} g^{-1}$  can be written as

$$C_p \approx xR\left(\frac{\theta}{T}\right)^2 e^{-\theta/T} \quad (3.9)$$

where  $R$  is the gas constant and  $x = 3N/M$  is the number of degrees of freedom per gram of molecule with molecular weight  $M$  and consisting of  $N$  atoms. A plot of  $\ln(T^2 C_p)$  versus  $1/T$  should be linear with the number of degrees of freedom and frequency of oscillation given by the intercept and slope respectively.

The data for PDOI were treated according to equation (3.9) over two temperature ranges, 110-170K and 215-250K and the result is shown in Table 3.18. The former corresponds to the glassy state where vibrational motions only contribute to  $C_p$ , while the latter corresponds to a state where the side chains are capable of undergoing independent relaxation.

TABLE 3.18

Theoretical  $C_p$  parameters for PDOI using equation 3.9.

<u>TEMP. RANGE/K</u>	<u>DEGREES OF FREEDOM</u> (per repeat unit)	<u>WAVENUMBER OF</u> <u>VIBRATION/cm<sup>-1</sup></u>
110 - 170	78	260
215 - 250	141	445

As can be seen, the glassy state heat capacity can be represented by 78 oscillations each with frequency corresponding to  $260 \text{ cm}^{-1}$ . After passing through  $T_g^L$  there is an increase by 63 in the number of the oscillators necessary to describe the heat capacity. Since the number of degrees of freedom of the repeat unit of PDOI should be 189 (3N), it appears that this treatment, invoking only one single frequency, is inadequate for a polymer of this complexity; although it has been used successfully with simpler structures such as poly(vinyl chloride) (PVC).<sup>(74)</sup> The increase in the number of degrees of freedom on going from below  $T_g^L$  to above can be given no physical significance since localised atomic vibrations are not frozen in at a glass transition.

### 3.5.2 HEAT CAPACITY FROM A VIBRATIONAL FREQUENCY SPECTRUM

More precise descriptions of heat capacity can be obtained by summing the contributions to  $C_v$  from each frequency present in the vibrational spectrum of the polymer, if this is known. For simpler structures, complete ir and Raman spectra

and the assignments are available in the literature, but for the complex structures considered here only incomplete information is available based on group contributions. The group contributions of interest are listed in Table 3.19 as "optical" frequencies.

Using Table 3.19 it is possible to calculate the total number of optical frequencies from the known structures of the itaconates. By evaluating equation (3.7) for each frequency and summing over all frequencies, an estimate of  $C_v (= C_p)$  can be made. To simplify the calculation, the  $CH_3$  and  $CH_2$  deformations and the  $CH_2$  wagging and twisting are assigned the same frequency of  $1400\text{ cm}^{-1}$  and the C- $CH_3$  and C-O stretches the same frequency of  $1150\text{ cm}^{-1}$ . The optical frequencies, and the number of vibrations at each frequency, for each homopolymer considered are listed in Table 3.20.

The total number of vibrations for each repeat unit (considered to be  $3N$  as before) is also listed, and the difference between  $3N$  and the total number of optical frequencies gives the number of low frequency vibrations making up the remainder of the frequency spectrum. These are not observable by normal infrared technique, so some estimate must be made. Two frequencies were chosen, one at a very low frequency of  $25\text{ cm}^{-1}$  (2) and one at around  $300\text{ cm}^{-1}$  (1). Frequencies in these regions have been used in the calculation of  $C_v$  for other polymers and correspond to skeletal vibrations and deformations. (34)

With the aid of an "Apple II" microcomputer, best fits to the experimental glassy state heat capacities for the PDHpI to PDDI homopolymer series were obtained using the low frequency vibrations listed in Table 3.21 and the optical frequencies in

TABLE 3.19

Group contribution to infrared absorption spectra

<u>GROUP</u>	<u>NUMBER OF MODES</u>	<u>TYPE</u>	<u>APPROXIMATE WAVENUMBER</u> ( $\text{cm}^{-1}$ )
CH <sub>3</sub>	3	stretching	3000
	3	deformation	1450
	2	rocking	1150
CH <sub>2</sub>	2	stretching	3000
	1	deformation	1450
	2	wagging/twisting	1300
	1	rocking	1150
C-CH <sub>3</sub>	1	stretching	1150
H <sub>2</sub> C-CH <sub>2</sub>	1	"	750
C-O	1	"	1250
C=O	1	"	1750

TABLE 3.20

Vibrational frequency spectrum for the indicated polymers

<u>FREQUENCY/cm<sup>-1</sup></u>	<u>NUMBER OF VIBRATIONS/REPEAT UNIT</u>			
	PDHpI	PDOI	PDNI	PDDI
3000	34	38	42	46
1750	2	2	2	2
1400	48	54	60	66
1150	24	26	28	30
750	15	17	19	21
-----				
TOTAL OPTICAL VIBRATIONS	123	137	151	165
3N	171	189	207	225
NUMBER OF LOW FREQUENCY VIBRATIONS	48	52	56	60

Table 3.20. Plots of the experimental and calculated  $C_p$  values versus temperature for the homopolymers are shown in figures 3.38-3.41.

TABLE 3.21

Low frequency vibration spectrum for indicated polymers

<u>POLYMER</u>	<u>WAVENUMBER (<math>\text{cm}^{-1}</math>) and NUMBER OF VIBRATIONS</u>	
	(1)	(2)
PDHpI	325/30	25/18
PDOI	265/33	25/19
PDNI	315/36	25/20
PDDI	300/39	25/21

The good agreement between theory and experiment for the four homopolymers considered shows that in the glassy state, the heat capacity can be adequately reproduced by vibrational contributions alone from a reasonable frequency spectrum. The figures 3.38-3.41 also show that, at  $T_g^L$ , the experimental heat capacity deviates dramatically from that based on atomic vibrations and that consequently additional molecular motion(s) have become activated. The possible nature of these added molecular motions is considered in the next section.

### 3.5.3 HINDERED INTERNAL ROTATION MODEL FOR $T_g^L$

For simple molecular motions it is possible to calculate heat capacity contributions by statistical mechanical methods. For example Pitzer<sup>(75)</sup> has evaluated  $C_v$  for a hindered rotation and has extended the treatment to allow an estimate to be made of the internal rotation contribution to the heat capacity of linear alkanes.<sup>(76)</sup> Since strong evidence has been

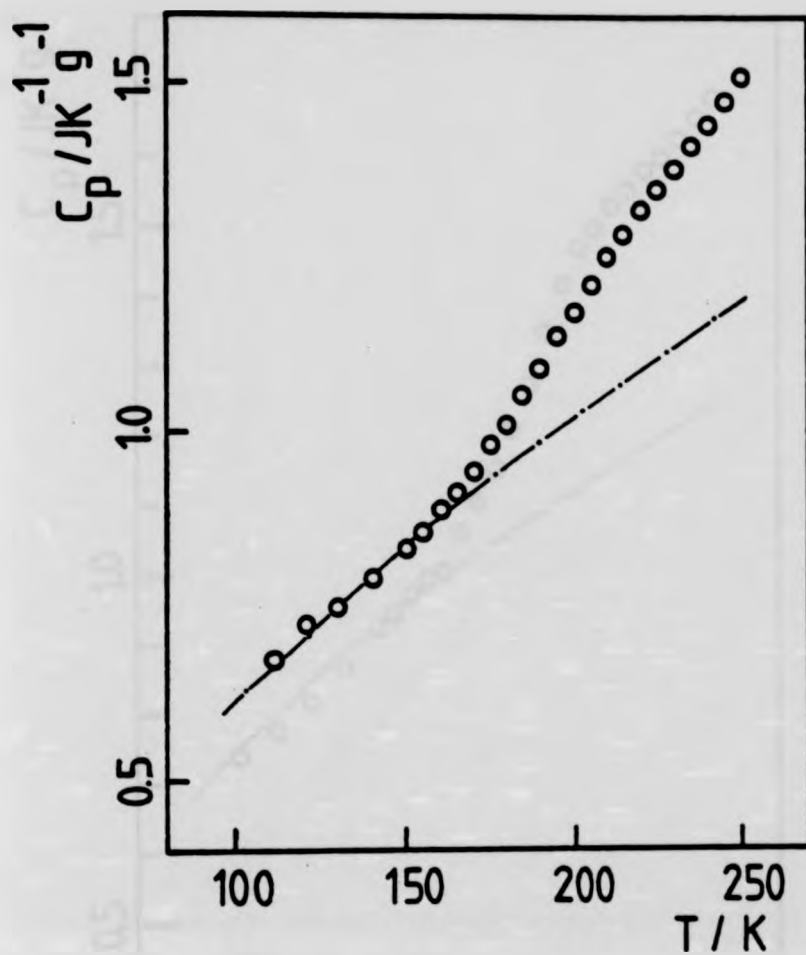


Figure 3.38: Plots of the experimental  $C_p / JK^{-1} g^{-1}$  values (o) and calculated glassy state heat capacity (----) versus temperature for PDHpI.



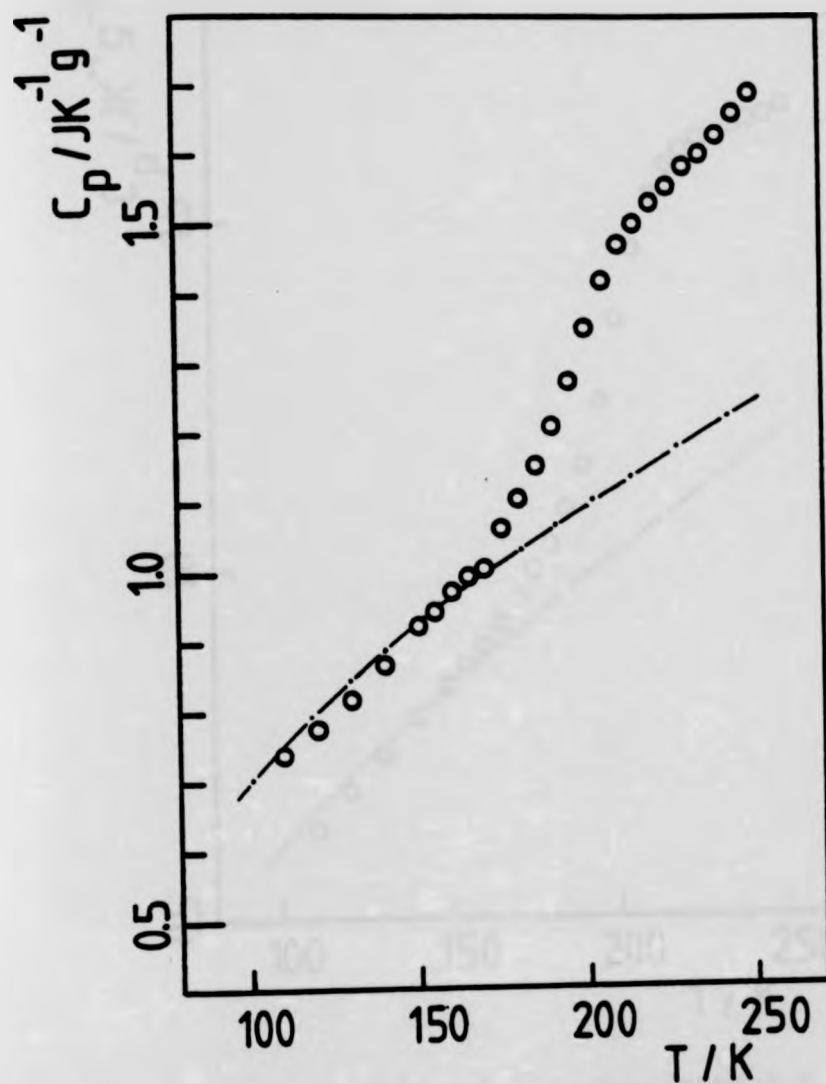


Figure 3.39: Plots of the experimental  $C_p / JK^{-1} g^{-1}$  (o) and calculated glassy state heat capacity (-.-.-) versus temperature for PDOI.

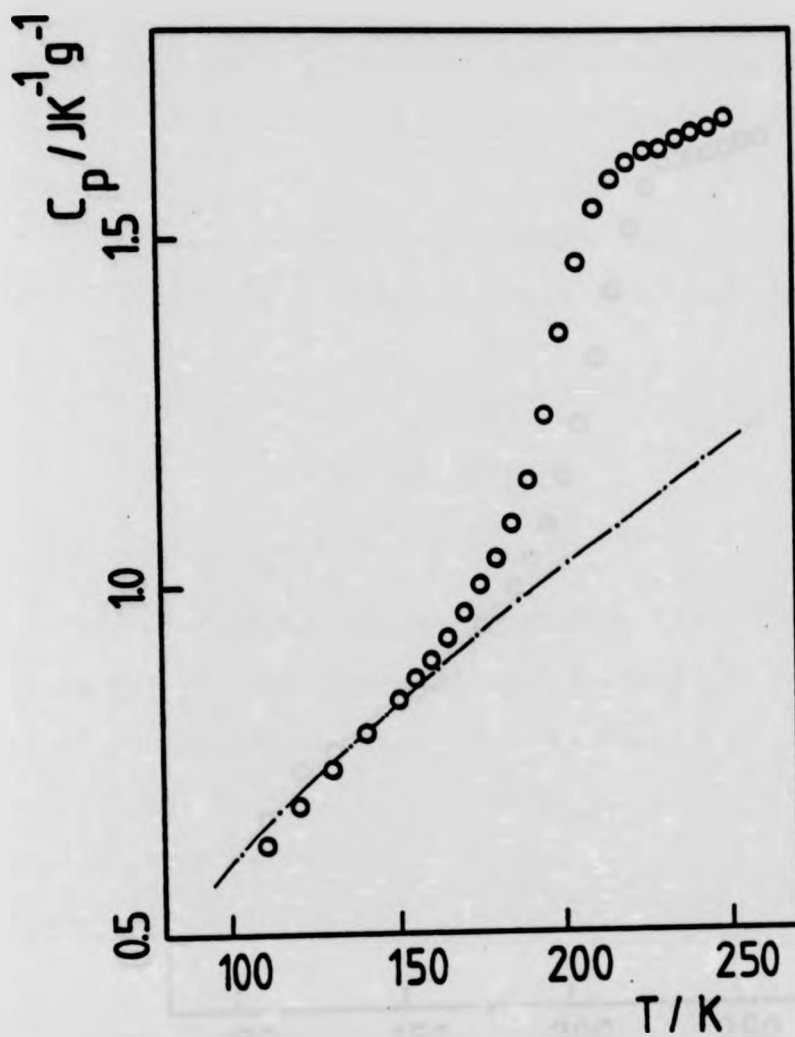


Figure 3.40: Plots of the experimental  $C_p/\text{JK}^{-1}\text{g}^{-1}$  values (o) and calculated glassy state heat capacity (---) versus temperature for PDNI.

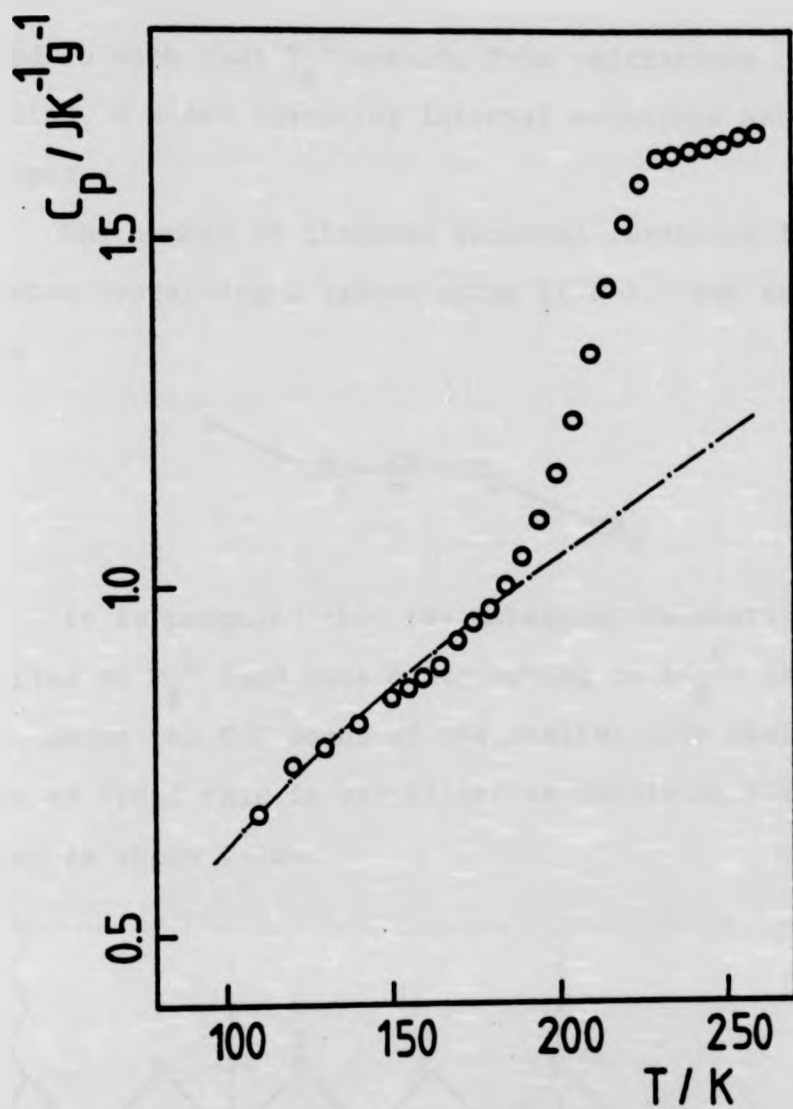
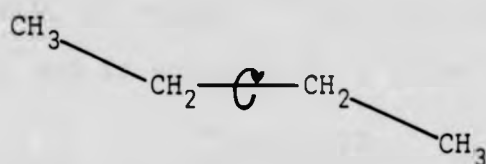


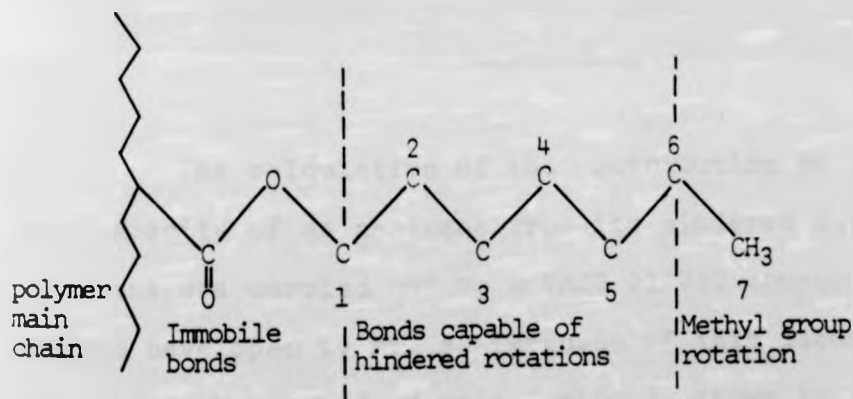
Figure 3.41: Plots of the experimental  $C_p / JK^{-1}g^{-1}$  values (o) and calculated glassy state heat capacity (-.-.-) versus temperature for PDDI:

presented to show that  $T_g^L$  results from relaxations of the n-alkyl side chains, a model involving internal rotations about C-C bonds is proposed.

The number of hindered internal rotations for a linear hydrocarbon containing N carbon atoms is N-3. For example, in n-butane



It is proposed that the molecular relaxation process giving rise to  $T_g^L$  (and thus contributing to  $\Delta C_p^L$ ) is hindered rotation about the C-C bonds of the n-alkyl side chains. In the case of PDHpI this is visualized as involving five such rotations as shown below.



Molecular models show that rotation about the carboxyl carbon-oxygen link is highly restricted and unlikely to be important, and rotation about the C<sub>6</sub>-C<sub>7</sub> is in fact methyl group rotation which is known to occur at low temperature<sup>(33)</sup> and will be already contributing to the experimental heat capacity at  $T_g^L$ .

This leaves rotations about the oxygen - C<sub>1</sub> bond and the five remaining C-C bonds. Calculations have been shown<sup>(77)</sup> that the O-C<sub>1</sub> bond has a rather high energy barrier to rotation (> 200 kJ mol<sup>-1</sup>) and is considered to be rigid in this model. The poly di-n-alkyl itaconates thus possess the numbers of hindered internal C-C rotations listed in Table 3.20. The hindering potential is chosen<sup>(76)</sup> as that about the centre C-C bond in n-butane and is equal to 15.1 kJ mol<sup>-1</sup>.

TABLE 3.22

<u>POLYMER</u>	<u>NUMBER OF C-C ROTATIONS PER SIDE CHAIN</u>	<u>FREEZING IN TEMP. (K)</u>
PDHpI	5	200
PDOI	6	209
PDNI	7	204
PDDI	8	210

The calculation of the contribution to the total heat capacity of an n-alkane from its hindered internal rotations was carried out on a VACS 11/780 computer using a program developed by Mr. R. Ferguson of this laboratory. An outline of the method of calculation is shown in Appendix 2.

The contribution from side chain relaxations to the experimental heat capacity of the polymer in question was estimated by a linear extrapolation of the data below  $T_g^L$  and evaluating the differences (at 5K intervals) between this extrapolation and the experimental  $C_p$  values above  $T_g^L$ . This procedure assumes that, in the absence of  $T_g^L$ , the heat capacity would be an increasing linear function of temperature and is obviously an approximation.

The differences thus obtained, as a function of temperature, from  $T_g^L$  to ca. 240K (where the influence of  $T_g^U$  becomes apparent) are assigned as the heat capacity due to the molecular motions involved in the relaxation of the two n-alkyl side chains. These are plotted (in  $J K^{-1}$  per mol of side chain) as a function of temperature in figures 3.42-3.45.

The theoretical values of heat capacity arising from respectively 5, 6, 7 and 8 hindered internal rotations are also shown in figures 3.42-3.45. These are smoothly increasing functions of temperature in the range considered.

A second proposal is now made - that the hindered rotations involved in the  $T_g^L$  process are frozen in at temperatures below  $T_g^L$  and that the freezing in temperature is the maximum temperature in the TBA relaxation assigned to  $T_g^L$ . The freezing in temperatures are also listed in Table 3.22. The hindered rotation heat capacity contribution below the freezing in temperature is consequently zero, but at temperatures above this it rises immediately to the full theoretical value. The calculated heat capacities are thus step functions as shown by the heavy full lines in figures 3.42-3.45. The agreement between the experimental values of the heat capacity deemed to arise from the n-alkyl side chains and the theoretical values is remarkably good for PDHpI, PDOI and PDNI and fair for PDDI. It should be remembered that the experimental values will depend on the extrapolated "base line" chosen.

The step nature of the theoretical heat capacity can be modified if it is recognised that the breadth of the damping peak for a  $T_g^L$  relaxation in the TBA spectrum represents the

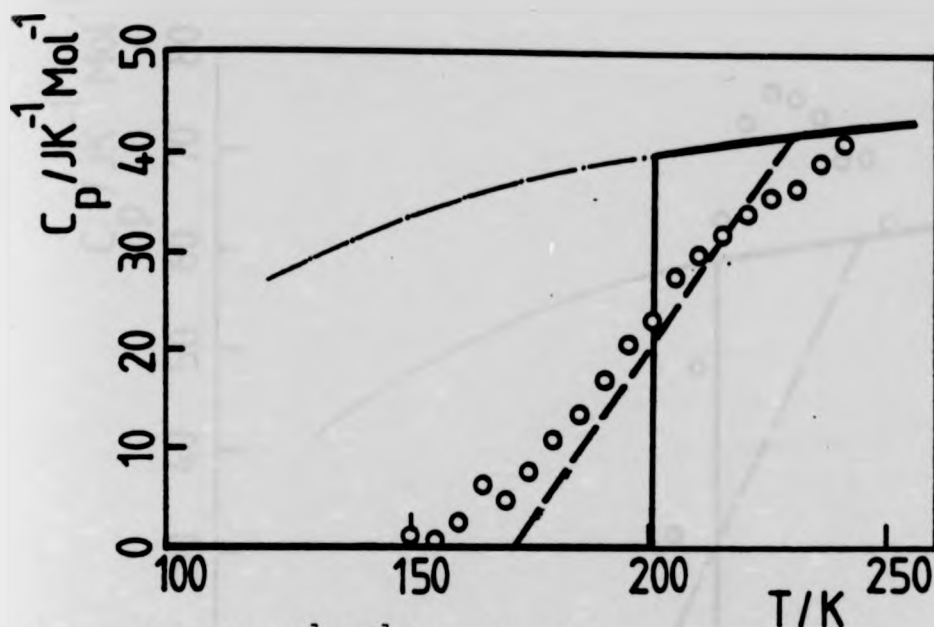


Figure 3.42:  $C_p/\text{JK}^{-1}\text{mol}^{-1}$  from side chain relaxation versus temperature evaluated as described in the text for PDHpI(o). Theoretical  $C_p$  versus temperature curve for 5 hindered internal rotations (-----). Heavy full and broken lines are described in the text.

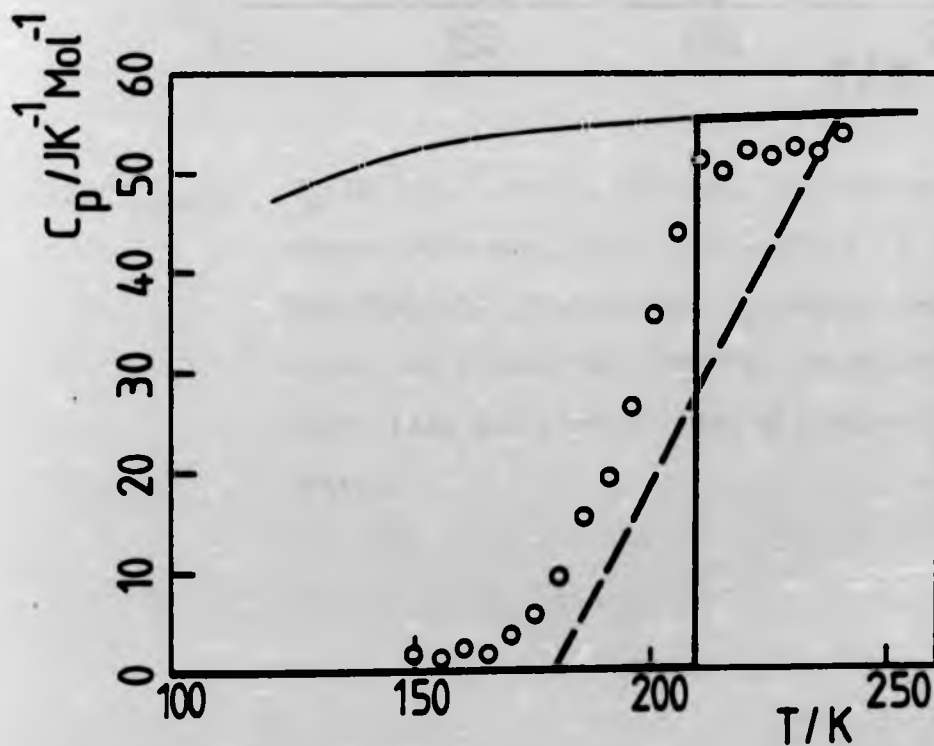


Figure 3.43:  $C_p/\text{JK}^{-1}\text{mol}^{-1}$  from side chain relaxation versus temperature evaluated as described in the text for PDOI(o). Theoretical  $C_p$  versus temperature curve for 5 hindered internal rotations (-----). Heavy full and broken lines are described in the text.

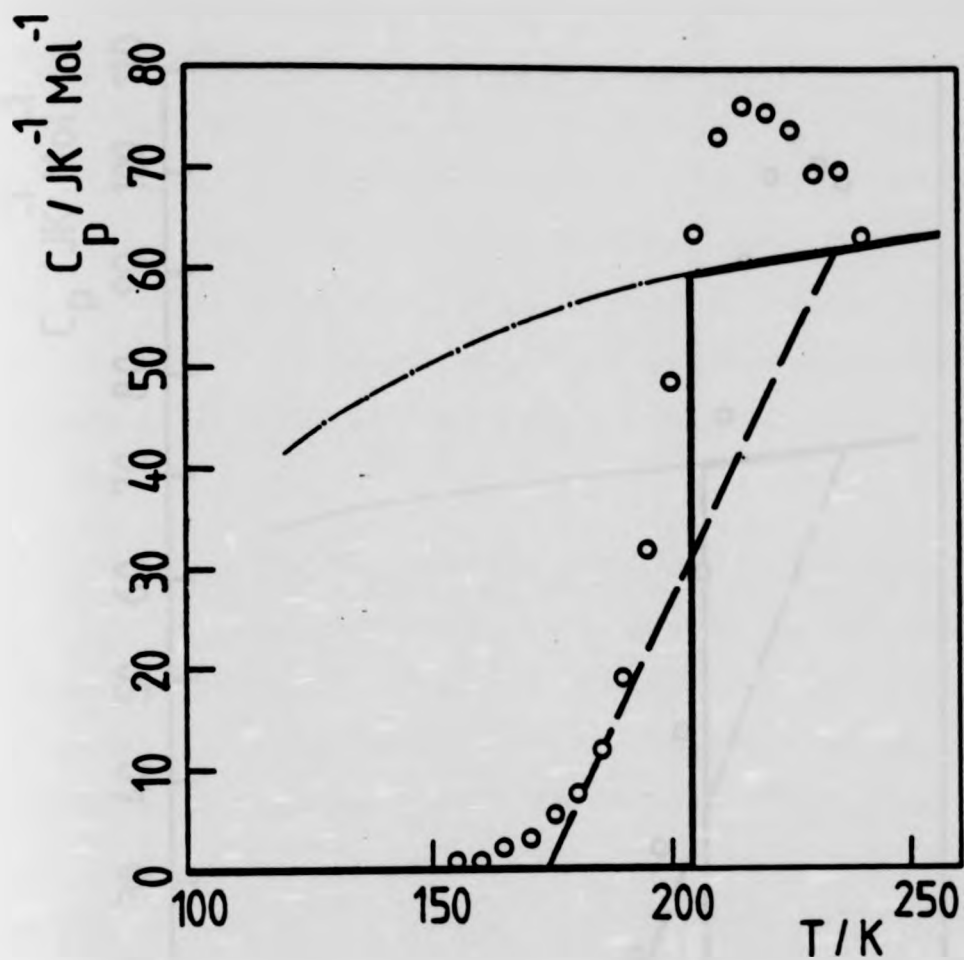


Figure 3.44:  $C_p / JK^{-1} mol^{-1}$  from side chain relaxation versus temperature evaluated as described in the text for PDNI(o). Theoretical  $C_p$  versus temperature curve for 5 hindered internal rotations (---). Heavy full and broken lines are described in the text.



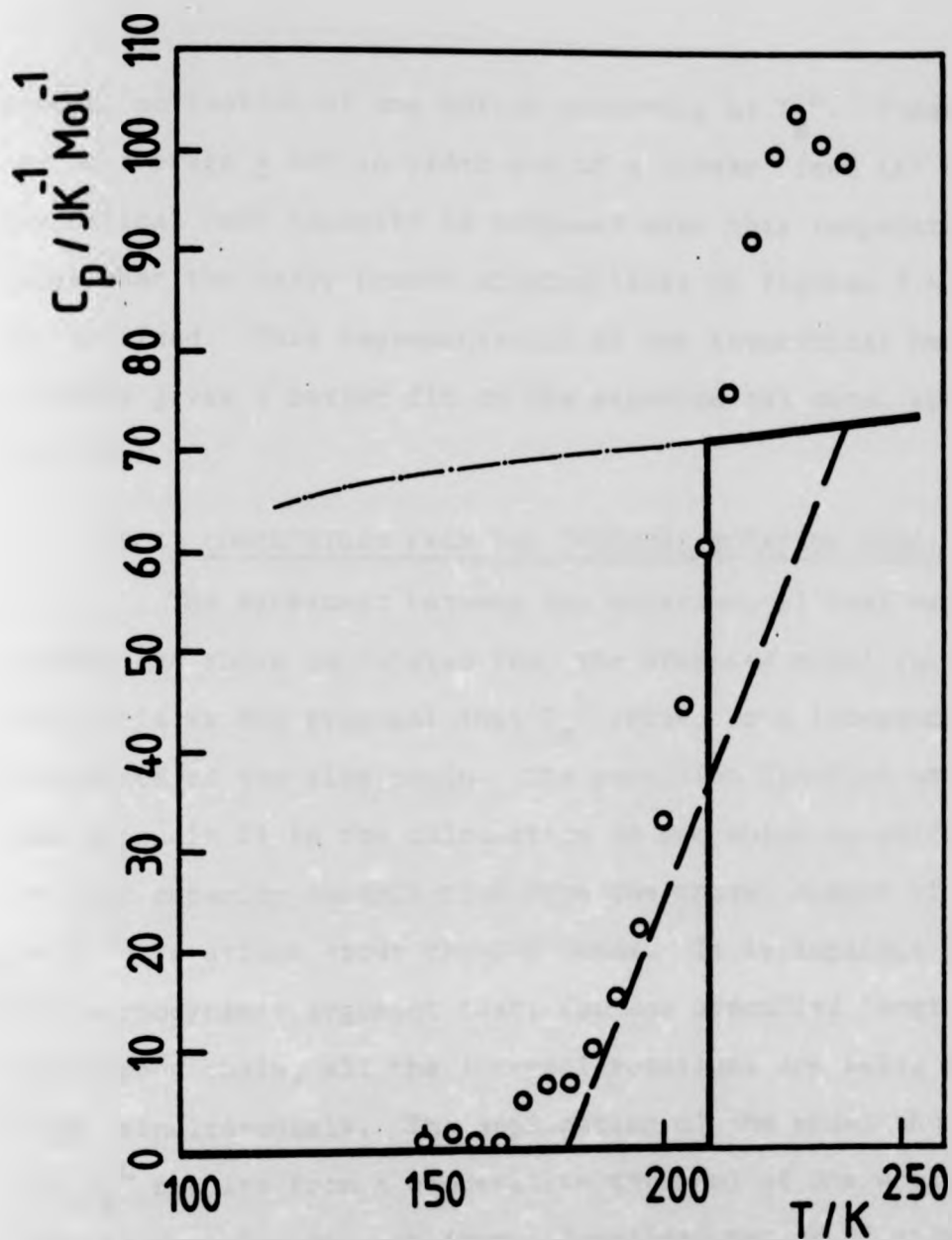


Figure 3.45:  $C_p / \text{JK}^{-1} \text{mol}^{-1}$  from side chain relaxation versus temperature evaluated as described in the text for PDDI(o). Theoretical  $C_p$  versus temperature curve for 5 hindered internal rotations (-----). Heavy full and broken lines are described in the text.

gradual activation of the motion occurring at  $T_g^L$ . These peaks are on average  $\pm 30K$  in width and if a linear "feed in" of the theoretical heat capacity is proposed over this temperature range then the heavy broken sloping lines of figures 3.43-3.46 are obtained. This representation of the theoretical heat capacity gives a better fit to the experimental data, specially for PDHpI.

#### 3.5.4 CONCLUSIONS FROM THE INTERNAL ROTATION MODEL

The agreement between the experimental heat capacity changes and those calculated from the proposed model further substantiates the proposal that  $T_g^L$  arises from independent relaxation of the side chain. The partition function used (see Appendix 2) in the calculation is one which quantifies the heat capacity contribution from the chosen number of hindered rotations about the C-C bonds. It is implicit in the thermodynamic argument that, for any specified length of hydrocarbon chain, all the internal rotations are being performed simultaneously. The application of the model thus implies that  $T_g^L$  results from a cooperative movement of the whole side chain in question and not from a localised motion of only a few units (such as  $T_y$ ).

The apparent activation energies ( $\Delta H^\ddagger$ ) of  $T_g^L$  have been measured for PDHpI, PDOI and PDNI as approximately 230, 170 and 150  $\text{kJ mol}^{-1}$  respectively.<sup>(24)</sup> These values do not fit the Heijboer relation (see equation 3.5, section 3.2) which describes molecular relaxations in which  $\Delta H^\ddagger$  is defined by the local barrier to rotation. If the activation energies of the  $T_g^L$ 's were derived from some sort of summation of the local

barriers to C-C rotation, then they would be expected to show an increase with increasing chain length. For example, in PDHPI, ten synchronous rotations could involve a maximum total activation energy of approximately  $320 \text{ kJ mol}^{-1}$ .<sup>\*</sup> This energy would reduce if the motions were non synchronous - which would be the case since any sort of synchronous movement of all the C-C bonds in a side chain would involve the chain in large scale excursions of a "whip-lash" motion. Models show that a more or less linear conformation must be maintained for sensible side chain packing. Nevertheless, activation energies entirely dependent on local barriers will still increase on going to longer n-alkyl side chains.

Since the experimental activation energies do not correlate with chain length, they are not solely derived from the internal rotation barriers. It is suggested that the apparent activation requirements of the  $T_g^L$ 's are mainly derived from matrix or free volume effects. That is, the cooperative relaxation process proposed occurs as a result of an increase in free volume and the movement no longer being matrix impeded.  $T_g^L$  therefore has all the characteristics of a "conventional" glass transition.

### 3.6 ANALYSIS OF THE VARIATION OF $T_g^U$ WITH COPOLYMER COMPOSITION

Polymer mixtures can be defined broadly as (1) polymer-small molecule (plasticiser) systems and (2) polymer-polymer

\* This is ten times the barrier for rotation about the middle bond of n-butane.

systems. Since random copolymers are mixtures of "mers" with varying  $T_g$  values, the composition dependence of  $T_g$  may be described by many of the polymer-polymer equations that have been developed.

### 3.6.1 EMPIRICAL $T_g$ VERSUS COMPOSITION EQUATION

The vast majority of copolymer systems do not exhibit linear  $T_g$  versus composition behaviour. The empirical equation already stated in section 3.3.1 can be used to describe non-linearity.

$$T_g = n_1 T_{g1} + n_2 T_{g2} + n_1 n_2 K \quad (3.10)$$

K may be regarded as a parameter reflecting the "non-ideality" of the system. All the copolymer data presented in section 3.3 have been fitted to this equation (see figures, 3.19, 3.22, 3.25, 3.28 and 3.31) and the values of K giving the best fits are shown in Table 3.23.

TABLE 3.23

Values of K parameters for indicated copolymer systems fitted

$$\text{to } T_g = n_1 T_{g1} + n_2 T_{g2} + n_1 n_2 K$$

<u>COPOLYMER SYSTEM</u>	<u>K</u>
P(DMI + DBI)	- 75
P(DMI + DHpI)	-155
P(DMI + DOI)	-140
P(DMI + DNI)	-230
P(DPrI + DOI)	- 70

The general trend is for K to increase with increasing difference in side chain length on the two comonomers, as would

be sensibly expected since the only difference between comonomers is the side chain length. However no further significance can be attached to this parameter.

### 3.6.2 GORDON-TAYLOR EQUATION

A number of equations have been proposed which are essentially modifications of the empirical relation used above and which have weighting factors stemming from the theories of  $T_g$  based on free volume concepts. One such equation is that of Gordon and Taylor<sup>(78)</sup> which is similar in form to an earlier general expression due to Wood.<sup>(72)</sup>

$$(T_g - T_{g1})w_1 + K(T_g - T_{g2})w_2 = 0 \quad (3.11)$$

Here  $w_i$  is the weight fraction of each monomer in the copolymer and  $K$  is defined in terms of the thermal expansion coefficients of the polymers.

$$K = \Delta\alpha_2 / \Delta\alpha_1 \quad (3.12)$$

where  $\Delta\alpha_i$  is the difference in thermal expansion coefficient between the liquid and the glassy state. Rearrangement of (3.11) gives

$$T_g = T_{g2} - \frac{1}{K}(T_g - T_{g1})\frac{w_1}{w_2} \quad (3.13)$$

so that a plot of copolymer glass transition ( $T_g$ ) against  $(T_g - T_{g1})\frac{w_1}{w_2}$  should be linear with slope =  $-\frac{1}{K}$ .

When the DSC data for the copolymer systems are treated according to equation (3.13) distinct non-linear behaviour is found, indicating that the Gordon-Taylor treatment does not adequately describe the copolymer data obtained here. This confirms the previous non-applicability of the Gordon-Taylor

approach to other itaconate copolymer systems. (18)

### 3.6.3 THE FOX EQUATION

Fox<sup>(79)</sup> derived a simplified version of the Wood<sup>(72)</sup> equation that takes the form

$$\frac{1}{T_g} = \frac{w_1}{T_{g1}} + \frac{w_2}{T_{g2}} \quad (3.14)$$

and can be expressed as the linear relation

$$\frac{1}{T_g w_2} = \frac{w_1}{w_2 T_{g1}} + \frac{1}{T_{g2}} \quad (3.15)$$

so that a plot of  $\frac{1}{T_g w_2}$  versus  $\frac{w_1}{w_2 T_{g1}}$  should be a straight line of slope unity and with  $\frac{1}{T_{g2}}$  given by the intercept.

When the copolymer data (see Appendix 1) are treated according to equation (3.15) good straight lines are obtained as can be seen from figure 3.46. The values of  $T_{g2}$  by this graphical method are compared with the experimental values in Table 3.24.

TABLE 3.24

Extrapolated values of  $T_{g2}$  obtained from Fox plots for indicated copolymer systems.  $T_{g2}$  is the glass transition for the longer side chain polymer.

<u>COPOLYMER SYSTEM</u>	<u>SLOPE</u>	<u><math>T_{g2}/K</math></u> (from intercept)	<u><math>T_{g2}/K</math></u> (DSC)
P(DMI + DBI)	1.04	285	282
P(DMI + DHpI)	1.10	246	248
P(DMI + DOI)	0.99	242	240
P(DMI + DNI)	1.01	230	(245)
P(DPrI + DOI)	1.04	234	240

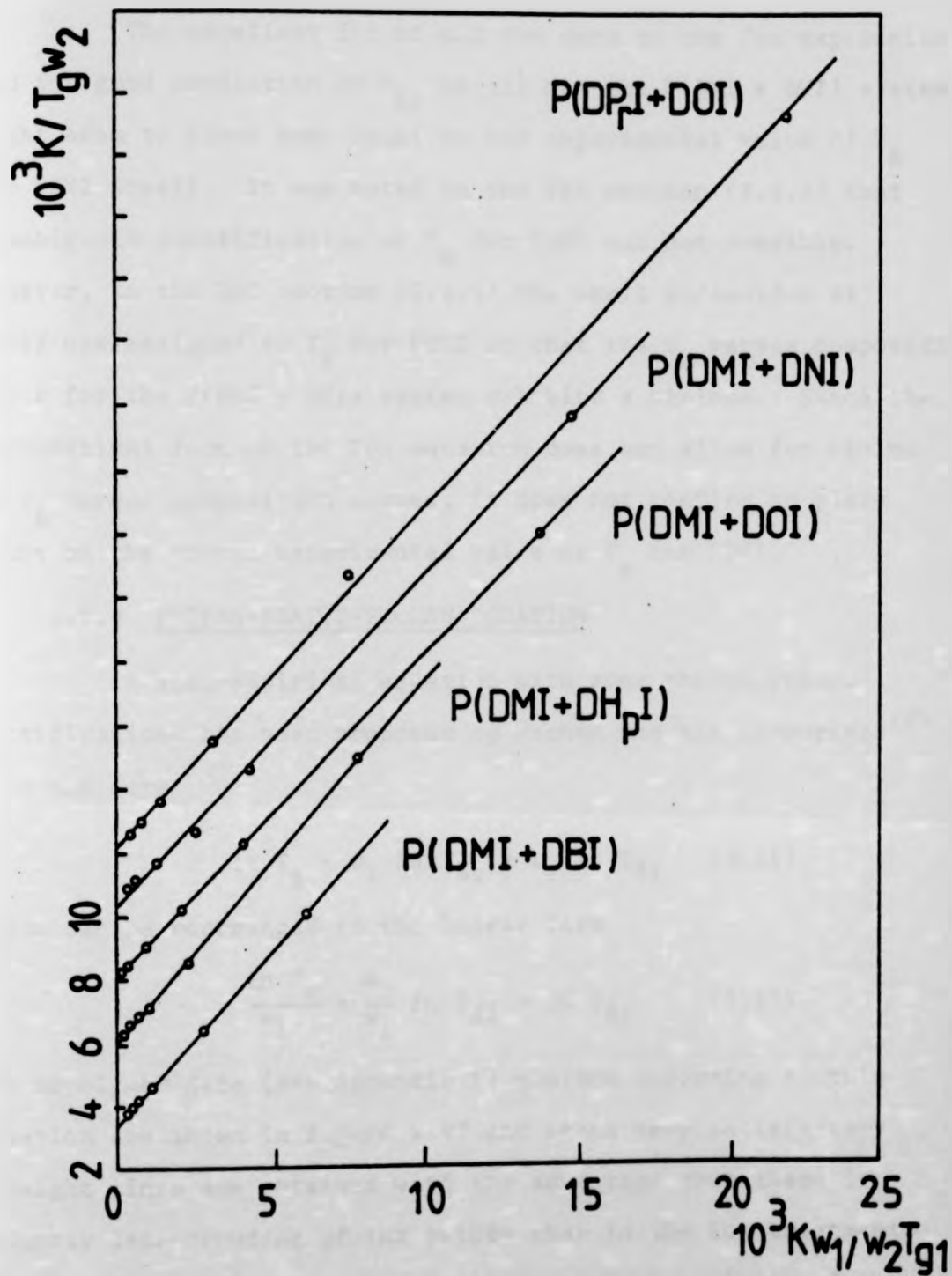


Figure 3.46: Plots of the Fox equation for indicated copolymer systems. The copolymer data are fitted to least square determined straight lines with the slopes and intercepts listed in Table 3.18. Each line is displaced from the one below by  $2 \times 10^{-3} K^{-1}$ .

The excellent fit of all the data to the Fox expression and the good prediction of  $T_{g2}$  in all but the P(DMI + DNI) system might seem to place some doubt on the experimental value of  $T_g$  for PDNI itself. It was noted in the TBA section (3.2.3) that unambiguous identification of  $T_g$  for PDNI was not possible. However, in the DSC section (3.3.4) the small inflection at  $\sim 245K$  was assigned to  $T_g$  for PDNI so that the  $T_g$  versus composition curve for the P(DMI + DNI) system exhibits a minimum. Since the mathematical form of the Fox equation does not allow for minima in  $T_g$  versus composition curves, it does not confirm or place doubt on the chosen experimental value of  $T_g$  for PDNI.

#### 3.6.4 POCHAN-BEATTY-POCHAN EQUATION

A semi-empirical equation with some thermodynamic justifications has been proposed by Pochan and his co-workers<sup>(80)</sup> with the form

$$\ln T_g = w_1 \ln T_{g1} + w_2 \ln T_{g2} \quad (3.16)$$

which can be rearranged to the linear form

$$\frac{\ln T_g}{w_1} = \frac{w_2}{w_1} \ln T_{g2} + \ln T_{g1} \quad (3.17)$$

The copolymer data (see Appendix 1) plotted according to this equation are shown in figure 3.47 and again very satisfactory straight lines are obtained with the advantage that there is slightly less crowding of the points than in the Fox treatment. Table 3.25 shows the  $T_{g1}$  values ( $T_{g1}$  = glass transition of the longer side chain homopolymer) from the intercepts of the lines of figure 3.47.



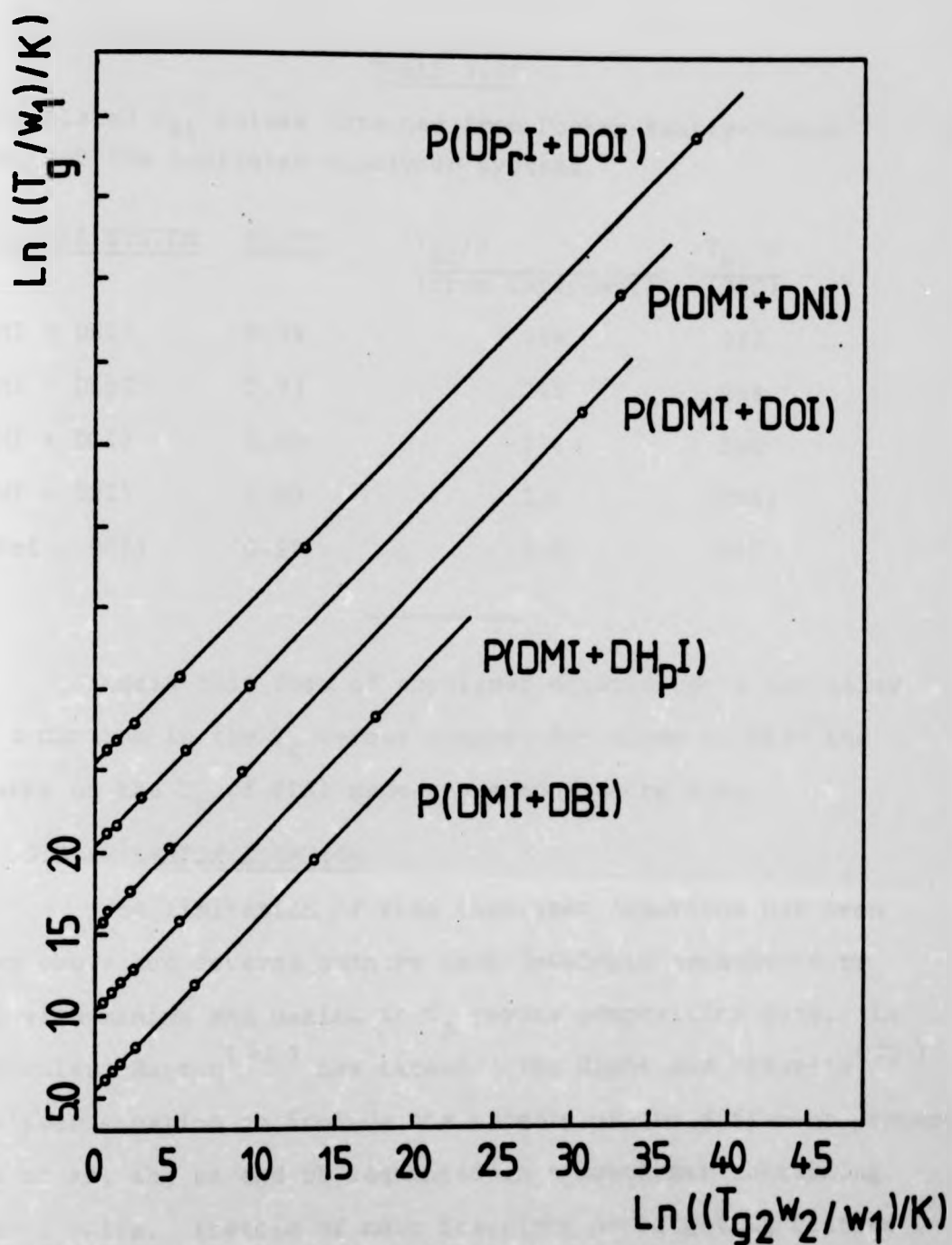


Figure 3.47: Plots of the Pochan-Beatty-Pochan equation for the indicated copolymer systems. The copolymer data are fitted to least square determined straight lines with the slopes and intercepts listed in Table 3.19. Each line is displaced from the one below by 5 units of the vertical axis.

TABLE 3.25

Extrapolated  $T_{g1}$  values obtained from Pochan-Beatty-Pochan plots for the indicated copolymer systems

<u>COPOLYMER SYSTEM</u>	<u>SLOPE</u>	$T_{g1}/K$ (from intercept)	$T_{g1}/K$ (DSC)
P(DMI + DBI)	0.99	284	282
P(DMI + DHpI)	0.98	245	248
P(DMI + DOI)	1.00	238	240
P(DMI + DNI)	1.00	224	(245)
P(DPrI + DOI)	0.99	232	240

Again this form of copolymer equation does not allow for a minimum in the  $T_g$  versus composition curve so that the remarks on the  $T_g$  of PDNI made above apply here also.

### 3.6.5 BARTON EQUATION

The limitation of some copolymer equations has been shown above and several authors have developed treatments to deal with minima and maxima in  $T_g$  versus composition data. In particular, Barton<sup>(81)</sup> has extended the Gibbs and DiMarzio<sup>(82)</sup> copolymer equation to include the effects of the different properties of aa, ab, ba and bb sequences in a copolymer containing a and b units. Instead of mole fractions as weighting factors the fractions of rotatable bonds per unit are chosen and the equation has the form

$$T_g = n'_{aa}T_{aa} + n'_{bb}T_{bb} + n'_{ab}T_{ab} + n'_{ba}T_{ba} \quad (3.18)$$

where  $n'_{ij}$  is the mole fraction of rotatable bonds (or groups)

in an  $ij$  sequence. The terms  $T_{aa}$  and  $T_{bb}$  are the glass transition temperatures of the homopolymers of  $a$  and  $b$  respectively and  $T_{ab} = T_{ba}$  is equated to the  $T_g$  of the strictly alternating copolymer  $(a-b)_n$  so that equation (3.18) may be rewritten as

$$T_g = n'_{aa}T_{aa} + n'_{bb}T_{bb} + (n'_{ab} + n'_{ba})T_{ab} \quad (3.19)$$

it can be shown that<sup>(83,84)</sup>

$$n_{aa} = r_a \chi / [r_a \chi + (\frac{r_b}{\chi}) + 2] \quad (3.20)$$

and

$$n_{bb} = \frac{r_b}{\chi} / [r_a \chi + (\frac{r_b}{\chi}) + 2] \quad (3.21)$$

where  $r_a$  and  $r_b$  are the reactivity ratios of comonomers  $A$  and  $B$  and  $\chi = [A]/[B]$ , the feed ratio necessary to give the copolymer composition defined by  $n_{aa}$  and  $n_{bb}$ , the mole fractions of  $aa$  and  $bb$  diads respectively. The sum of the mole fractions of  $ab$  and  $ba$  diads is given by

$$n_{ab} + n_{ba} = 1 - n_{aa} - n_{bb} \quad (3.22)$$

with  $n_{ab} = n_{ba}$ .

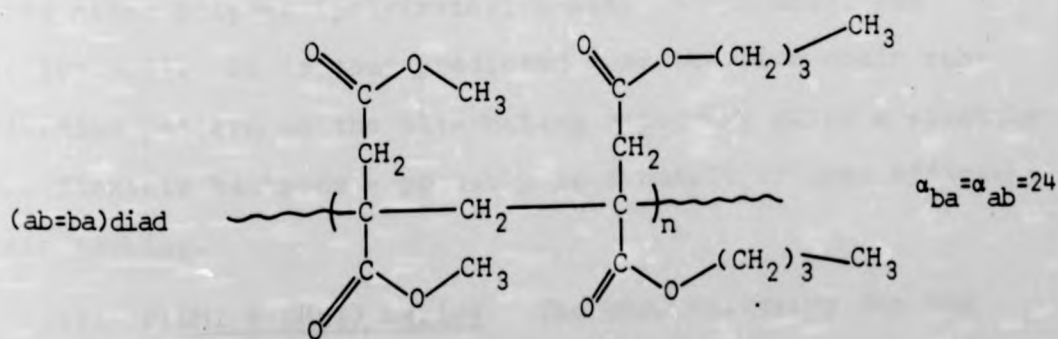
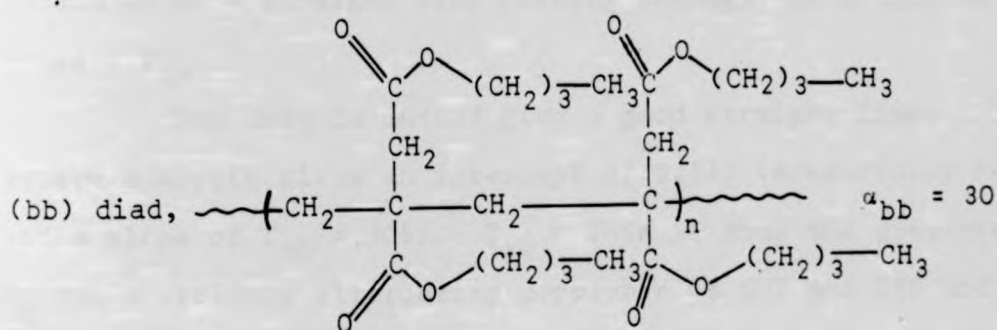
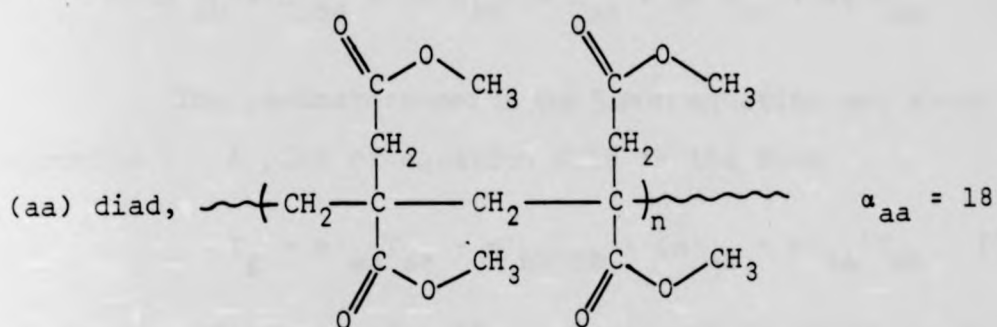
The rotatable bond fractions  $n'_{ij}$  are given by

$$n'_{ij} = n_{ij} \alpha_{ij} / \sum_{i,j} (n_{ij} \alpha_{ij}) \quad (3.23)$$

where  $\alpha_{ij}$  is the number of rotatable bonds in an  $ij$  sequence.

The application of the Barton equation is described in detail for the P(DMI + DBI) system below.

(i) P(DMI + DBI) series. The values of  $\alpha_{ij}$  for the three possible sequences are obtained by counting all rotatable bonds in the sequence in question. DMI is labelled monomer a and DBI monomer b.



$n'_{aa}$  is then given by

$$\begin{aligned} n'_{aa} &= n_{aa} \alpha_{aa} / n_{aa} \alpha_{aa} + n_{bb} \alpha_{bb} + n_{ab} \alpha_{ab} + n_{ba} \alpha_{ba} \\ &= 18 n_{aa} / 18 n_{aa} + 30 n_{bb} + 48 n_{ab} \end{aligned} \quad (3.24)$$

similarly

$$n'_{bb} = 30 n_{bb}/18 n_{aa} + 30 n_{bb} + 48 n_{ab} \quad (3.25)$$

$$n'_{ab} = n'_{ba} = 24 n_{ab}/18 n_{aa} + 30 n_{bb} + 48 n_{ab} \quad (3.26)$$

The parameters used in the Barton equation are shown in Appendix 1. A plot of equation 3.19 in the form

$$T_g - n'_{aa}T_{aa} - n'_{bb}T_{bb} = (n'_{ab} + n'_{ba})T_{ab} \quad (3.27)$$

is shown in figure 3.48. If the treatment is valid the points should be on a straight line passing through the origin with slope =  $T_{ab}$ .

The data do indeed give a good straight line, a least square analysis gives an intercept of 0.13K (essentially zero) and a slope of  $T_{ab} = 305K$ .  $T_{ab} = 305K$  is thus the predicted  $T_g$  for a strictly alternating copolymer of DMI and DBI and can be compared with the value of  $T_g = 315$  for the corresponding mixed ester polymer (poly(methyl n-butyl itaconate), see section 4.3). It is thus predicted that the side chain substitution pattern on the alternating copolymer gives a slightly more flexible backbone - probably as a result of less efficient chain packing.

(ii) P(DMI + DHbI) series. The data necessary for the Barton equation are listed in Appendix 1 and are plotted in figure 3.49.

A least square analysis of the data yields an intercept of -2.4K ( $\approx 0$ ) and slope of 254K which is the predicted  $T_g$  for the alternating copolymer. Again this value is less than that

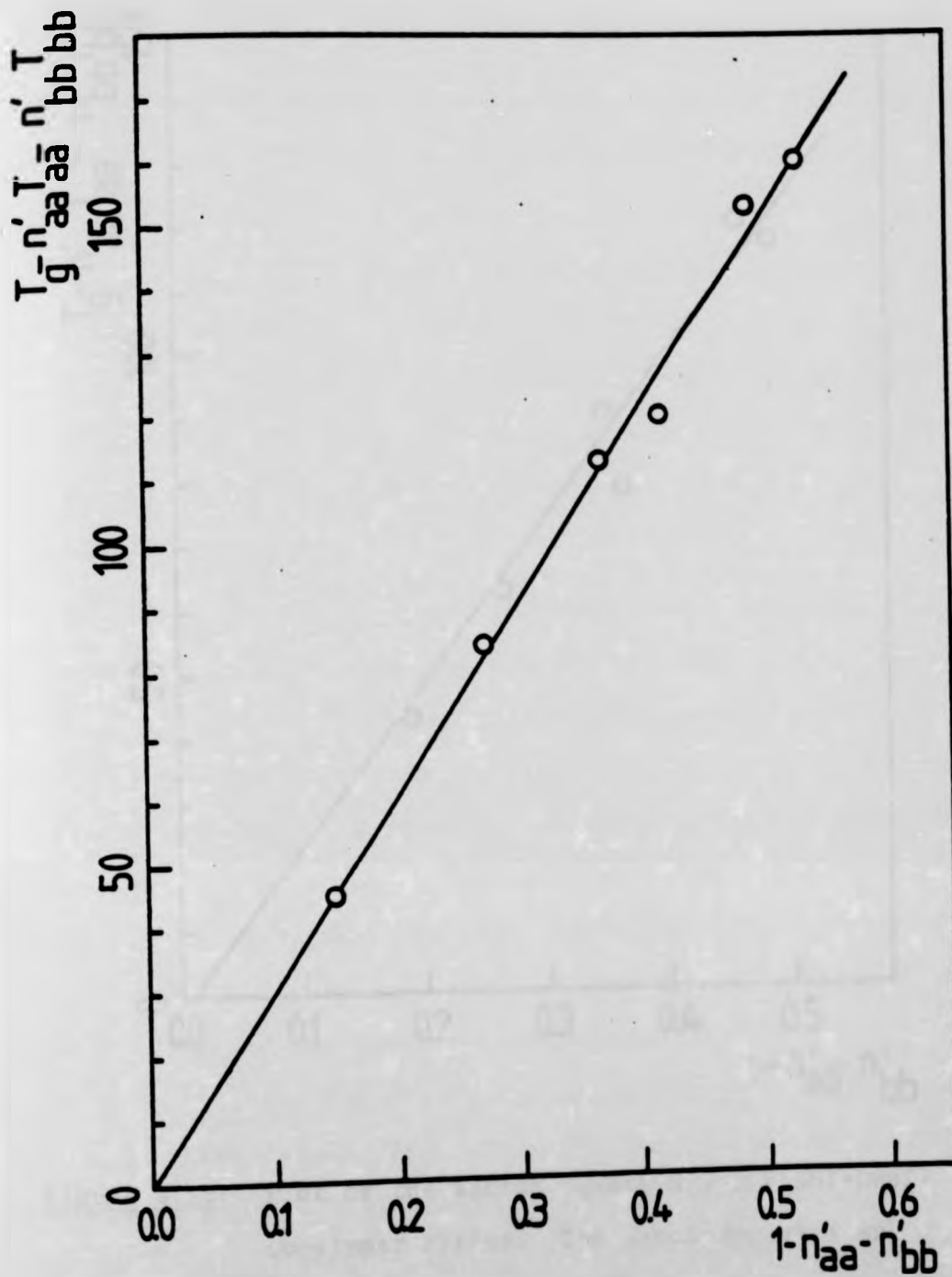


Figure 3.48: Plot of the Barton equation for P(DMI+DBI) copolymer series. The copolymer data are fitted to a least square determined straight line with slope = 305K.

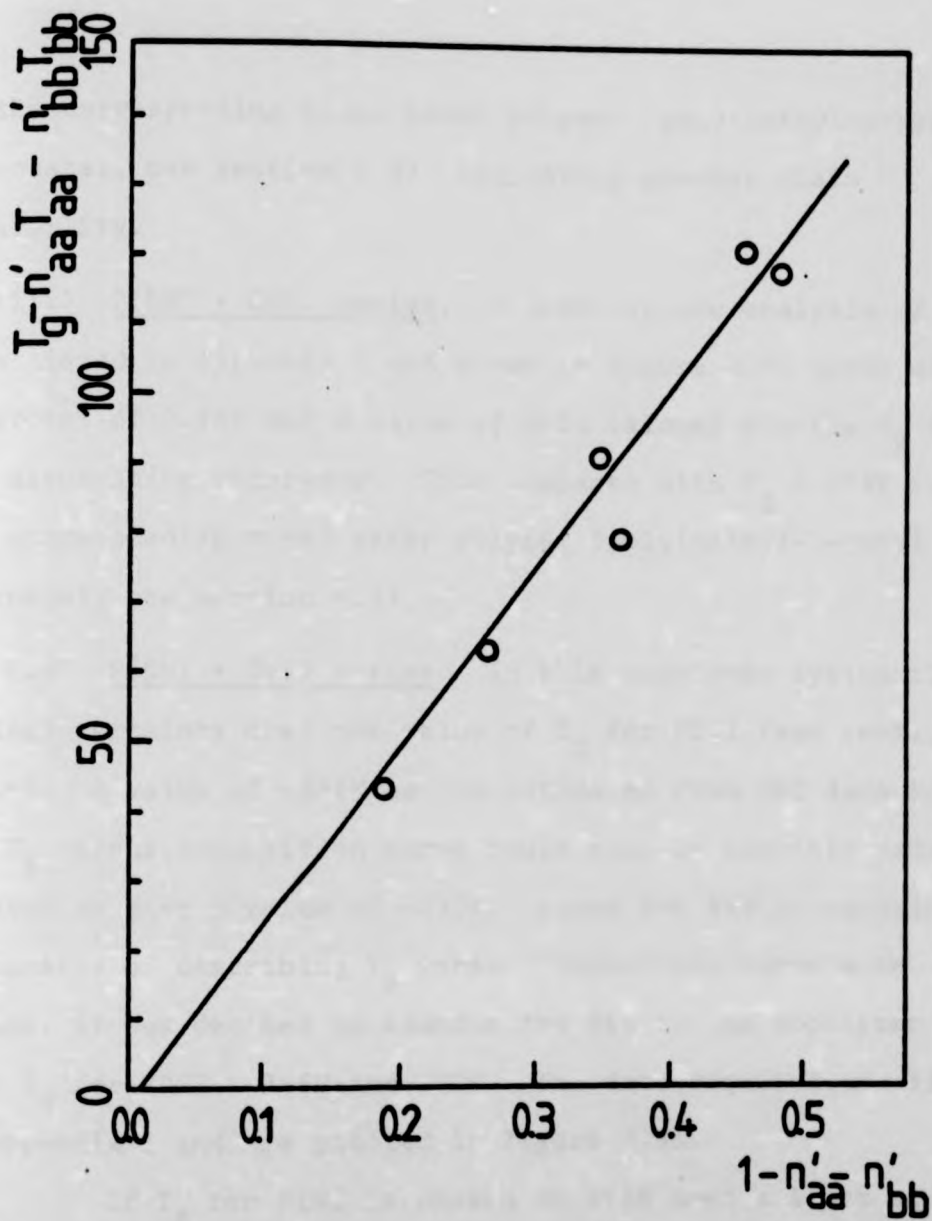


Figure 3.49: Plot of the Barton equation for P(DMI+DHpI) copolymer series. The copolymer data are fitted to a least square determined straight line with slope = 254K.

of the corresponding mixed ester polymer (poly(methyl-n-heptyl itaconate), see section 4.3) indicating greater chain flexibility.

(iii) P(DMI + DOI) series. A least square analysis of the data listed in Appendix 1 and shown in figure 3.50 gives an intercept of 0.26K and a value of 263K (slope) for the  $T_g$  of the alternating copolymer. This compares with  $T_g = 278K$  for the corresponding mixed ester polymer (poly(methyl-n-octyl itaconate), see section 4.3).

(iv) P(DMI + DNI) series. In this copolymer system there is less certainty over the value of  $T_g$  for PDNI (see section 3.3.4). A value of  $\sim 245K$  can be estimated from DSC data but the  $T_g$  versus composition curve could also be sensibly extrapolated to give a value of  $\sim 230K$ . Since the Barton equation is capable of describing  $T_g$  versus composition curve with minima, it was decided to examine the fit to the copolymer data with  $T_g$  for PDNI = 245K and 230K. The data required are listed in Appendix 1 and are plotted in figure 3.51.

If  $T_g$  for PDNI is chosen as 245K then a least square analysis of the data gives a slope of 253K but a definite non-zero intercept of -6.5K. When  $T_g$  for PDNI is chosen as 230K then the slope is similar at 251K with a reduced non-zero intercept of -2.9K. On the basis of the better fit to the Barton equation, an extrapolated value of  $T_g = 230K$  may be chosen for PDNI, which is very different from the DSC determined value of 245K. The  $T_g$  for the alternating copolymer is roughly the same in both cases and again indicates that alternating placement gives a more flexible backbone than that of the corresponding



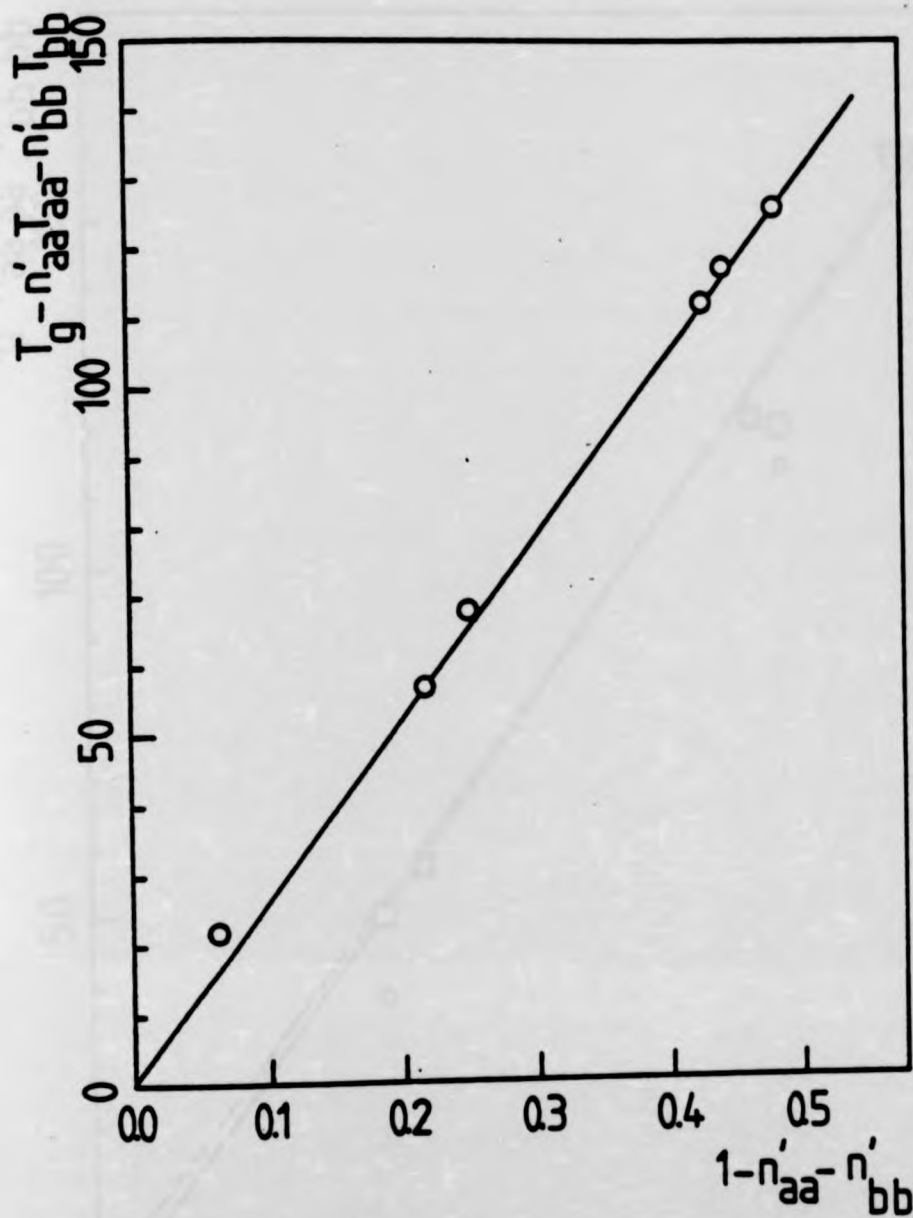


Figure 3.50: Plot of the Barton equation for P(DMI+DOI) copolymer series. The copolymer data are fitted to a least square determined straight line with slope = 263K.

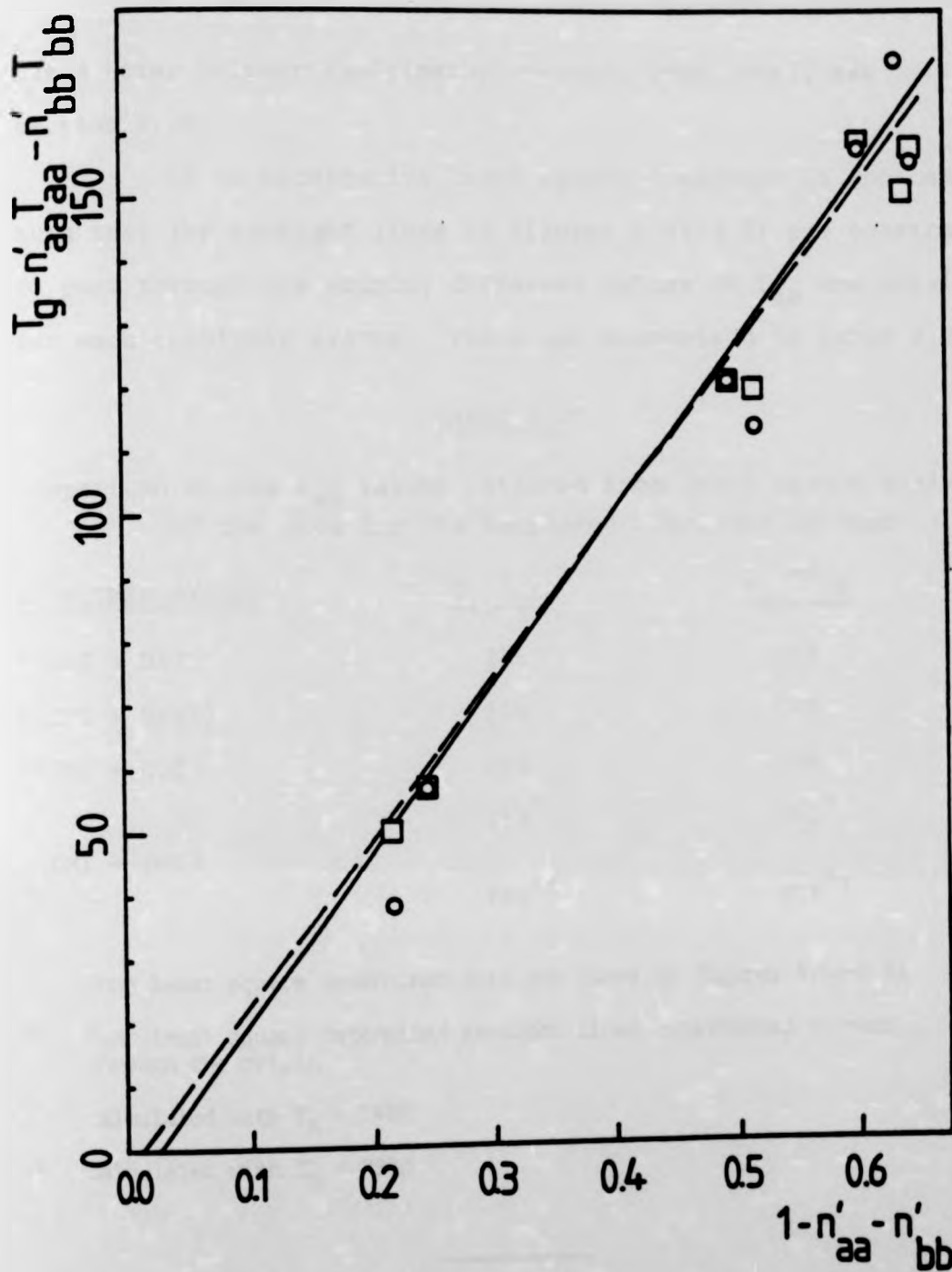


Figure 3.51: Plot of the Barton equation for P(DMI+DNI) copolymer series. (—○—), drawn with  $T_g$  for PDNI = 245K. The copolymer data are fitted to a least square determined straight line with slope = 253K; (---□---) drawn with  $T_g$  for PDNI = 230K and the copolymer data are fitted to a least square determined straight line with slope = 251K.

mixed ester polymer (poly(methyl-n-nonyl itaconate), see section 4.3).

If an alternative least square treatment is applied such that the straight lines in figures 3.48-3.51 are constrained to pass through the origin, different values of  $T_{ab}$  are obtained for each copolymer system. These are summarised in Table 3.26.

TABLE 3.26

Comparison of the  $T_{ab}$  values obtained from least square analysis of the data for the indicated copolymer systems

<u>COPOLYMER SYSTEM</u>	$T_{ab}^*/K$	$T_{ab}^{**}/K$
P(DMI + DBI)	305	305
P(DMI + DHpI)	254	248
P(DMI + DOI)	263	264
	253 <sup>†</sup>	241 <sup>†</sup>
P(DMI + DNI)	251 <sup>††</sup>	246 <sup>††</sup>

\* From least square determined straight lines in figures 3.48-3.51

\*\* From least square determined straight lines constrained to pass through the origin

† calculated with  $T_b = 245K$

†† calculated with  $T_b = 230K$

---

Only in the case of the P(DMI + DNI) system is there a significant change in the  $T_{ab}$  predicted but the values still imply a more flexible backbone for the alternating copolymers.

The decision as to the correct value of  $T_g$  for PDNI

is still not clear cut. The DSC trace for PDNI does show a small, but definite, inflection at  $\sim 245\text{K}$ . Previously published TBA data<sup>(24)</sup> also agrees with this. Perhaps more copolymer data in the high DNI composition range would help to resolve this problem.

In conclusion, the copolymer data derived in this study can be fitted well to the Fox and Pochan-Beatty-Pochan equations, both involve no adjustable or other parameters. The non-applicability of the Gordon-Taylor equation, where a separate free volume parameter is used, is interesting. Similarly poor fits were obtained when the copolymer data was treated according to the Couchman and Karasz equation<sup>(85)</sup> which also uses free volume parameters ( $\Delta C_p$  values for the homopolymers). Perhaps these series of copolymers with their high concentration of long side chain branches, are not amenable to simple free volume treatments.

The Barton equation is successful in describing the copolymers studied here as well as many other simpler systems.<sup>(81)</sup> This equation seems to have more general utility than others but is limited in that it requires both reactivity ratios and  $T_a$  and  $T_b$  data before it could be used in a predictive manner.

CHAPTER 4

MIXED ESTER POLYMERS FROM ITACONIC ACID

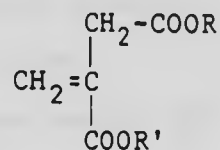
RESULTS AND DISCUSSIONS

Abbreviated names of mixed ester polymers used in this chapter.

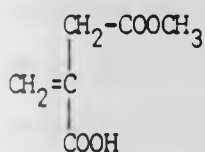
poly(methyl ethyl itaconate)	PMeEI
poly(methyl-n-propyl itaconate)	PMePrI
poly(methyl-n-butyl itaconate)	PMeBI
poly(methyl-n-pentyl itaconate)	PMePI
poly(methyl-n-hexyl itaconate)	PMeHxI
poly(methyl-n-heptyl itaconate)	PMeHpI
poly(methyl-n-octyl itaconate)	PMeOI
poly(methyl-n-nonyl itaconate)	PMeNI
poly(methyl-n-decyl itaconate)	PMeDI

4.1 MIXED ESTERS

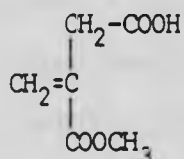
Mixed esters of itaconic acid



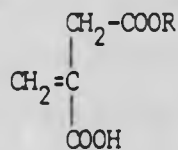
were prepared as described in section 2.1(iii). The method used was acid catalysed esterification of monomethylitaconate (MMI) so it is reasonable to expect an equilibrium product mixture containing all the possible isomers of mono- and diesters I-VIII below.



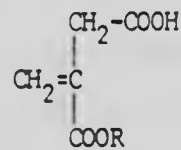
(I)



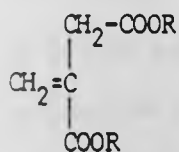
(II)



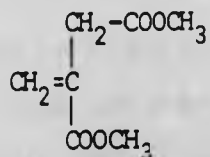
(III)



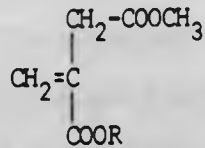
(IV)



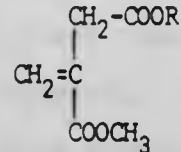
(V)



(VI)



(VII)



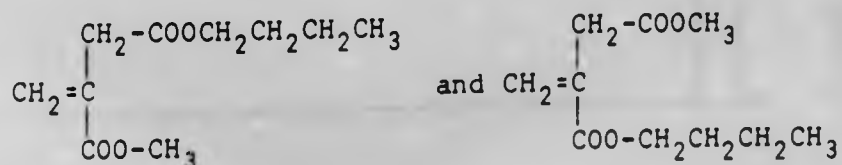
(VIII)

In general, monoesters I-IV will have higher boiling points than any of the corresponding diesters<sup>(18)</sup> and the diesters V and VI should have boiling points higher and lower respectively than either of the desired products VII and VIII. Consequently careful fractional distillation under vacuum with fractions monitored by nmr was expected to separate VII and VIII from

the other unwanted products. The separation of products VII and VIII would be expected to be extremely difficult, and nmr analysis showed separation was not achieved under the conditions used here.

The nmr spectrum of MMI shows in addition to the acid proton signal at  $\sim$  11-12 ppm, singlet absorptions at 6.45 and 5.81 ppm ( $H_2C=$ ), 3.69 ppm ( $-OCH_3$ ) and at 3.33 ppm ( $CH_2-\overset{O}{\parallel}C-$ ), whereas the corresponding signals in dimethyl itaconate (DMI) are at 6.22 and 5.68 ppm, a resolved doublet at 3.63 and 3.72 ppm and at 3.31 ppm (see figures 4.1 and 4.2). The resolved doublet in DMI indicates that the two  $-OCH_3$  groups experience different environments on either side of the molecule. This dissymmetry is also reflected in the coupling constant of the methine protons, 0.54 ppm in the DMI and 0.64 ppm in MMI.

The nmr spectrum of a mixed ester would be expected to exhibit a singlet for the  $-OCH_3$  at ca. 3.6-3.7 ppm. If the nmr spectrum in figure 4.3 is examined it is seen that it contains a resolved doublet with roughly equal integrals similar to that in DMI at ca. 3.6-3.7 ppm. No acid proton signal above 10 ppm was detected. This is consistent with an equimolar mixture of the diesters



which will provide the dissimilar  $-OCH_3$  environments. The



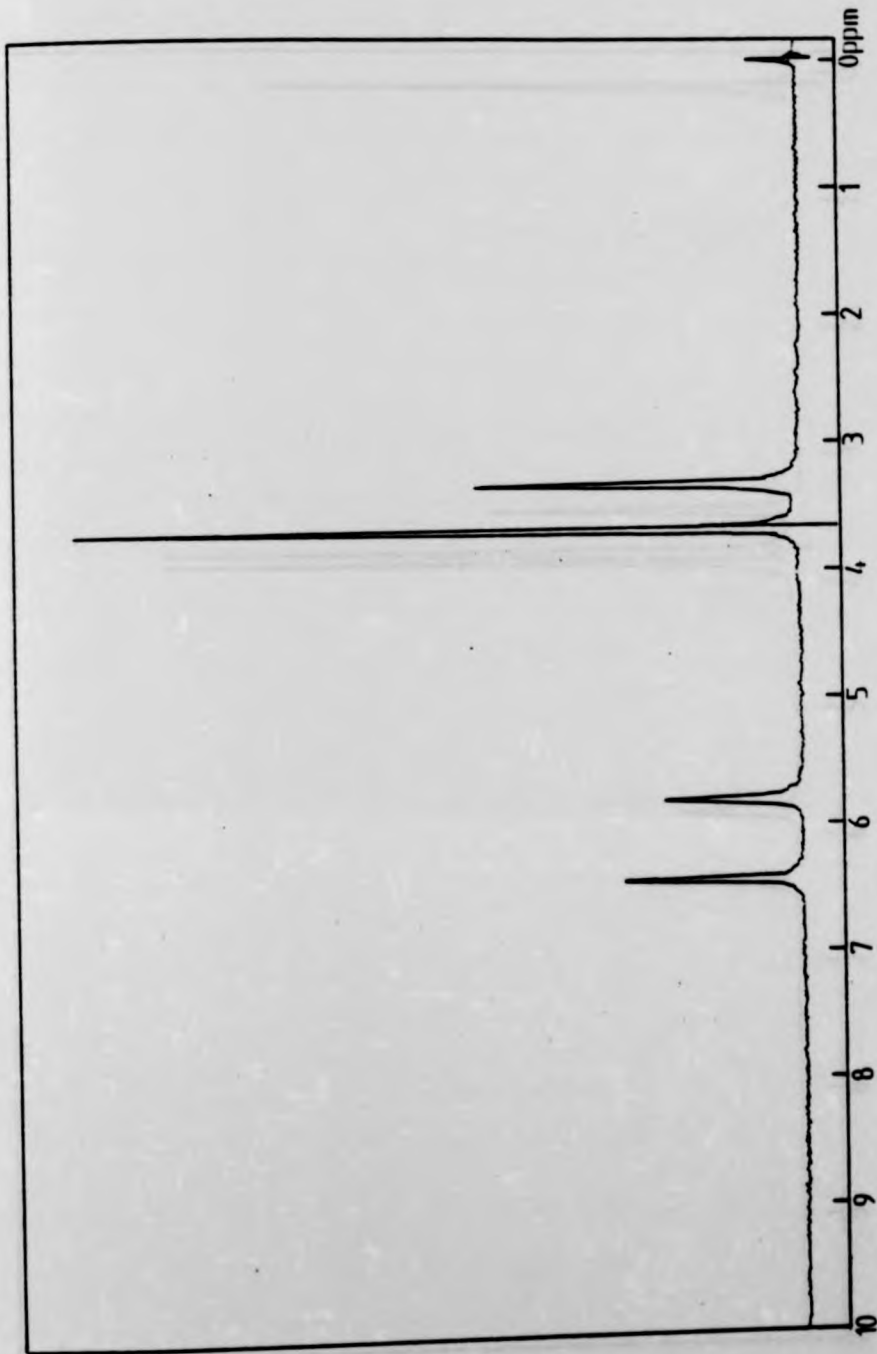


Figure 4.1: nmr spectrum of MMI

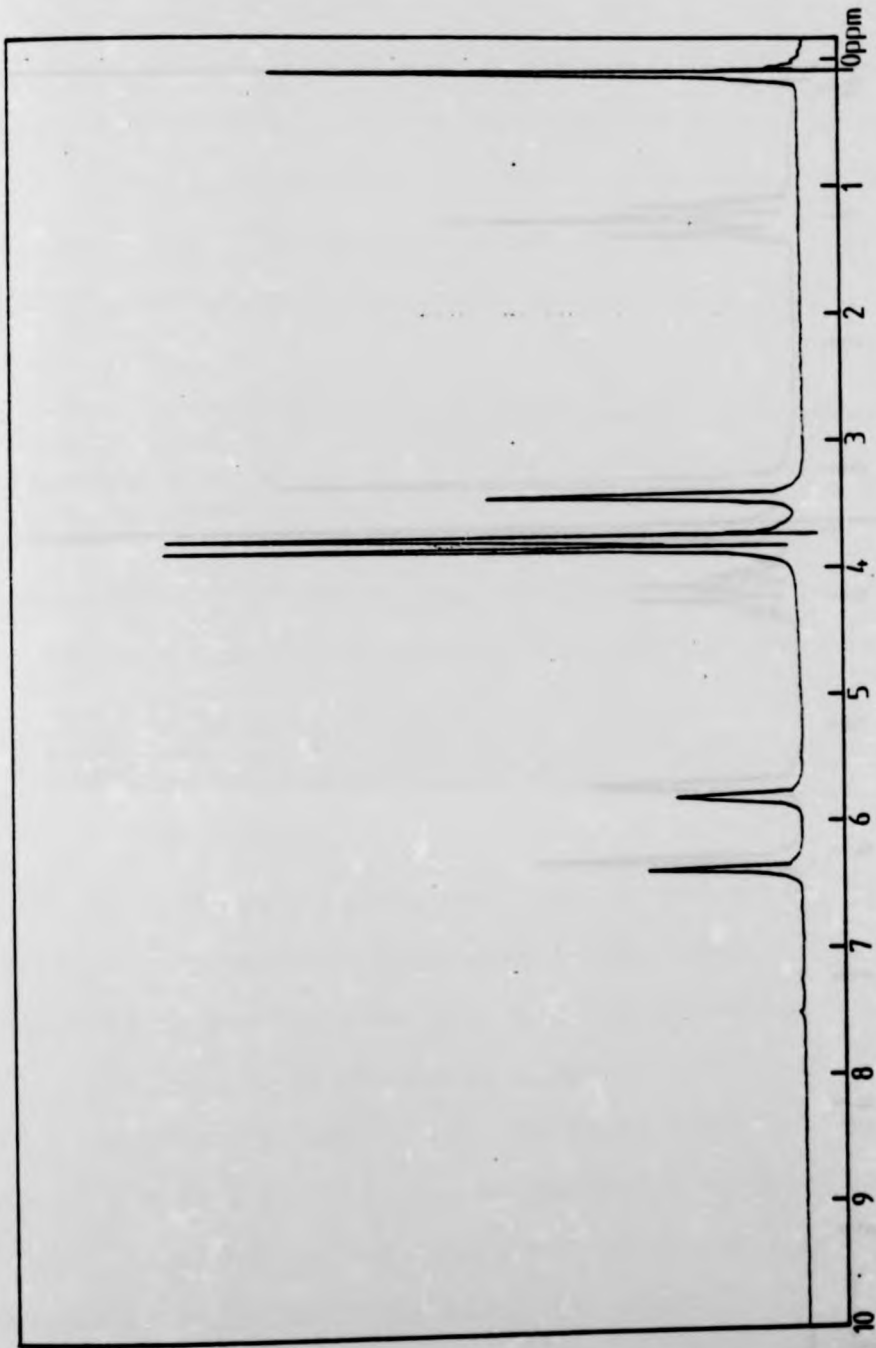


Figure 4.2: nmr spectrum of DMI

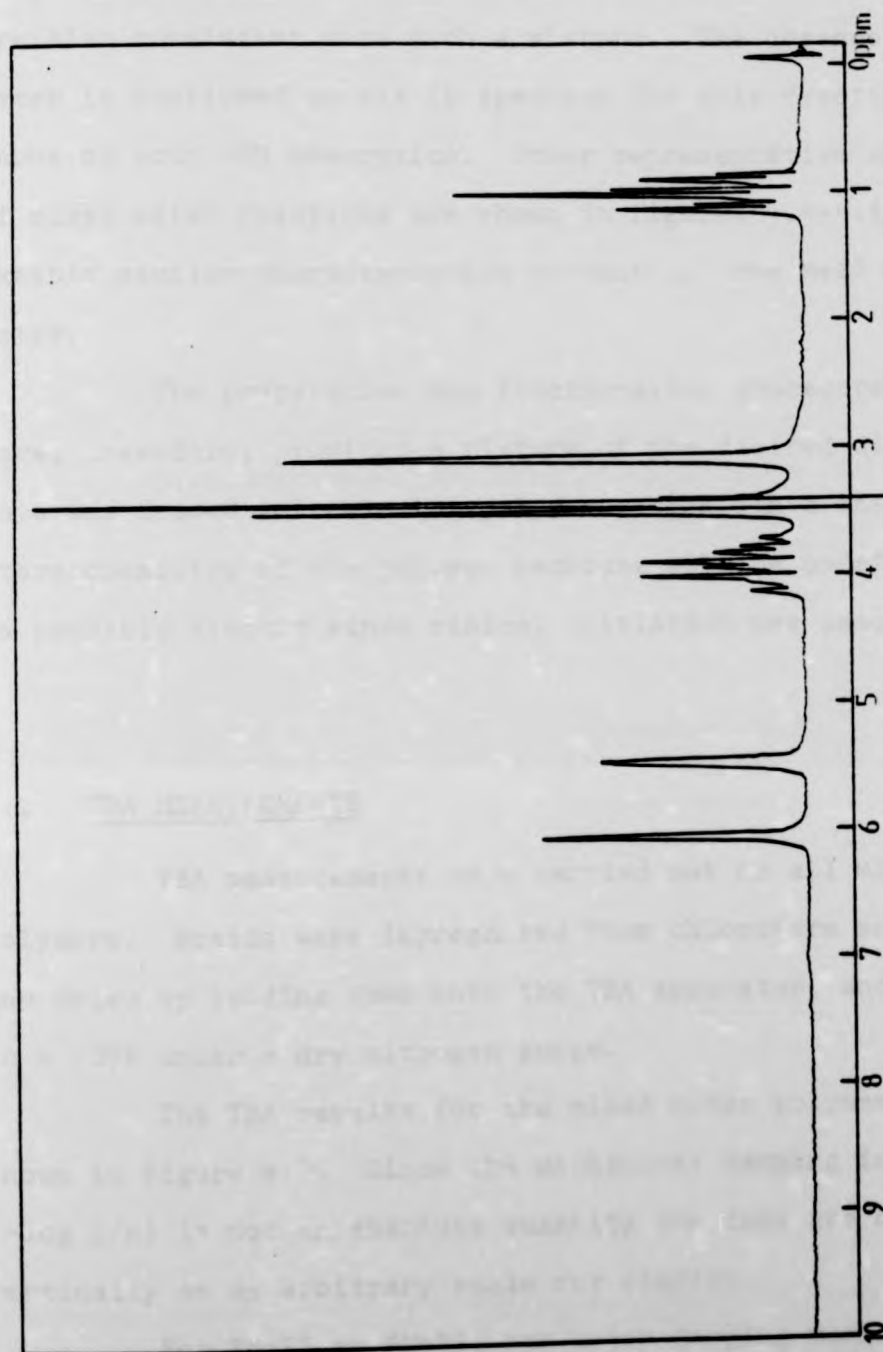


Figure 4.3: nmr spectrum of MeEI

multiplet at ca. 4.0 ppm is for the  $-OCH_2-$  protons and the  $-CH_2CH_2CH_3$  signals appear at higher field ; the integrals are also consistent with such a mixture. The absence of mono-ester is confirmed by the ir spectrum for this fraction which shows no acid  $-OH$  absorption. Other representative nmr spectra of mixed ester fractions are shown in figures 4.4-4.6 and these exhibit similar characteristics to that of the MeBI mixed ester.

The preparation and fractionation procedure used here, therefore, provides a mixture of the desired diesters. This was deemed suitable for polymerization since the precise stereochemistry of the polymer backbone will be undefined but is probably atactic since radical initiation was used.

#### 4.2 TBA MEASUREMENTS

TBA measurements were carried out on all mixed ester polymers. Braids were impregnated from chloroform solutions and dried by loading them into the TBA apparatus, and preheating to  $\sim 400K$  under a dry nitrogen purge.

The TBA results for the mixed ester polymers are shown in figure 4.7. Since the mechanical damping index ( $-\log 1/n$ ) is not an absolute quantity the data are displaced vertically on an arbitrary scale for clarity.

For PMeEI to PMeDI, one major damping maximum is apparent which is due to the  $T_g$  of each polymer and which moves progressively to higher temperatures as the number of carbon atoms in the larger alkyl side group decreases. The  $T_g$  for

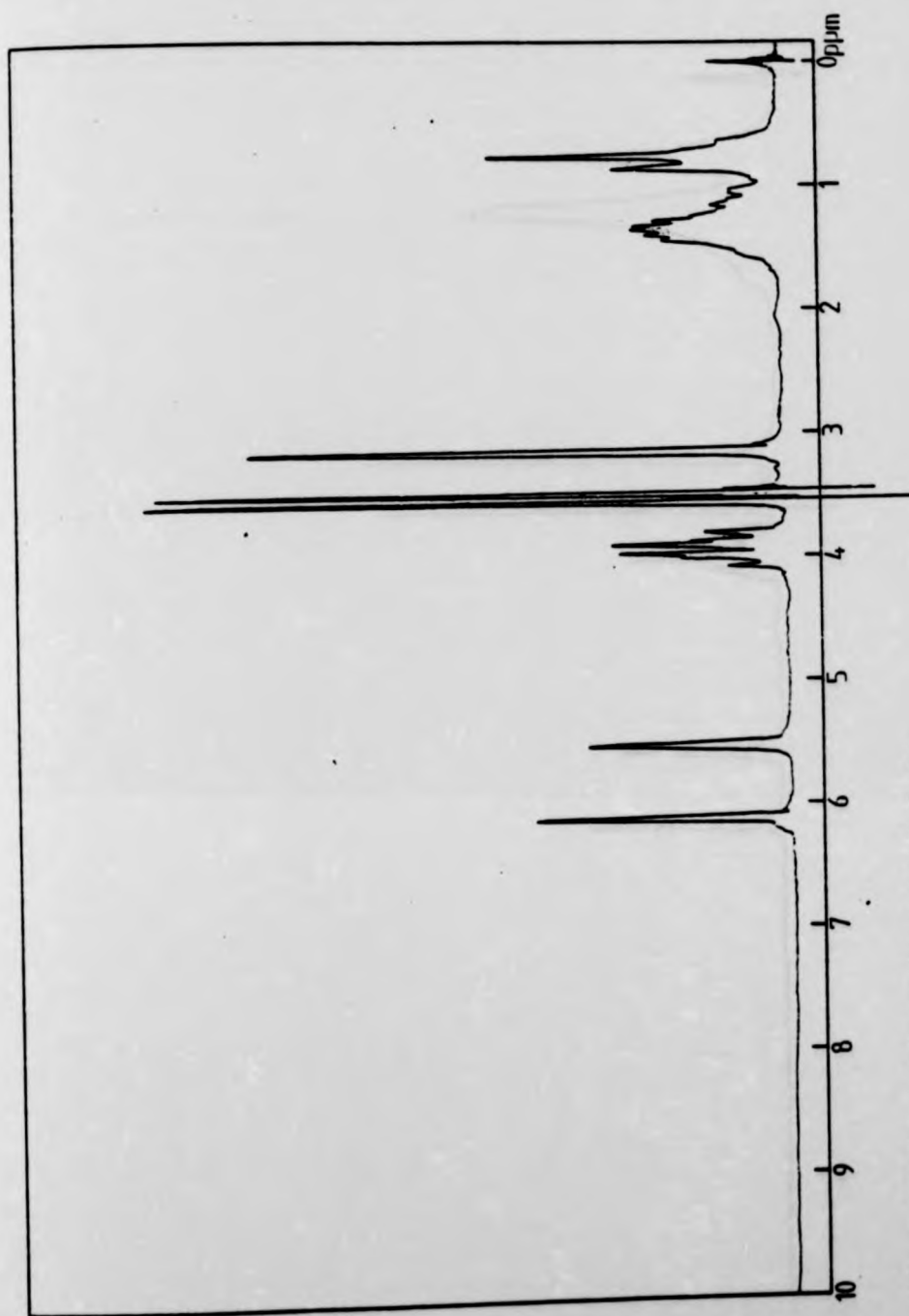


Figure 4.4: nmr spectrum of MeBI

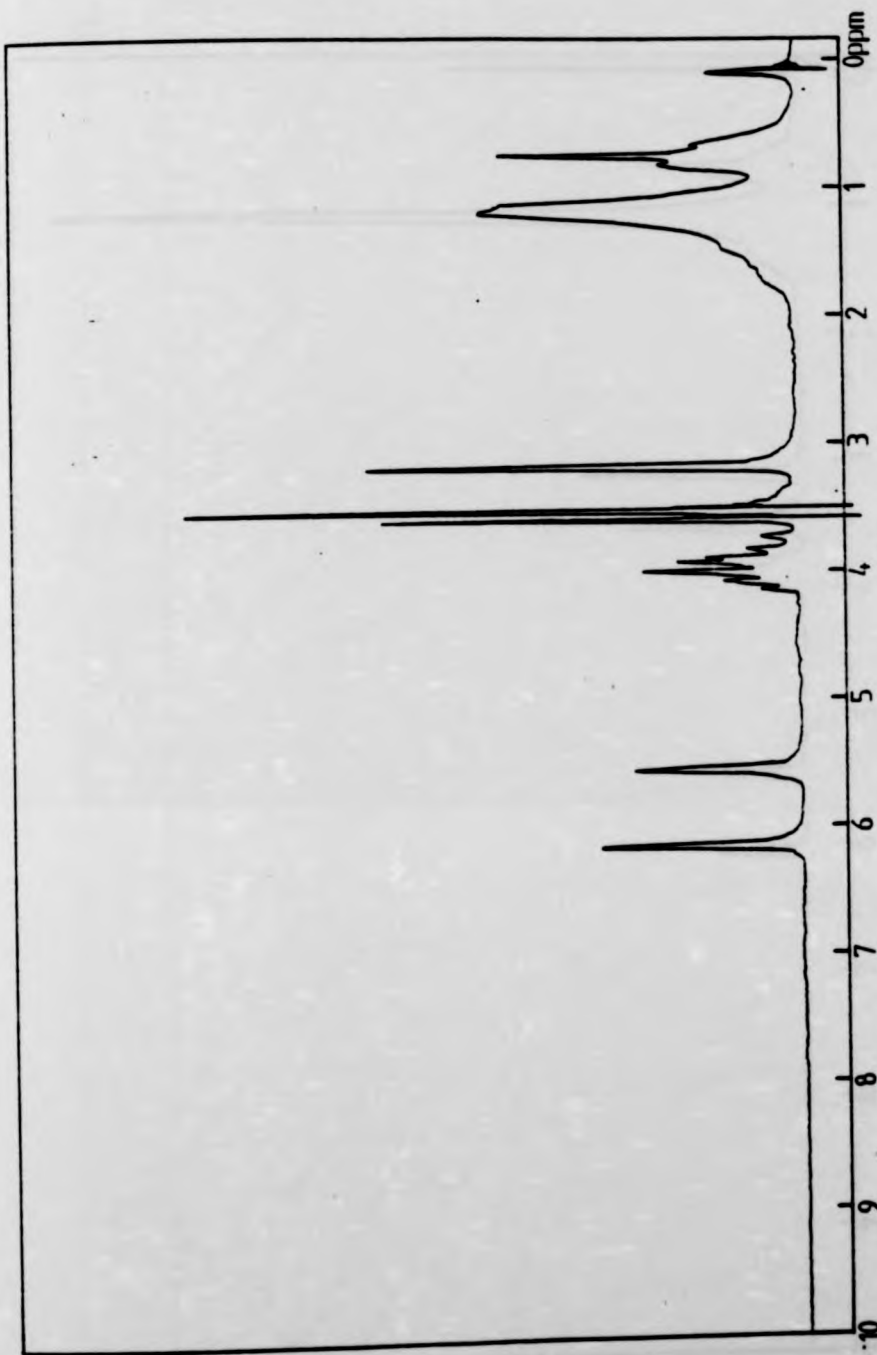


Figure 4.5: nmr spectrum of MeHxI

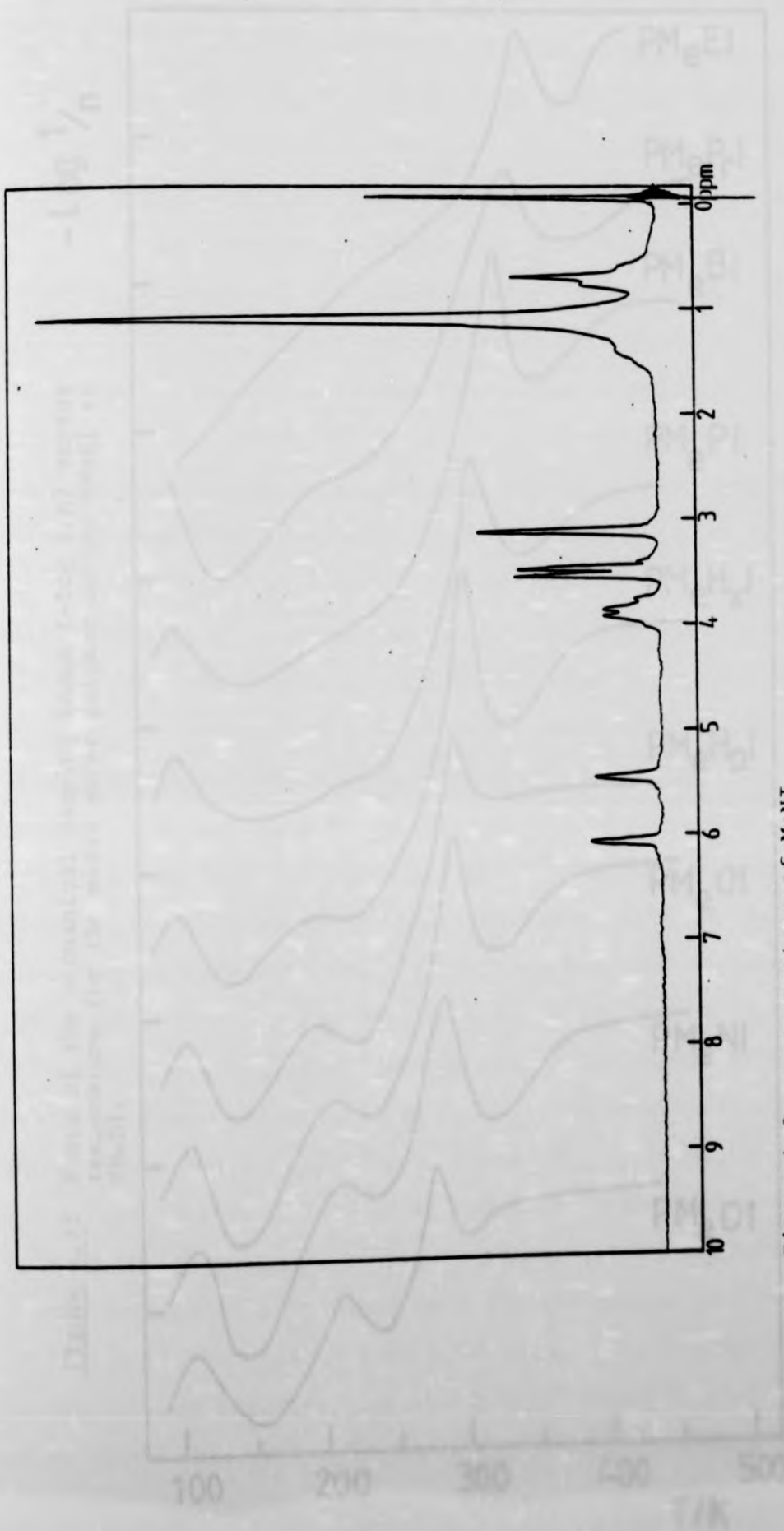
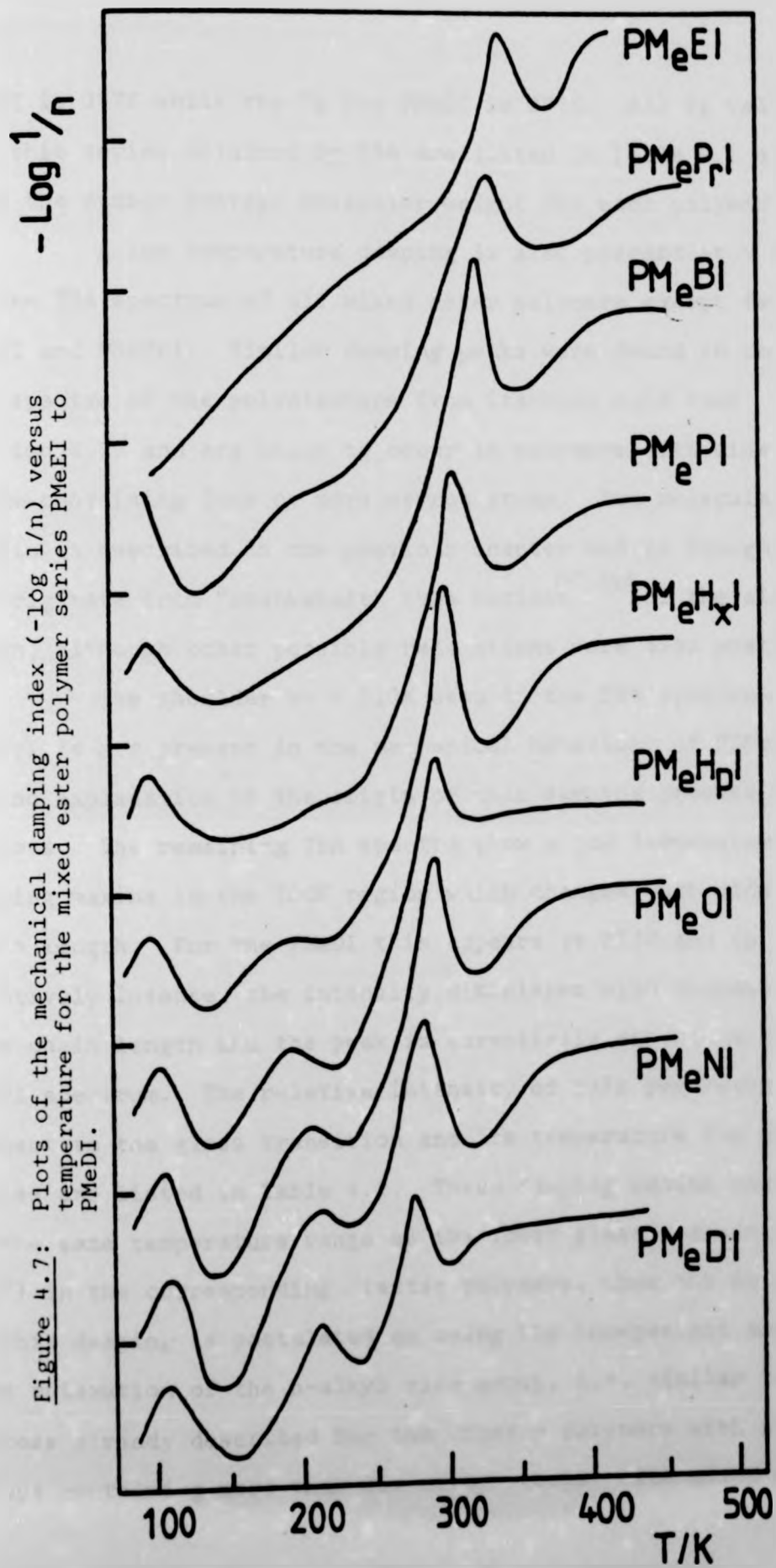


Figure 4.6: nmr spectrum of MeNI





PMeEI is 347K while the  $T_g$  for PMeDI is 277K. All  $T_g$  values for this series obtained by TBA are listed in Table 4.1 along with the number average molecular weight for each polymer.

A low temperature damping is also present at  $\sim 100K$  in the TBA spectrum of all mixed ester polymers except for PMeEI and PMePrI. Similar damping peaks were found in the TBA spectra of the polydiesters from itaconic acid (see section 3.2) and are known to occur in polymers with side chains containing four or more carbon atoms. Its molecular origin is described in the previous chapter and is thought to originate from "crankshaft" type motions<sup>(67,68)</sup> of the side chain, although other possible relaxations were also postulated<sup>(33)</sup>.

The shoulder at  $\sim 210K$  seen in the TBA spectrum of PMePrI is not present in the mechanical behaviour of PDPPrI<sup>(21)</sup> and no explanation of the origin of this damping process is obvious. The remaining TBA spectra show a low temperature damping maxima in the 200K region which changes with side chain length. For the PMeDI this appears at 213K and is relatively intense, the intensity diminishes with decreasing side chain length and the peak is essentially absent in the PMePI spectrum. The relative intensity of this peak with respect to the glass transition and its temperature for the series are listed in Table 4.2. These damping maxima occur in the same temperature range as the lower glass transitions ( $T_g^L$ ) in the corresponding diester polymers, thus the origin of this damping is postulated as being the independent cooperative relaxation of the n-alkyl side group, i.e. similar to the process already described for the diester polymers with side groups containing more than six carbon atoms. The mixed ester

TABLE 4.1T<sub>g</sub> and  $\bar{M}_n$  values for the mixed ester polymers

<u>SAMPLE CODE:</u>	<u>T<sub>g</sub></u> (K)	<u><math>\bar{M}_n \times 10^5</math></u> (g mol <sup>-1</sup> )
PMeEI	347	0.93
PMePrI	333	2.39
PMeBI	325	1.34
PMePI	309	1.49
PMeHxI	301	1.20
PMeHpI	294	1.31
PMeOI	290	0.74
PMeNI	283	1.14
PMeDI	277	0.95

---

TABLE 4.2

<u>SAMPLE CODE:</u>	$\frac{T_g^L}{(K)}$	<u>PEAK RELATIVE INTENSITY*</u> ( $T_g^L/T_g^U$ )
PMeHpI	193	0.38
PMeOI	207	0.45
PMeNI	214	0.56
PMeDI	213	0.72

\* Relative intensity of a peak is arbitrary

measured as  $\frac{-\log 1/n \text{ at peak } T_g^L}{-\log 1/n \text{ at peak } T_g^U}$

polymers are thus further examples of polymers with a second glass transition ( $T_g^L$ ). Since the "concentration" of the longer side chain in the mixed ester polymers is only 50% of that in the corresponding diester polymers, the relaxation is of lower relative intensity.

It is interesting to note that an apparent  $T_g^L$  is present in the PMeHxI sample at  $\sim 200\text{K}$ . No evidence for a  $T_g^L$  was found in PDHxI either by TBA or DSC<sup>(21)</sup>. Whether or not the  $\sim 200\text{K}$  peak is due to a  $T_g^L$  in the sense described above is not readily established. The  $T_g^L$  values for PMeDI to PMeHpI tend to lower temperatures (reflecting a slightly reduced energy requirement for the motion) just as the corresponding lower glass transitions for PDDI to PDHpI do (see section 3.3). The  $\sim 200\text{K}$  relaxation in PMeHxI does not continue this trend. This, taken with the DSC determined  $\Delta C_p$  values for  $T_g^L$  in the PDHpI to PDDI series (see section 3.4.1), which indicate that at least seven carbon atoms are necessary, and the absence of any detectable  $C_p$  inflection in the DSC trace for PMeHxI (see section 4.3), suggests that the relaxation is not a  $T_g^L$ .

When the values of  $T_g^L$  in the mixed ester polymers are compared with those in the corresponding diester polymers, they are found to be slightly higher for all but the heptyl pair. Notwithstanding the difficulties of obtaining precise temperatures from TBA maxima, it seems that the side chain environment in the mixed ester polymers (with side chains containing seven or more carbon atoms) is slightly more restricted than in a diester polymer with similar side chain. This could be due to slightly tighter packing when the methyl group is present.

#### 4.3 DSC MEASUREMENTS

The DSC results for the series of mixed ester polymers are shown as  $C_p$  versus temperature plots in figure 4.8. For polymers containing short side chain one distinct inflection in  $C_p$  is seen. This is the  $T_g$  for these polymers. For polymers with side chains equal to heptyl or longer the DSC traces are similar in appearance to those of the corresponding diester polymers, i.e. a low temperature inflection corresponding to  $T_g^L$  is present. However the inflection is rather weak and ill-defined and only approximate values of  $T_g^L$  are listed in Table 4.3 along with the glass transitions for the main chain relaxation ( $T_g$ ). These confirm the values obtained by TBA (see Tables 4.1 and 4.2).

#### 4.4 CONCLUSIONS

A comparison of the thermal and mechanical behaviour of homopolymers and random copolymers from diesters of itaconic acid with that of the mixed ester polymers, all prepared under the same conditions, is now possible.

In the previous chapter and from already published work<sup>(24)</sup> it has been established that polymers from diesters of itaconic acid show a minimum in  $T_g$  at a side chain length of about seven carbon atoms. At sufficiently long side chain length (eleven carbons and greater) crystallisation of the side chain occurs. When the  $T_g$  values for the mixed ester polymer series are plotted as a function of the number of carbon atoms in the longer side chain (see figure 4.9) a similar trend is observed, the increasing length of the single

Figure 4.8: Plots of  $C_p / JK^{-1}g^{-1}$  values versus temperature for the mixed ester polymer series. Polymers are indicated in the diagram.

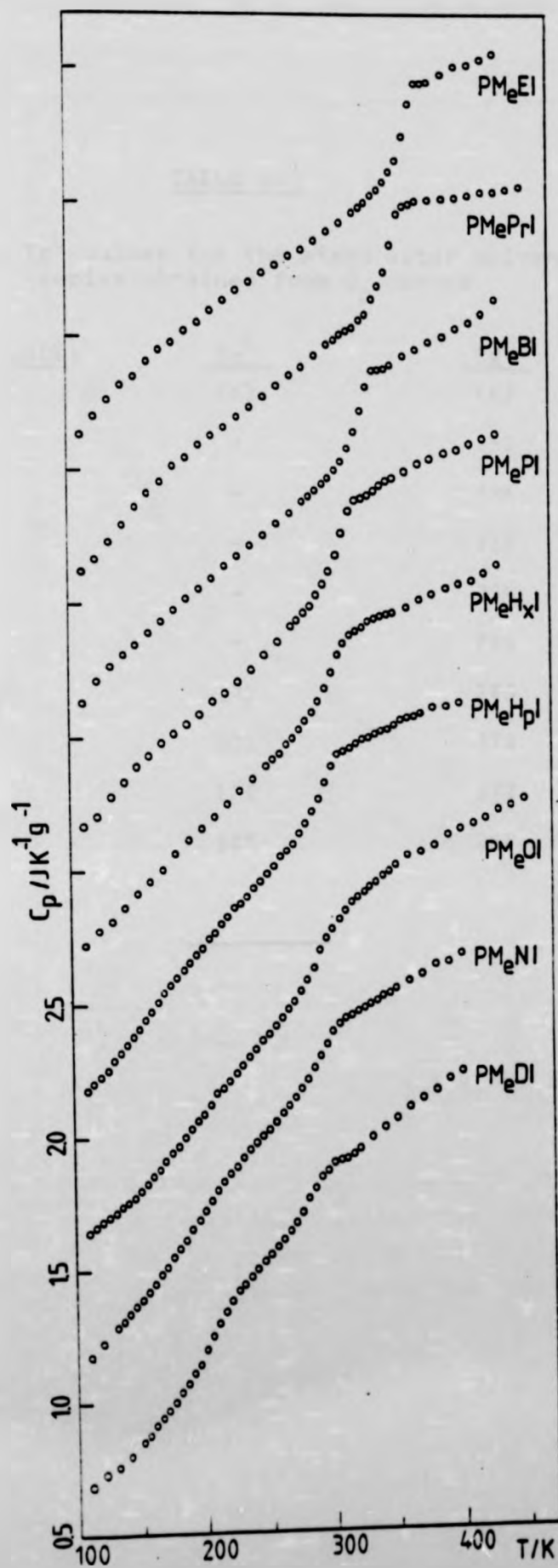


TABLE 4.3

$T_g^L$  and  $T_g^U$  values for the mixed ester polymer series obtained from  $C_p$  curves

<u>SAMPLE CODE:</u>	<u><math>T_g^L</math></u> (K)	<u><math>T_g^U</math></u> (K)
PMeEI	-	352
PMePrI	-	336
PMeBI	-	315
PMePI	-	294
PMeHxI	-	285
PMeHPI	172	280
PMeOI	201	278
PMeNI	172	272
PMeDI	186	266

---

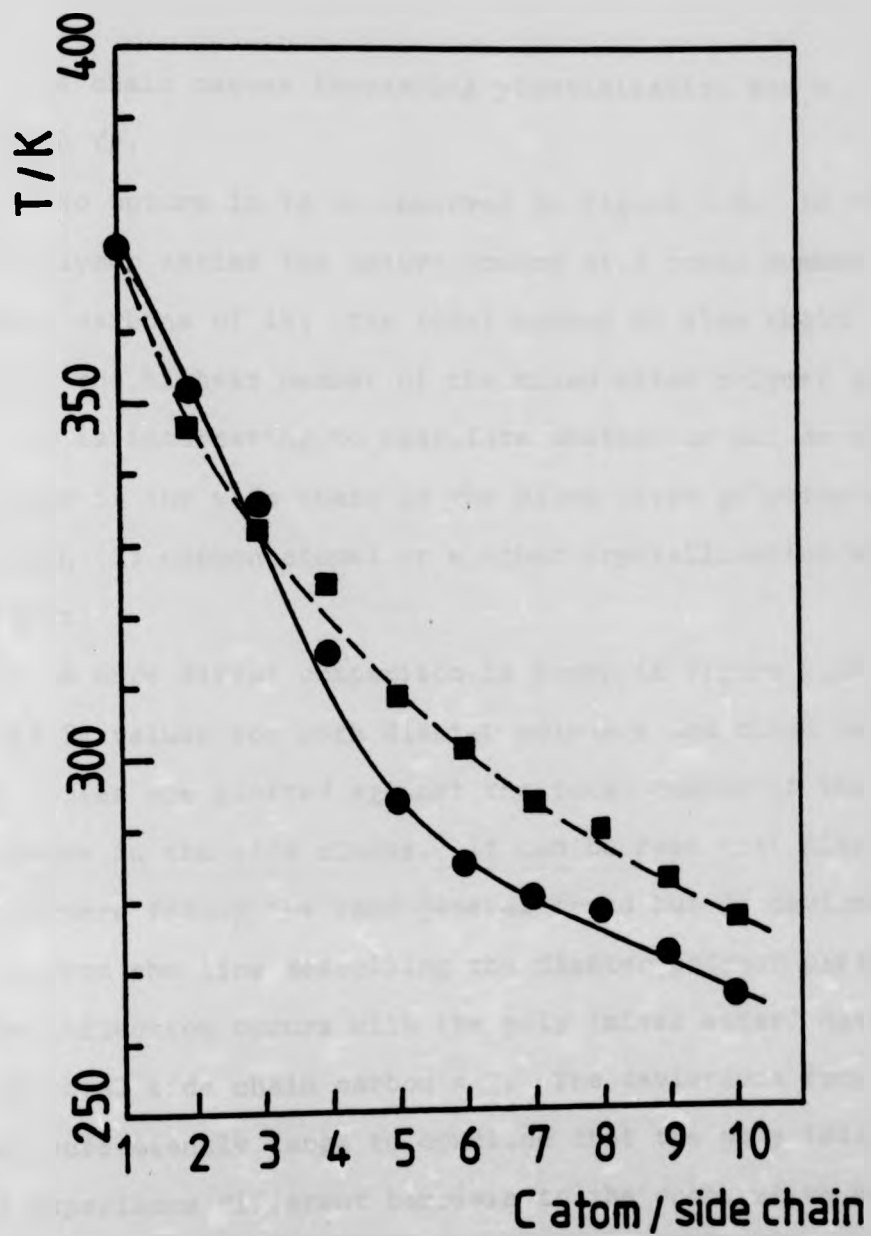


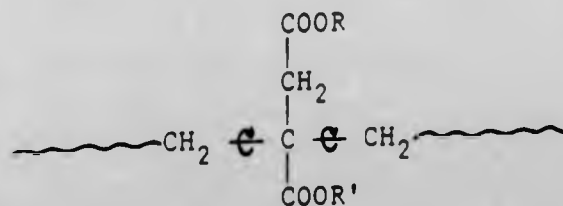
Figure 4.9: Plots of the  $T_g^U$  values determined by DSC (●) and TBA (■) against the number of carbon atoms in the longer ester side chain for the mixed ester polymer series PMeEI to PMeDI.



longer side chain causes increasing plasticisation and a decrease in  $T_g$ .

No upturn in  $T_g$  is observed in figure 4.9. In the diester polymer series the upturn occurs at a total number of side chain carbons of 14; the total number of side chain carbons of the highest member of the mixed ester polymer series is 11. It is interesting to speculate whether or not an upturn would occur if the side chain in the mixed ester polymers were long enough (13 carbon atoms) or whether crystallisation would occur first.

A more direct comparison is shown in figure 4.10 where the  $T_g$  values for both diester polymers and mixed ester polymer series are plotted against the total number of the carbon atoms in the side chains. It can be seen that mixed ester polymers follow the same general trend but do deviate slightly from the line describing the diester polymer series. A slight inflection occurs with the poly (mixed ester) data at about total side chain carbon = 7. The deviations from the line are sufficiently large to conclude that the poly (mixed esters) experience different barriers to the cooperative motion which define  $T_g$ . It seems unlikely that the difference lies in the actual rotational barrier of the main chain since in a diester polymer and a mixed ester polymer the alkyl side group is decoupled from the main chain by the ester links. In other words, the rotational barriers



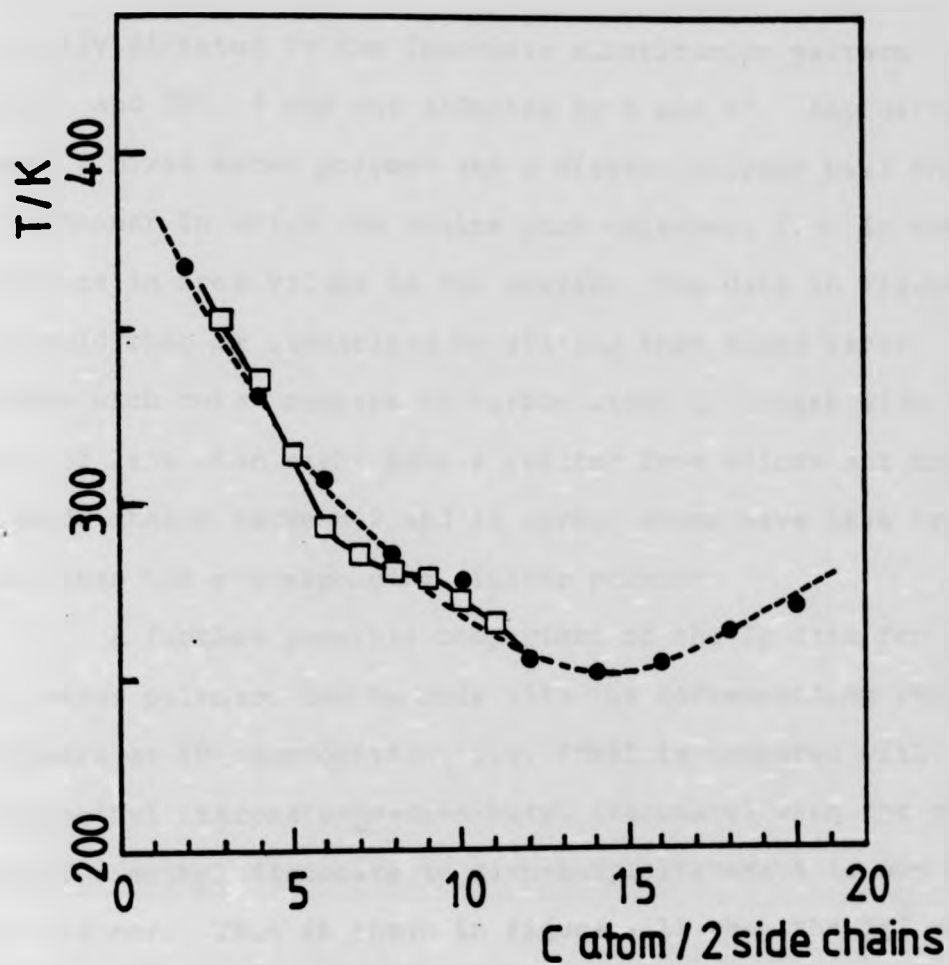


Figure 4.10: Plots of the DSC determined  $T_g$  values versus total number of carbon atoms in the side chains for poly(di-n-alkyl itaconates), (---●---) and for the mixed ester polymer series PMeEI to PMeDI, (—□—).

are mostly dictated by the immediate substitution pattern ( $\text{CH}_2\text{COO}$  and  $\text{COO}$  ) and not affected by R and R'. Any difference between a mixed ester polymer and a diester polymer will then lie in the manner in which the chains pack together, i.e. in the difference in free volume in the system. The data in figure 4.10 could then be summarised by stating that mixed ester polymers with total numbers of carbon atoms in longer side chains of less than eight have a greater free volume but those with side chains between 8 and 12 carbon atoms have less free volume than the corresponding diester polymer.

A further possible comparison of the Tg data for the mixed ester polymers can be made with the corresponding random copolymers at 50% composition, i.e. PMeBI is compared with poly(dimethyl itaconate-co-di-n-butyl itaconate) when the mol ratio of dimethyl itaconate to di-n-butyl itaconate is one in the copolymer. This is shown in figure 4.11 when the  $T_g^U$  values are compared for four systems. If the mixed ester polymers and the random copolymers have equivalent restriction to backbone motion then a straight line relation would be obtained. The experimental data approximate to this for the PMeBI, PMeHpI and PMeOI system but there is a distinct deviation at PMeNI.

As argued before the actual side chain length should not affect Tg through variation in rotational barriers. It must be again the case that significant differences in free volume are present between the PMeNI and the corresponding random copolymer systems from dimethyl itaconate and di-n-nonyl itaconate but not for the shorter chain systems.

In conclusion it can be said that the mixed ester

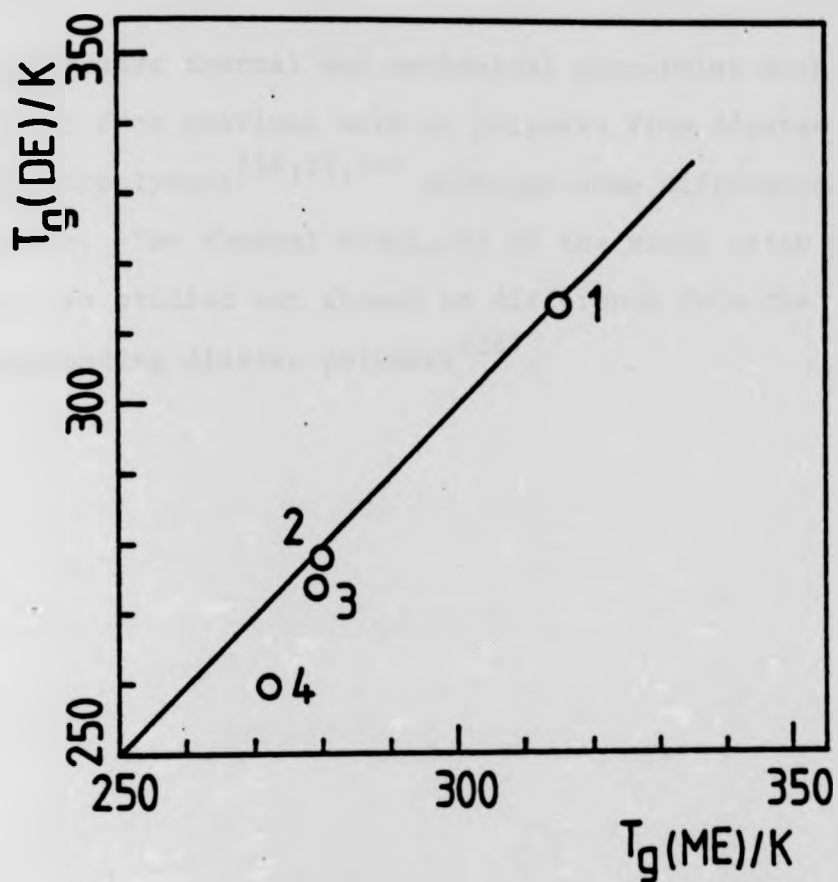


Figure 4.11: Plots of  $T_g$  for indicated mixed ester polymers ( $T_g(\text{ME})$ ) versus  $T_g$  at 50 mol % composition for the corresponding random diester copolymers ( $T_g(\text{DE})$ ).

<u>Point number</u>	<u>Mixed ester polymer</u>	<u>Diester copolymer</u>
1	PMeBI	P(DMI+DBI)
2	PMeHpI	P(DMI+DHpI)
3	PMeOI	P(DMI+DOI)
4	PMeNI	P(DMI+DNI)

polymers have thermal and mechanical properties much as expected from previous work on polymers from diesters and random copolymers<sup>(18,21,24)</sup> although some differences are apparent. The thermal stability of the mixed ester polymers were also studied but showed no difference from the corresponding diester polymers<sup>(18)</sup>.

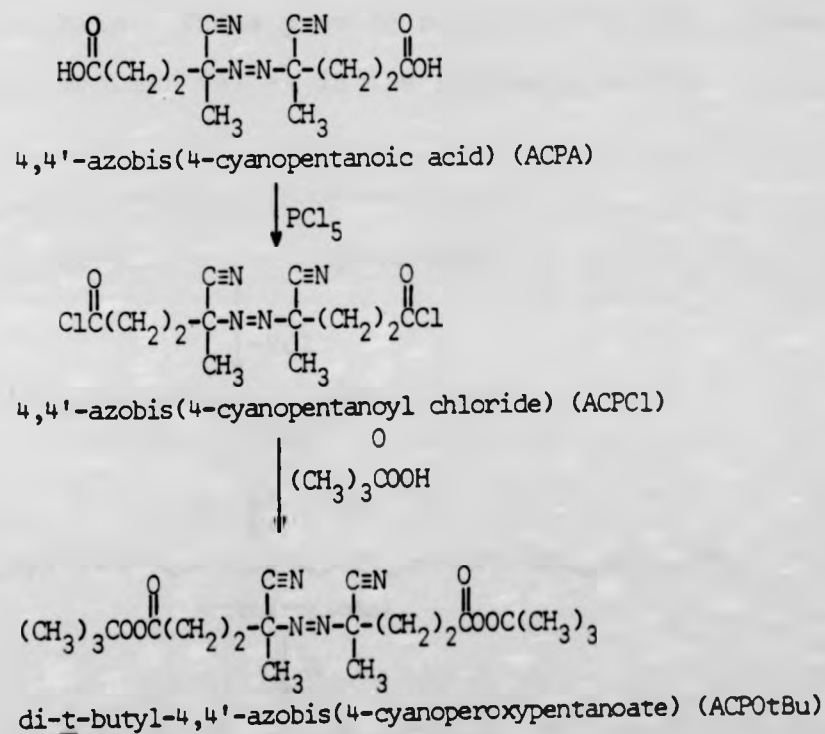
CHAPTER 5

BLOCK COPOLYMERS

RESULTS AND DISCUSSION

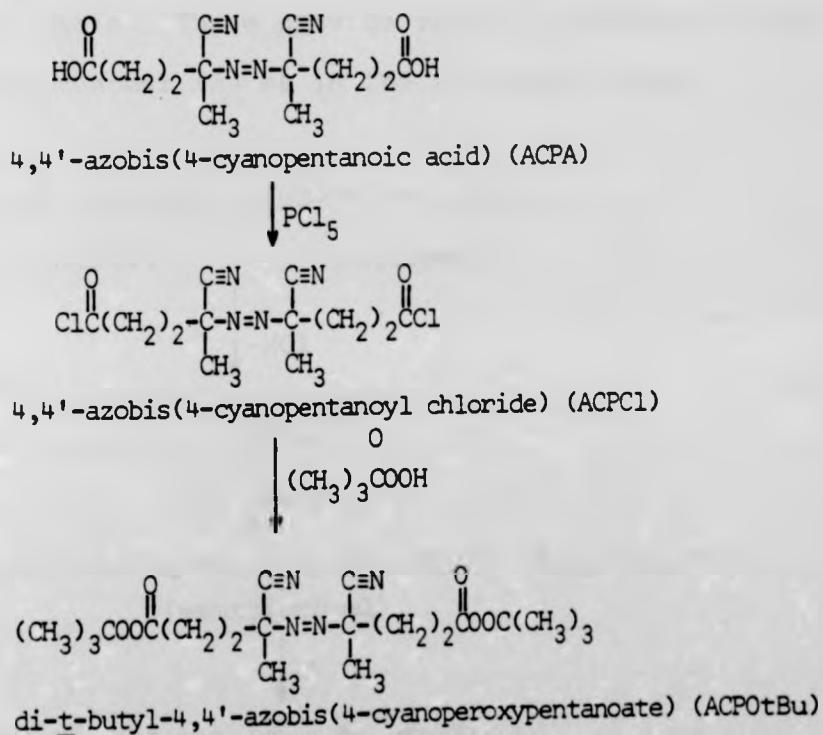
5.1 SEQUENTIAL INITIATORS

Preparation of block copolymers by a free radical method can be carried out by performing one of the blocks with a latent free radical-forming site at one or both end groups. Under chosen conditions, in the presence of a second monomer, this site is then activated and chain growth of the second monomer will proceed.<sup>(49,42,86,87)</sup> Two reaction schemes were employed in this work, using the sequential initiators synthesized as described in sections 2.1 (iv) and (v).



## 5.1 SEQUENTIAL INITIATORS

Preparation of block copolymers by a free radical method can be carried out by performing one of the blocks with a latent free radical-forming site at one or both end groups. Under chosen conditions, in the presence of a second monomer, this site is then activated and chain growth of the second monomer will proceed.<sup>(49,42,86,87)</sup> Two reaction schemes were employed in this work, using the sequential initiators synthesized as described in sections 2.1 (iv) and (v).

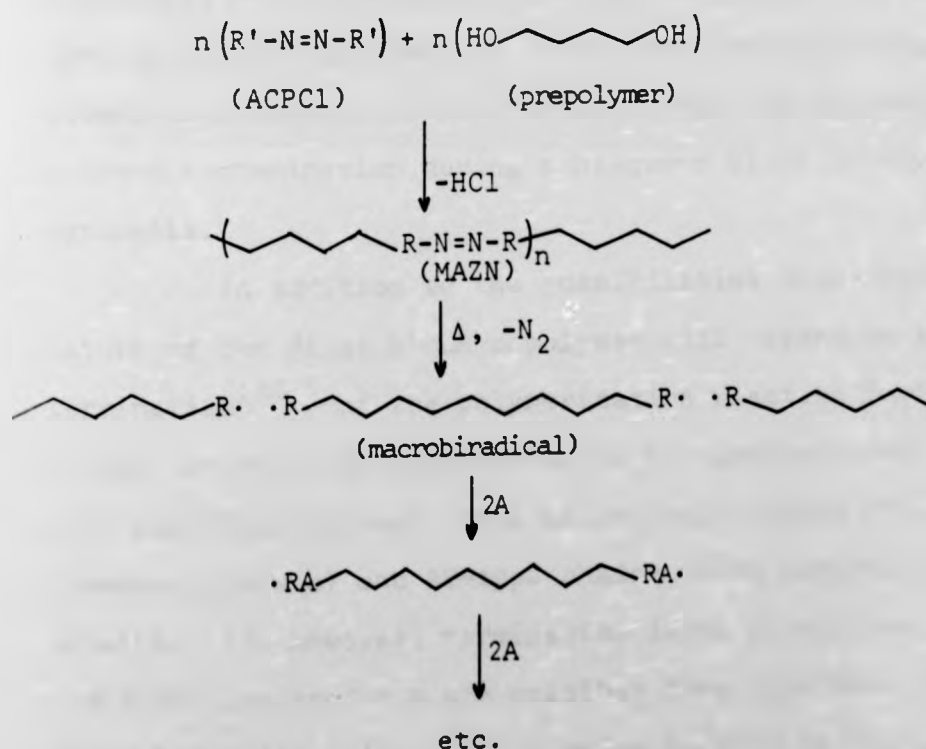




5.1.1 USE OF ACPCl - SCHEME 1

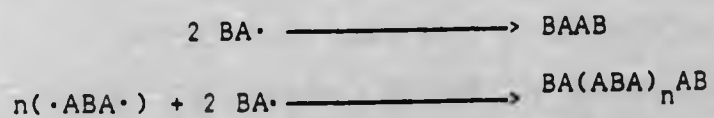
The ACPCl preparation yielded a white crystalline solid with a melting point of 364-367K, which compares with the literature value of 366-368K.<sup>(48)</sup> The ir spectrum has the expected absorbances at  $2250\text{ cm}^{-1}$  ( $\text{C}\equiv\text{N}$ ) and  $1800\text{ cm}^{-1}$  ( $\text{COCl}$ ) and the nmr spectrum is identical with that already published.<sup>(49)</sup>

ACPCl is a diacid chloride capable of condensing with hydroxyl-terminated prepolymers to give a linear macro-azonitrile (MAZN) which possesses thermally labile  $-\text{N}=\text{N}-$  links in the main chain. These provide radical initiation sites for a second monomer (A) as in the following scheme.



The product will be an ABA-type block copolymer where the B block derives from the original prepolymer and, in this work, the A block from dimethyl itaconate (DMI). In order to ensure that a significant number of macrobiradicals are formed, it is necessary that the degree of condensation (n) of the MAZN be reasonably high, since other initiating species will unavoidably be created from the MAZN end groups. These may be  $\sim\text{R-N=N-R}'$  if ACPCl is in excess during the condensation, or  $\sim\text{R-N=N-R}\sim\text{OH}$  if the prepolymer is used in excess. In the former case, homopolymer of the second monomer will be formed in addition to the desired ABA-type block copolymer. In the latter, a macromonomer radical will result from scission of the end azo linkage and this will lead to an AB-type block copolymer. In this work prepolymer was used in excess (see tables 2.5 and 2.10) in order to minimise homopolymer contamination during subsequent block copolymer synthesis.

In addition to the possibilities described above the nature of the final block copolymer will depend on the mode of termination<sup>(42)</sup> of the polymerization reaction involving the second monomer. If termination is by disproportionation only, then the final products will be ABA-type chains (from macrobiradical growth) and AB-type chains (from macromonomer radical growth). If, however, termination is by recombination then the following products are possible from a mixture of growing macrobiradicals (.ABA.) and growing macromonomer radicals (BA.),



in other words the block copolymeric products will be of the BAB-type or  $(ABA)_n$ -type.

The mode of termination of n-alkyl itaconates is not known, so it is not possible to predict the type of block copolymer which will be formed.

#### 5.1.2 USE OF ACPOtBu - SCHEME 2

ACPOtBu was obtained as a white crystalline solid with melting point of 374-377K. Elemental analysis gave C, 55.6%; H, 7.1%; N, 13.4%; which compares with the expected values C, 56.6%; H, 7.5%; N, 13.2%. The ir spectrum is shown in figure 5.1 and the nmr spectrum in figure 5.2.

ACPOtBu contains two peroxy links and one azo link which are both thermally labile but have widely differing activation energies. The peroxy link has a half life of  $\sim 5$  hours at 410K but the azo bond only requires 340K for a  $\sim 5$  hours half life.<sup>(88)</sup> The two groups can thus be selectively and sequentially activated in block copolymerizations.

The activation energy for peroxide decomposition may be lowered dramatically by using a redox system. The use of a reducing agent to activate peroxy decomposition enables initiation to be performed at significantly lower temperatures.<sup>(42)</sup> Tetraethylenepentamine (TEPA) is an effective activator for the perester links of ACPOtBu. The mechanism of this reaction is not known.

ACPOtBu was used in two temperature regions (a) 307-310K in the presence of TEPA to promote scission of the



Figure 5.1: ir spectrum of ACP0tBu

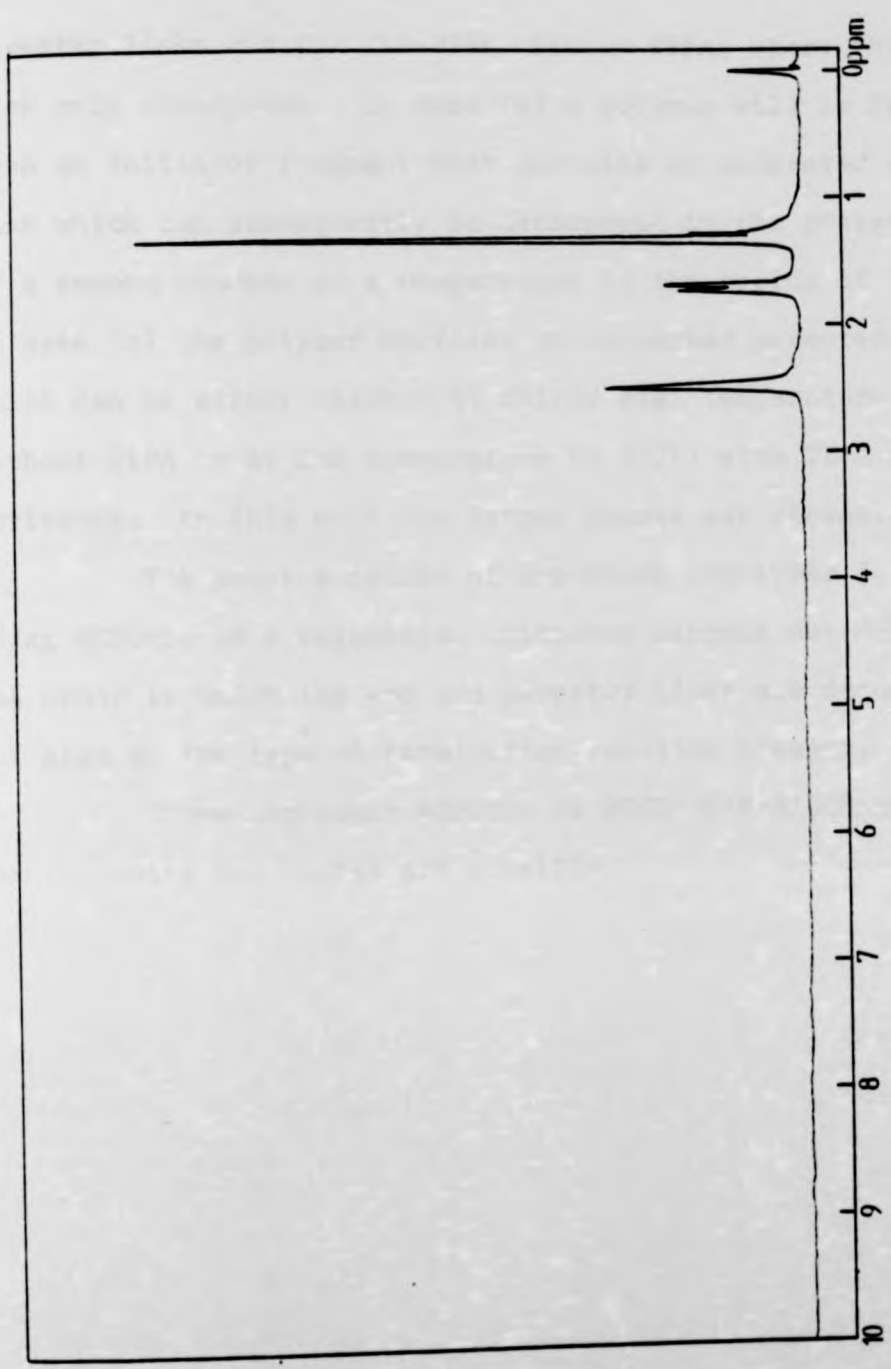


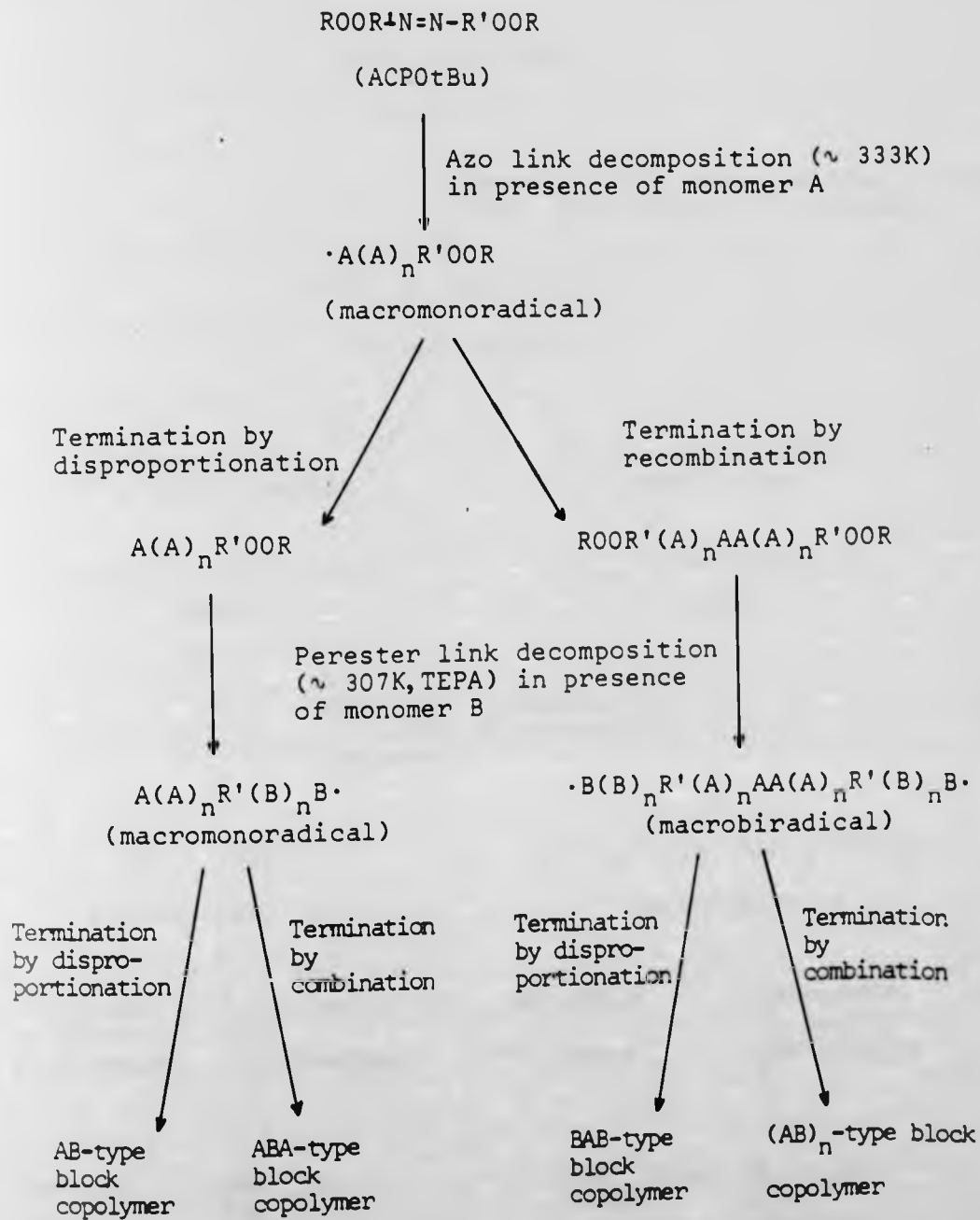
Figure 5.2: nmr spectrum of ACP0tBu

perester links and (b) 333-338K without TEPA, where the azo link only decomposes. In case (a) a polymer will be formed from an initiator fragment that contains an unreacted azo link which can subsequently be decomposed in the presence of a second monomer at a temperature in the region of 333K. In case (b) the polymer contains an unreacted perester link which can be either reacted at fairly high temperature ( $> 373\text{K}$ ) without TEPA or at low temperature ( $\sim 307\text{K}$ ) with TEPA as activator. In this work the latter course was chosen.

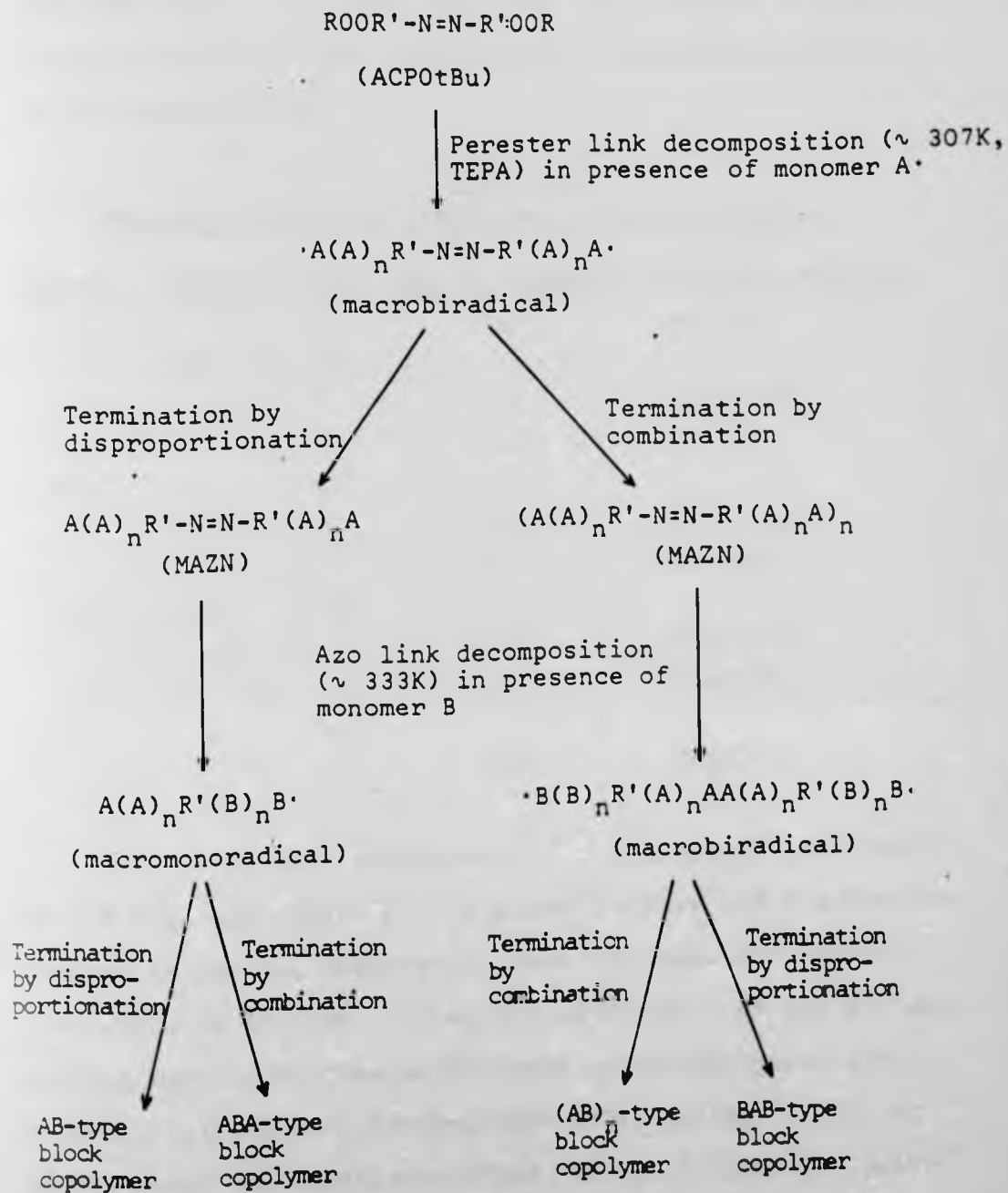
The precise nature of any block copolymer formed using  $\text{ACPOtBu}$  as a sequential initiator depends not only on the order in which the azo and perester links are decomposed, but also on the type of termination reaction present.

If we represent  $\text{ACPOtBu}$  by  $\text{ROOR}'\text{-N=N-R}'\text{OOR}$  then the following two routes are possible.

(i)



(ii)





The monomers chosen in this work were isoprene (I) and DMI. Since isoprene is known to terminate via a recombination reaction<sup>(42)</sup> so the copolymer types listed in Table 5.1 are possible if (a) DMI terminates by disproportionation or (b) by recombination.

TABLE 5.1  
Possible copolymer structures formed by Scheme 2

<u>MONOMER A</u>	<u>MONOMER B</u>	<u>ROUTE</u>	<u>MODE OF TERMINATION</u>	<u>COPOLYMER STRUCTURE</u>
I	DMI	(i)	(a)	DMI-I-DMI
			(b)	(DMI-I-DMI) <sub>n</sub>
DMI	I	(i)	(a)	DMI-I-DMI
			(b)	(I-DMI-I) <sub>n</sub>
I	DMI	(ii)	(a)	DMI-I-DMI
			(b)	(DMI-I-DMI) <sub>n</sub>
DMI	I	(ii)	(a)	DMI-I-DMI
			(b)	(I-DMI-I) <sub>n</sub>

It is well established<sup>(38)</sup> that block copolymers of the type ABA, where A is a glassy polymer and B a rubbery polymer at the use temperature, are far superior in their properties to AB-type and BAB-type polymers. It was the aim of this work to synthesize ABA-type block copolymers via scheme 1 using hydroxyl-terminated polybutadiene (PBD) (or hydrogenated polybutadiene (HPBD)) as the B block and poly-(dimethyl itaconate) (PDMI) as the A block. The possibility of forming similar ABA-type block copolymers with polyisoprene (PI) as the B block was investigated using scheme 2.

## 5.2 BLOCK COPOLYMERS OF BUTADIENE AND DIMETHYL ITACONATE

### 5.2.1 CHARACTERISATION OF BUTADIENE PREPOLYMERS

Low molecular weight  $\alpha$ ,  $\omega$ -hydroxy polybutadienes were available commercially and used without further purification. It was necessary, however, to characterize these with respect to structure and molecular weight.

Molecular weights of the butadiene prepolymers used were determined by VPO (see section 2.3.3), and the number average molecular weight ( $\bar{M}_n$ ) values obtained are listed in Table 5.2.

TABLE 5.2

$\bar{M}_n$  values for polybutadiene prepolymers

<u>POLYBUTADIENE</u>	$\frac{\bar{M}_n}{(g\ mol^{-1})}$	<u>TYPE</u>
<u>CODE:</u>		
PBD-1350*	1220	polybutadiene
PBD-3000*	3270	polybutadiene
HPBD-3000	3900	hydrogenated polybutadiene

\* Numbers refer to  $\bar{M}_n$  quoted by manufacturer.

As can be seen the sample of polybutadiene recovered after hydrogenation shows an  $\bar{M}_n$  value higher than that expected from simple addition of hydrogen ( $3390\ g\ mol^{-1}$ ). However,  $\bar{M}_n$  determinations by VPO are only considered accurate to  $\pm 10\%$ <sup>(89)</sup> and, moreover, the molecular weight distribution of the sample will have been altered by reprecipitation during sample recovery and purification.

The microstructure of the polybutadienes was determined by ir spectroscopy using the method of Binder<sup>(90)</sup> and is shown in Table 5.3.

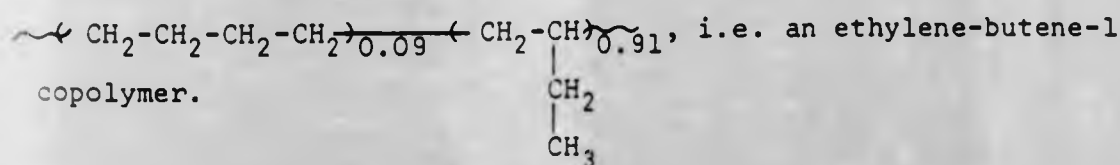
TABLE 5.3

Microstructure of polybutadiene prepolymers

<u>SAMPLE CODE:</u>	<u>% cis (1,4)</u>	<u>% trans (1,4)</u>	<u>% (1,2)</u>
PBD-1350	0.5	8.5	91.0
PBD-3000	0.3	8.0	91.7

The ir spectrum of PBD-1350 is shown in figure 5.3(a) the amount of cis, trans and 1,2 units were determined from the absorbances at 675, 972 and 911  $\text{cm}^{-1}$  respectively.

The extent of hydrogenation of the hydrogenated polybutadiene was evaluated from its ir spectrum (see figure 5.3(b)). The absorption at 1645  $\text{cm}^{-1}$  ( $\text{>C=C<}$ ) is effectively zero after hydrogenation, thus hydrogenation was estimated to have gone to  $\sim 100\%$  completion. The structure of 100% hydrogenated polybutadiene containing  $\sim 91\%$  1,2 units will be



### 5.2.2 MACROINITIATORS FROM POLYBUTADIENE PREPOLYMERS

The desirability to produce a MAZN with hydroxyl end groups was mentioned in section 5.1.1. The ir spectra of the PBD(MAZN)'s are shown in figures 5.4-5.6.

In the original hydroxyl-terminated polybutadienes the OH stretching vibration is centred on 3330  $\text{cm}^{-1}$  and, albeit

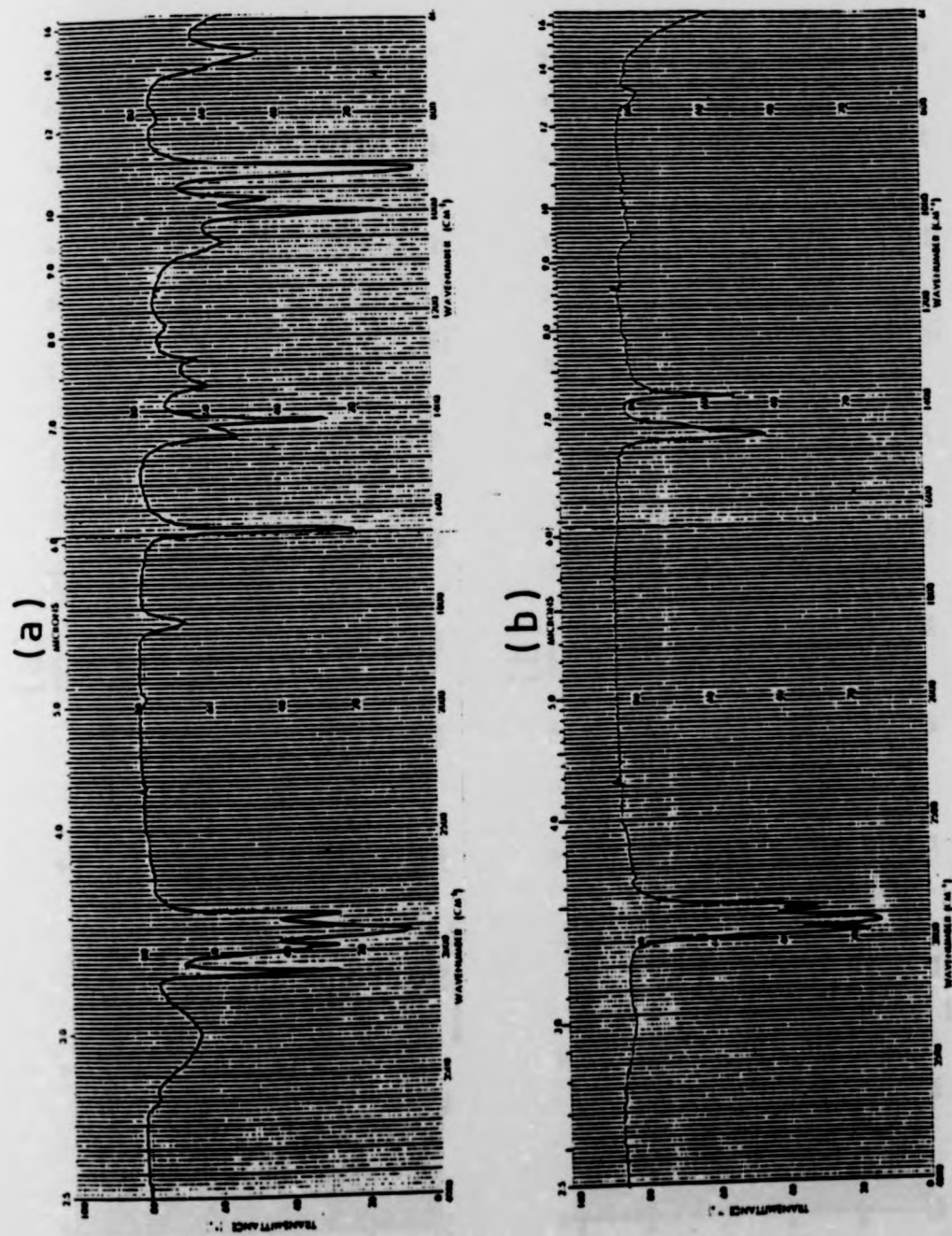


Figure 5.3 (a) ir spectrum of PBD-1350, and (b) ir spectrum of HPBD-3000.

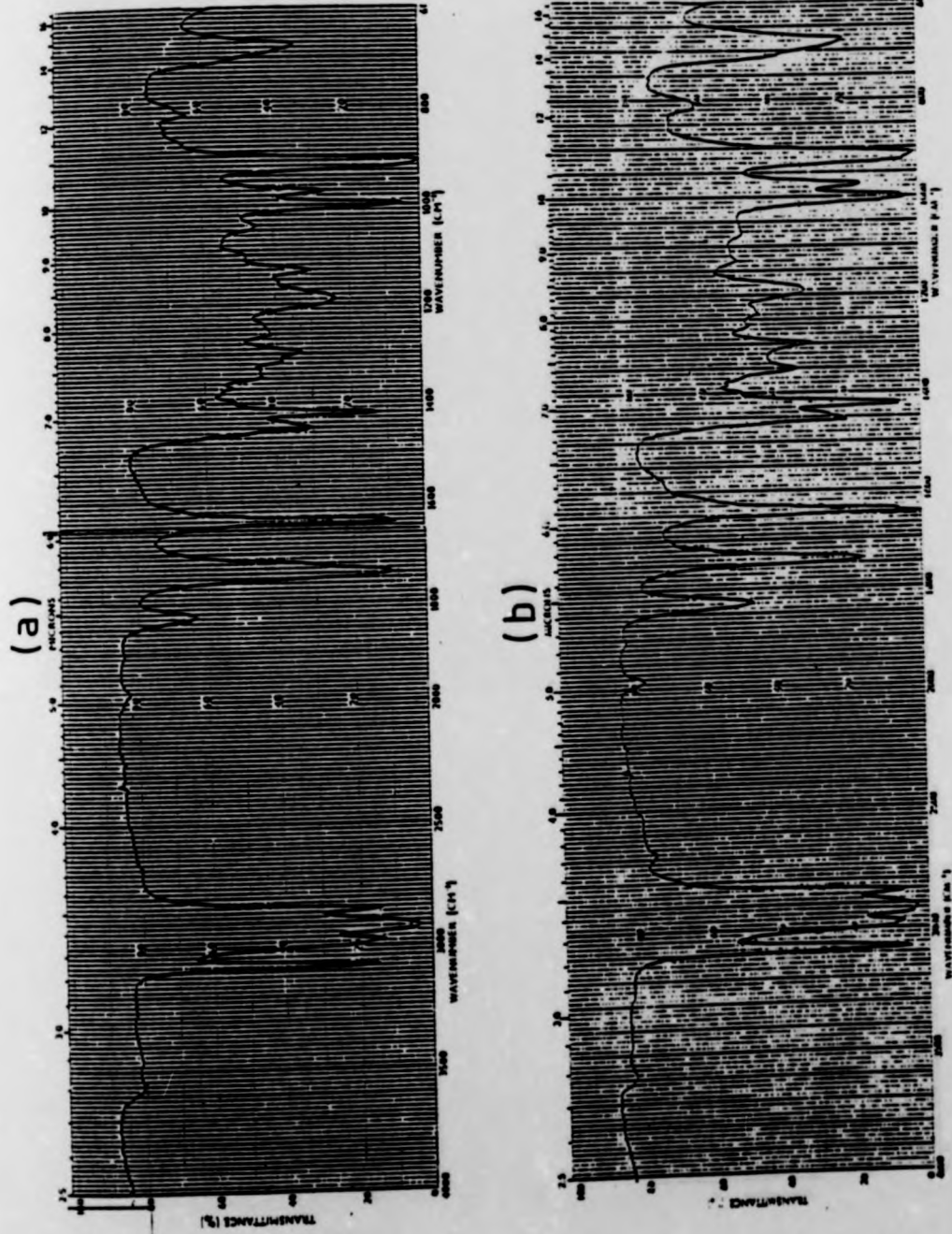


Figure 5.4 (a) ir spectrum of PBD(MAZN-IV) and (b) ir spectrum of PBD(MAZN-B).

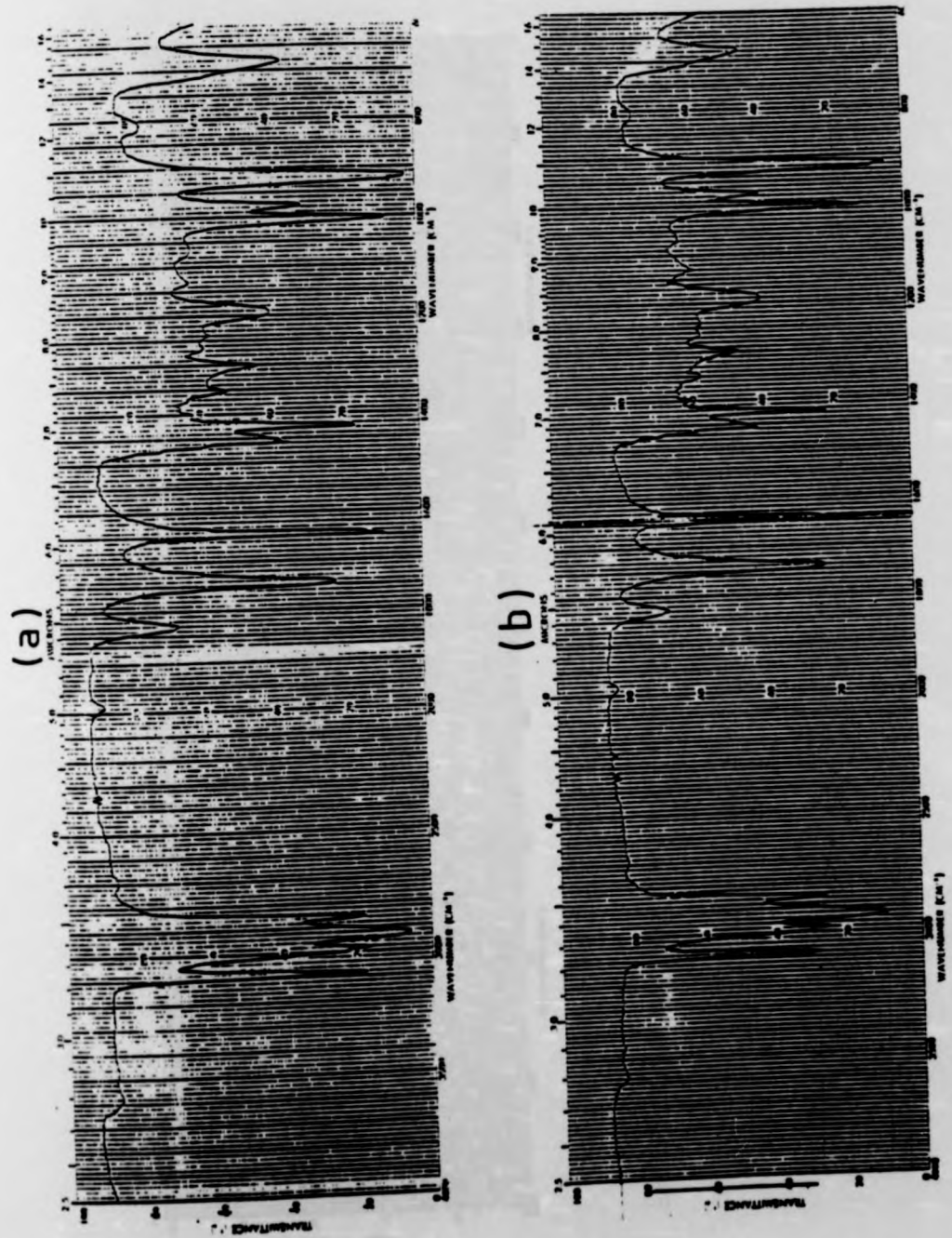


Figure 5.5: (a) ir spectrum of PBD(MAZN-V), and (b) ir spectrum of PBD(MAZN-VI).

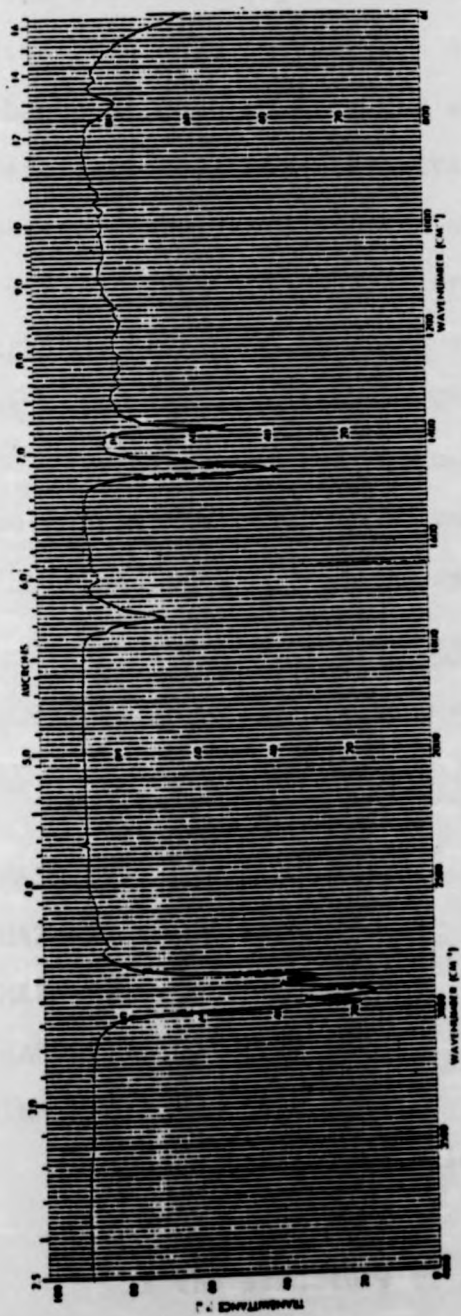


Figure 5.6: ir spectrum of HPBD(MAZN-C).

small, absorptions are observed in the spectra of all MAZN's, confirming OH end groups to be present. This would be expected from the stoichiometry of the reaction with ACPCl where polybutadiene was used in excess. A plot of the ratio of the absorbance at  $3330\text{ cm}^{-1}$  to the absorbance at  $675\text{ cm}^{-1}$  (due to C-H deformation of cis 1,4 units) against  $1/\bar{M}_n$  is shown for the two parent prepolymers and the unhydrogenated MAZN's (see figure 5.7). The points fall on a reasonable line passing through the origin ( $A_{3330}/A_{675} \rightarrow 0$  as  $\bar{M}_n \rightarrow \infty$ ) giving further evidence for the retention of OH end groups after coupling.

The number average molecular weights of the MAZN products from the reaction of butadiene prepolymers with ACPCl were obtained by VPO, and the results collected in Table 5.4.

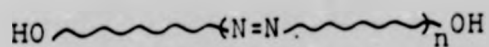
TABLE 5.4

$\bar{M}_n$  values for polybutadiene macroinitiators (PBD(MAZN)'s)

SAMPLE CODE:	$\bar{M}_n$ OF PREPOLYMER (g mol <sup>-1</sup> )	ACPCl/PBD (mol ratio)	$\bar{M}_n$ (g mol <sup>-1</sup> )	n
PBD(MAZN-IV)	1220	0.72	5560	3
PBD(MAZN-B)	3270	0.98	14710	3
PBD(MAZN-V)	1220	0.64	4610	2
PBD(MAZN-VI)	1220	0.95	5650	3
HPBD(MAZN-C)*	3900	0.96	11800	2

\*Hydrogenated polybutadiene macroinitiator.

If the structure of a MAZN is represented by



then it is possible to calculate the average value of n from



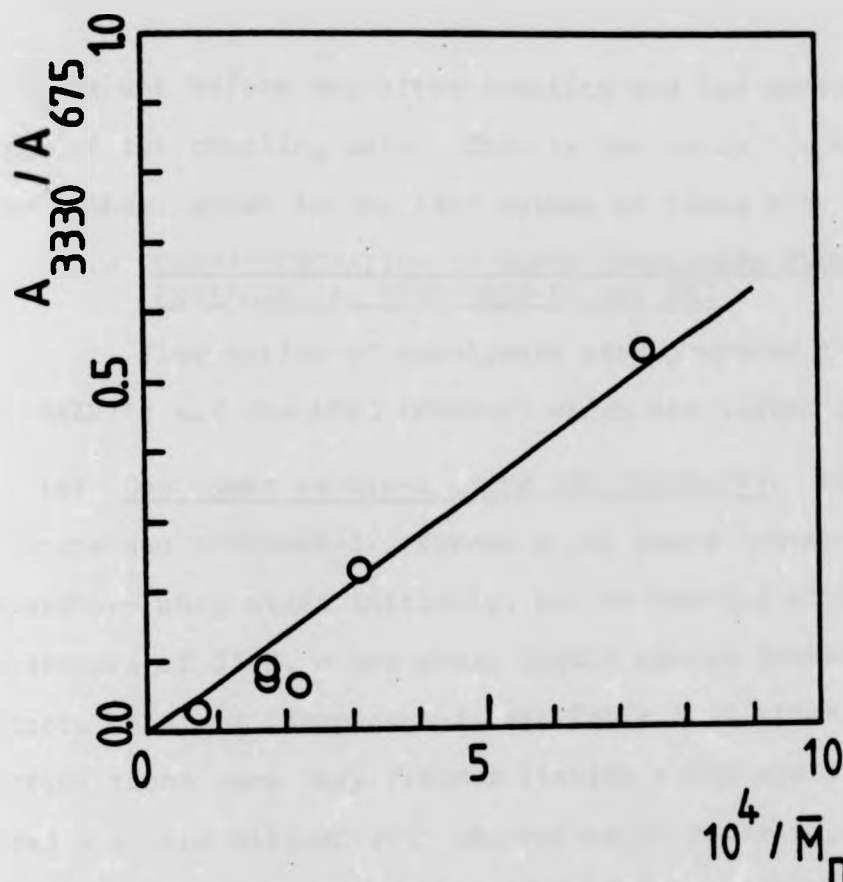


Figure 5.7: Plot of the ratio of absorbances ( $A_{3330}/A_{675}$ ) due to terminal OH groups and cis 1,4 units of the PBD-1350, PBD-3000, and PBD(MAZN)'s versus reciprocal  $\bar{M}_n$ .

the  $\bar{M}_n$  values before and after coupling and the molecular weight of the coupling unit. This is the value (to the nearest whole number) shown in the last column of Table 5.4.

### 5.2.3 CHARACTERISATION OF BLOCK COPOLYMERS FROM PBD(MAZN)'s, HPBD(MAZN-C) and DMI

Five series of copolymers were prepared from the PBD (MAZN)'s and the HPBD (MAZN-C) which are listed in Table 5.4.

(a) Copolymer series-I using PBD (MAZN-IV). Dimethyl itaconate and PBD(MAZN-IV) formed a two phase system at room temperature when mixed initially, but on heating to the reaction temperature of 338K, a one phase liquid system formed. The products obtained (samples 1-5, see Table 5.5) after the desired reaction times were very viscous liquids which could not be poured and were diluted with chloroform in order to facilitate reprecipitation into methanol. After drying, samples (1) and (2) were glassy at room temperature, but samples (3), (4) and (5) were increasingly elastomeric.

All samples were insoluble in toluene which is a solvent for PBD prepolymer and the MAZN's but a non-solvent for PDMI; it was not possible to find a solvent for PDMI which was a non-solvent for the copolymer. However from the structure of the PBD(MAZN)'s used there should be little or no homopoly-(dimethyl itaconate) formed.

A representative ir spectrum of sample (3) is shown in figure 5.8(a). The ir spectra of PDMI and PBD prepolymer are shown in figure 5.8(b) and 5.3(a) respectively; the copolymer spectrum shows characteristic bands of both.

Compositions for this series of copolymers (and for the other series II, III and IV) were estimated from their nmr

TABLE 5.5

$\bar{M}_n$  values and copolymer compositions for poly(butadiene-b-dimethyl itaconate) (Copolymer series-I) using PBD(MAZN-IV) as initiator

SAMPLE CODE	FEED MOL. RATIO		-N-N-# (mol %)	COPOLYMER COMPOSITION MOL RATIO**		CONVERSION† (wt. %)	$\frac{\bar{M}_n}{(\text{g mol}^{-1} \times 10^{-4})}$
	BD	DMI		BD	DMI		
P(BD- <u>b</u> -DMI)-I (1)	6.70	93.3	0.22	14	86	40	10.8
P(BD- <u>b</u> -DMI)-I (2)	13.0	87.0	0.43	30	70	28	10.1
P(BD- <u>b</u> -DMI)-I (3)	22.6	77.4	0.85	39	61	39	7.60
P(BD- <u>b</u> -DMI)-I (4)	37.0	63.0	1.71	62	38	28	3.40
P(BD- <u>b</u> -DMI)-I (5)	59.5	40.5	4.27	75	25	38	3.40

\* Mol % azobonds with respect to DMI monomer, based on the whole number values of  $n$  shown in Table 5.4

\*\* From nmr analysis

† With respect to weight of DMI monomer used

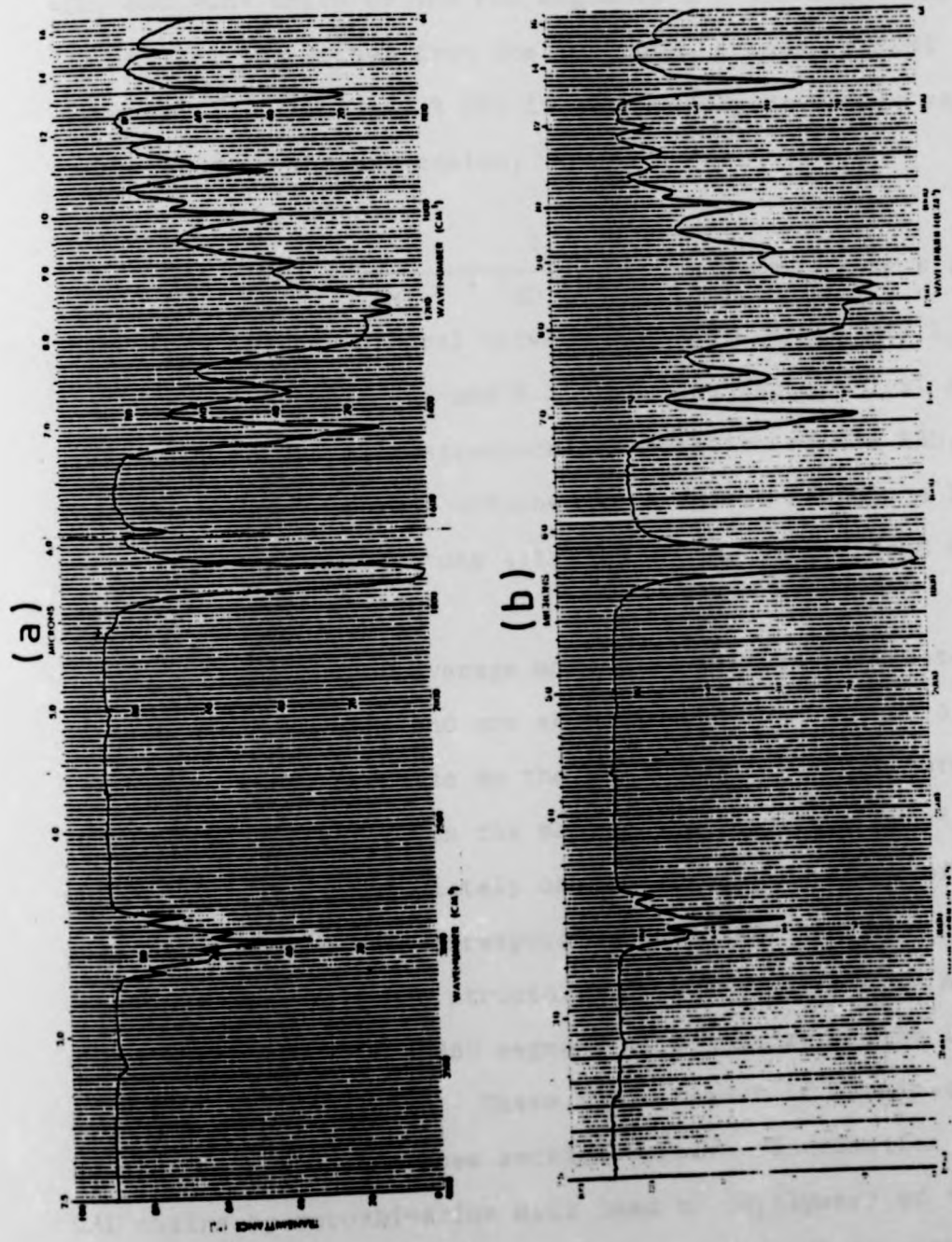


Figure 5.8 (a) ir spectrum of P(BD-b-DMI)-I(3) and (b) ir spectrum of PDMI.

spectra (see figure 5.9 for a representative nmr spectrum of sample (3)) the signals between 4.4 and 6.1 ppm are due to the =CH<sub>2</sub> and =CH- units of the PBD segments and the signal between 3.1 and 4.1 ppm arises from the two -OCH<sub>3</sub> groups of PDMI segments<sup>(73)</sup>. The mol % DMI in each copolymer sample was evaluated from the expression,

$$\text{Mol \% DMI} = \frac{I_{\text{DMI}}/6}{I_{\text{DMI}}/6 + I_{\text{BD}}/(0.91 \times 3 + 0.09 \times 2)} \times 100$$

where  $I_{\text{DMI}}$  is the integral between 3.1 and 4.1 ppm and  $I_{\text{BD}}$  is the integral between 4.1 and 6.1 ppm. The factors 0.91 and 0.09 refer to the microstructural composition of the PBD, i.e. there are 3 protons attached to a double bond in a 1,2 unit (91%) and two protons attached to the double bond of a 1,4 unit (9%).

The number average molecular weights were determined by membrane osmometry and are shown in the last column of Table 5.5, these decrease as the mol % initiator (in terms of -N=N- units) increases, in the manner expected from previous work<sup>(18)</sup>. It is immediately obvious from the values of  $\bar{M}_n$  obtained and from the corresponding butadiene contents of the copolymer samples, that structures of the type -ABA or AB, where the B block is a PBD segment of molecular weight 1220 g mol<sup>-1</sup>, are impossible. These would result if termination was by disproportionation (see section 5.1.1). Termination of growing DMI chains by recombination will lead to copolymers of the (AB)<sub>n</sub>-type. That this structure is more compatible with the  $\bar{M}_n$  and composition values obtained for the series can be shown by the following analysis.

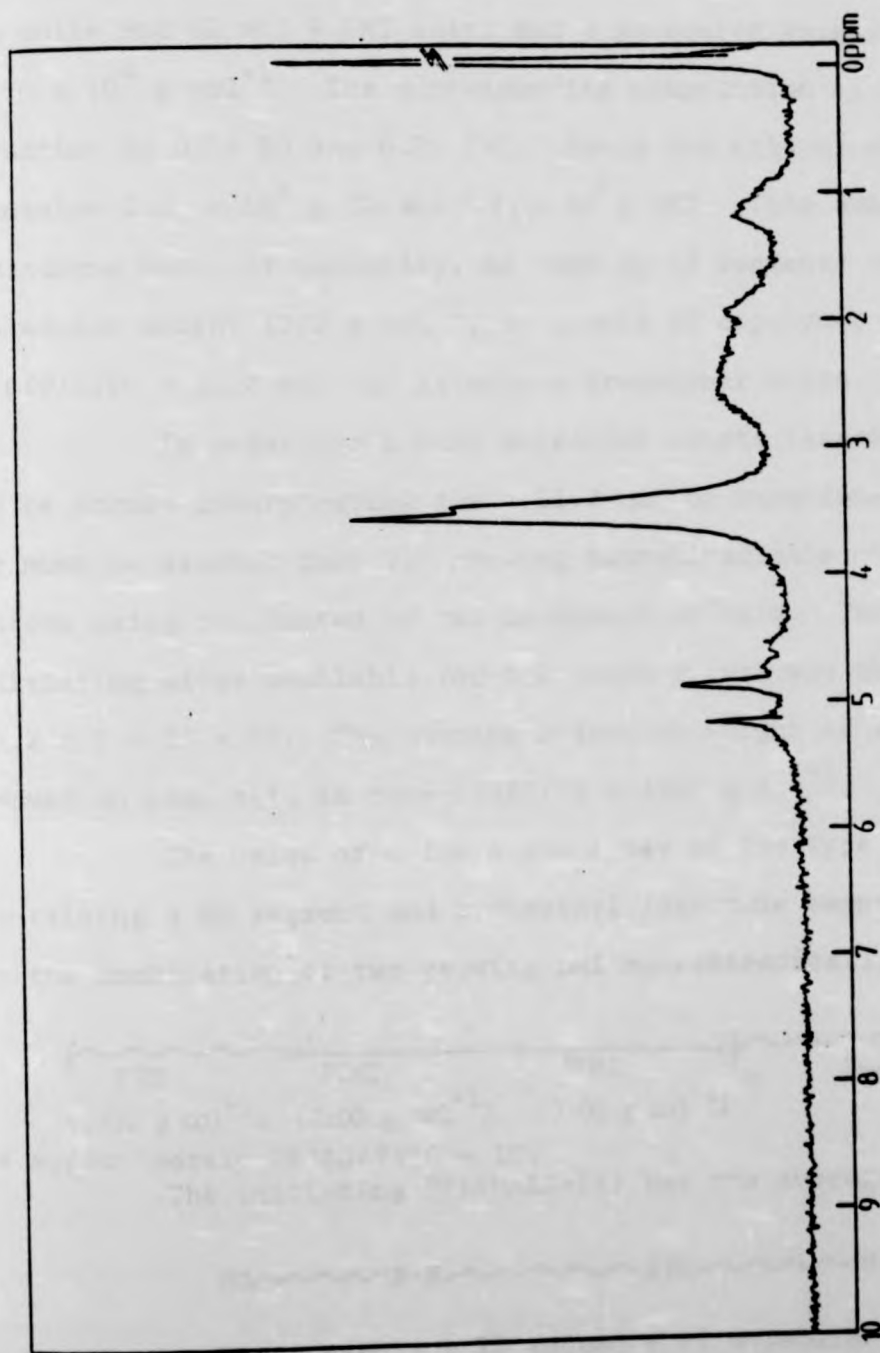
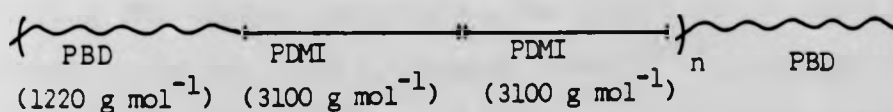


Figure 5.9: nmr spectrum of P(BD-b-DMI)-I (3).

Consider sample P(BD-b-DMI)-I(3) which has 39 mol % BD units and 61 mol % DMI units and a molecular weight of  $7.60 \times 10^4 \text{ g mol}^{-1}$ . The corresponding composition by weight fraction is 0.18 BD and 0.82 DMI. Hence one mole of copolymer contains  $1.37 \times 10^4 \text{ g BD}$  and  $6.23 \times 10^4 \text{ g DMI}$ . This amount of butadiene must, of necessity, be made up of segments with molecular weight  $1220 \text{ g mol}^{-1}$ , so a mole of copolymer contains  $13680/1220 = 11.2 \text{ mol}$  of butadiene prepolymer units.

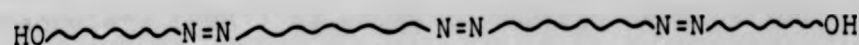
In order for a high molecular weight linear copolymer to be formed incorporating these 11.2 mol of butadiene units, it must be assumed that 9.2 growing macrobiradicals combined before being terminated by two macromonomer radicals. The number of initiating sites available for DMI chain growth was thus  $(9.2 \times 2 + 2) \approx 20$ . The average molecular weight of a DMI chain formed on each site is thus  $62320/20 \approx 3100 \text{ g mol}^{-1}$ .

The value of  $n$  for a copolymer of the type  $-(AB)_n$  containing a BD segment and a dimethyl itaconate segment formed by the combination of two growing DMI macrobiradicals,



is approximately  $76000/7420 \approx 10$ .

The initiating PBD(MAZN-IV) has the average structure



where  $\sim$  represents a BD sequence of molecular weight  $1220 \text{ g mol}^{-1}$ . On decomposition this yields two macrobiradicals



and two macromonomer radicals,



The ratio of macromonomer radicals to macrobiradicals available

is thus 1:1 which is different from that proposed in the final copolymer (2:9.2). It is unreasonable to suppose that macromonomer radicals are less reactive in any way and they should have an equal chance of forming copolymer. The analysis and structure proposed is thus an "ideal" one, however considerable amounts of other structures (such as BAB copolymers) must be present.

From this analysis, sample P(BD-b-DMI)-I(3) is an  $(AB)_n$ -type copolymer with A segments formed from PDMI of average molecular weight  $6200 \text{ g mol}^{-1}$  and B segments from the original PBD prepolymer of molecular weight  $1220 \text{ g mol}^{-1}$ .

When this analysis is applied to the other samples of the series the results shown in Table 5.6 are obtained for "ideal" copolymers formed by recombination of growing macrobiradicals and terminated by recombination with macromonomer radicals giving the structure  $(BA)_n B$ .

This ideal situation, as noted above, can never be achieved. All radical sites formed will not be successful in initiating DMI chains, and, since the half life of the azo link in a MAZN is of order of 5.5 hours (343K)<sup>(88)</sup>, not all the azo linkages will have been used. Additionally it seems unreasonable to expect termination of PDMI to be exclusively by recombination. Polymethylmethacrylate (PMMA) is known to undergo termination predominately by recombination below  $\sim 333\text{K}$  but by disproportionation above this temperature. PDMI is structurally very similar to PMMA and at the temperature used here both termination mechanisms could be operative.

However, it does appear that the copolymers must approximate to these ideal "segmented" structures with relatively



TABLE 5.6

Details of the structure analysis for poly(butadiene-b-dimethyl itaconate) (Copolymer series-I)

SAMPLE CODE	COMP. MOL FRACT.		COMP. WT. FRACT.		WT. BD	WT. DMI	PBD(PREPOLYMER UNITS)	RADICAL SITES	$\bar{M}_n$ (PDMI SEGM.)	$\bar{\nu}_n$ *
	BD	DMI	BD	DMI	(g)	(g)	(mol)	(mol)	( $\text{g mol}^{-1} \times 10^{-3}$ )	
P(BD- <u>b</u> -DMI)-I(1)	0.14	0.86	0.05	0.95	5400	102600	4.4	6.8	30.16	3
P(BD- <u>b</u> -DMI)-I(2)	0.30	0.70	0.13	0.87	13130	87870	10.8	19.6	8.960	10
P(BD- <u>b</u> -DMI)-I(3)	0.39	0.61	0.18	0.82	13680	62320	11.2	20.4	6.110	10
P(BD- <u>b</u> -DMI)-I(4)	0.62	0.38	0.36	0.64	12240	21760	10.0	18.0	2.416	9
P(BD- <u>b</u> -DMI)-I(5)	0.75	0.25	0.50	0.50	17000	17000	14.0	26.0	1.306	13

\* Nearest whole number value of  $n$  for (AB)<sub>n</sub>-type copolymer.

short sequence of A and B in order to explain the compositions found. The products from the remaining MAZN's are analysed as above and are discussed in the following sections.

(b) Copolymer series-II using PBD(MAZN-B). In this series of copolymers the PBD prepolymer segment was of higher molecular weight ( $3270 \text{ g mol}^{-1}$ ) and the feeds chosen were higher in PBD content (see Table 5.7). Only samples (1) and (2) were isolated by precipitation as before, reaction products (3) and (4) were found to be insoluble in chloroform. These were presumably cross-linked in some manner resulting from high conversion and high butadiene content and were discarded. Table 5.8 shows the analysis for samples (1) and (2).

(c) Copolymer series-III using PBD(MAZN-V). Again a high butadiene prepolymer feed was used (see Table 5.9) and all samples could be isolated as soluble products. However, the molecular weights were low and the polymers were "crumbly" rather than elastomeric. The MAZN used for this series would yield only one macrobiradical and two macromonoradicals. The opportunity for the formation of  $(AB)_n$ -type structures, even under ideal condition (see Table 5.10) is consequently lower and a considerable amount of BAB-type structure must be present.

(d) Copolymer series-IV using PBD(MAZN-VI). The PBD(MAZN-VI) used in this series had a similar structure to that used in (a), the details are shown in Table 5.11. No cross-linked products were obtained and samples (3), (4) and (5) were increasingly elastomeric in nature although samples (1) and (2) were glassy at room temperature. The analysis was carried out as before and results are shown in Table 5.12.

TABLE 5.7

$\bar{M}_n$  values and copolymer compositions for poly(butadiene-b-dimethyl itaconate) (Copolymer series-II) using PBD(MAZN-B) as initiator

SAMPLE CODE	FEED MOL RATIO		-N=N- <sup>*</sup> (mol %)	COPOLYMER COMPOSITION MOL RATIO <sup>**</sup>		CONVERSION <sup>†</sup> (wt. %)	$\bar{M}_n$ (g mol <sup>-1</sup> × 10 <sup>-4</sup> )
	BD	DMI		BD	DMI		
P(BD- <u>b</u> -DMI)-II (1)	57.5	42.5	1.5	85	15	17	3.82
P(BD- <u>b</u> -DMI)-II (2)	63.5	36.5	2.0	90	10	40	3.69
P(BD- <u>b</u> -DMI)-II (3)	70.0	30.0	2.6	-	-	> 50	-
P(BD- <u>b</u> -DMI)-II (4)	77.0	23.0	3.7	-	-	> 60	-

\* Mol % azobonds with respect to DMI monomer, based on the whole number values of n shown in Table 5.4

\*\* From nmr analysis

† With respect to weight of DMI monomer used

TABLE 5.8

Details of the structure analysis for poly(butadiene-*b*-dimethyl itaconate) (Copolymer series-II)

SAMPLE CODE	COMP. MOL. FRACT.		COMP. WT. FRACT.		WT. BD (g)	WT. DMI (g)	PBD(PREPOLYMER UNITS) (mol)	RADICAL SITES (mol)	$\bar{M}_n$ (PDMI SEGM) (g mol <sup>-1</sup> × 10 <sup>-3</sup> )	$\bar{v}_n^*$
	BD	DMI	BD	DMI						
P(BD- <i>b</i> -DMI)-II(1)	0.85	0.15	0.66	0.34	25232	12998	7.7	13.4	0.970	7
P(BD- <i>b</i> -DMI)-II(2)	0.90	0.10	0.75	0.25	27693	9231	8.4	14.8	0.623	8

\* Nearest whole number value of  $n$  for (AB)<sub>*n*</sub>-type copolymer

TABLE 5.9

$\bar{M}_n$  values and copolymer compositions for poly(butadiene-*b*-dimethyl itaconate) (Copolymer series-III) using PBD(MAZN-V) as initiator

SAMPLE CODE	FEED MOL RATIO		-N=N- <sup>*</sup> (mol %)	COPOLYMER COMPOSITION MOL RATIO <sup>**</sup>		CONVERSION <sup>†</sup> (wt. %)	$\bar{M}_n$ (g mol <sup>-1</sup> × 10 <sup>-4</sup> )
	BD	DMI		BD	DMI		
P(BD- <i>b</i> -DMI)-III (1)	43.0	57.0	1.8	69	31	28	1.40
P(BD- <i>b</i> -DMI)-III (2)	54.0	46.0	2.8	77	23	33	1.15
P(BD- <i>b</i> -DMI)-III (3)	62.0	38.0	3.8	88	12	35	1.10
P(BD- <i>b</i> -DMI)-III (4)	59.5	40.5	3.4	50	50	38	1.30

\* Mol % azobonds with respect to DMI monomer, based on the whole number values of *n* shown in Table 5.4

\*\* From nmr analysis

† With respect to weight of DMI monomer used

TABLE 5.10

Details of the structure analysis for poly(butadiene-b-dimethyl itaconate) (Copolymer series-III)

SAMPLE CODE	COMP. MOL FRACT.		COMP. WT. FRACT.		WT. BD (g)	WT. DMI (g)	PBD(PREPOLYMER UNITS) (mol)	RADICAL SITES (mol)	$\bar{M}_n$ (PDMI SEGM) (g mol <sup>-1</sup> x 10 <sup>-3</sup> )	$\nu n^*$
	BD	DMI	BD	DMI						
P(BD- <u>b</u> -DMI)-III(1)	0.69	0.31	0.43	0.57	6020	7980	4.9	7.8	2.046	4
P(BD- <u>b</u> -DMI)-III(2)	0.77	0.23	0.53	0.47	6095	5405	5.0	8.0	1.350	4
P(BD- <u>b</u> -DMI)-III(3)	0.88	0.12	0.71	0.29	7100	2900	5.8	9.6	0.604	6
P(BD- <u>b</u> -DMI)-III(4)	0.50	0.50	0.25	0.75	3250	9750	2.7	3.4	5.734	2

\* Nearest whole number value of n for (AB)<sub>n</sub>-type copolymer

TABLE 5.11

$\bar{M}_n$  values and copolymer compositions for poly(butadiene-*b*-dimethyl itaconate) (Copolymer series-IV) using PBD(MAZN-VI) as initiator

SAMPLE CODE	FEED MOL RATIO		-N=N-*		COPOLYMER COMPOSITION MOL RATIO <sup>***</sup>		CONVERSION <sup>†</sup> (wt. %)	$\bar{M}_n$ (g mol <sup>-1</sup> × 10 <sup>-4</sup> )
	BD	DMI	(mol %)	DMI	BD	DMI		
P(BD- <i>b</i> -DMI)-IV (1)	22.6	77.4	0.84	60	40	60	15	4.7
P(BD- <i>b</i> -DMI)-IV (2)	37.0	63.0	1.7	50	50	50	10	4.5
P(BD- <i>b</i> -DMI)-IV (3)	47.0	53.0	2.5	40	60	40	13	3.9
P(BD- <i>b</i> -DMI)-IV (4)	59.5	40.5	4.2	27	73	27	10	2.4
P(BD- <i>b</i> -DMI)-IV (5)	64.0	36.0	5.1	23	77	23	10	2.2

\* Mol % azobonds with respect to DMI monomer, based on the whole number values of n shown in Table 5.4

\*\* From nmr analysis

† With respect to weight of DMI monomer used

TABLE 5.12

Details of the structure analysis for poly(butadiene-*b*-dimethyl itaconate) (Copolymer series-IV)

SAMPLE CODE	COMP. MOL FRACT.		COMP. WT. FRACT.		WT. BD (g)	WT. DMI (g)	PBD(PREPOLYMER UNITS) (mol)	RADICAL SITES (mol)	$\bar{M}_n$ (PDMI SEGM) (g mol <sup>-1</sup> × 10 <sup>-3</sup> )	$\nu_{n1}$ *
	BD	DMI	BD	DMI						
P(BD- <i>b</i> -DMI)-IV (1)	0.40	0.60	0.19	0.81	8930	38070	7.3	12.6	6.042	6
P(BD- <i>b</i> -DMI)-IV (2)	0.50	0.50	0.25	0.75	11250	33750	9.2	16.4	4.116	8
P(BD- <i>b</i> -DMI)-IV (3)	0.60	0.40	0.34	0.66	13260	25740	10.8	19.6	2.626	10
P(BD- <i>b</i> -DMI)-IV (4)	0.73	0.27	0.48	0.52	11520	12480	9.4	16.8	1.484	9
P(BD- <i>b</i> -DMI)-IV (5)	0.77	0.23	0.53	0.47	11660	10340	9.6	17.2	1.202	9

\* Nearest whole number value of n for (AB)<sub>n</sub>-type copolymer



(e) Copolymer series-V using HPBD(MAZN-C). Table 5.13 shows the details of this series of copolymers. Hydrogenated butadiene prepolymer was used in order to investigate the changes brought about by a rubbery segment of different characteristics to polybutadiene and to remove all possibility of cross-linking. A representative ir spectrum is shown in figure 5.10 and a representative nmr spectrum in figure 5.11. Compositions were estimated for each copolymer sample from its nmr spectrum by the following expression,

$$\text{mol \% DMI} = \frac{I_{\text{DMI}}/6}{I_{\text{DMI}}/6 + I_{\text{HBD}}/3 \times 0.91} \times 100$$

$I_{\text{HBD}}$  is the integral of the signal between 0.5 and 1.1 ppm due to the protons of the  $-\text{CH}_3$  side chains of HBD 1,2 units which will form 91% of the chain.

In this series of copolymers a small amount of PDMI homopolymer (8%) was found in sample (1) by extraction of the sample with toluene. Toluene is a non-solvent for PDMI but a solvent for the copolymer. This relatively low amount of homopolymer formed confirms the assertion that the macroazobitriles have predominantly  $-\text{OH}$  end groups.

A similar "ideal" analysis was carried out for these copolymer samples and the result is shown in Table 5.14. However only samples (2) and (3) were elastomeric while sample (1) was crumbly and sample (4) was tacky liquid. Here again the ratio of the macromonomer radicals to macrobiradicals is 2:1 and this would seem to have some bearing on the nature of the products obtained.

TABLE 5.13

$\bar{M}_n$  values and copolymer compositions for poly(hydrogenated butadiene-*b*-dimethyl itaconate)  
(Copolymer series-V) using HPBD(MAZN-C) as initiator

SAMPLE CODE	FEED MOL RATIO		-N-N- <sup>*</sup>		COPOLYMER COMPOSITION MOL RATIO <sup>**</sup>		CONVERSION <sup>†</sup> (wt. %)	$\frac{\bar{M}_n}{10^{-4}}$ (g mol <sup>-1</sup> × 10 <sup>-4</sup> )
	HBD	DMI	(mol %)	DMI	HBD	DMI		
P(HBD- <u>b</u> -DMI)-V (1)	47.7	52.3	0.87	38	62	38	36	2.70
P(HBD- <u>b</u> -DMI)-V (2)	70.0	30.0	2.3	15	85	15	41	1.85
P(HBD- <u>b</u> -DMI)-V (3)	74.3	25.7	2.8	13	87	13	51	1.70
P(HBD- <u>b</u> -DMI)-V (4)	85.4	14.6	5.6	7.0	93	7.0	49	1.40

\* Mol % azobonds with respect to DMI monomer, based on the whole number values of n shown in Table 5.4

\*\* From nmr analysis

† With respect to weight of DMI monomer used

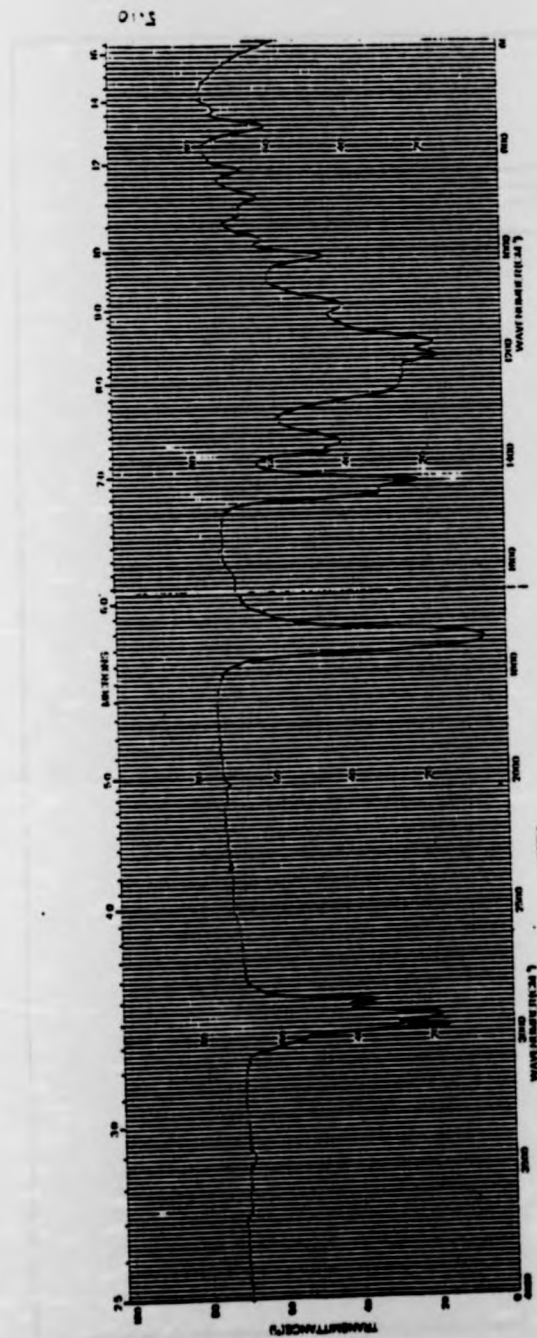


Figure 5.10: ir spectrum of P(HBD-b-DMI)-V(2).

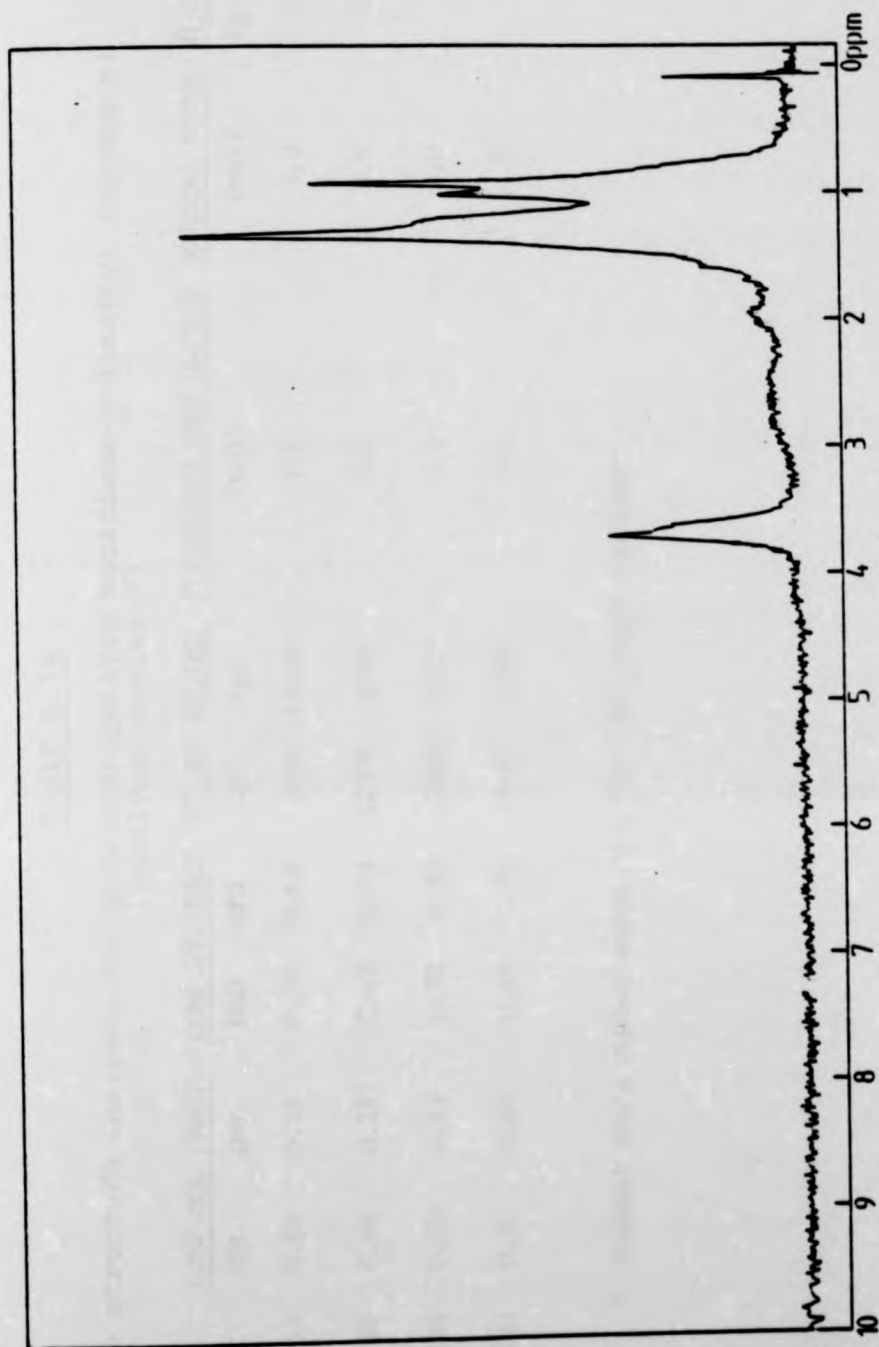


Figure 5.11: nmr spectrum of P(HBD-b-DMI)-V(1).

TABLE 5.14

Details of the structure analysis for poly(hydrogenated butadiene-*b*-dimethyl itaconate)  
(Copolymer series-V)

SAMPLE CODE	COMP. MOL FRACT.		COMP. WT. FRACT.		WT. BD (g)	WT. DMI (g)	PBD(PREPOLYMER UNITS) (mol)	RADICAL SITES (mol)	$\bar{M}_n$ (PDMI SEGM) (g mol <sup>-1</sup> × 10 <sup>-3</sup> )	$\eta_{sp}^*$
	HBD	DMI	HBD	DMI						
P(HBD- <i>b</i> -DMI)-V (1)	0.62	0.38	0.37	0.63	9990	17010	2.5	3.0	11.340	2
P(HBD- <i>b</i> -DMI)-V (2)	0.85	0.15	0.67	0.33	12395	6105	3.2	4.4	2.774	3
P(HBD- <i>b</i> -DMI)-V (3)	0.87	0.13	0.70	0.30	11900	5100	3.0	4.0	2.550	2
P(HBD- <i>b</i> -DMI)-V (4)	0.93	0.07	0.82	0.18	11480	2520	3.0	4.0	1.260	3

\* Nearest whole number value of  $n$  for (AB)<sub>*n*</sub>-type copolymer

### 5.3 THERMAL AND MECHANICAL PROPERTIES OF COPOLYMERS FROM POLYBUTADIENES, HYDROGENATED POLYBUTADIENE AND DIMETHYL ITACONATE

Samples of copolymers from series I-V were studied using DSC and TGS. RV measurements were made on samples from series I, II and V and creep measurements done on samples from series IV. Tensile testing was carried out on only one sample from series IV.

#### 5.3.1 DSC MEASUREMENTS

In order to evaluate the results from the copolymers, DSC measurements on the PBD prepolymers were first carried out to determine their glass transition temperatures ( $T_g$ ). The traces are shown in figure 5.12 and results collected in Table 5.15.

$T_g$  was taken as the intercept of the extrapolated baseline with the line of greatest slope during inflection.

TABLE 5.15

Glass transition temperatures for polybutadiene prepolymers

<u>SAMPLE CODE</u>	<u><math>T_g</math> /K</u>	<u><math>\bar{M}_n</math> /g mol<sup>-1</sup></u>
PBD-1350	247	1220
PBD-3000	259	3270
HPBD-3000	240	3900

The  $T_g$  values for the unhydrogenated polybutadiene prepolymers are in accord with their relative molecular weights. The lowering of  $T_g$  on hydrogenation of PBD-3000 shows that the hydrogenated backbone has a greater flexibility than the

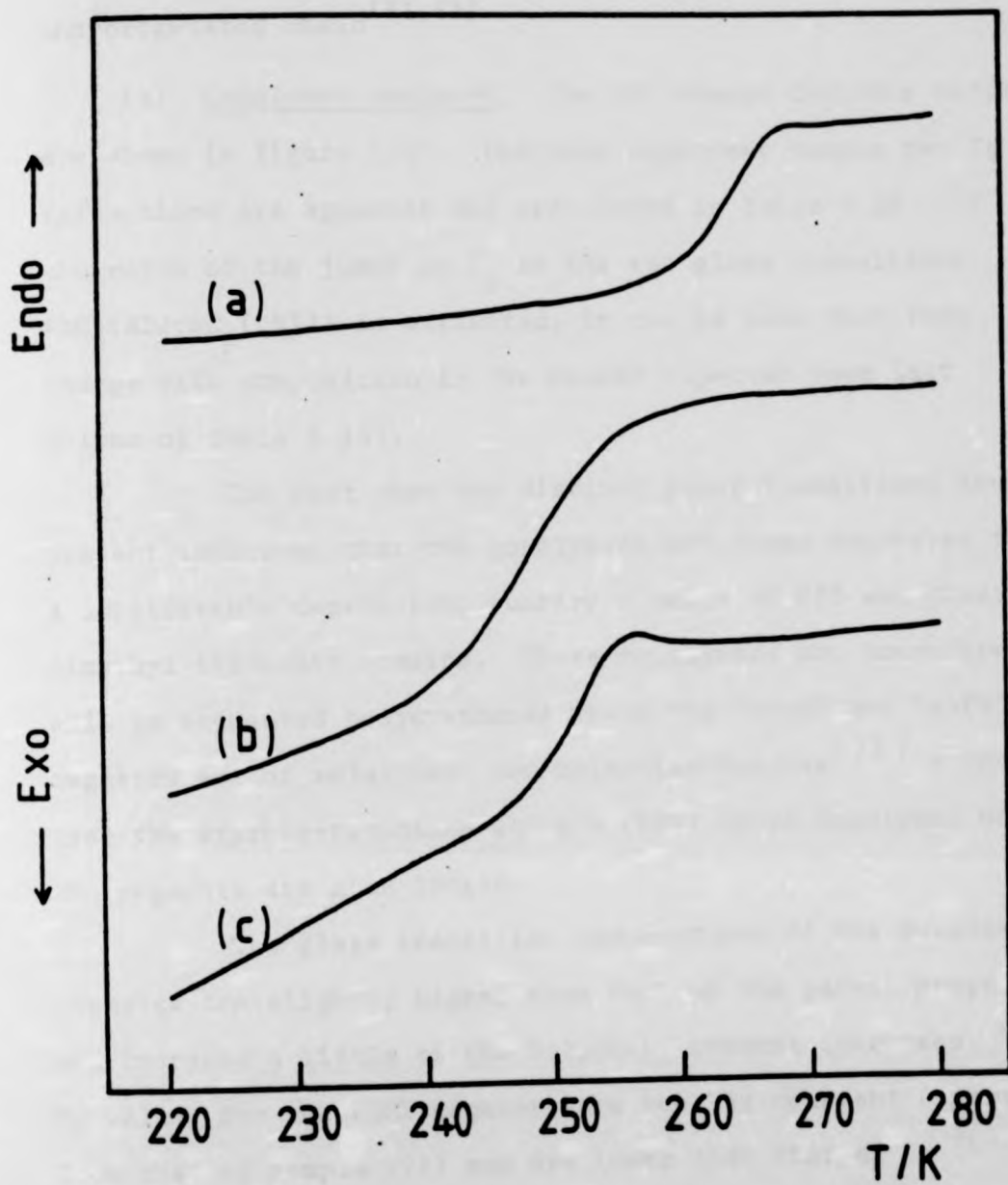


Figure 5.12: DSC traces for:

(a) PBD-3000;

(b) HPBD-3000;

and (c) PBD-1350.

unhydrogenated chain<sup>(91,92)</sup>

(a) Copolymer series-I. The DSC traces for this series are shown in figure 5.13. For each copolymer sample two T<sub>g</sub> inflections are apparent and are listed in Table 5.16. If the ratio of the jumps in C<sub>p</sub> at the two glass transitions ( $\Delta C_p(\text{BD}) : \Delta C_p(\text{DMI})$ ) is estimated, it can be seen that they change with composition in the manner expected (see last column of Table 5.16).

The fact that two distinct glass transitions are present indicates that the copolymers are phase separated to a considerable degree into rubbery domains of PBD and glassy dimethyl itaconate domains. These copolymers are therefore akin to segmented polyurethanes where the "hard" and "soft" segments are of relatively low molecular weights<sup>(93)</sup> rather than the styrene-butadiene-styrene (SBS) block copolymer where the segments are much longer.

The glass transition temperatures of the butadiene segments are slightly higher than that of the parent prepolymer and increase a little as the butadiene content increases. The T<sub>g</sub> values for the PDMI segments are roughly constant (apart from that of sample (2)) and are lower than that of PDMI (T<sub>g</sub> = 377K).<sup>(18)</sup> This "inward shift" of the glass transition temperatures is usually taken as evidence for some degree of mixing,<sup>(94,95)</sup> i.e. the domains are not pure PDMI and pure PBD. However an alternative reason for the lowered PDMI segment's T<sub>g</sub> values would be the presence of relatively short PDMI sequences since T<sub>g</sub> is dependent on molecular weight<sup>(61)</sup>.



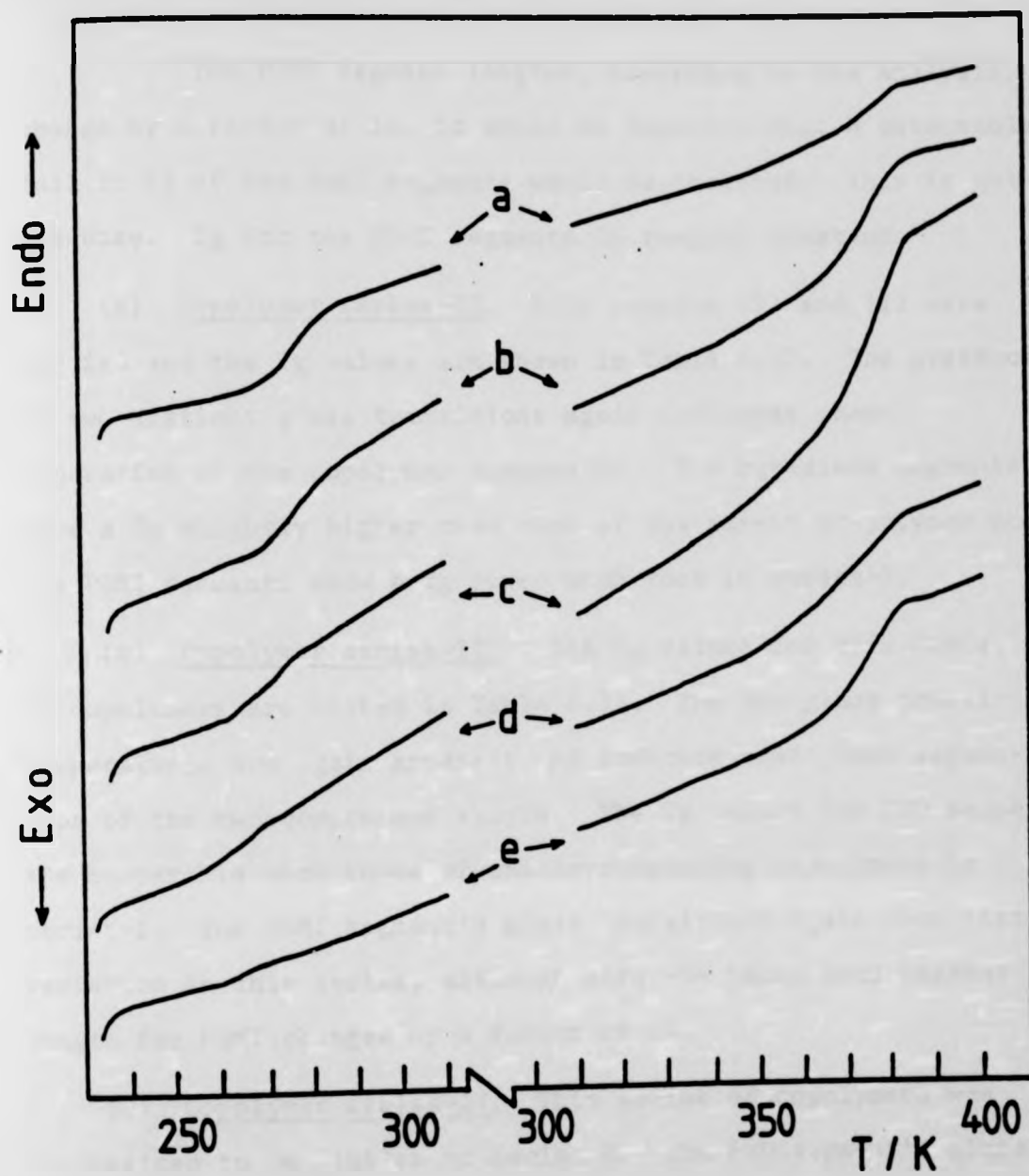


Figure 5.13: DSC traces for P(BD-b-DMI)-I copolymer series:

- (a) Sample (5);
- (b) Sample (4);
- (c) Sample (3);
- (d) Sample (2);
- and (e) Sample (1).

The PDMI segment lengths, according to the analysis, change by a factor of 10, it would be expected that a detectable fall in  $T_g$  of the PDMI segments would be observed. This is not the case.  $T_g$  for the PDMI segments is roughly constant.

(b) Copolymer series-II. Only samples (1) and (2) were studied and the  $T_g$  values are shown in Table 5.17. The presence of two distinct glass transitions again indicates phase separation of the copolymer components. The butadiene segments have a  $T_g$  slightly higher than that of the parent prepolymer and the PDMI segments show a  $T_g$  lower than that in series-I.

(c) Copolymer series-III. The  $T_g$  values for this series of copolymers are listed in Table 5.18. The two glass transition temperatures are again apparent and indicate that phase separation of the two components exists. The  $T_g$  values for PBD segments are comparable with those of the corresponding copolymers in series-I. The PDMI segment's glass transitions again show little variation in this series, although here the calculated segment length for PDMI changes by a factor of 10.

(d) Copolymer series-IV. This series of copolymers was synthesized to be similar to series-I. The PBD segment's glass transitions are comparable as are the  $T_g$  of PDMI segments. However, the latter now show a small decline with decreasing DMI content (see Table 5.19) as would be expected from the calculated change in PDMI segment length through the series.

(e) Copolymer series-V. The  $T_g$  values of the HPBD segments are very close to that of the parent prepolymer (see Table 5.20) and the glass transition temperatures of the PDMI segments reduce with DMI content, as it should if it reflects the shortening of

TABLE 5.16

Glass transition temperatures for poly(butadiene-b-dimethyl itaconate) (Copolymer series-I)

<u>SAMPLE</u> <u>CODE:</u>	<u>T<sub>g</sub>/(K)</u>		<u>Block <math>\bar{M}_n</math>/(g mol<sup>-1</sup>)</u>		<u>BD CONTENT</u>	<u><math>\Delta C_p</math></u>
	BD	DMI	BD	DMI	(mol %)	BD/DMI
P(BD- <u>b</u> -DMI)-I (1)	~259	364	1220	30.16x10 <sup>3</sup>	14	~0.045
P(BD- <u>b</u> -DMI)-I (2)	~258	353	"	8.96x10 <sup>3</sup>	30	~0.075
P(BD- <u>b</u> -DMI)-I (3)	263	364	"	6.11x10 <sup>3</sup>	39	0.15
P(BD- <u>b</u> -DMI)-I (4)	267	364	"	2.416x10 <sup>3</sup>	62	0.60
P(BD- <u>b</u> -DMI)-I (5)	270	362	"	1.306x10 <sup>3</sup>	75	1.30

TABLE 5.17

Glass transition temperatures for poly(butadiene-b-dimethyl itaconate) (Copolymer series-II)

<u>SAMPLE</u> <u>CODE:</u>	<u>T<sub>g</sub>/(K)</u>		<u>Block <math>\bar{M}_n</math>/(g mol<sup>-1</sup>)</u>		<u>BD CONTENT</u>
	BD	DMI	BD	DMI	(mol %)
P(BD- <u>b</u> -DMI)-II (1)	265	353	3270	970	85
P(BD- <u>b</u> -DMI)-II (2)	264	354	"	620	90

TABLE 5.18

Glass transition temperatures for poly(butadiene-b-dimethyl itaconate) (Copolymer series-III)

SAMPLE CODE:		T <sub>g</sub> /(K)		Block $\bar{M}_n$ /(g mol <sup>-1</sup> )		BD CONTENT (mol %)
		BD	DMI	BD	DMI	
P(BD- <u>b</u> -DMI)-III	(1)	263	366	1220	2.046x10 <sup>3</sup>	69
P(BD- <u>b</u> -DMI)-III	(2)	265	365	"	1.350x10 <sup>3</sup>	77
P(BD- <u>b</u> -DMI)-III	(3)	270	364	"	0.604x10 <sup>3</sup>	88
P(BD- <u>b</u> -DMI)-III	(4)	260	362	"	5.734x10 <sup>3</sup>	50

TABLE 5.19

Glass transition temperatures for poly(butadiene-b-dimethyl itaconate) (Copolymer series-IV)

SAMPLE CODE:		T <sub>g</sub> /(K)		Block $\bar{M}_n$ /(g mol <sup>-1</sup> )		BD CONTENT (mol %)
		BD	DMI	BD	DMI	
P(BD- <u>b</u> -DMI)-IV	(1)	260	364	1220	6.042x10 <sup>3</sup>	40
P(BD- <u>b</u> -DMI)-IV	(2)	261	362	"	4.116x10 <sup>3</sup>	50
P(BD- <u>b</u> -DMI)-IV	(3)	260	361	"	2.626x10 <sup>3</sup>	60
P(BD- <u>b</u> -DMI)-IV	(4)	268	356	"	1.484x10 <sup>3</sup>	73
P(BD- <u>b</u> -DMI)-IV	(5)	270	354	"	1.202x10 <sup>3</sup>	77

TABLE 5.20

Glass transition temperatures for poly(hydrogenated butadiene-b-dimethyl itaconate) (Copolymer series-V)

SAMPLE CODE:		T <sub>g</sub> /(K)		Block $\bar{M}_n$ /(g mol <sup>-1</sup> )		HBD CONTENT (mol %)
		HBD	DMI	HBD	DMI	
P(HBD- <u>b</u> -DMI)-V	(1)	238	352	3900	11.34x10 <sup>3</sup>	62
P(HBD- <u>b</u> -DMI)-V	(2)	240	344	"	2.774x10 <sup>3</sup>	85
P(HBD- <u>b</u> -DMI)-V	(3)	240	342	"	2.550x10 <sup>3</sup>	87
P(HBD- <u>b</u> -DMI)-V	(4)	241	340	"	1.260x10 <sup>3</sup>	93

PDMI segments length as the composition is varied. The actual values are lower than in the other series for segment lengths of comparable calculated molecular weights.

### 5.3.2 DYNAMIC MECHANICAL MEASUREMENTS - RV

(a) Copolymer series-I. From this series, samples (3), (4) and (5) formed transparent films when melt pressed at 413K. The RV traces for these are shown in figures 5.14, 5.15 and 5.16 respectively. In each case the damping curves ( $\tan \delta$ ) show two maxima corresponding to the glass transitions of the PBD and PDMI segments. In sample (3) the lower temperature damping peak is of very low intensity, corresponding to its lower diene content. The appearance of two distinct damping maxima is evidence for a phase separated system<sup>(95)</sup>. The BD content of sample (3) must just be sufficient to generate a phase separated system. Sample (4) and (5) show a relative increase in the PBD  $\tan \delta$  maxima and a relative decrease in PDMI  $\tan \delta$  maxima as the composition of DMI decreases.

Corresponding to the  $\tan \delta$  maxima, are step reductions in the complex moduli ( $E^*$ ). This is not very apparent in sample (3) but quite obvious in the others. The relative modulus drops are in proportion to the DMI contents.

The values of  $E^*$  around room temperature for samples (4) and (5) are  $\sim 10^8 \text{ Nm}^{-2}$  and the material behaves as a tough elastomer. Sample (3) is a rather less useful copolymer, being somewhat more brittle and easily broken. Samples (4) and (5) are elastomeric materials conforming to the requirements of a

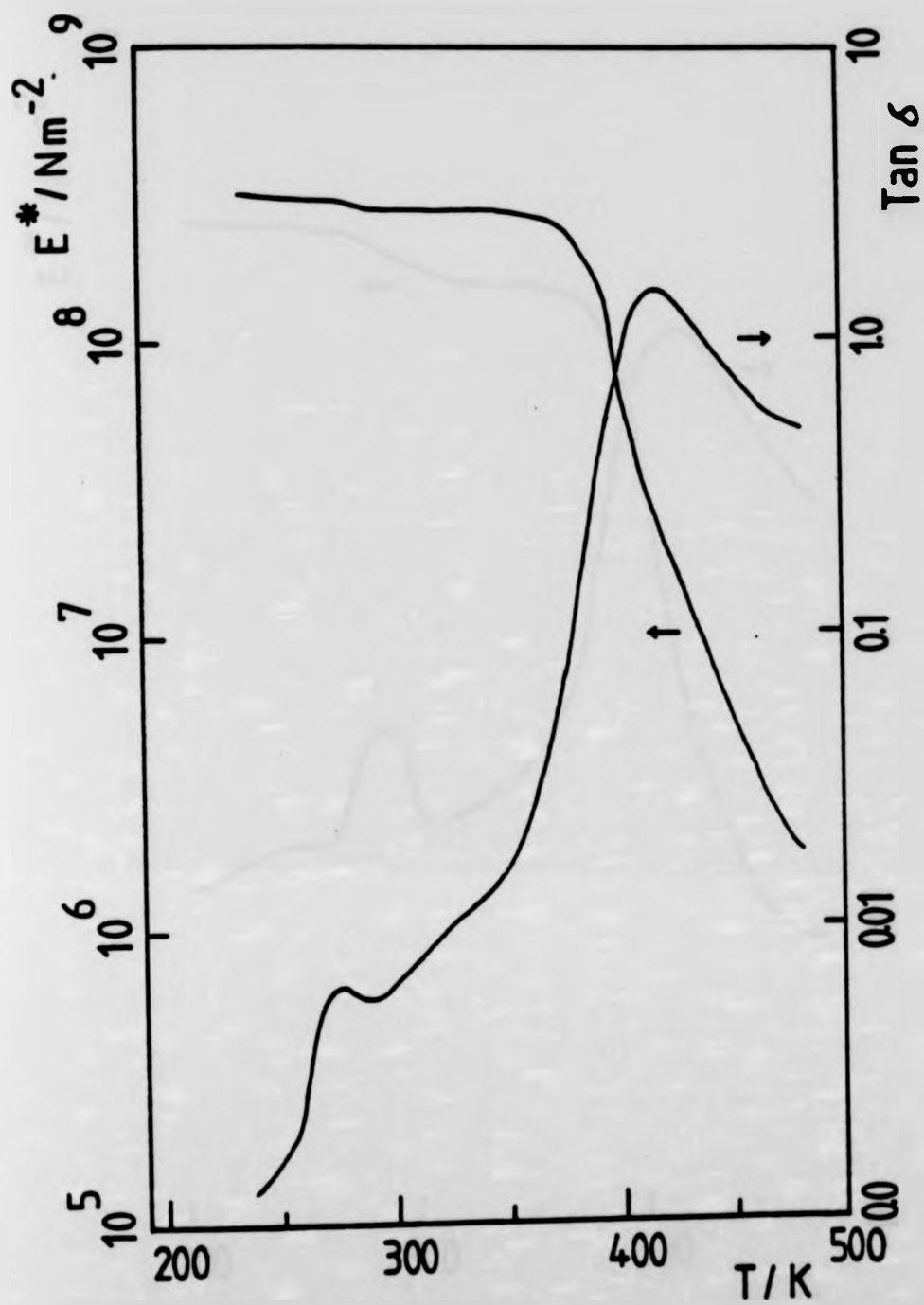


Figure 5.14: Complex modulus ( $E^*/Nm^{-2}$ ) and  $\tan \delta$  versus temperature curves for P(BD-p-DMI)-I(3), pressed film.

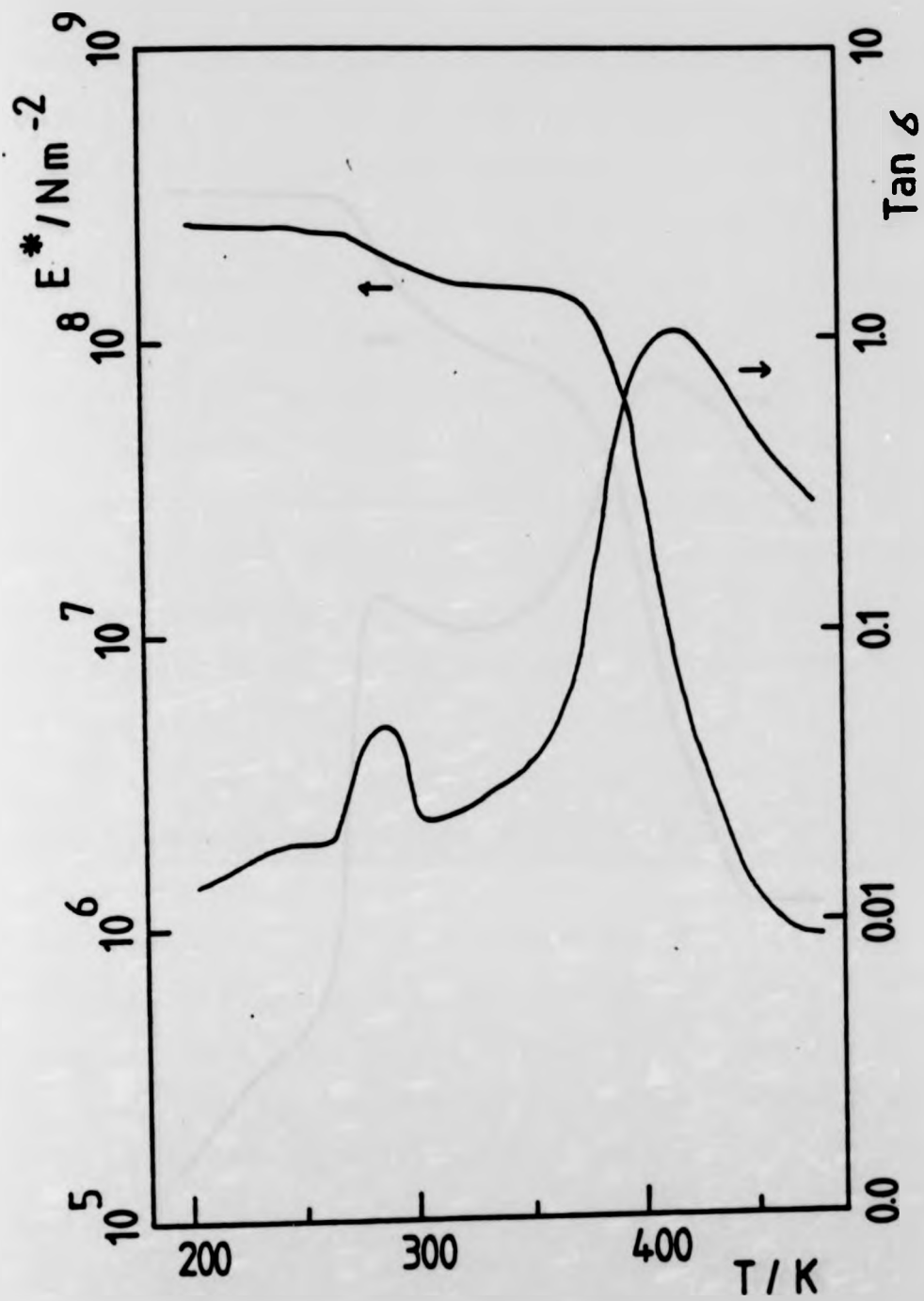


Figure 5.15: Complex modulus ( $E^*/Nm^{-2}$ ) and  $\tan \delta$  versus temperature curves for P(BD-b-DMI)-I(4), pressed film.

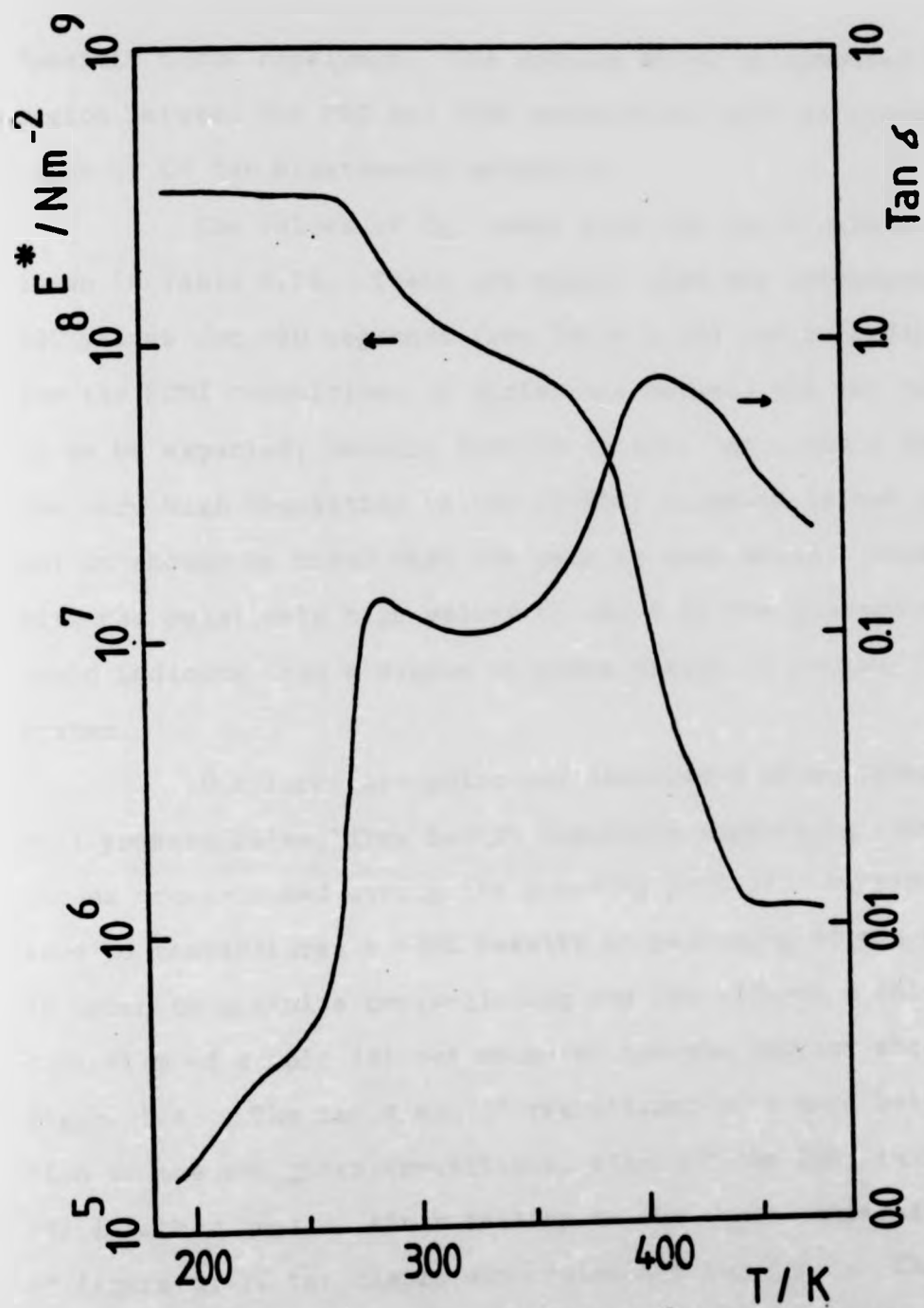


Figure 5.16: Complex modulus ( $E^*/Nm^{-2}$ ) and  $\tan \delta$  versus temperature curve for P(BD-p-DMI)-I(5), pressed film.



"useful" block copolymer. The modulus shows an extended plateau region between the PBD and PDMI transitions with an appropriate value of  $E^*$  for elastomeric behaviour.

The values of  $T_g$ , taken from the  $\tan \delta$  maxima are shown in Table 5.21. These are higher than the corresponding DSC values for PBD segments (see Table 5.16) and markedly higher for the PDMI transition. A difference between the two techniques is to be expected, usually from 10 to 20K. An obvious reason for the very high transition values of PDMI segments is not apparent, but it should be noted that the peak is very broad. This, along with the relatively high values of  $\tan \delta$  in the plateau region could indicate that a degree of phase mixing is present in the system.

One important point was discovered after forming the melt pressed films, they became insoluble suggesting that they became cross-linked during the pressing process. Continued exposure to temperatures  $\sim 420K$  results in yellowing of the films. In order to minimize cross-linking and its effects, a chloroform cast film of sample (5) was measured and the results shown in figure 5.17. The  $\tan \delta$  and  $E^*$  transitions show much better separation of the two glass transitions, although the PDMI  $\tan \delta$  peak is still rather broad. After testing to the upper temperature limit of figure 5.17, the sample was cooled and run again. The result is shown in figure 5.18 where the  $\tan \delta$  peaks are now much more broadened and the moduli drops are also less distinct. The sample was cross-linked after the first run and figure 5.18 must reflect the effect of cross-linking on the sample's mechanical response.

To what extent broadening in the RV traces of melt

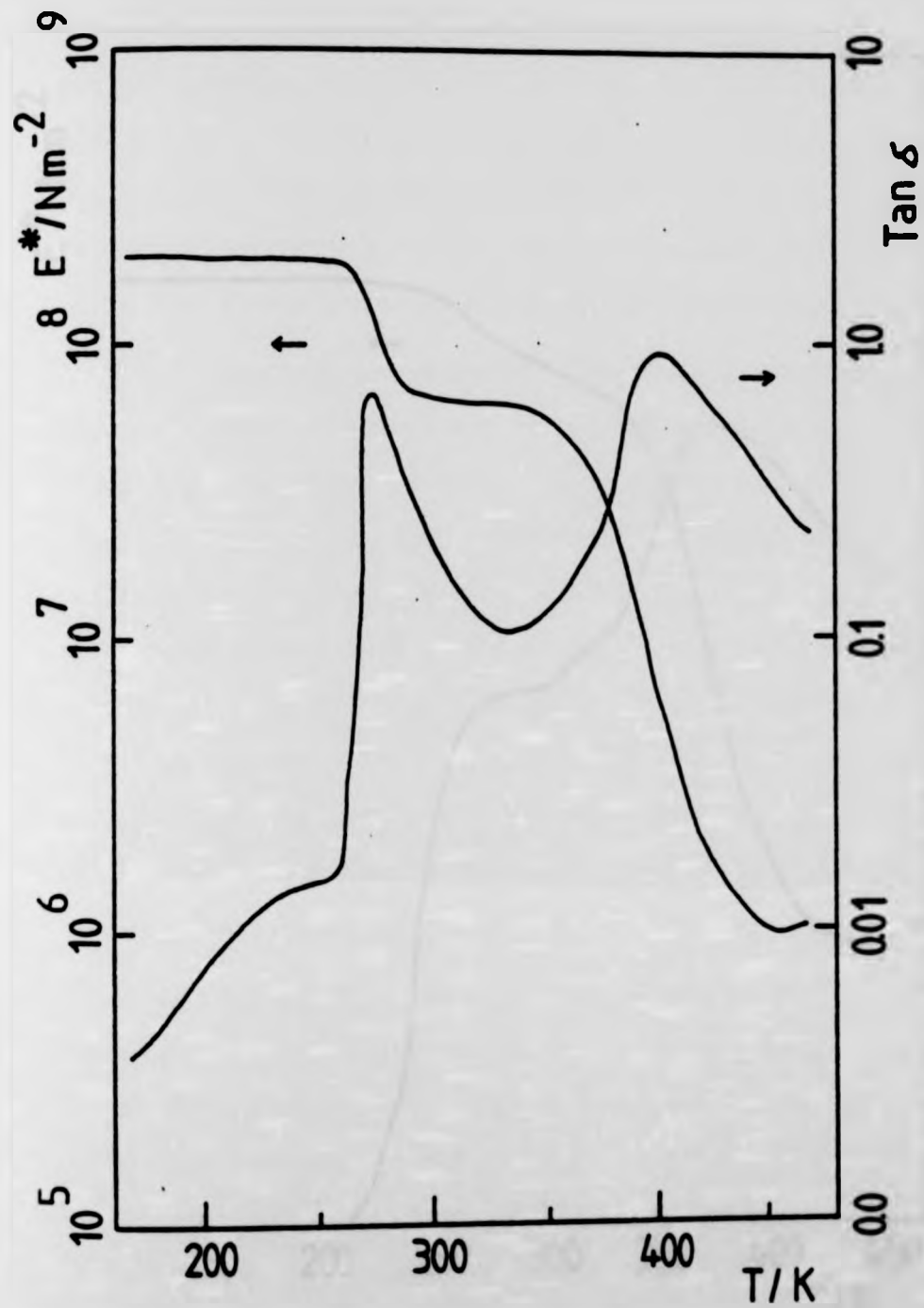


Figure 5.17: Complex modulus ( $E^*/Nm^{-2}$ ) and  $\tan \delta$  versus temperature curves for P(BD-b-DMI)-I(5), cast film.

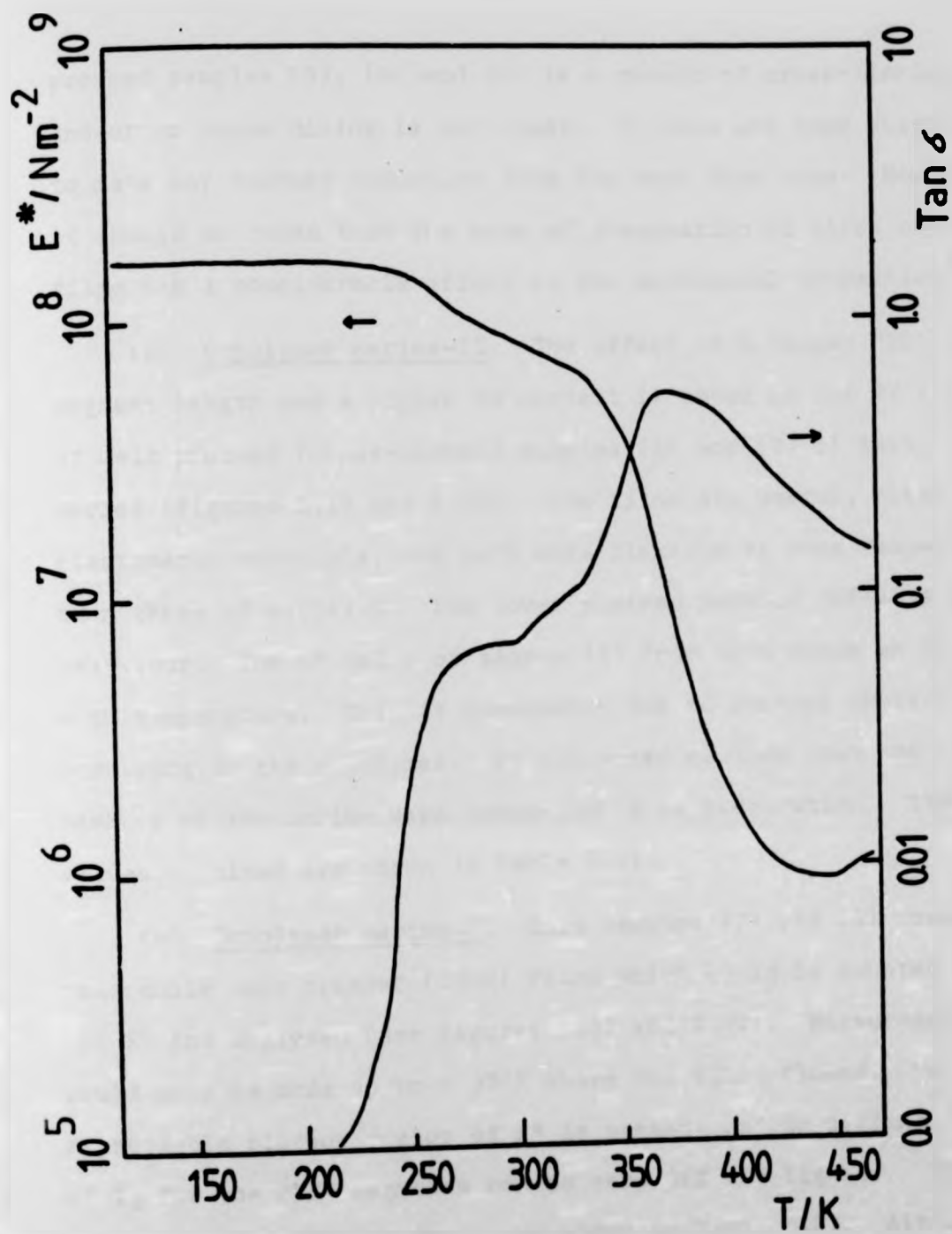


Figure 5.18: Complex modulus ( $E^*/Nm^{-2}$ ) and  $\tan \delta$  versus temperature curves for P(BD-b-DMI)-I(5), recycled film.

pressed samples (3), (4) and (5) is a result of cross-linking and/or of phase mixing is not clear. It does not seem possible to make any further deduction from the work done here. However it should be noted that the mode of preparation of block copolymer films has a considerable effect on the mechanical properties.<sup>(96,97)</sup>

(b) Copolymer series-II. The effect of a longer PBD segment length and a higher BD content is shown by the RV traces of melt pressed (cross-linked) samples (1) and (2) of this series (figures 5.19 and 5.20). The films are useful, clear elastomeric materials, but much more flexible at room temperature than those of series-I. The lower plateau modulus reflects this behaviour. The  $E^*$  value of sample (2) from 423K shows an increase with temperature. This is presumably due to further cross-linking occurring in the copolymer. It was noted earlier that the other members of the series were cross-linked on preparation. The  $T_g$  values obtained are shown in Table 5.22.

(c) Copolymer series-V. Only samples (2) and (3) formed reasonable melt pressed (333K) films which could be mounted in the RV and analysed (see figures 5.21 and 5.22). Measurements could only be made up to  $\sim 370K$  where the films flowed. No appreciable plateau region of  $E^*$  is present and no distinct value of  $T_g$  for the PDMI segments can be read off the figures. The  $T_g$  values for the HPBD segments are shown in Table 5.23. Although these copolymers do not cross-link, the properties of the films are disappointing. No further work was done on this system.

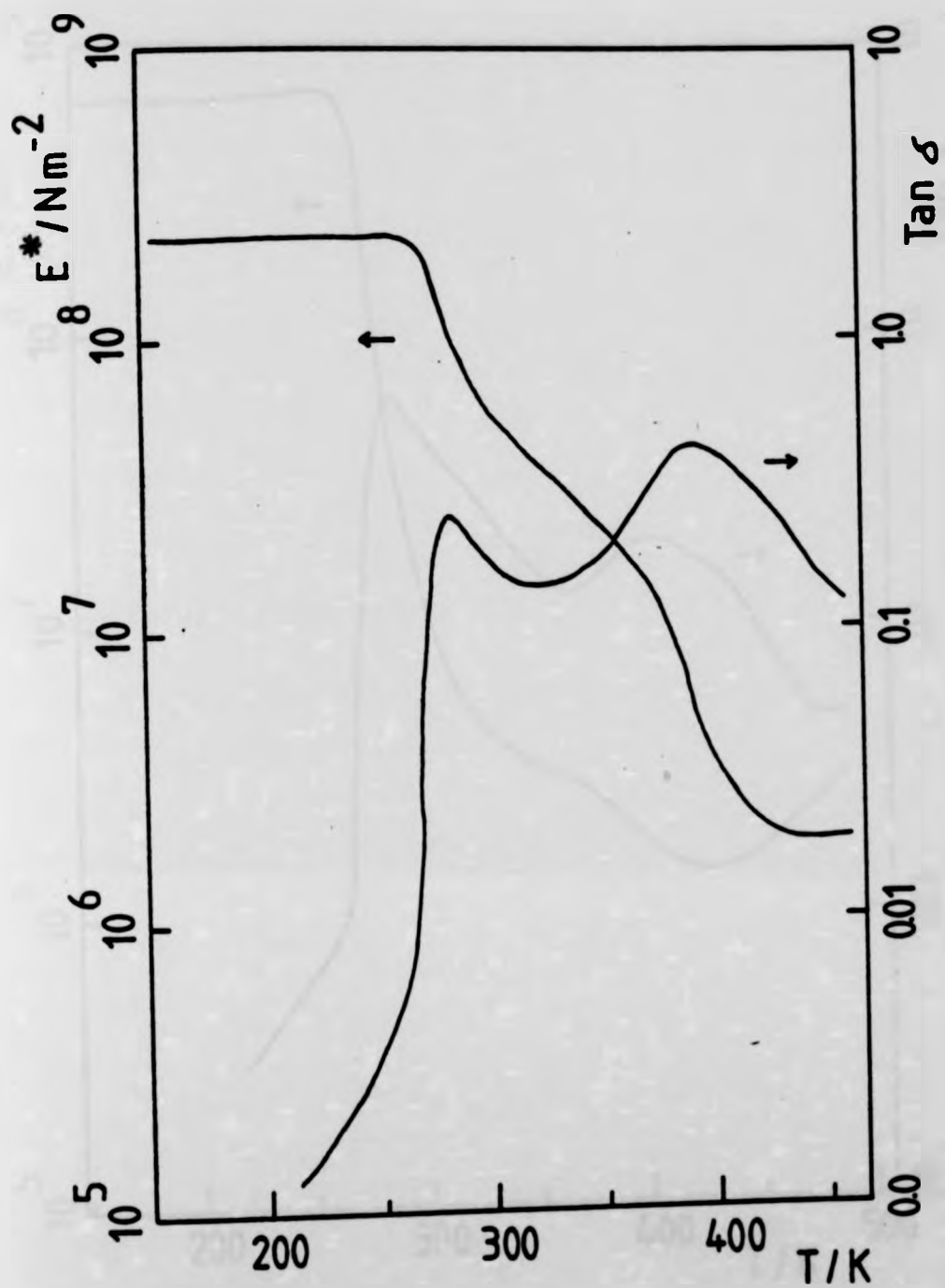


Figure 5.19: Complex modulus ( $E^*/Nm^{-2}$ ) and  $\tan \delta$  versus temperature curves for P(BD-b-DM)-II(1), pressed film.

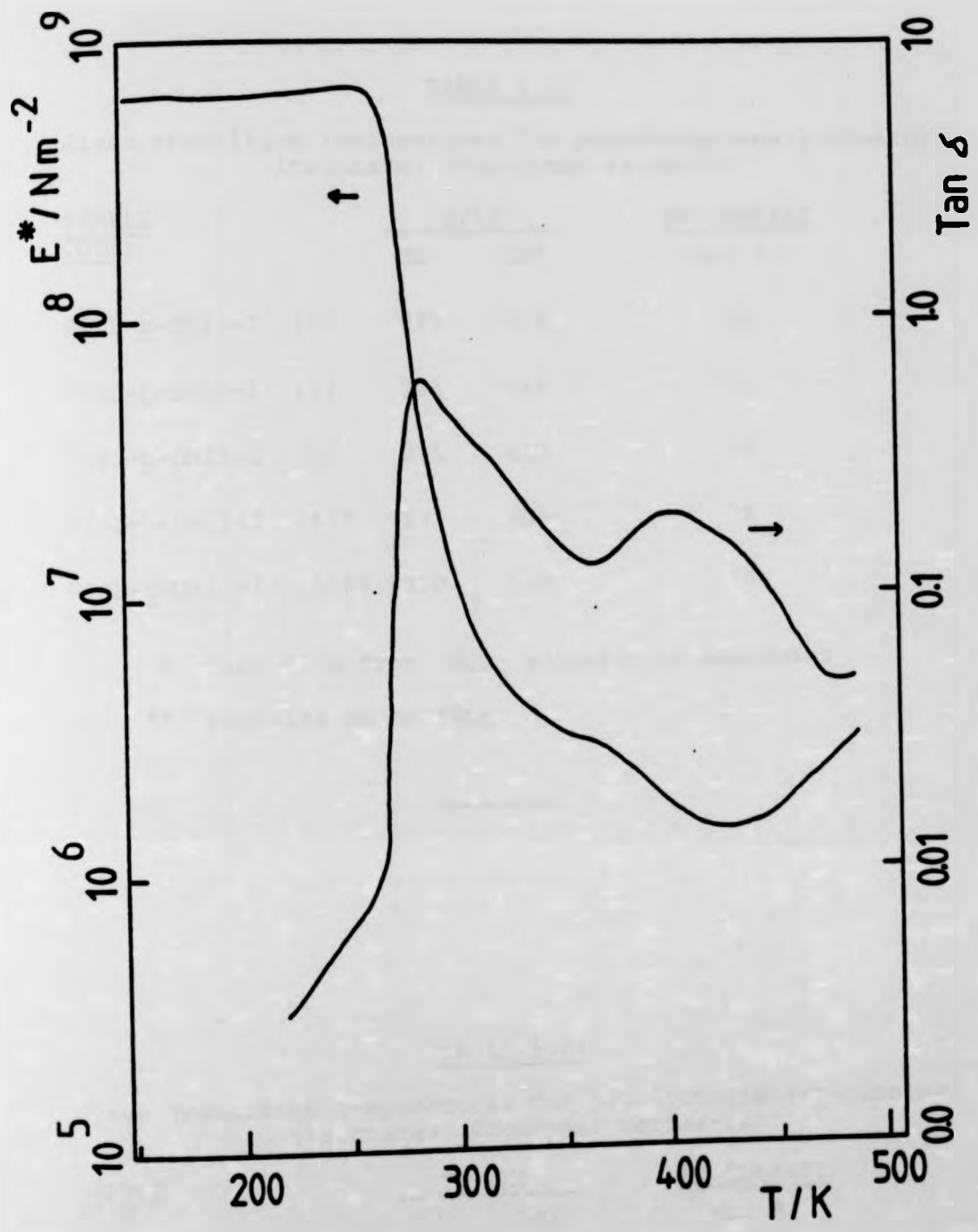


Figure 5.20: Complex modulus ( $E^*/Nm^{-2}$ ) and  $\tan \delta$  versus temperature curves for P(BD-p-DMI)-II(2), pressed film.

TABLE 5.21

Glass transition temperatures for poly(butadiene-b-dimethyl itaconate) (Copolymer series-I)

<u>SAMPLE</u> <u>CODE:</u>	<u>T<sub>g</sub>/(K)</u>		<u>BD CONTENT</u>
	BD	DMI	(mol %)
P(BD- <u>b</u> -DMI)-I (3)	279	416	39
P(BD- <u>b</u> -DMI)-I (4)	285	415	62
P(BD- <u>b</u> -DMI)-I (5)	285	410	75
P(BD- <u>b</u> -DMI)-I (5)*	277	405	75
P(BD- <u>b</u> -DMI)-I (5)**	~310	408	75

\* Cast film from CHCl<sub>3</sub> solution of copolymer

\*\* Recycled on heating

TABLE 5.22

Glass transition temperatures for poly(butadiene-b-dimethyl itaconate) (Copolymer series-II)

<u>SAMPLE</u> <u>CODE:</u>	<u>T<sub>g</sub>/(K)</u>		<u>BD CONTENT</u>
	BD	DMI	(mol %)
P(BD- <u>b</u> -DMI)-II (1)	287	397	85
P(BD- <u>b</u> -DMI)-II (2)	289	407	90

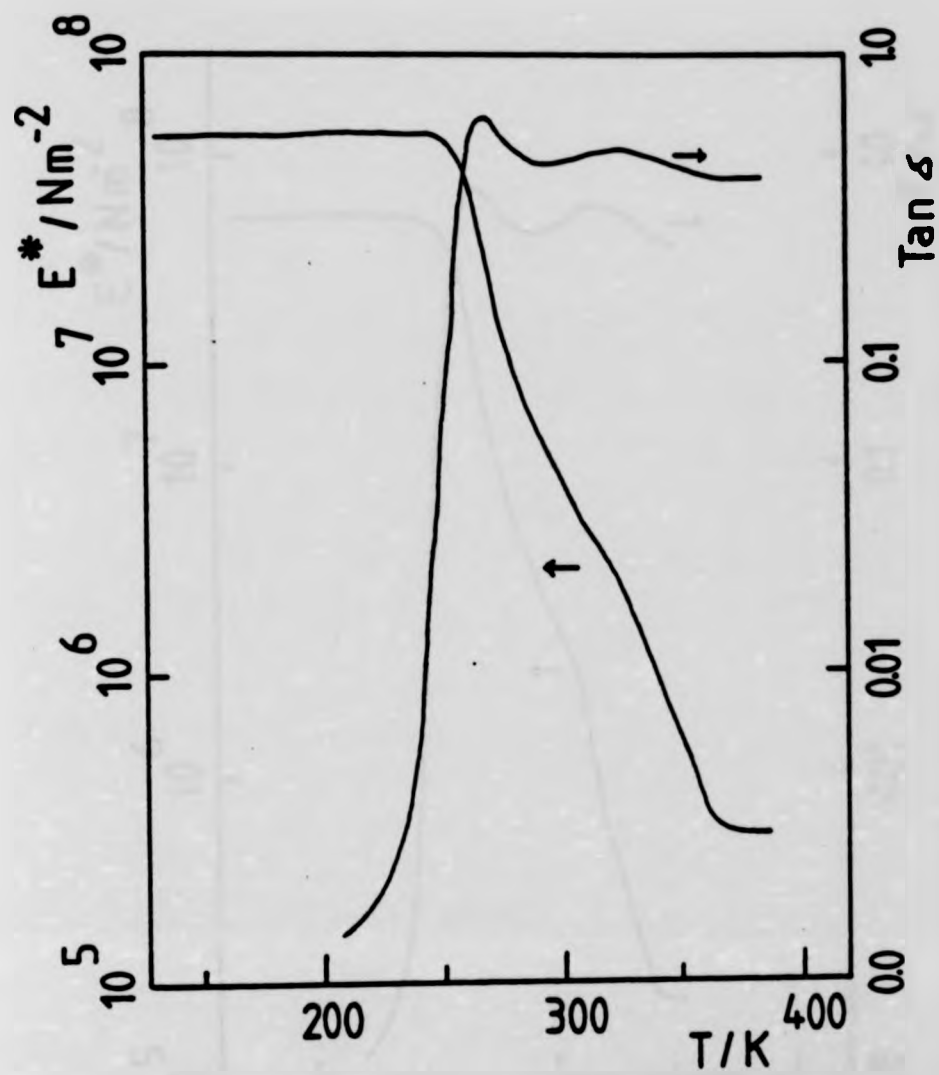


Figure 5.21: Complex modulus ( $E^*/\text{Nm}^{-2}$ ) and  $\tan \delta$  versus temperature curves for P(HBD-b-DMI)-V(2), pressed film.



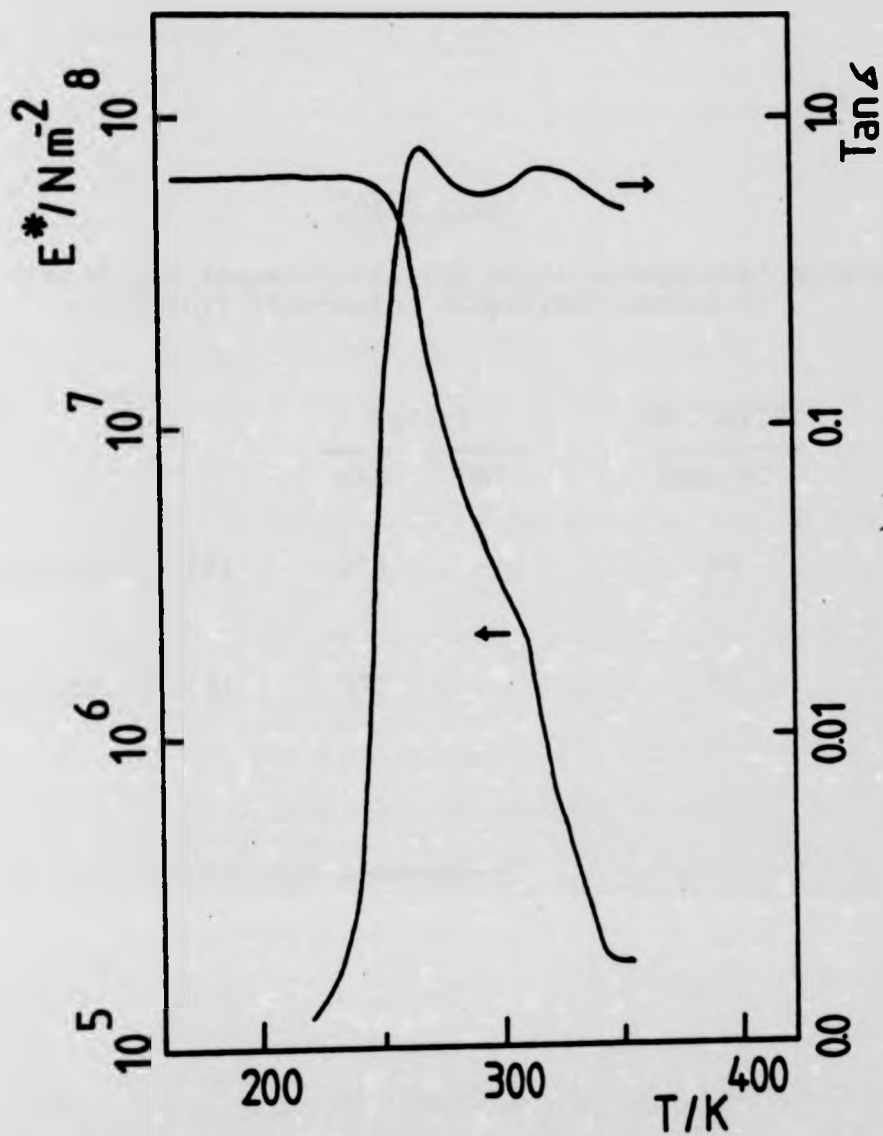


Figure 5.22: Complex modulus ( $E^*/Nm^{-2}$ ) and  $\tan \delta$  versus temperature curves for P(HBD-b-DMI)-V(3), pressed film.

TABLE 5.23

Glass transition temperatures for poly(hydrogenated butadiene-  
b-dimethyl itaconate) (Copolymer series-V)

<u>SAMPLE</u> <u>CODE:</u>	<u>Tg/(K)</u>		<u>BD CONTENT</u>
	HBD	DMI	(mol %)
P(HBD- <u>b</u> -DMI)-V (2)	273	-	85
P(HBD- <u>b</u> -DMI)-V (3)	272	-	87

---

#### 5.3.4 TENSILE TESTING AND CREEP

In order to get some idea of the response of the copolymers under load both tensile and creep measurements were carried out on samples from series-IV.

The tensile response of sample (5) (the most flexible of this series) as a chloroform cast film is recorded in figure 5.23. Four separate runs are shown up to their break point. The shape of the curves is characteristic for a material which cold draws after "necking". The neck point occurs at  $\sim 10-20\%$  elongation. This type of behaviour is typical of elastomeric block copolymers<sup>(98)</sup>. The drawing mechanism for block copolymers containing hard and soft domains is thought to involve distortion and realignment of the hard domains in the rubbery matrix<sup>(99)</sup>.

Creep behaviour was recorded for samples (3) and (4) and is shown by the compliance,  $J(t)$ , as a function of  $\log(t)$ . The effect of increasing butadiene content on two pressed films of samples (3) and (4) is as expected, the sample with lower  $J$  values having the greater DMI content. The difference between a cast and pressed film of sample (4) is again as expected. Since pressing induces cross-linking the pressed films have lower  $J$  values than the cast sample.

All three films show an initial increase in  $J$  followed by a plateau region from  $\log(t/\text{sec}) = 1-2.5$ . This plateau is due to chain entanglements or cross-links and is followed by a second region when viscous flow occurs. The creep behaviour is quite typical of this type of copolymer<sup>(31)</sup> and traces are shown in figure 5.24.

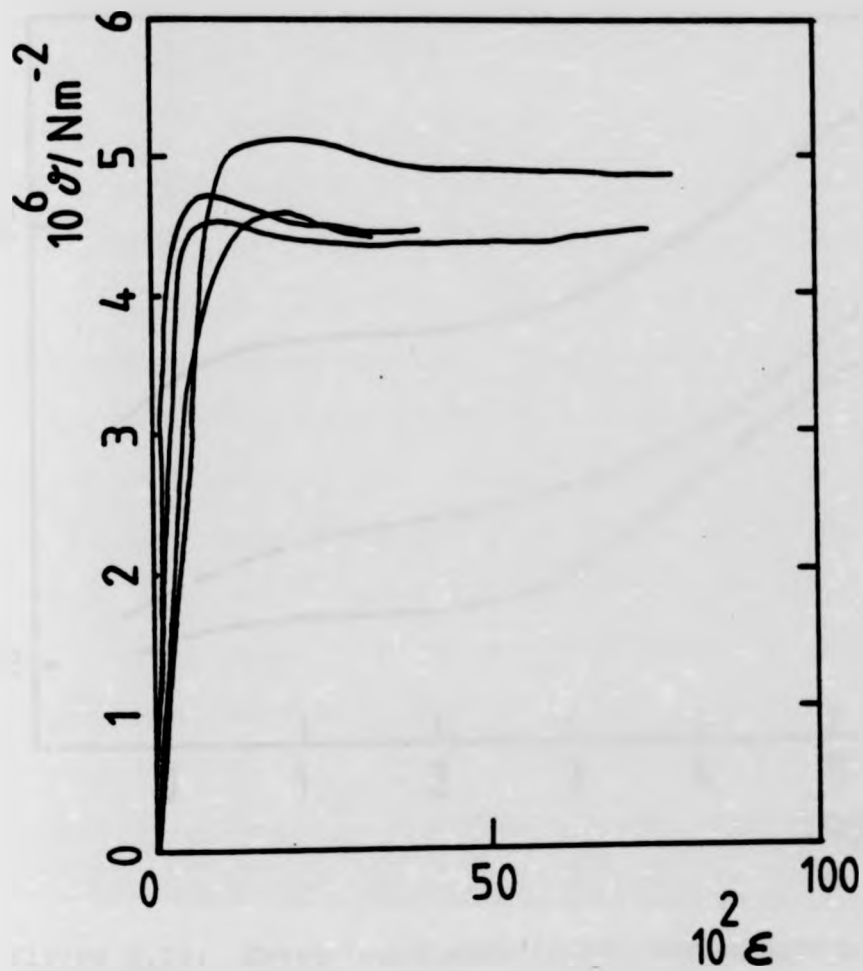


Figure 5.23: Stress-strain behaviour for P(BD-b-DMI)-IV(5).  
 Plots of stress  $\sigma/\text{Nm}^{-2}$  versus % extension.  
 ( $\epsilon$ ) for 4 runs on the same film prepared  
 by casting from chloroform.

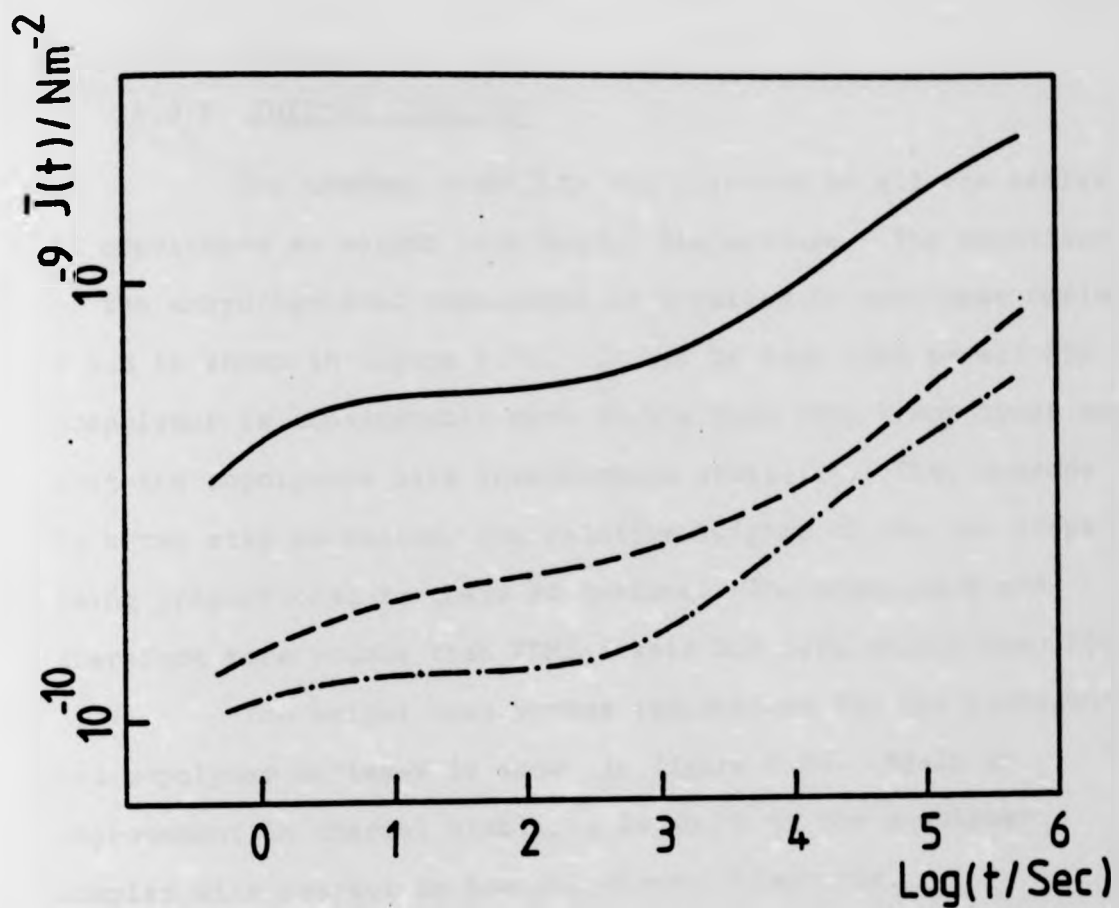


Figure 5.24: Creep compliance ( $J(t)$ ) versus  $\log(\text{time})$  behaviour of P(BD-b-DMI)-IV sample (4) cast film (—), sample (4) pressed film (----), and sample (3) pressed film (-.-.-).

#### 5.3.5 THERMAL STABILITY

The thermal stability was measured on all the series of copolymers as weight loss versus temperature. The behaviour of the unhydrogenated copolymers is typified by copolymer series-I and is shown in figure 5.25. It can be seen that parent PBD prepolymer is considerably more stable than PDMI homopolymer and that the copolymers have intermediate stability. They degrade by a two step mechanism, the relative heights of the two steps being proportional to their BD content. The copolymers are therefore more stable than PDMI itself but less stable than PBD.

The weight loss versus temperature for the hydrogenated copolymer series-V is shown in figure 5.26. Again an improvement in thermal stability is shown by the copolymer samples with respect to homopolydimethylitaconate.

#### 5.3.6 CONCLUSIONS ON BLOCK COPOLYMERS FROM PBD AND DMI

In terms of producing a useful elastomeric product the synthesis is gauged successful. When the BD content is roughly between 60 and 80 mol % a tough clear and flexible material is obtained. The major disadvantage is its willingness to cross-link thermally, however even after cross-linking the desirable mechanical properties are present. The creep and tensile behaviours are as expected for this type of material and thermal stability is enhanced when compared with homopoly(dimethylitaconate).

The ideal analysis yields structures in accord with the molecular weights and compositions of the copolymers, but it must be admitted that the DSC determined Tg values for the PDMI

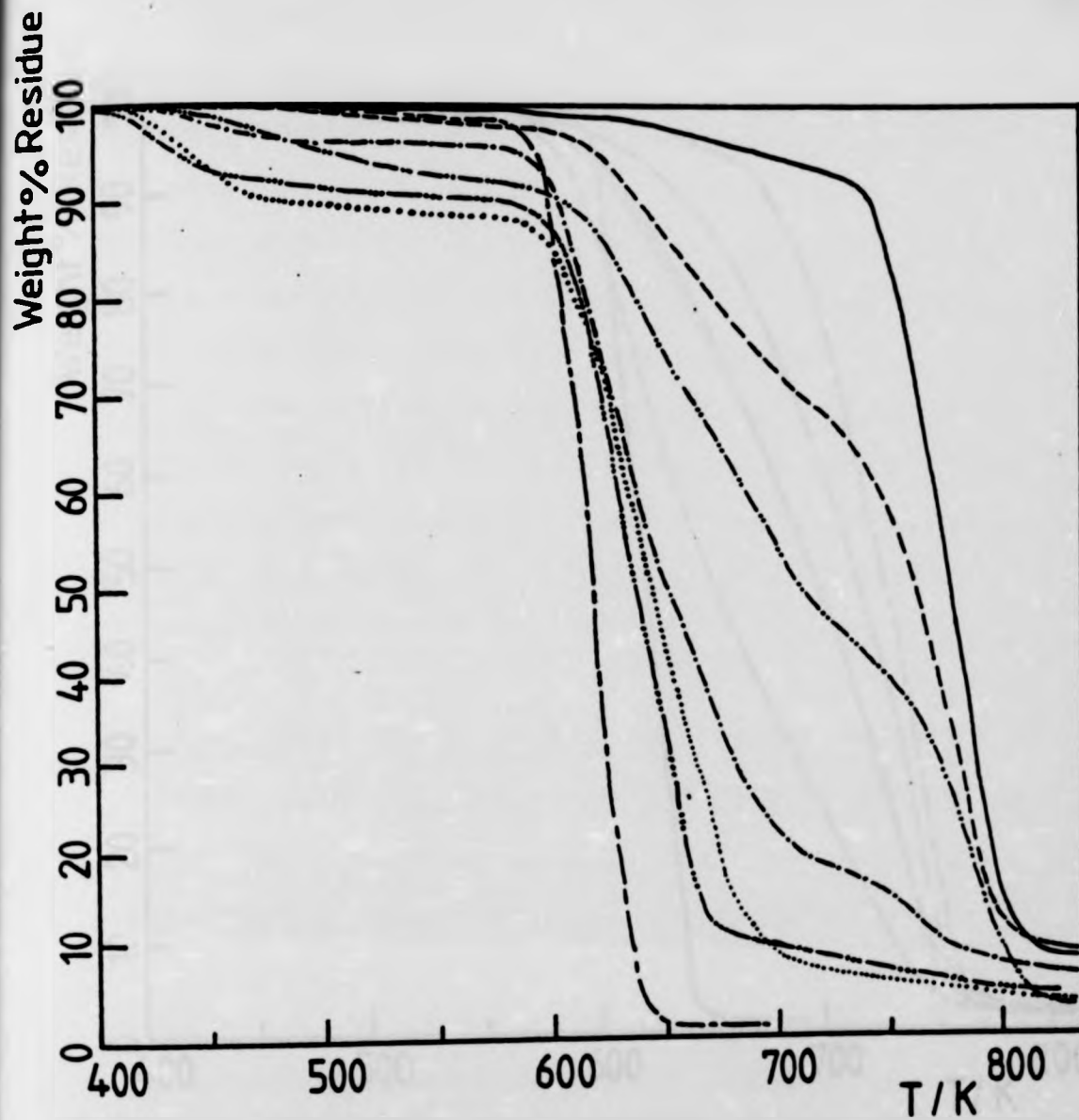


Figure 5.25: % weight loss versus temperature curves for P(BD-b-DMI)-I series; (---), sample (1); (.....), sample (2); (-----), sample (3); (---), sample (4); (-----), sample (5) and homopolymers PDMI(-----), PBD (——).

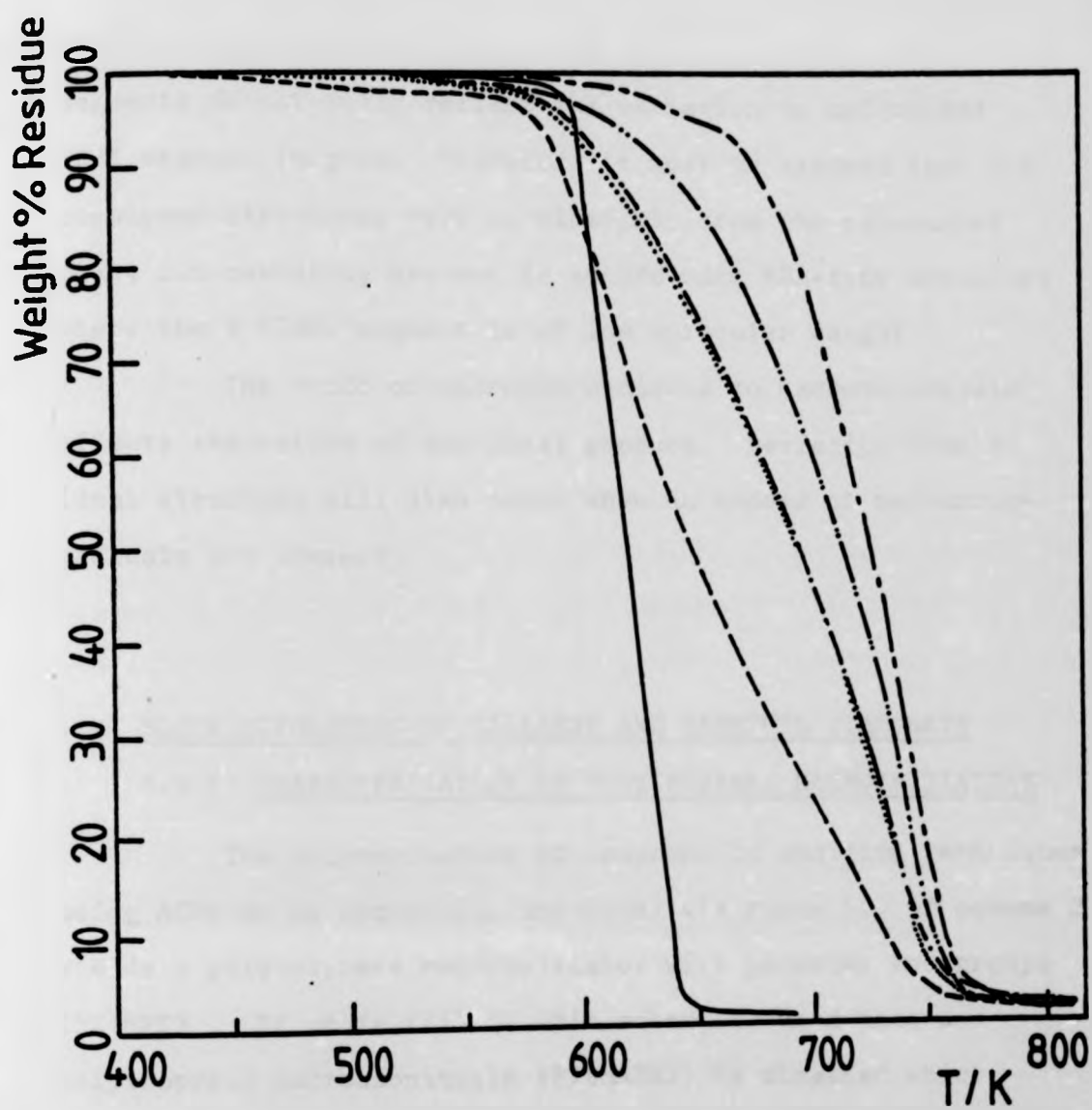


Figure 5.26: % weight loss versus temperature curves for P(HBD-b-DMI)-V series; (----), sample (1); (.....), sample (2); (-·-·-·-·-), sample (3); (-·-·-·-·-), sample (4), and homopolymers PDMI (—), PBD(— — — —).



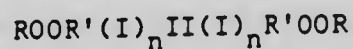
segments do not fully reflect the variation in calculated PDMI segment lengths. Therefore it must be assumed that the copolymer structures vary considerably from the calculated ones, but certainly are not in accord with ABA-type structure where the B (PBD) segment is of low molecular weight.

The ratio of macromonomer radicals to macrobiradicals affects the nature of the final product. Deviation from an ideal structure will also occur when an excess of macromonomer radicals are present.

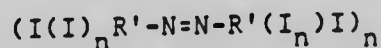
#### 5.4 BLOCK COPOLYMERS OF ISOPRENE AND DIMETHYL ITACONATE

##### 5.4.1 CHARACTERISATION OF POLYISOPRENE MACROINITIATORS

The polymerization of isoprene by emulsion techniques using  $\text{ACPOtBu}$  as sequential initiator via route (i) of scheme 2 yields a polyisoprene macroinitiator with perester end groups (PI(MPE)). If route (ii) of this scheme is used then a polyisoprene macroazobitrile (PI(MAZN)) is obtained which contains azo links in the main chain as the active sites. The termination mechanism in isoprene polymerization is known to be exclusively by a recombination mechanism, thus the PI(MPE) has the structure,



and the PI(MAZN) the following structure,



Emulsion techniques were used only because of the low reactivity of isoprene in bulk or solution which yields low molecular weight products<sup>(42)</sup>.

Polyisoprene macroinitiators prepared were characterised with respect to structure using ir spectroscopy<sup>(90)</sup> and molecular weight using membrane osmometry. The following microstructural composition was obtained, 65% cis and trans 1,4 units ( $840\text{ cm}^{-1}$ ), 22% 3,4 units ( $890\text{ cm}^{-1}$ ) and 13% 1,2 units ( $910\text{ cm}^{-1}$ ).  $\bar{M}_n$  values for the polyisoprene macroinitiators are listed in Table 5.24. The preparation of the PI(MPE)-I-III yielded soluble products. However, three attempted preparations of the PI(MAZN) gave an insoluble and presumably cross-linked material each time and no further work was done on these products.

#### 5.4.2 CHARACTERIZATION OF POLY(DIMETHYL ITACONATE) MACROINITIATORS

Three poly(dimethyl itaconate) macroinitiators were prepared from ACP0tBu and DMI by both route (i) of scheme 2 to give polymers with perester links (PDMI(MPE)) and by route (ii) of scheme 2 to give polymer with azo links (PDMI(MAZN)). Six soluble PDMI macroinitiators were isolated and characterised by ir spectroscopy and membrane osmometry and are listed in Table 5.25. The use of benzene as solvent (samples IV and V) caused very low yields to be obtained, for this reason the emulsion polymerization (sample VI) was carried out.

TABLE 5.24

$\bar{M}_n$  values for polyisoprene macroinitiators (PI(MPE)'s) and (PI(MAZN)) using ACPOtBu as initiator

<u>SAMPLE CODE:</u>	<u>INITIATOR</u> (mol %)	<u>TEMP.</u> (K)	<u>CONVERSION</u> (wt. %)	$\bar{M}_n$ (g mol <sup>-1</sup> x 10 <sup>-4</sup> )
PI(MPE-I)	1.00	328	25	2.83
PI(MPE-II)	0.70	333	53	2.60
PI(MPE-III)	0.65	333	83	3.58
PI(MAZN-I)	1.00	308	60	-

TABLE 5.25

$\bar{M}_n$  values for poly(dimethyl itaconate) macroinitiators (PDMI(MPE)'s) and (PDMI(MAZN)'s) using ACPOtBu as initiator.

<u>SAMPLE CODE:</u>	<u>INITIATOR</u> (mol %)	<u>TEMP.</u> (K)	<u>CONVERSION</u> (wt. %)	$\bar{M}_n$ (g mol <sup>-1</sup> x 10 <sup>-5</sup> )
PDMI(MPE-I)	1	333	78	1.70
PDMI(MPE-II)	3	333	53	0.94
PDMI(MPE-III)	4	338	30	0.60
PDMI(MAZN-I)	1	301	4.0	1.20
PDMI(MAZN-II)	2	310	4.7	0.84
PDMI(MAZN-III)	2	310	60	0.86

#### 5.4.3 ATTEMPTED COPOLYMERIZATION OF POLYISOPRENE MACROINITIATORS WITH DIMETHYL ITACONATE

An attempt to form a copolymer by decomposing the PI(MPE-I), PI(MPE-II) and PI(MPE-III) in the presence of DMI monomer at 307K led to the formation of (insoluble) cross-linked products. Extraction with chloroform yields very small amounts of non-cross-linked material with  $\bar{M}_n = 3-4 \times 10^4 \text{ g mol}^{-1}$ . The ir and nmr spectra showed bands of both polyisoprene and poly-(dimethyl itaconate) but no further attempts were made to characterize these materials. It was possible to take an ir spectrum of the cross-linked polymer and this showed it to be almost 100% polyisoprene. Heating polyisoprene macroinitiator to  $\sim 330\text{K}$  in the presence of free radicals results predominately in a self cross-linking reaction.

It was noted that when dimethyl itaconate monomer was added to the benzene solution of polyisoprene macroinitiator a two phase system developed. The polymerization systems were thoroughly agitated but it seems likely from the above results that DMI monomer was effectively excluded from the isoprene phase.

#### 5.4.4 ATTEMPTED COPOLYMERIZATION OF POLY(DIMETHYL ITACONATE) MACROINITIATORS WITH ISOPRENE

All the attempted preparations listed in Tables 2.18-2.23 resulted in obtaining insoluble cross-linked products. Again the polymer systems were two phase and no attempts were made to characterize any of the products.

#### 5.4.5 CONCLUSIONS ON ATTEMPTED BLOCK COPOLYMER FORMATION USING ISOPRENE AND DIMETHYL ITACONATE

This can easily be summarized as unsuccessful. The choice of polyisoprene as rubbery block is possibly a bad one since it is well known that cross-linking is facile. The incompatibility of the second monomer with the macroinitiator is possibly equally responsible for the failure to produce block copolymer. Macroinitiators were successfully synthesized and future work could be done with these but in a more compatible system. Block copolymers have been successfully prepared by these methods<sup>(42)</sup> using methylmethacrylate and butylacrylate which are, of course, much more compatible systems than the pair chosen here.

EXPERIMENTAL PROCEDURE

In order to study the effect of the concentration of the monomer on the rate of polymerization, a series of experiments were carried out in which the concentration of the monomer was varied while the concentration of the initiator was kept constant. The results are shown in Figure 1.

It is seen from Figure 1 that the rate of polymerization increases with increasing monomer concentration. This is to be expected since the rate of polymerization is proportional to the concentration of the monomer.

CHAPTER 6

IONOMERS

RESULTS AND DISCUSSION

The results of the experiments are shown in Figure 1. It is seen that the rate of polymerization increases with increasing monomer concentration. This is to be expected since the rate of polymerization is proportional to the concentration of the monomer.

The results of the experiments are shown in Figure 1. It is seen that the rate of polymerization increases with increasing monomer concentration. This is to be expected since the rate of polymerization is proportional to the concentration of the monomer.

## 6.1 COPOLYMER CHARACTERIZATION

In order to form ionomers from itaconic acid-based polymers it is necessary to synthesize copolymers with ionisable functional groups in the main chain. This is most easily accomplished by allowing an itaconic acid monoester to copolymerize with a diester.

Previous work<sup>(22)</sup> has shown that useful ionomers can be formed from copolymers of mono- and di-n-heptyl itaconate. In this thesis an investigation of the mechanical properties of ionomers from poly(mono-n-pentyl itaconate-co-di-n-pentyl itaconate) (P(MPI + DPI)) was undertaken.

### 6.1.1 UNIONISED COPOLYMERS

The compositions of the copolymers synthesized as described in section 2.2(ii) were estimated by titration of their solutions in 90% ethanol + 10% water. Representative pH curves are shown in figure 6.1. The unionised copolymers are coded by the abbreviation P(MPI + DPI) followed by the numbers indicating the mole ratio of MPI to DPI in the copolymers. The end points were taken as the inflection points on the curves and occur at pH = 10.5-11. The calculated MPI contents for each copolymer are shown in Table 6.1 along with their number average molecular weights determined by membrane osmometry.

The reactivity ratios ( $r_1$  and  $r_2$ ) of the copolymer system MPI (monomer 1) + DPI (monomer 2) were evaluated from the compositions of those samples whose conversion was 10% or less (to avoid errors from composition drift effects). The



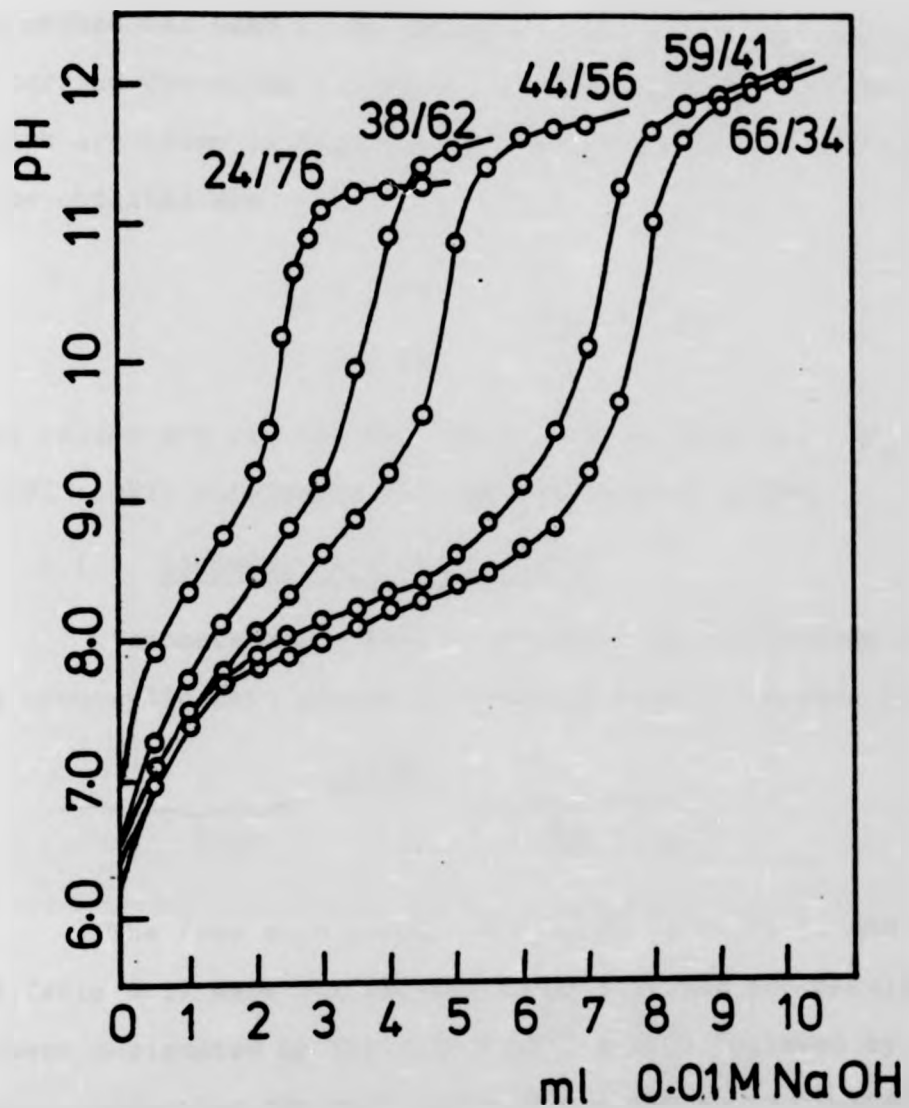


Figure 6.1: pH curves for representative samples from P(MPI+DPI) copolymer series.

From left to right curves are for sample 1, 5, 6, 8 and 9. Numbers alongside curves refer to mole ratio MPI/DPI calculated from end points.

(62)

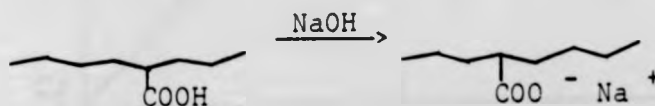
same method was used as described in Chapter 3. The calculation was carried out using an "Apple II" microcomputer and the results are shown in figure 6.2. The values of the reactivity ratios obtained are

$$\begin{aligned} r_1 &= 1.69 \\ r_2 &= 0.78 \\ r_1 r_2 &= 1.31 \end{aligned}$$

These values are not too far from the ideal case ( $r_1 = r_2 = 1$ ) so (MPI + DPI) copolymers will be essentially random.

#### 6.1.2 IONOMERS FROM P(MPI + DPI)

Ionomers were readily formed by neutralisation of the free carboxylic acid groups by either sodium or caesium hydroxide



The free acid groups of samples 1, 5, 8, 11 and 14 (see Table 6.1) were neutralised completely and the resulting ionomers designated by the code PI(MPI + DPI) followed by the numbers indicating the mole ratio of mono-ester to diester in the copolymer.

Small angle x-ray scattering (SAXS) studies were kindly carried out on three samples (sodium ionomers) by Dr. D. H. Handlin of the University of Massachusetts and the results shown in figures 6.3, 6.4 and 6.5. There appear to be two peaks present in each scattering pattern and it is possible to relate the scattering intensity maxima to the Bragg spacing ( $d$ ) of the scattering sources from the Bragg equation,

$$\lambda = 2d \sin \theta \quad (6.1)$$

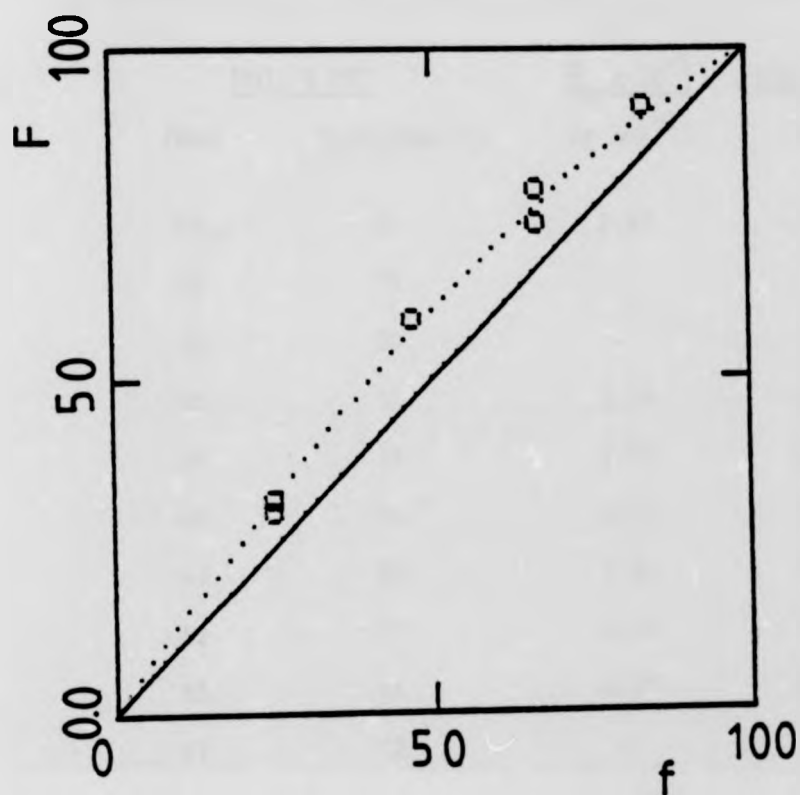


Figure 6.2: Plot of mol fraction MPI in feed ( $f$ ) versus mol fraction MPI in copolymer ( $F$ ) for P(MPI+DPI) copolymer series.  
 $\square$ , Experimental points; (.....) calculated curve with  $r_1 = 1.69$  and  $r_2 = 0.78$ .

TABLE 6.1

Copolymer compositions and  $\bar{M}_n$  values for poly(mono-n-pentyl itaconate-co-di-n-pentyl itaconate) series

<u>SAMPLE</u>	<u>Mol. % MPI</u>		$\bar{M}_n \times 10^{-5}$ (g mol <sup>-1</sup> )	<u>Conversion</u> (%)
	Feed	Copolymer		
1	24	24	2.97	14
2	25	22	-	-
3	25	30	-	6
4	25	32	2.24	9
5	39	38	2.52	12
6	45	44	2.82	11
7	47	59	2.80	5
8	52	59	4.16	17
9	59	66	5.37	23
10	67	73	-	10
11	67	78	3.18	7
12	71	80	-	-
13	84	88	-	14
14	84	91	3.97	8
PMPI	-	-	1.16	36
PDPI	-	-	0.74	59

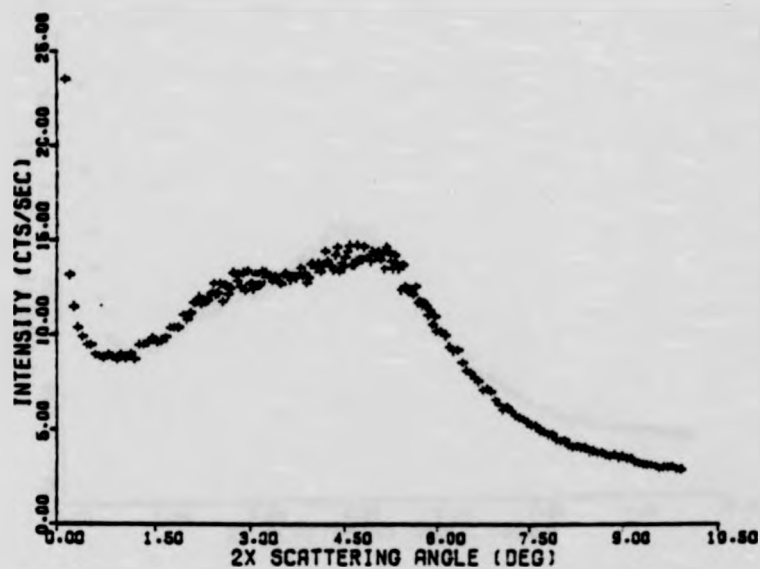


Figure 6.3: SAXS behaviour for PI(MPI+DPI) 24/76, plot of the scattering intensity versus scattering angle ( $2\theta$ ).

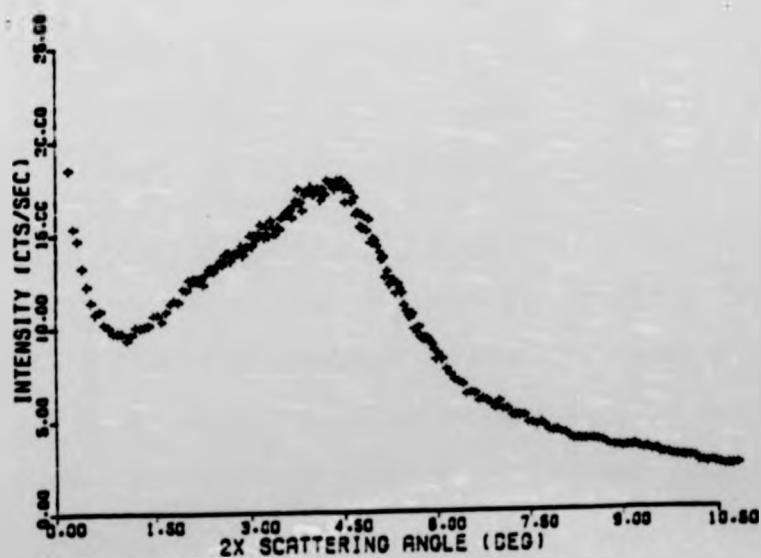


Figure 6.4: SAXS behaviour for PI(MPI+DPI) 38/62, plot of the scattering intensity versus scattering angle ( $2\theta$ ).

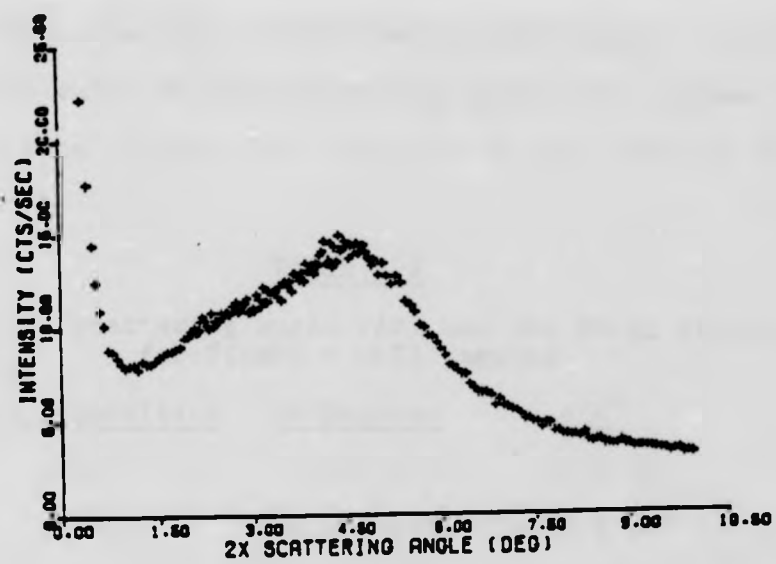


Figure 6.5: SAXS behaviour for PI(MPI+DPI) 59/41, plot of scattering intensity versus scattering angle ( $2\theta$ ).

where  $\lambda$  = the wavelength of the X-ray used ( $\text{CuK}_\alpha = 1.54 \text{ \AA}$ ) and  $\theta$  is the value of the scattering angle. The values of  $d$  calculated from figures 6.3, 6.4 and 6.5 are listed in Table 6.2.

TABLE 6.2

Values of the scattering angle ( $2\theta$ ) and the Bragg spacing ( $d$ ) for PI(MPI + DPI) samples

<u>Sample Composition</u>	<u><math>2\theta</math>/Degrees</u>	<u><math>d/\text{\AA}</math></u>
24/76	2.9 & 4.7	30 & 19
38/62	$\sim$ 2.3 & 4.2	$\sim$ 38 & 21
59/41	$\sim$ 2.6 & 4.6	$\sim$ 34 & 19

A large number of SAXS studies on ionomers have shown that a scattering intensity peak is always present at  $2\theta \sim 4^\circ$ <sup>(100)</sup>. The appearance of this so-called "ionic peak" is independent of the cation present but is intensified by the incorporation of large cations such as caesium. The presence of increasing amounts of water in the sample destroys the ionic peak.

Various models have been proposed to account for the ionic peak and these are described briefly below.

(a) Model of Longworth and Vaughan,<sup>(101)</sup> This model proposes microphase separation of domains containing the ionic groups. Since the cations themselves are not regarded as scattering units the model fails to account for the cation dependent intensity of the ionic peak. A schematic diagram of Longworth-Vaughan<sup>(101)</sup> model for ionic aggregates is shown in figure 6.6(a).

(b) Model of Marx, Caulfield and Cooper. <sup>(102)</sup>

This model invokes no phase separation, but rather proposes that the cations act as point scatterers on a quasi-lattice and that the acid groups exist as aggregates. Figure 6.6(b) represents a schematic diagram for this model <sup>(103)</sup> proposed by the authors.

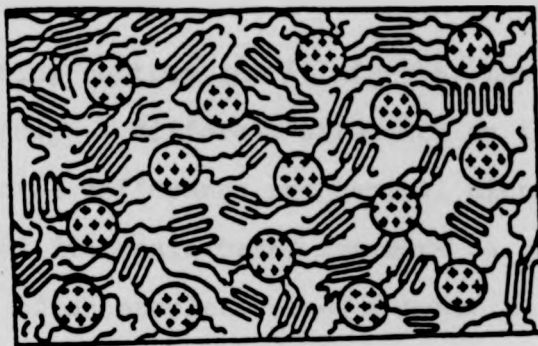
(c) Model of Macknight, Taggart and Stein. <sup>(100)</sup>


These authors propose a model based on an analysis of the scattering radial distribution function which is quite different from (a) and (b) above (see figure 6.6(c)). It is proposed that an ionic cluster of 8-10 Å radius exists and this is shielded from surrounding matrix ions (not incorporated in ionic clusters) by a shell of hydrocarbon chains. The distance between cluster and matrix is assumed to be ca. 20 Å and is the origin of the ionic peak.

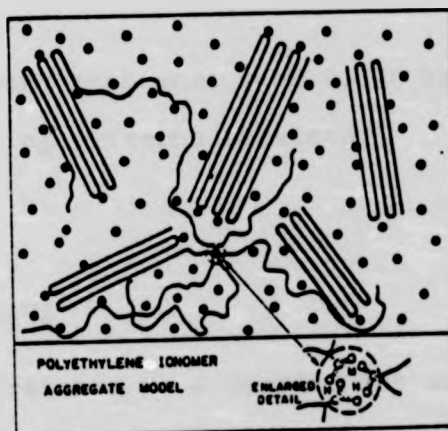
The data shown in figures 6.3, 6.4 and 6.5 are consistent with the scattering results from ionomers already published except for the important difference that they seem to be composed of two peaks. The appearance of two scattering intensities has been noted before in ionomers, but the second peak is present at significantly different scattering angles and has been ascribed to crystallinity.<sup>(104)</sup>

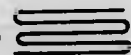
It should be noted that the majority of all previous studies have been on ethylene/acrylic or methacrylic acid-type ionomers with ion contents less than 10% or so. The ionomers studied here have much greater ion concentration even if account is taken of the "dilution" by the relatively long hydrocarbon side chains. Not one of the models proposed would predict two

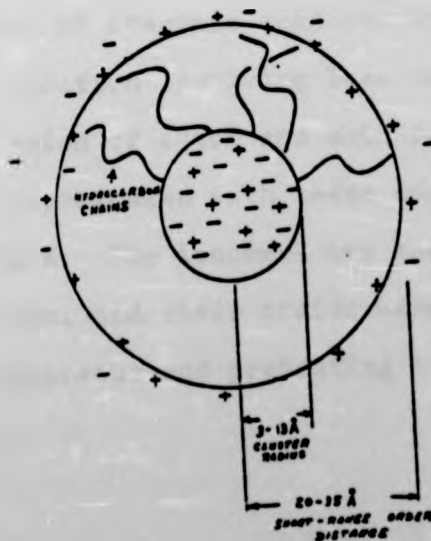




(a) Model of Longworth and Vaughan,  represents ionic cluster.



(b) Model of Marx, Caulfield and Cooper,  represents crystalline domains.



(c) Model of Macknight, Taggart and Stein.

types of scattering centres and it might be that these itaconate-based ionomers adopt a different structure on ionisation due to a quite fundamental difference in chemical microstructure. The main chain of itaconate-based ionomers is considerably more polar than that of an ethylene-based ionomer as there are two ester groups per repeat unit. The driving force which causes ionic sites to cluster or aggregate in a hydrocarbon medium must be considerably modified and this could have an effect on the final structure.

In any event much more work would have to be done to explain the scattering patterns obtained.

## 6.2 TBA MEASUREMENTS

TBA measurements were carried out on representative samples from both the unionised and fully ionised copolymers listed in Table 6.1. Braids were impregnated from ethanol or ethanol + chloroform solutions. Since unionised copolymers containing monoesters of itaconic acid are known to undergo a facile dehydration reaction involving loss of water and/or alcohol from interaction of ester and acid functions<sup>(18)</sup> at  $\sim 400\text{K}$ , the braids impregnated with these copolymers were dried under vacuum at  $\sim 310\text{K}$ . The ionomers are thermally stable with respect to dehydration, and their braids were dried by loading them into the TBA apparatus and preheating to  $\sim 400\text{K}$  under a dry nitrogen purge.

### 6.2.1 TBA RESULTS FOR P(MPI + DPI) SERIES

The TBA results for this series of copolymers are shown in figures 6.7 and 6.8. Since both the mechanical damping index ( $-\log 1/n$ ) and the relative rigidity ( $1/p^2$ ) are non-absolute quantities, the data are displaced vertically in both figures on an arbitrary scale for clarity.

For PDPI itself and the two copolymers containing 24 mol % and 38 mol % of MPI, one major damping maximum is apparent. There are corresponding dramatic falls in the relative rigidity, confirming that these maxima are due to the  $T_g$  in each copolymer.

A smaller damping maximum is also present at  $\sim 100K$  in the TBA spectra of all the copolymers up to a MPI content of 78 mol %. Damping peaks in this temperature region are commonly found in polymers with side chains containing four or more carbon atoms and the molecular origin of this damping process has been ascribed to a "crankshaft" type motion<sup>(67,68)</sup>, although other motions have been postulated<sup>(33)</sup>.

In the copolymers with an MPI content greater than 38 mol % the TBA spectrum of each shows another prominent peak above  $T_g$  at  $\sim 400K$  and higher. This peak is also discernable in P(MPI + DPI) 24/76 and in P(MPI + DPI) 38/62 and is almost certainly due to the dehydration reaction already mentioned. Since, in the copolymers with higher MPI content, this is also accompanied by a rise in the relative rigidity, dehydration reaction must be leading to a cross-linked (more rigid system). This was confirmed by the observation that copolymers heat treated to  $\sim 400K$  were completely insoluble.

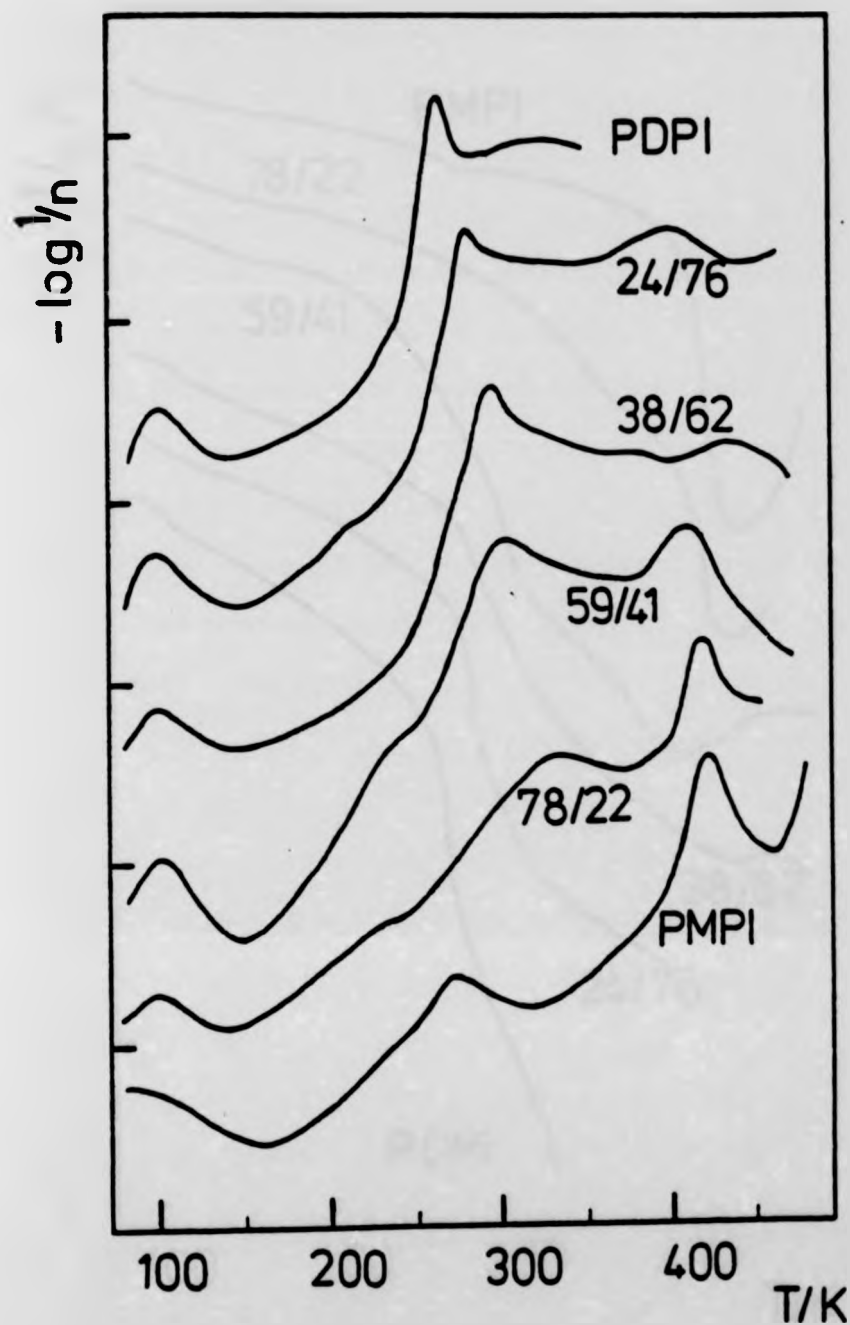


Figure 6.7: Plots of the mechanical damping index ( $-\log 1/n$ ) versus temperature for P(MPI+DPI) 24/76, 38/62, 59/41, 78/22 and for PMPI.

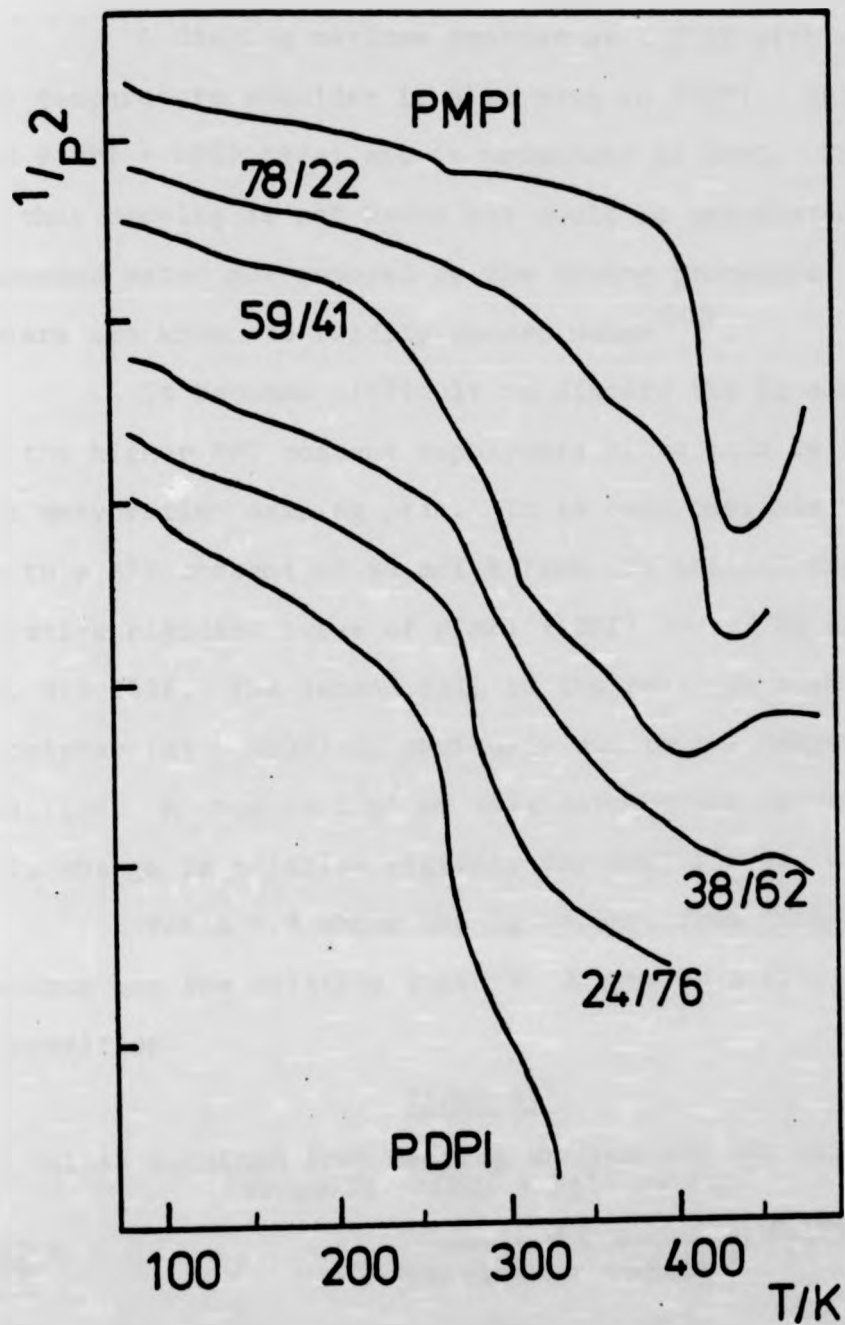


Figure 6.8: Plots of the relative rigidity ( $1/p^2$ ) versus temperature for PMPI, P(MPI+DPI) 78/22, 59/41, 38/62, 24/76 and PDPI.

A damping maximum centred at  $\sim 273\text{K}$  with a small low temperature shoulder is also seen in P(MPI + DPI) 78/22 and P(MPI + DPI) 59/41 and is prominent in PMPI. The origin of this damping is not known but could be associated with absorbed water not removed by the drying procedure. Polymonoesters are known to readily absorb water<sup>(105)</sup>.

It becomes difficult to discern the Tg damping maximum in the higher MPI content copolymers since this is absorbed into the dehydration damping peak. It is only possible to define Tg up to a MPI content of 59 mol % from the initial drop in the relative rigidity curve of P(MPI + DPI) 78/22, Tg is probably ca. 323-333K. The second fall in the relative rigidity for this copolymer (at  $\sim 400\text{K}$ ) is obviously due to the dehydration reaction. A drop in  $1/p^2$  at this temperature is virtually the only change in relative rigidity for PMPI itself.

Table 6.3 shows the Tg values, from both the damping maximum and the relative rigidity drops, as a function of composition.

TABLE 6.3

Tg values obtained from damping maximum and the relative rigidity drops for p(MpI + DpI) series

SAMPLE CODE:	Tg/K		wt.Fract.DPI in copolymer, (w <sub>1</sub> )
	from $-\log 1/n$	from $1/p^2$ *	
PDPI	264	263	-
P(MPI + DPI) 24/76	279	276	0.82
P(MPI + DPI) 38/62	294	290	0.69
P(MPI + DPI) 59/41	303	302	0.48
P(MPI + DPI) 78/22	337	345	0.28
PMPI	-	-	-

\* from point of maximum slope in  $1/p^2$  curve.

From the extrapolation of the data in Table 6.3,  $T_g$  for pMpI is somewhere in the region of 400K. It is, of course, not possible to observe this directly since, in this temperature region, the dehydration reaction is chemically modifying the polymer.

A linear extrapolation is possible using the Fox equation<sup>(79)</sup>, which relates the  $T_g$  of a copolymer to its composition via,

$$\frac{1}{T_g} = \frac{w_1}{T_{g_1}} + \frac{w_2}{T_{g_2}} \quad (6.2)$$

where  $T_g$  is the copolymer glass transition,  $T_{g_1}$  and  $T_{g_2}$  the glass transitions of the homopolymer 1 and 2 whose weight fractions are  $w_1$  and  $w_2$  respectively. A plot of equation (6.2) from the data in Table 6.3 is shown in figure 6.9. This is a straight line with slope = 1.02 and gives the  $T_g$  for pMpI from the intercept as 408K.

In summary, the P(MPI + DPI) series of copolymers have  $T_g$  values which increase with MPI content but whose mechanical behaviour is modified by a dehydration reaction involving the monoester units.

#### 6.2.2 TBA RESULTS FOR PI(MPI + DPI) SERIES

The TBA spectra for pI(MPI + DPI) 24/76, 59/41, 78/22 and 91/9 are shown in figures 6.10 and 6.11. All previously reported mechanical studies on ionomers have been limited to copolymers with ion contents of up to 8% or thereby<sup>(43)</sup>. In general, these ionomers show similar properties to their parent, unionised, precursors, except for the very important enhancement

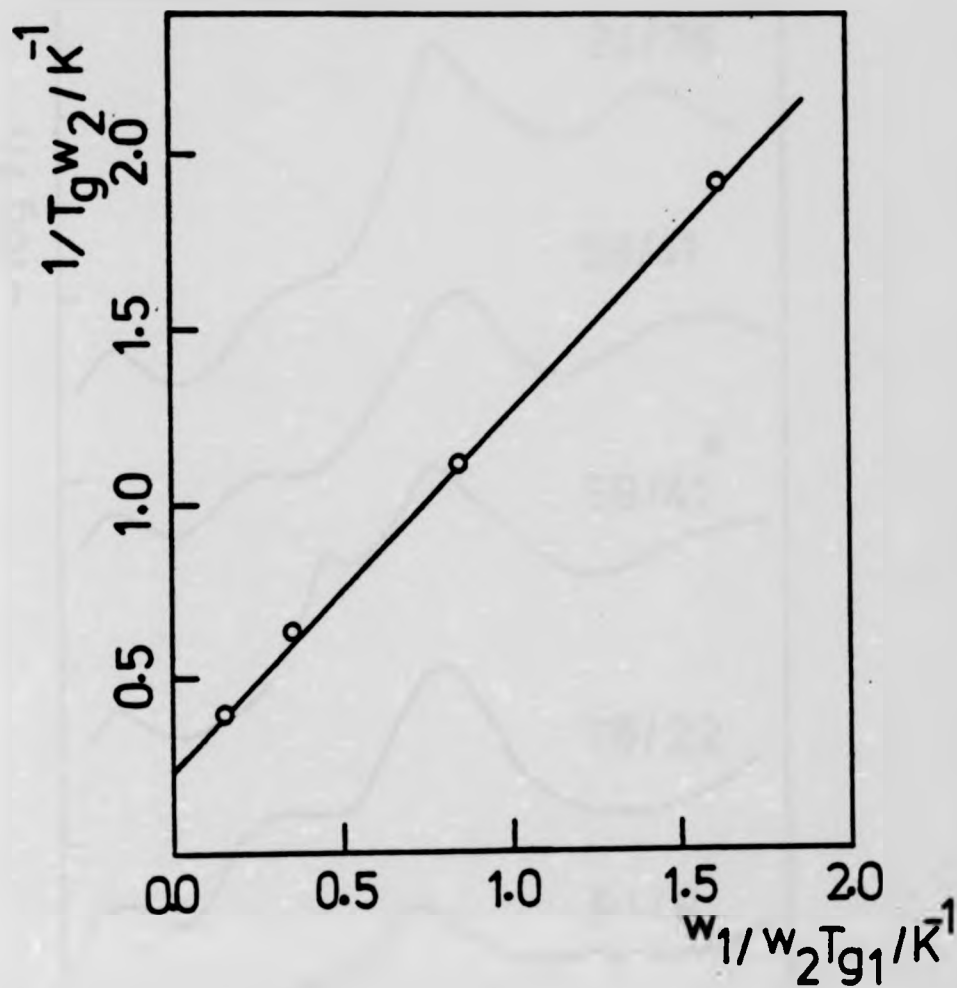


Figure 6.9: Extrapolation of  $T_g$  data for P(MPI+DPI) series according to equation 6.2.  $w_1$  and  $w_2$  are the weight fractions of DPI and MPI respectively in the copolymer,  $T_g$  is the copolymer glass transition and  $T_{g1}$  is the glass transition for PDPI.



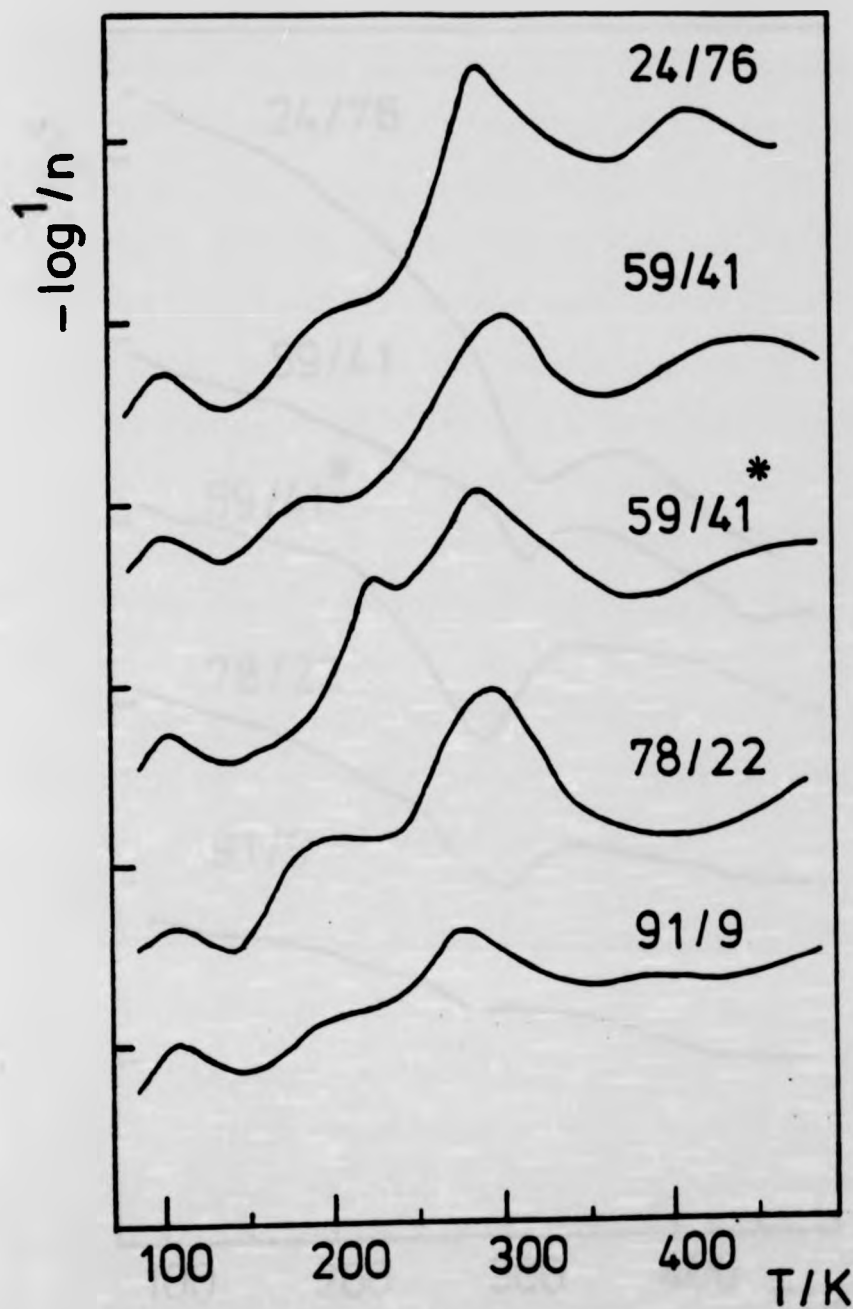


Figure 6.10: Plots of the mechanical damping index ( $-\log 1/n$ ) versus temperature for PI(MPI+DPI) 24/76 (Cs salt), 59/41 (Cs salt), 59/41\* (Cs salt, recycled sample), 78/22 (Na salt) and 91/9 (Na salt).

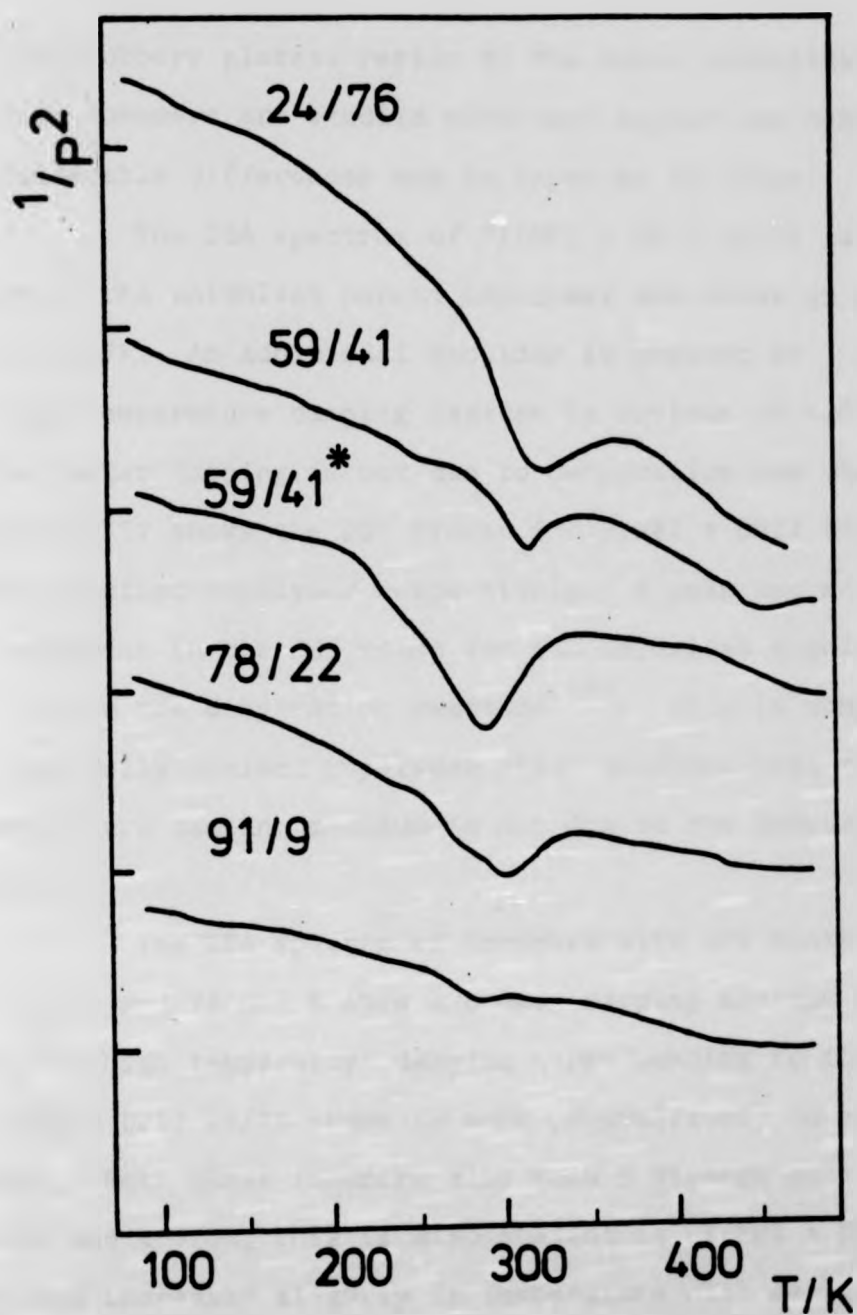


Figure 6.11: Plots of the relative rigidity ( $1/p^2$ ) versus temperature for PI(MPI+DPI) 24/76 (Cs salt), 59/41 (Cs salt), 59/41\* (Cs salt, recycled sample), 78/22 (Na salt) and 91/9 (Na salt).

of the rubbery plateau region by the ionic crosslinks. In this thesis ionomers are studied with much higher ion contents, where considerable differences may be expected to occur.

The TBA spectrum of PI(MPI + DPI) 24/76 is similar to that of the unionised parent copolymer and shows an obvious  $T_g$  at 287K. An additional shoulder is present at  $\sim 200$ K and a high temperature damping feature is obvious at 420K. That this latter damping is not due to dehydration was checked by DSC. Figure 6.12 shows the DSC traces for P(MPI + DPI) 59/41 and its fully ionised copolymer respectively. A peak centred at 450K is apparent in the DSC trace for the unionised copolymer which is due to the dehydration reaction<sup>(18)</sup>. This is completely absent in the fully ionised copolymer which confirms that the high temperature damping maximum is not due to the dehydration cross-link.

The TBA spectra of ionomers with MPI contents of 59 mol % and 78 mol % show a common damping maximum at  $\sim 290$ K but the high temperature damping corresponding to that in PI(MPI + DPI) 24/76 seems to move progressively to higher temperatures. Both these ionomers also show a strange rise in  $1/p^2$  at  $\sim 310$  and  $\sim 320$ K, this is also present in PI(MPI + DPI) 24/76 but has increased slightly in temperature with decreasing ion content. What causes such behaviour (an increase in relative rigidity) is a matter for speculation at this time. The phenomenon is reversible, since on re-running PI(MPI + DPI) 59/41 the behaviour is still present, indeed even enhanced slightly. It is tentatively suggested that some reorganisation of the ion clusters may be involved which leads to a greater degree of

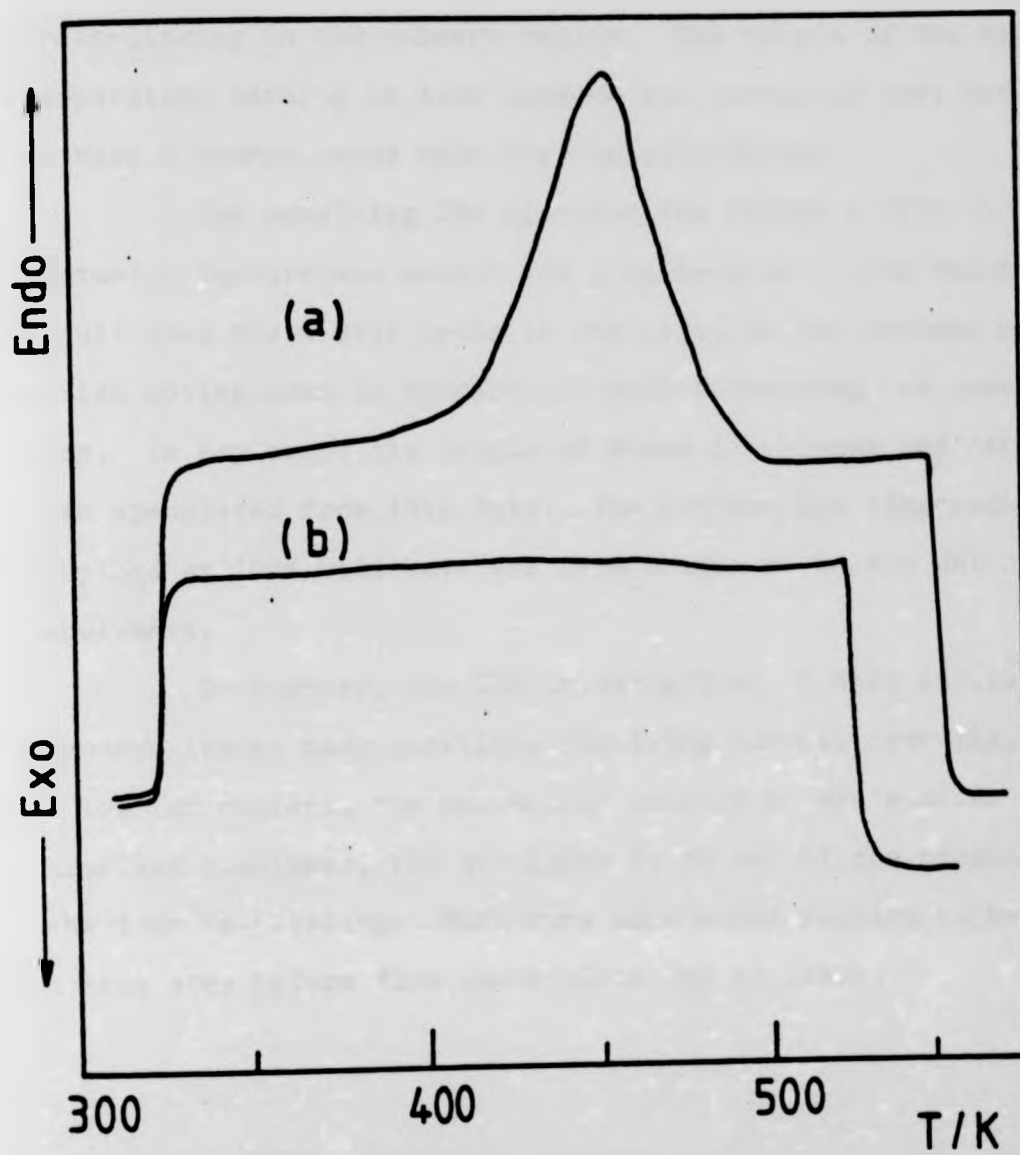


Figure 6.12: (a) DSC trace for P(MPI+DPI) 59/41;  
(b) DSC trace for PI(MPI+DPI) 59/41.

cross-linking in the rubbery region. The origin of the high temperature damping is also unknown and certainly does not seem to have a common cause with the rigidity change.

The remaining TBA spectrum for PI(MPI + DPI) 91/9 is virtually featureless except for a maximum at  $\sim 275\text{K}$  which could result from the  $\sim 290\text{K}$  peaks of the previous two members of the series moving down in temperature with increasing ion concentration. In any event the origin of these is unknown and cannot be even speculated from this data. The extreme low temperature dampings at  $100\text{K}$  will have the same origin as in the unionised copolymers.

In summary, the TBA investigation of this series of ionomers leaves many questions requiring further investigation. At low ion content, the mechanical properties are similar to the unionised copolymer, but at higher ( $\geq 24$  mol %) the mechanical behaviour is puzzling. Much more work would require to be done in this area before firm conclusions can be drawn.

REFERENCES

1. S. Baup, Ann., 19, 29 (1837).
2. H. Stobbe and A. Lippold, J.Prkt.Chem., 95, 336 (1914).
3. K. Kinoshita, Acta Phytochim.Japan, 5, 272 (1931).
4. S. Swarts, Bull.Acad.Royal Belg., 36, (2) 64 (1873).
5. Pfizer Chemicals, Pfizer Ltd., Kent, Product Information Sheets No. 403 and 404.
6. C. S. Marvel and T. H. Shepherd, J.Org.Chem., 24, 599 (1959).
7. S. Nagai, I. Yoshida and T. Uno, Chem.High Polym.Japan, 17, 117 (1960).
8. B. E. Tate, Adv.Polym.Sci., 5, 214 (1967).
9. B. E. Tate, "The polymerization of itaconic acid and esters", published by Pfizer Europe Chemicals, Sandwich, Kent.
10. B. R. Baker, R. E. Shaub and G. H. Williams, J.Org.Chem., 17, 122 (1952).
11. J. Velickovic and J. Vukajlovic-Filipovic, Die Angew.Makromol.Chemie, 13, 79 (1970).
12. J. Velickovic, V. Juranicova and J. Filipovic, Die Angew. Makromol.Chemie, 24, 77 (1972).
13. J. Velickovic and S. Vasovic, Die Makromolek.Chemie, 153, 207 (1972).
14. J. Velickovic, S. Coseva and R. J. Fort, Europ.Polym.J., 11, 377 (1975).
15. J. Velickovic, J. Filipovic and S. Coseva, Europ.Polym.J., 15, 521 (1979).
16. Ye. A. Bekturov, L. A. Bimendina and S. V. Bereza, Vysokomol.Soyed., A12, 2179 (1970).

17. Ye. A. Bekturov, L. A. Bimendina, V. V. Roganov and S. R. Rafikov, *Vysokomol.Soyed.*, A14, 343 (1972).
18. Z. Haq, Ph.D. Thesis, Chemistry Dept., University of Stirling (1976).
19. S.A.E. Henshall, Ph.D. Thesis, Chemistry Dept., University of Stirling (1974).
20. J.M.G. Cowie and I. J. McEwen, *Polymer*, 16, 869 (1975).
21. J.M.G. Cowie, S.A.E. Henshall, I. J. McEwen and J. Velickovic, *Polymer*, 18, 612 (1977).
22. J.M.G. Cowie and Z. Haq, *Polymer*, 19, 1052 (1978).
23. J.M.G. Cowie, Z. Haq and I. J. McEwen, *J.Polym.Sci: Polym.Lett.Ed.*, 17, 771 (1979).
24. J.M.G. Cowie, Z. Haq and I. J. McEwen, *Polymer*, 22, 327 (1981).
25. J.M.G. Cowie and I. J. McEwen, *Europ.Polym.J.*, 17, 619 (1981).
26. J.M.G. Cowie and I. J. McEwen, *Macromolecules*, 14, (5), 1374 (1981).
27. J. D. Ferry, "Viscoelastic properties of polymers", John Wiley & Sons, New York (1970).
28. N. G. McCrum, B. E. Read and G. Williams, "Anelastic and dielectric effects in polymeric solids", John Wiley & Sons, London (1967).
29. J. F. Rabek, "Experimental Methods in Polymer Chemistry", John Wiley & Sons, New York (1980).
30. D. J. Meier Ed., "Molecular Basis of Transitions and Relaxations", Gordon and Breach, New York (1978).
31. L. E. Nielsen, "Mechanical properties of polymers", Reinhold, New York (1962).

32. J. Heijboer, Ann.New York Acad.Sci., 279, 104 (1976).
33. J.M.G. Cowie, J. Macromol.Sci.-Phys., B18, (4) 569 (1980).
34. B. Wunderlich and H. Bauer, Adv.Polymer Sci., 7, 151 (1970).
35. U. Gaur, Hua-Cheng Shu, A. Mehta and B. Wunderlich, J.Phys.Chem.Ref.Data, 10, (1) 89 (1981).
36. E. A. DiMarzio and F. Dowell, J.Appl.Phys., 50, (10) 6061 (1979).
37. J.M.G. Cowie, R. Ferguson and I. J. McEwen, Polymer, 23, 605 (1982).
38. A. Noshay and J. E. McGrath, "Block Copolymers", Academic Press, New York (1977).
39. R. B. Seymour, D. R. Owen and G. A. Stahl, Polymer, 14, 324 (1973).
40. C. I. Simionescu, B. Simionescu, M. Leanca and C. Ananiescu, Polymer Bulletin, 5, 61 (1981).
41. M.J.M. Abadie, F. Schue and T. Souel, Polymer, 22, 1076 (1981).
42. Binnur Z. Gunerin-Minard, Ph.D. Thesis, University of Akron (1978).
43. L. Holliday, Ed., "Ionic Polymers", Applied Science Publishers, London (1975).
44. M. Rigdahl, B. A. Reinhardt, F. W. Harris and A. Eisenberg, Macromolecules, 14, 851 (1981).
45. E. D. Andreeva, V. N. Nikitin and Yu. M. Boyartchuk, Macromolecules, 9, (2) 238 (1976).
46. E. J. Roche, R. S. Stein and W. J. MacKnight, J.Polym.Sci.:Polym.Phys.Ed., 18, 1035 (1980).
47. D. L. Handlin, W. J. MacKnight and E. L. Thomas, Macromolecules, 14, 795 (1981).



48. D. A. Smith, Makromolek.Chem., 103, 301 (1967).
49. John J. Laverty and Zack G. Gardlund, J.Polym.Sci., Polym.Chem.Ed., 15, 2001 (1977).
50. Perkin-Elmer DSC-2 Instruction Manual, Perkin-Elmer Corporation, Norwalk, Conn., USA.
51. E. S. Watson, M. J. O'Neill, J. Justin and N. Brenner, Anal.Chem., 36, 1233 (1964).
52. M. J. O'Neill, Anal.Chem., 36, 1238 (1964).
53. M. J. O'Neill, Anal.Chem., 38, 1331 (1968).
54. Thermal Analysis Newsletter, No. 3 Perkin-Elmer Corporation, Norwalk, Conn., USA.
55. E. M. Barrall ii and J. F. Johnson, Tech.Methods.Polym. Evaln., 2, 1 (1970).
56. D. C. Ginnings and G. T. Furukawa, J.Amer.Chem.Soc., 75, 522 (1953).
57. A. F. Lewis and J. K. Gillham, J.Appl.Polym.Sci., 7, 685 (1963).
58. J. K. Gillham, Review paper, AIChE Journal, 6, 20, 1066 (1974).
59. T. Murayama, "Dynamic Mechanical Analysis of Polymeric Material", Vol.1 Elsevier Scientific Publishing Company, Amsterdam (1978).
60. P. J. Flory, "Principles of Polymer Chemistry", Cornell University Press, Ithaca, New York, (1953).
61. J.M.G. Cowie, Europ.Polym.J., 11, 297 (1975).
62. D. Braun, W. Brendlein and G. Mott, Europ.Polym.J., 9, 1007 (1973).
63. R. F. Boyer in "Molecular basis of transitions and relaxations", Gordon and Breach, New York (1978).

64. I. J. McEwen, Personal communication.
65. K. Shimizu, O. Yano and Y. Wada, *J. Polym. Sci.; Polym. Phys. Ed.*, 13, 1959 (1975).
66. J. Dale, *Acta. Chemica. Scand.*, 27, 1115 (1973).
67. R. F. Boyer, *Rubber Chem. Technol.*, 36, 1303 (1963).
68. T. F. Schatzki, *J. Polym. Sci.*, 57, 496 (1962).
69. R. H. Boyd and S. M. Breitling, *Macromolecules*, 7, 855 (1974).
70. L. Mandelker, G. M. Martin and F. A. Quinn, *J. Res. Nat. Bur. Stds.*, 58, 137 (1957).
71. R.-Joon Roe and A. E. Tonelli, *Macromolecules*, 11, (1) 114 (1978).
72. L. A. Wood, *J. Polym. Sci.*, 28, 319 (1958).
73. D. Lath and I. J. McEwen, unpublished work.
74. S. Alford and M. Dale, *J. Amer. Chem. Soc.*, 77, 4774 (1955).
75. K. S. Pitzer and W. D. Gwinn, *J. Chem. Phys.*, 10, 428 (1942).
76. K. S. Pitzer, *J. Chem. Phys.*, 8, 711 (1940).
77. J. M. G. Cowie and R. Ferguson, unpublished work.
78. M. Gordon and J. S. Taylor, *J. Appl. Chem.*, 2, 493 (1952).
79. T. G. Fox, *Bull. Amer. Phys. Soc.*, 1, 123 (1956).
80. J. M. Pochan, C. L. Beatty and D. F. Pochan, *Polymer*, 20, 879 (1979).
81. J. M. Barton, *J. Polym. Sci.*, Part C, (30) 573 (1970).
82. E. A. Di Marzio and J. H. Gibbs, *J. Polym. Sci.*, 40, 121 (1959)
83. B. D. Coleman and T. G. Fox, *J. Polym. Sci.*, Part A1, 3183 (1963).
84. K. Ito and Y. Yamashita, *J. Polym. Sci.*, Part A3, 2165 (1965).
85. P. R. Couchman and F. E. Karasz, *Macromolecules*, 11, (1) 117 (1978).
86. J. J. Laverty and Z. G. Gardlund, *Polymer Preprints*, 15, (2) 306 (1974).

87. R. Walez and W. Heitz, *J. Polym. Sci.; Polym. Chem. Ed.*, 16, 1807 (1978).
88. *Polymer Handbook*, J. Brandrup and E. H. Immergut, Eds. Interscience Publishers, New York (1967).
89. C.E.M. Morris and R. A. Humphreys, "Modification of a Vapour Pressure Osmometer", Report No. 616, Materials Research Laboratories, Melbourne, Australia, (1974).
90. J. L. Binder, *Appl. Spectrosc.*, 28, 17 (1969).
91. J.M.G. Cowie and I. J. McEwen, *Macromolecules*, 10, (5) 1124 (1977).
92. M. Yazadani Pedram, MSc thesis, Chemistry Dept., University of Stirling (1977).
93. D. C. Allport and A. A. Mohajer in "Block Copolymers", D. C. Allport and W. H. Janes, Eds. Applied Science Publishers Ltd., Essex (1973).
94. M. Matsuo, *Japan Plastics*, 2, 6 (1968).
95. L. J. Hughes and G. L. Brown, *J. Appl. Polym. Sci.*, 5, 580 (1961) and *J. Appl. Polym. Sci.*, 5, 337 (1961).
96. R. Séguéla and J. Prud'homme, *Macromolecules*, 11, (5) 1007 (1978).
97. J.M.G. Cowie, D. Lath and I. J. McEwen, *Macromolecules*, 12, 52 (1979).
98. J. V. Dawkins in "Block Copolymers", D. C. Allport and W. H. Janes, Ed. Applied Science Publishers Ltd., Essex (1973).
99. J.M.G. Cowie and I. J. McEwen, *J. Macromol. Sci.-Phys.*, B16, (4) 611 (1979).
100. W. J. Macknight, W. P. Taggart, and R. S. Stein, *J. Polym. Sci.; Polym. Symp.*, 45, 113 (1974).

101. R. Longworth and D. J. Vaughan, *Polymer Preprints*, 9, (1) 525 (1968).
102. C. L. Marx, D. F. Caulfield, and S. L. Cooper, *Macromolecules*, 6, (3) 344 (1973).
103. C. L. Marx, D. F. Caulfield and S. L. Cooper, *Polymer Preprints*, 14, (2) 890 (1973).
104. M. Fujimura, T. Hashimoto and H. Kawai, *Macromolecules*, 14, (5) 1309 (1981).
105. J.M.G. Cowie and C. Y. Ho, unpublished work.

APPENDIX 1TABLE A1

Calculated parameters of the Fox equation for P(DMI + DBI) series with DMI = 1 and DBI = 2

<u>SAMPLE</u>	$T_g/K$	$w_1$	$w_2$	$\frac{10^3 K}{T_g w_2}$	$\frac{10^3 w_1 K}{w_2 T_{g1}}$
PDMI	377	1.00	0.00	-	-
1	334	0.70	0.30	9.98	6.19
2	321	0.51	0.49	6.36	2.76
3	308	0.29	0.71	4.57	1.08
4	296	0.19	0.81	4.17	0.62
5	292	0.14	0.86	3.98	0.43
6	286	0.08	0.92	3.80	0.23
PDBI	282	0.00	1.00	3.55	0.00

TABLE A2

Calculated parameters of the Fox equation for P(DMI + DHpI) series with DMI = 1 and DHpI = 2

<u>SAMPLE</u>	$T_g/K$	$w_1$	$w_2$	$\frac{10^3 K}{T_g w_2}$	$\frac{10^3 w_1 K}{w_2 T_{g1}}$
PDHpI	248	0.00	1.00	-	-
1	246	0.05	0.95	4.28	0.14
2	250	0.13	0.87	4.60	0.39
3	260	0.20	0.80	4.81	0.66
4	274	0.28	0.72	5.07	1.03
5	290	0.47	0.53	6.50	2.35
6	312	0.75	0.25	12.82	7.95
PDMI	377	1.00	0.00	-	0.00

TABLE A3

Calculated parameters of the Fox equation for P(DMI + DOI) series with DMI = 1 and DOI = 2

<u>SAMPLE</u>	$T_g/K$	$w_1$	$w_2$	$\frac{10^3 K}{T_g w_2}$	$\frac{10^3 w_1 K}{w_2 T_{g1}}$
PDMI	377	1.00	0.00	-	-
1	350	0.84	0.16	17.86	13.92
2	313	0.61	0.39	8.19	4.15
3	290	0.44	0.56	6.16	2.08
4	269	0.26	0.74	5.02	0.93
5	252	0.11	0.89	4.46	0.32
6	242	0.03	0.97	4.26	0.08
PDOI	240	0.00	1.00	4.16	0.00

TABLE A4

Calculated parameters of the Fox equation for P(DMI + DNI) series with DMI = 1 and DNI = 2

<u>SAMPLE</u>	$T_g/K$	$w_1$	$w_2$	$\frac{10^3 K}{T_g w_2}$	$\frac{10^3 w_1 K}{w_2 T_{g1}}$
PDMI	377	1.00	0.00	-	-
1	341	0.85	0.15	19.55	15.03
2	306	0.62	0.38	8.56	4.33
3	296	0.49	0.51	6.62	2.55
4	264	0.33	0.67	5.65	1.31
5	238	0.18	0.82	5.12	0.58
6	231	0.11	0.89	4.86	0.33
PDNI	(245)	0.00	1.00	(4.08)	0.00

TABLE A5

Calculated parameters of the Fox equation for P(DPrI + DOI) series with DPrI = 1 and DOI = 2

<u>SAMPLE</u>	$T_g/K$	$w_1$	$w_2$	$\frac{10^3 K}{T_g w_2}$	$\frac{10^3 w_1 K}{w_2 T_{g1}}$
PDPPrI	304	1.00	0.00	-	-
1	284	0.87	0.13	27.08	22.01
2	264	0.70	0.30	12.62	7.67
3	257	0.48	0.52	7.48	3.04
4	253	0.30	0.70	5.64	1.41
5	248	0.19	0.81	4.98	0.77
6	245	0.12	0.88	4.63	0.45
PDOI	240	0.00	1.00	4.16	0.00

TABLE A6

Calculated parameters of the Pochan-Beatty-Pochan equation for P(DMI + DBI) series with DBI = 1 and DMI = 2

<u>SAMPLE</u>	$T_g/K$	$w_1$	$w_2$	$\frac{\ln T_g}{w_1}$	$\frac{w_2}{w_1} \ln T_{g2}$
PDMI	377	0.00	1.00	-	-
1	334	0.30	0.70	19.37	13.84
2	321	0.49	0.51	11.78	6.17
3	308	0.71	0.29	8.07	2.42
4	296	0.81	0.19	7.02	1.39
5	292	0.86	0.14	6.60	0.96
6	286	0.92	0.08	6.15	0.52
PDBI	282	1.00	0.00	5.64	0.00

TABLE A7

Calculated parameters of the Pochan-Beatty-Pochan equation for P(DMI + DHpI) series with DHpI = 1 and DMI = 2

<u>SAMPLE</u>	$T_g/K$	$w_1$	$w_2$	$\frac{\ln T_g}{w_1}$	$\frac{w_2}{w_1} \ln T_{g2}$
PDHpI	248	1.00	0.00	5.513	0.000
1	246	0.95	0.05	5.795	0.312
2	250	0.87	0.13	6.346	0.886
3	260	0.80	0.20	6.951	1.483
4	274	0.72	0.28	7.796	2.307
5	290	0.53	0.47	10.698	5.260
6	312	0.25	0.75	22.972	17.796
PDMI	377	0.00	1.00	-	-

TABLE A8

Calculated parameters of the Pochan-Beatty-Pochan equation for P(DMI + DOI) series with DOI = 1 and DMI = 2

<u>SAMPLE</u>	$T_g/K$	$w_1$	$w_2$	$\frac{\ln T_g}{w_1}$	$\frac{w_2}{w_1} \ln T_{g1}$
PDMI	377	0.00	1.00	-	-
1	350	0.16	0.84	36.612	31.144
2	313	0.39	0.61	14.734	9.278
3	290	0.56	0.44	10.125	4.661
4	269	0.74	0.26	7.560	2.084
5	252	0.89	0.11	6.213	0.733
6	242	0.97	0.03	5.658	0.183
PDOI	240	1.00	0.00	5.480	0.000



TABLE A9

Calculated parameters of the Pochan-Beatty-Pochan equation for P(DMI + DNI) series with DNI = 1 and DMI = 2

<u>SAMPLE</u>	$T_g/K$	$w_1$	$w_2$	$\frac{\ln T_g}{w_1}$	$\frac{w_2}{w_1} \ln T_{g1}$
PDMI	377	0.00	1.00	-	-
1	341	0.15	0.85	38.880	33.616
2	306	0.38	0.62	15.062	9.680
3	296	0.51	0.49	11.157	5.700
4	264	0.67	0.33	8.322	2.922
5	238	0.82	0.18	6.673	1.302
6	231	0.89	0.11	6.115	0.733
PDNI	(245)	1.00	0.00	(5.501)	0.000

TABLE A10

Calculated parameters of the Pochan-Beatty-Pochan equation for P(DPrI + DOI) series with DOI = 1 and DPrI = 2

<u>SAMPLE</u>	$T_g/K$	$w_1$	$w_2$	$\frac{\ln T_g}{w_1}$	$\frac{w_2}{w_1} \ln T_{g2}$
PDPrI	304	0.00	1.00	-	-
1	284	0.13	0.87	43.453	38.260
2	264	0.30	0.70	18.586	13.340
3	257	0.52	0.48	10.671	5.277
4	253	0.70	0.30	7.905	2.450
5	248	0.81	0.19	6.806	1.341
6	245	0.88	0.12	6.251	0.779
PDOI	240	1.00	0.00	5.480	0.000



TABLE A12

Calculated parameters of the Barton equation for P(DMI+DHpI) series with  $r_a = 1.81$ ,  $r_b = 0.678$ ,  $\alpha_{aa} = 18$ ,  $\alpha_{bb} = 40$  and  $\alpha_{ab} = \alpha_{ba} = 29$

SAMPLE	$T_g$ (K)	$n_a$ (Feed)	$T_g^{-n'_{aa}} T_{aa}^{-n'_{bb}} T_{bb}$	$1 - n'_{aa} - n'_{bb}$
PDHpI(b) 248	-	-	-	-
1	246	0.098	43	0.186
2	250	0.146	63	0.261
3	260	0.213	91	0.347
4	274	0.338	121	0.454
5	290	0.556	118	0.481
6	312	0.740	79	0.362
PDMI(a) 377	-	-	-	-

TABLE A13

Calculated parameters of the Barton equation for P(DMI+DOI) series with  $r_a = 1.361$ ,  $r_b = 1.031$ ,  $\alpha_{aa} = 18$ ,  $\alpha_{bb} = 44$  and  $\alpha_{ab} = \alpha_{ba} = 31$

SAMPLE	$T_g$ (K)	$n_a$ (Feed)	$T_g^{-n'_{aa}} T_{aa}^{-n'_{bb}} T_{bb}$	$1 - n'_{aa} - n'_{bb}$
PDMI(a) 377	-	-	-	-
1	350	0.900	57	0.216
2	313	0.733	112	0.425
3	290	0.600	126	0.481
4	269	0.430	117	0.441
5	252	0.200	68	0.248
6	242	0.065	22	0.086
PDOI(b) 240	-	-	-	-

TABLE A14

Calculated parameters of the Barton equation for P(DMI+DNI) series with  $r_a = 1.171$ ,  $r_b = 0.316$ ,  $\alpha_{aa} = 18$ ,  $\alpha_{bb} = 48$  and  $\alpha_{ab} = \alpha_{ba} = 33$ .

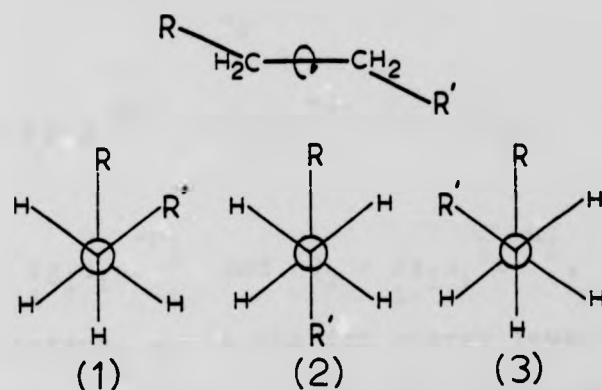
<u>SAMPLE</u>	<u>T<sub>g</sub>/K</u>	<u>n<sub>a</sub></u> (Feed)	T <sub>g</sub> <sup>-n'</sup> <sub>aa</sub> T <sub>aa</sub> <sup>-n'</sup> <sub>bb</sub> T <sub>bb</sub> <sup>*</sup>	T <sub>g</sub> <sup>-n'</sup> <sub>aa</sub> T <sub>aa</sub> <sup>-n'</sup> <sub>bb</sub> T <sub>bb</sub> <sup>**</sup>	1-n' <sub>aa</sub> -n' <sub>bb</sub>
PDMI(a)	377	-	-	-	-
1	341	0.906	57	57	0.244
2	306	0.747	121	121	0.495
3	296	0.617	158	159	0.604
4	264	0.447	156	158	0.648
5	238	0.213	114	120	0.517
6	231	0.060	38	50	0.216
PDNI(b)	(245 (230	-	-	-	-

\* calculated with T<sub>(b)</sub> = 245K

\*\* calculated with T<sub>(b)</sub> = 230K

## APPENDIX 2

The total heat capacity of a molecule is a measure of its ability to store thermal energy, and can be expressed as a sum of heat capacity contributions from the various sets of energy levels possessed by the molecule. In section 3.5.3 the heat capacity contribution from the internal rotation about C-C bonds of linear alkanes is required and this problem has been solved by Pitzer<sup>(75,76)</sup> who recognised that the asymmetric internal rotation barrier to rotation of the unit



can be regarded as comprising a 3-fold symmetric ethane-type barrier plus a steric contribution from the two high energy gauche conformers (1) and (3).  $C_v$  for this type of hindered internal rotation may then be expressed as

$$C_v = (n-3)C_v^{ir} + C_v^{steric} \quad (1)$$

where there are  $n$  carbon atoms in the alkyl chain,  $C_v^{ir}$  is the heat capacity due to hindered internal rotation about a symmetric 3-fold barrier and  $C_v^{steric}$  is the heat capacity contribution due to the high energy conformers.

For the purpose of this application the difference between

$C_p$  and  $C_v$  is neglected (see equation 3.9, section 3.5.1).

In general,  $C_v$  may be described by the familiar statistical thermodynamic relationship

$$C_v = \frac{R}{T^2} \cdot \frac{\partial^2 \ln Q}{\partial (1/T)^2} \quad (2)$$

where  $Q$  is the appropriate partition function. This may be rearranged to give

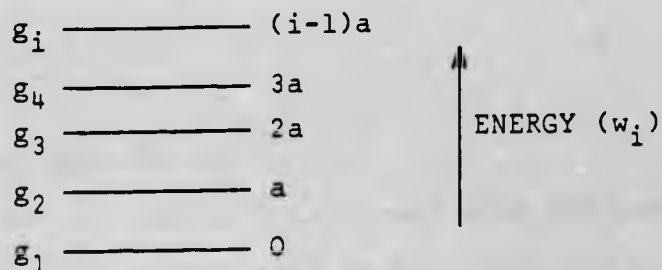
$$C_v = \frac{R(Q_0 Q_2 - Q_1^2)}{Q_0^2} \quad (3)$$

where  $Q_0 = \sum_i g_i e^{-\frac{w_i}{kT}} = \sum_i g_i e^{-u_i}$ , ( $u_i = \frac{w_i}{kT}$ ),

$$Q_1 = \sum_i g_i u_i e^{-u_i} \quad \text{and} \quad Q_2 = \sum_i g_i u_i^2 e^{-u_i},$$

$k$  is the Boltzman constant,  $w_i$  is the  $i$ th energy level of the system and  $g_i$  is the degeneracy of the  $i$ th energy level.

(a)  $C_v^{\text{steric}}$  may be evaluated from equation (3) if the number of high energy conformers for a given linear alkane is calculated and steric energy of these conformations is known. Pitzer provides the following energy level diagram in terms of the adjustable parameter  $a$



where  $g_i$  is thus the number of conformations with a steric energy  $(i-1)a$  and the following table which allows the energy and number of conformations to be selected.  $a$  is chosen to be  $3.35 \text{ kJ mol}^{-1}$  so that theory and experiment fit.

<u>Number of atoms in linear alkane</u>	<u>Number of conformations with energy</u>					
	<u>0</u>	<u>a</u>	<u>2a</u>	<u>3a</u>	<u>4a</u>	<u><math>\infty^*</math></u>
4	1	2	0	0	0	0
5	1	4	2	0	0	2
6	1	6	8	2	0	10
7	1	8	18	12	2	40

\* This column takes account of inaccessible conformers where the alkane chain ends are in contact

(b)  $C_v^{ir}$  may be evaluated from the wave equation for a hindered internal rotation with a symmetric 3-fold potential barrier  $V$ .

$$\frac{-h^2}{8\pi^2 I} \cdot \frac{d^2 \psi}{d\phi^2} + \frac{1}{2}V(1 - \cos 3\phi)\psi = w\psi \quad (4)$$

where  $h$  = Planck's constant,  $I$  the reduced moment of inertia of the rotation,<sup>(75,76)</sup>  $\phi$  is the angle of rotation and  $\psi$  is the wave function.  $w_i$  is given by

$$w_i = \frac{9 h^2 \theta_{0i}}{32 \pi^2 I} + \frac{1}{2}V \quad (5)$$

where  $\theta_{0i}$  is the eigen value.

Equation (4) can be transformed into the Matheu equation and the eigen values used to calculate the energy levels  $w_i$  of the rotor.  $C_v^{ir}$  can then be calculated from equation (3).

A Fortran program for use on the VACS computer for the calculation of the  $C_v$  contribution from hindered internal rotation of a linear alkane of any length via equations (3) and (1) has been developed by Mr. R. Ferguson in this laboratory. The number of hindered internal rotations for side chains of poly di-n-alkyl itaconates was established as indicated in Table 3.22 and the hindered internal rotation heat capacity of the n-alkane with the same number of hindered rotors evaluated. For example, side chain of PDHpI has 5 internal rotations and the calculated  $C_v$  for n-octane is used to represent this.



copyright of this thesis rests with its author.

This copy of the thesis has been supplied on condition that anyone who consults it is understood to recognise that its copyright rests with its author and that no quotation from the thesis and no information derived from it may be published without the author's prior written consent.

307

D47328/83

YAZDANI PEDRAM M

307